E.O. Paton Electric Welding Institute of the National Academy of Sciences of Ukraine

International Scientific-Technical and Production Journal

The Paton WELDING JOURNAL

May/June 2016
No. 5-6

Published since 2000

English translation of the monthly «Avtomaticheskaya Svarka» (Automatic Welding) journal published in Russian since 1948

International Conference
ADVANCED WELDING TECHNOLOGIES
13–15 June, 2016, Kiev, Ukraine
E.O. Paton Electric Welding Institute

Organizers
National Academy of Sciences of Ukraine
E.O. Paton Electric Welding Institute
International Association «Welding»

CONTENTS

HYBRID TECHNOLOGIES OF WELDING

3D ADDITIVE TECHNOLOGIES

ECOLOGY IN WELDING PRODUCTION

FLASH-BUTT WELDING OF HIGH-STRENGTH RAILS OF NOWADAYS PRODUCTION

S.I. KUCHUK-YATSENKO, A.V. DIDKOVSKY, V.I. SHVETS, P.M. RUDENKO and **E.V. ANTIPIN**

E.O. Paton Electric Welding Institute, NASU

11 Kazimir Malevich Str., 03680, Kiev, Ukraine. E-mail: office@paton.kiev.ua

Over the recent five years, the high-strength rails of the new generation of type R65 of steel grade K76F of the production of the plant «MK Azovstal» as well as high-strength rails of type R65 of steel grade 76F of Russian production with their welding in continuous welded track are more and more often laid at the railroads of Ukraine. At the E.O. Paton Electric Welding Institute the comprehensive investigations of weldability of these rails were carried out using flash-butt method with the aim of development of industrial technologies. In welding of all the investigated batches of high-strength rails the required values of mechanical properties of welded joints were obtained at welding modes, characterizing by energy input 1.5–2 times lower than that in welding of rails of previous generations. The welding technology using pulsed flashing was developed providing a highly-concentrated heating and formation of quality joints of high-strength rails of different production, as well as the new generation of machines for flash-butt welding of high-strength rails under the stationary and field conditions was developed. 10 Ref., 11 Figures, 3 Tables.

The laying of high-strength rails of the new generation with their welding in continuous track is more and more widely used at the railroads of Ukraine. Mostly high-strength rails R65 of steel grade K76F of production of «MK Azovstal», as well as high-strength rails R65 of steel grade 76F of Russian production are applied. At the PWI the comprehensive investigations of weldability of these rails were carried out using flash-butt method with the aim of development of industrial technologies for their welding. At the same time, the weldability of modern high-strength rails R350HT produced by well-known companies «Voestalpine Schienen GmbH» (Austria), and rails VS-

350Ya 350LDT of «Nippon Steel» (Japan) was also investigated. Table 1 shows chemical composition and mechanical properties of the mentioned steels.

In the manufacture of all the investigated rails the advanced technologies of converter production with the continuous casting of steel and continuous rolling are used.

For the rails of steel K76F the differentiated hardening and for steel 76F the volumetric one are used. The hardness of layer of steel K76F hardened over the surface of rail head is *HV* 374–401 (Figure 1), the depth of the hardened layer is different and amounts from 7 to 15 mm. The hardness of the base material is

Table 1. Chemical composition of rails steel of different manufacturers and grades

Steel grade (country)	Chemical composition, wt.%					
	C	Mn	Si	V	Ti	Cr
K76F (Ukraine)	0.71–0.82	0.80–1.30	0.25–0.45	0.03–0.07	–	–
76F (Russia)	0.71–0.82	0.75–1.05	0.25–0.45	0.03–0.15	–	–
VS-350Ya 350LDT (Japan)	0.72–0.82	0.7–1.2	0.35–1	0.01	0.025	0.3–0.7
R350HT (Austria)	0.72–0.82	0.15–0.60	0.65–0.75	0.03	–	0.15

Table 1 (cont.)

Steel grade (country)	Chemical composition, wt.%			Mechanical properties		
	P	Al	S	Tensile strength σ_t, MPa	Yield strength $\sigma_{0.2}$, MPa	Hardness *HB*
K76F (Ukraine)	0.035	0.015	0.045	1196	800	341–388
76F (Russia)	0.025	0.02	0.03	1280	870	370–409
VS-350Ya 350LDT (Japan)	0.025	0.005	0.02	1240	860	362–400
R350HT (Austria)	0.025	0.004	0.03	1175	840	350–390

in the range of *HV* 250–300. The microstructure of all the rail steels mentioned in Table 1 is sorbite, the precipitates of free ferrite are almost absent (Figure 2). The characteristic feature of hypereutectoid rail steel VS-350Ya is the presence of primary austenitic grains, and precipitates of iron carbide along the boundaries. It should be noted that R350HT rails are characterized by a coarse primary austenitic grain, the grain number is estimated as 3–4. A somewhat smaller austenitic grain size is in rails K76F. The structure of steel for rails VS-350Ya and 76F is finer, the number of their austenitic grain is 5–6.

The welding modes using continuous flashing (CF) are determined by the programs of changing the basic parameters given for rails R65 in works [1, 2]. As the basic parameter determining energy input, the duration of flashing was accepted, which for rail R65 amounts to 180 s. The welding of reference batches of rails of 10 pcs was carried out in stationary machine K1000 and also in mobile machine K922 (both machines are of the PWI design and manufactured at Kakhovka Plant of Electric Welding Equipment. After flash removal the welded specimens of rails of 1.22 m length were tested for static mechanical bending according to the standard procedure accepted in the world practice [3]. The metallographic examinations of welded joints were carried out in light microscope «Neophot 32», fractographic investigations and micro X-ray analysis of the fracture surface were performed in the JEOL Auger-microprobe JAMP 9500F. The batches of rails 76F were preliminary welded using CF welding technology [4]. Such a technology is successfully applied at the railroads of Ukraine,
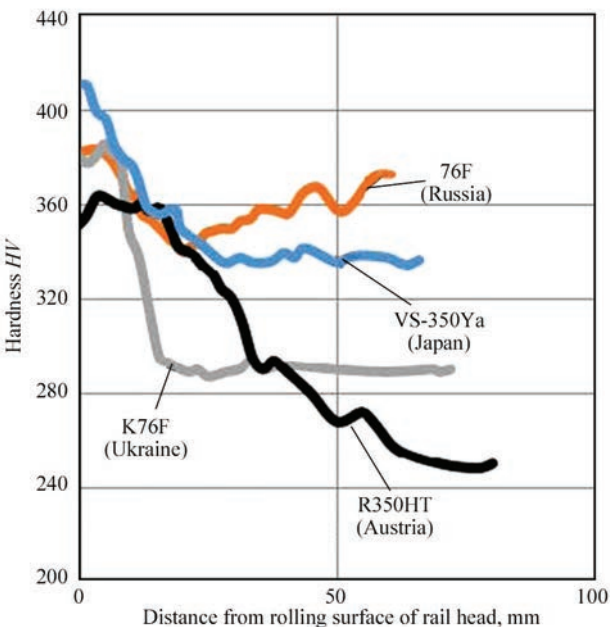
Figure 1. Distribution of hardness in the rail base metal in the vertical plane

CIS countries and other countries where rail welding equipment, designed at the PWI, is used. At the same time, the required values of mechanical properties of welded joints of non-hardened rails are provided.

For welded joints of high-strength rails the minimum values of fracture loads and bending deflections, specified by the Technical Specifications, are given in Table 2. In the Table (mode 2) the test results on static bending of high-strength batch of rails, welded using CF, are given. As is seen from the data, the fracture load in the tests meets the standard requirements and the values of deflection are significantly lower. On the
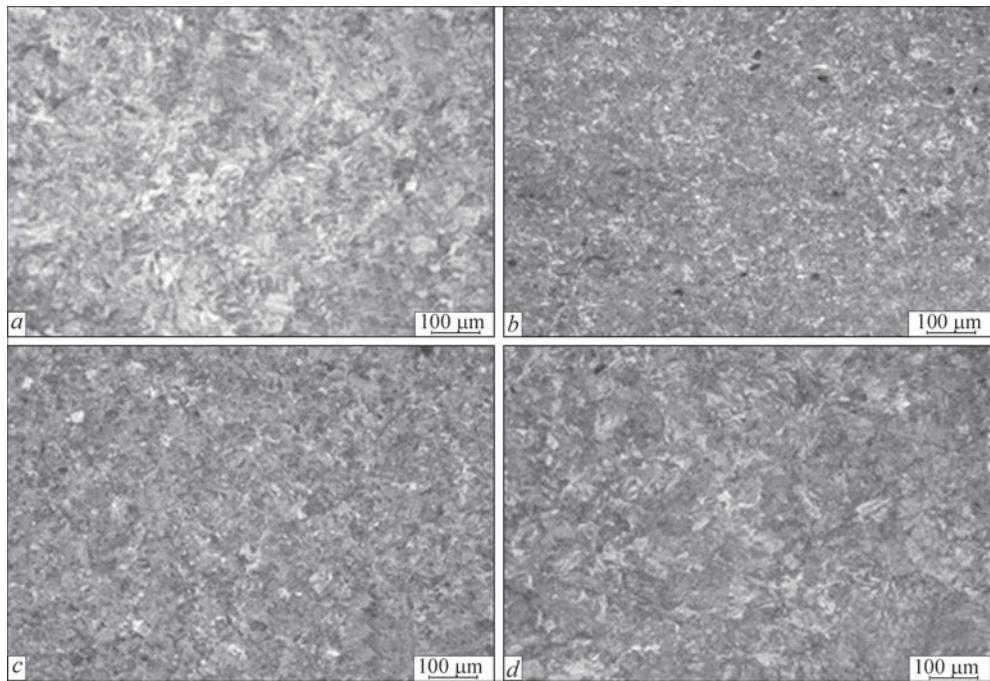
Figure 2. Microstructure of base metal of rail steel: *a* — K76F; *b* — 76F; *c* — VS-350Ya; *d* — R350HT

Table 2. Results of tests on static mechanical bending of different grades of batches of rails welded at different modes

Number of mode	Standard and steel grade	Welding time, s	Fracture load, kN	Bending deflection, mm	Note
	Ukraine		160	≥30	TU U 24.1-40075815-002:2016
	Russia	–	210	≥27	STO RZhD 1.08.002–2009
	Eurostandard		160	≥20	EN 14587-1:2007 E
1	K76F	180–200	$\frac{1750–2100}{2100}$	$\frac{17–32}{20}$	Continuous flashing
2	K76F	130–140	$\frac{1800–2000}{1900}$	$\frac{14–30}{19}$	Same
3	K76F	70–80	$\frac{2150–2400}{2250}$	$\frac{35–55}{40}$	Pulsed flashing
4	K76F	30–40	$\frac{1750–2000}{1950}$	$\frac{25–35}{28}$	Same
5	K76F	70–80	$\frac{2000–2300}{2150}$	$\frac{35–45}{38}$	»
5	76F	70–80	$\frac{2300–2600}{2450}$	$\frac{30–46}{38}$	»
5	VS-350Ya	70–80	$\frac{2620–2660}{2650}$	$\frac{32–40}{40}$	»
5	R350NT	70–80	$\frac{2770–3050}{3000}$	$\frac{58–66}{60}$	»

surface of welds fracture the defects were not detected. Along the joining line and the adjacent layers of metal a coarse structure of primary austenitic grains (Figure 3, *a*) is observed with grain number of 2–3. Along the grain boundaries of primary austenite the solid net of ferrite precipitates is clearly observed indicating the lower ductile properties of this area.

From the practice of flash-butt welding (FBW) it is well-known [5–7] that the reduction in welding energy input allows improving the structure of metal along the joining line and adjacent areas, in particular, reducing the grain sizes and precipitates of ferrite along their boundaries.

The batch of rails K76F was welded using CF with the low (t_w = 130–140 s) energy input (temperature field corresponding to mode 2 is shown in Figure 4, curve *3*). At the tests of welded specimens of this batch the decrease in values of ductility was observed (see Table 2). The reason for reduction of ductile properties in most cases is the formation of defects in the plane of the joints determined as dull spots (DS), the area of which is 10–50 mm² (Figure 5).

As the carried out investigations showed, in the DS microstructure on the background of the matrix pit fracture mainly (single cleavage facets are found),
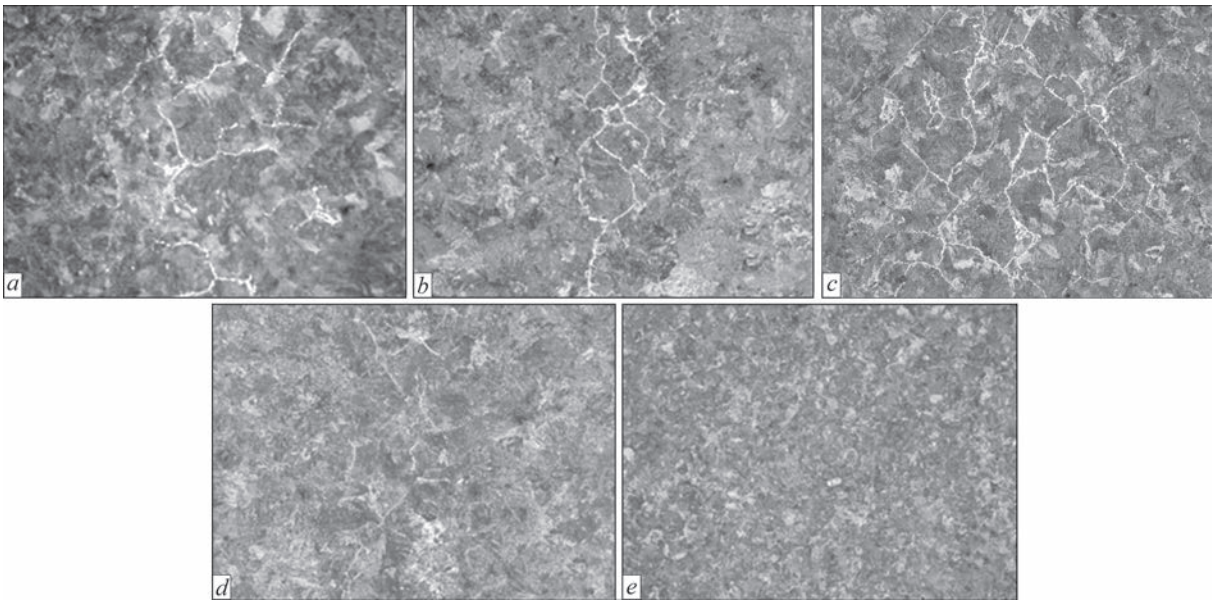
Figure 3. Microstructure (×100) of HAZ metal of welded joints: *a* — K76F (CF); *b* — K76F (PF); *c* — 76F (PF); *d* — VS-350Ya (PF); *e* — R350HT (PF)
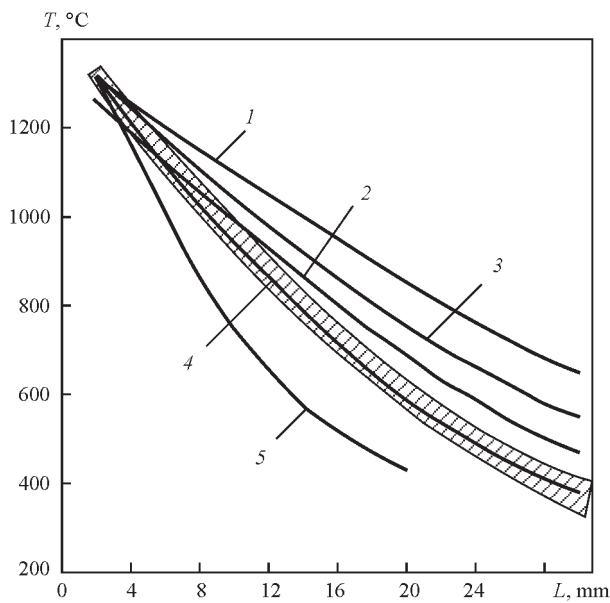
Figure 4. Distribution of temperature in HAZ before upsetting in welding rails R65 at different modes: *1–3* — CF with program decrease in voltage at t_w, s: *1* — 210–240; *2* — 180–200; *3* — 140–160; *4, 5* — PF at t_w, s: *4* — 70–80; *5* — 30–40

Number of area	C	O	F	Al	Si	Mn	Fe	Place of investigation
1	3.27	66.66	3.49	1.11	16.48	8.12	0.86	Silicate
2	1.63	61.08	2.73	2.15	16.70	14.73	0.99	Same
3	2.41	68.91	3.16	1.32	16.39	6.90	0.90	»
4	4.43	1.57	0	0.11	0	0.80	93.09	Matrix
5	5.51	0.86	1.88	0	0.18	0.81	90.76	Same
6	4.70	1.50	0	0	0.15	1.11	92.54	»

Figure 5. Macro- (*a*), microstructure (*b*) and results of chemical analysis of fracture surface of the joints of rails with DS

the numerous silicate inclusions of fused type of up to 10 μm size are present.

The defects of larger than 30 mm sizes reduce noticeably the results of investigations on bending, especially if they are located in the zone of tension. In the majority of standard documents in different countries regulating the quality evaluation, the presence of DS with total area of up to 30 mm² is not a rejection sign. If the spots of larger area are present in several specimens from a single reference batch, the decision is taken on the need in modifying the technology.

The aim of the carried out investigations was looking for the ways to prevent the formation of DS-type defects in welding at a reduced energy input. It was found that the formation of the mentioned defects is largely determined by flashing processes running at its final stage envisaged by the program (intensive flashing passing to upsetting). During this period at the edges of the flashed parts a melt is formed (Figure 6). In the melt the products of its oxidation by air from spark gap are always present. If the melt has a time to solidification before upsetting, then it fails to be completely removed due to deformation. The duration of solidification for melt at the edges of flashed parts is

$$t_m \rightarrow \frac{A\delta_l}{\lambda \frac{d\theta}{dx}} \geq \frac{\delta_{g\,max}}{v_f},$$

$$\frac{d\theta}{dx} \rightarrow f(\theta, v_{flash}, A_2),$$

(1)

where $\delta_{g\,max}$ is the maximum value of spark gap; v_f is the final flashing rate; Q is the melting point of ma-

terials to be welded; $\lambda(d\theta/dx)$ is the gradient of temperature field at flashing before upsetting; δ_l is the gap size in the places, where flashing values are maximum at the surface; A, A_2 is the dimensionless parameter which depends on thermophysical constants of material to be welded (c_m, γ, Q_m, θ_l).

It follows from the expression (1) that the admitted duration of the melt solidification decreases with the increase in the gradient of temperature field, and the probability of defects formation is increased.

The decrease in $\delta_{g\,max}$ value or increase in δ_l helps to increase the duration of existence of the melt before solidification. The maximum δ_l value is determined by thermophysical properties of the melt and forces of surface tension retaining the melt on the flashed surface. In the real conditions the thickness of the melt layer is unstable (Figure 6, CF), which is determined
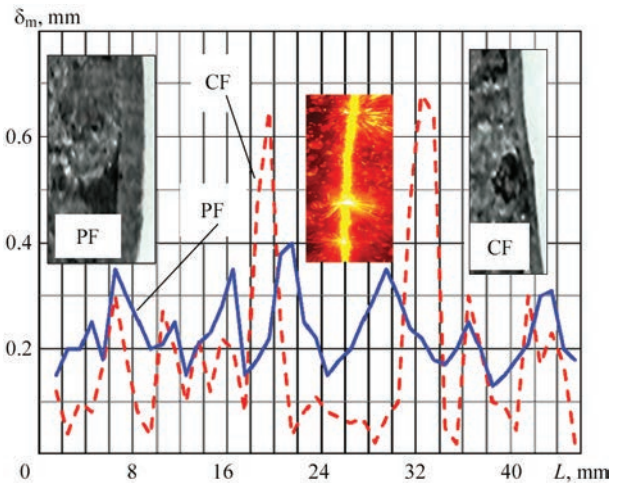
Figure 6. Distribution of melt on flashing surface of the head of rail K76F in welding with CF and PF
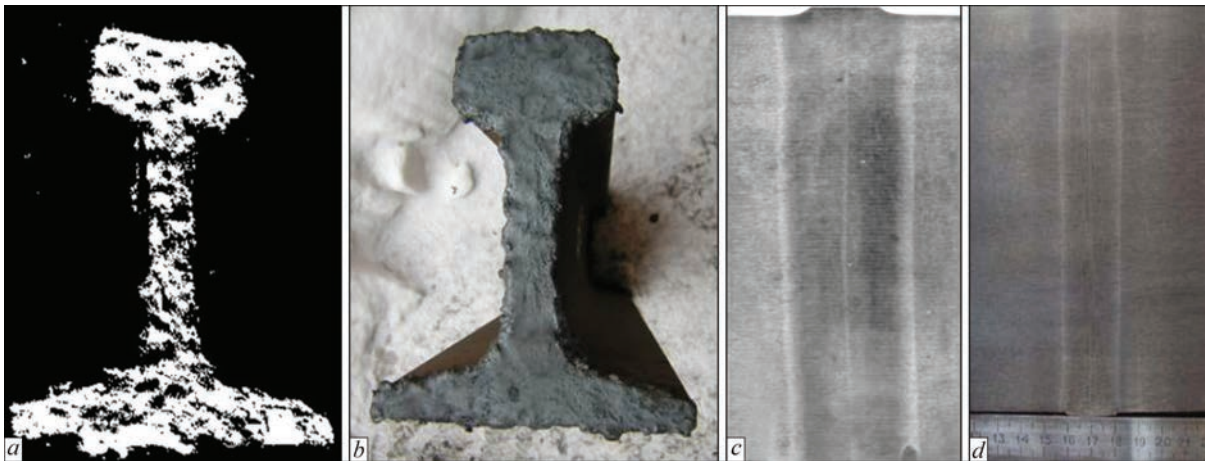
Figure 7. Flashing surface of rails R65 before upsetting during CF (*a*) and PF (*b*), and macrostructure of welded joints of rails at CF (*c*) and PF (*d*)

by explosive nature of flashing. The δ_g value is largely determined by the value of voltage during flashing.

The use of pulsed flashing [8] allows applying multifactor control of voltage, current and speed of movement of parts to suppress the explosive process of destroying the elementary contacts in flashing. It makes possible to maintain the high thermal efficiency of the process for the whole period of flashing and obtaining a highly-concentrated heating. Moreover, the flashing surface during PF is smoother (Figure 7 *a*, *b*), the depth of the craters, and respectively δ_g is 1.5–2 times decreased, and the thickness of the melt on the rail surface is stably maintained constant at a sufficiently high value (see Figure 6, PF).

Figure 8 shows record of the basic PF process parameters during welding rails. At PF, as well as CF, the basic process parameters are preset by the programs of changing the voltage, welding current, flashing rate and displacement. A typical program is shown in the Figure 8 (curve I). The initial period of the process takes place at CF mode with the subsequent PF. The welding current during transition to PF is almost 3 times increased, the rate of flashing remains at a con-

stant level, and the energy input is determined by the duration of flashing process.

While using PF process it appears to be possible to produce high-quality joints 2–3 times reducing the energy input as compared to conventional welding modes accepted during CF and with resistance heating, at the same time there is no danger of DS arising. For example, in welding the rails of steel K76F using PF the quality joints were produced at welding duration of 30–40 s (see Figure 4, curve *5*). The values of tests on bending meet the requirements of Technical Specifications (see Table 2, mode 4), and in the fractures of joints no defects were revealed. On the basis of the carried out investigations the optimum levels of energy input were identified for each of the mentioned rail steels, providing the highest values of strength and ductility.

Curve *4* in Figure 4 shows the optimum distribution of temperature in welding zone of rail of steel K76F, which provided the highest values of mechanical properties during tests of welded rails on static bending (see Table 2, mode 5). From the comparison of macrosection structure in Figure 7 it is seen that the total width of HAZ in welding using PF is twice smaller than that using conventional CF welding technology. The values of mechanical tests on static bending exceed the standard values specified by the Technical Specifications both on fracture load as well as on bending deflection.

In the industrial conditions the accurate reproduction of optimum heating modes at the rigidly preset programs of changing the basic parameters is rather problematic. Throughout the investigations carried out in the laboratory and industrial conditions, the main factors were established influencing the stability of reproduction of the preset heating modes and sustainable flashing. In particular, the influence of accuracy of rail edge preparation before welding and also
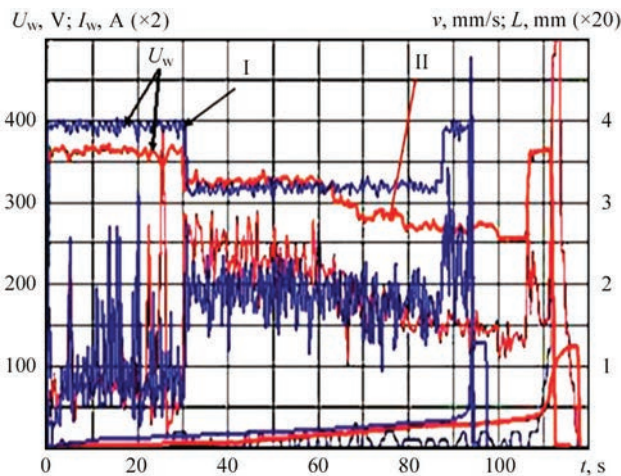
Figure 8. Record of the basic parameters of PF process

voltage fluctuations in the electric mains of the power source on heating stability was found. Inaccurate cutting (more than ±1 mm) as well as voltage fluctuations in the mains result in unstable heating.

To eliminate these difficulties the improvement of technology was performed on both directions. The investigations were carried out to determine the influence of different factors on the accuracy of energy input, and their acceptable deviations in the process of production were established. At the same time, the development of automatic control systems of heating and flashing process was carried out, which allow correcting the heating program in a way to provide a constant energy input. The areas were determined (see Figure 4) characterizing heating at the maximum allowable changes in energy input, at which the required mechanical properties of welded joints are provided according to the standards.

Technologies for FBW of high-strength rails of steel K76F, 76F, VS-350Ya and R350HT. On the basis of the developed technologies, the programs for changing the main parameters were accepted, approved in welding the rails of steel K76F under the production conditions. The main values accepted for each type of rails and welding modes (see Figure 4) are based on the developed programs and are characterized by duration of heating process, gradient of the temperature field and, respectively, energy input, as well as necessary upsetting force. The value of voltage, average consumed power, shortening of parts in welding are supported by the systems of automatic control at a constant level. The limits of permissible deviations for given values of energy input differ greatly. For the rails of steel 76F more rigid limitations of energy input are established than for other batches of the investigated high-strength rails. It is caused by a high content of non-metallic inclusions in the rails of «Evraz» Metallurgical Works, RF. In microstructure of joints of all the investigated batches, welded at optimal modes (see Figure 3), the overall HAZ is 2 times smaller than it is accepted in CF welding. In the welding zone of rails of all the batches the increase in hardness with some decrease along the boundaries of the zone and in the center was observed (Figure 9). It is caused by change in the metal structure in the tempering zone at the boundaries of HAZ and decrease in carbon content in the plane of the joints. The width of these areas is negligible and does not influence the wear resistance of the surface of the rail rolling head.

In the areas with increased hardness the sorbite structure is observed. In general, the change in hardness is occurred in the ranges admissible for the mentioned rails, and while carrying out comprehensive
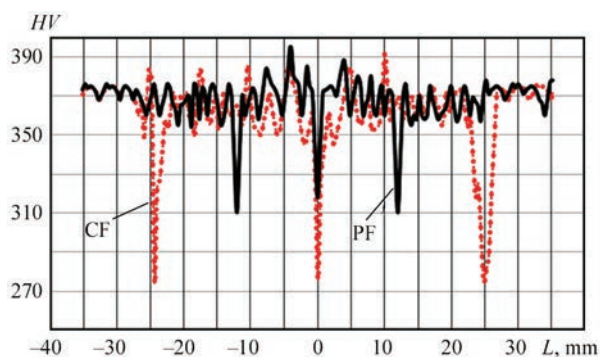
Figure 9. Distribution of hardness on rolling surface of R65 rail butt produced using CF and PF

metallographic examinations the martensitic structures in HAZ were not found.

The reference batches of the welded rails passed comprehensive tests. During checking using destructive and non-destructive testing methods in all the reference batches the defects were not revealed. The results of reference batches tests on static bending according to the international principles (see Table 2) meet the standards in Ukraine and the EU. It is necessary to consider that all the welded joints were not subjected to postweld heat treatment.

Self-adjustment system for automatic control of the FBW process of high-strength rails using pulsed flashing. The same as in CF, in PF the program of the main parameters of flashing process is preset determining its stability and preset energy input in welding, they include voltage and current in welding circuit, flashing rate, voltage value, force developed by the drive of welding machines and amount of deformation during upsetting. The programs are automatically corrected using feedbacks. The developed algorithms for control of the parameters envisage their correlation with the change of open-circuit voltage in the electrical mains, as well as short-circuit of welding circuit of the machine during welding process.

In typical recording of parameters in welding rails of type R65 of steel K76F under the industrial conditions at one of the rail welding enterprises of Ukraine curve I (see Figure 8) corresponds to welding at the optimal modes, curve II was registered when the mains voltage decreased by 50 V, that could significantly influence the quality of the joints, if the program would not be adjusted in welding process.

Due to the presence of feedbacks in the system, the program changed so that the energy input remained constant. The automatic correction of the preset program occurs also at the change of other parameters of the process, for example, increasing the short-circuit resistance of welding machine as a result of overheating or unsatisfactory state of the secondary circuit, as

well as unsatisfactory cleaning of the surface of the rails to be welded. Naturally, the capabilities of the automatic system for control of the parameters are not unlimited and can not prevent grave violations of the accepted service conditions of the equipment. It allows extending the range of permissible deviations and providing a high reproducibility of the preset welding programs. At the same time, an additional possibility appears to control the quality of the joints according to the analysis of changes of all the mentioned parameters in welding process.

For each welded butt of the rails the computer system for control of welding machine issues a certificate, where both in text as well as in graphical form the change of basic parameters is registered, as well as their actual deviations from the preset optimum values. The control algorithms were developed, basing on which the system provides quality evaluation of welded butt in real time. The inspection results are provided immediately after welding on the display of the welding machine for information of the operator and at the same time are transmitted via e-mail to the diagnostic center, where a more thorough analysis is produced, taking into account the results of non-destructive testing and reference tests of specimens.

The results of operational control in the form of exchangeable report are introduced as a regulating document in the approved Technical Specifications for welding performance and are successfully applied at all rail-welding plants of Company «Ukrzaliznytsya». Together with the Diagnostic Center of «Ukrzaliznytsya» the unified system is created performing remote monitoring of rail joints quality not only in the stationary but also in the field conditions, where today the main volume of welding works is transferred.

PWI together with the Diagnostic Center processed a large volume of information (several tens of thousands of butts) on the quality of welding the joints of high-strength rails and related information on the state of welding equipment. On the basis of this information, the algorithms of evaluation of quality of welded joints during in-process control were specified. The proposals on maintenance of welding equipment and its preventive inspection were introduced.

Welding of rails with tension. During construction and repair of continuous tracks [9, 10], the problem of stabilization of temperature and stressed state of the track arises. In the majority of middle latitudes the temperature range is 90 °C. The level of stresses in rails varies in the temperature range from +50 to –40 °C. It is reduced due to the more rigid fixing of rails on the sleepers, which requires the complex of measures on tightening the base of the track, and the periodic unloading of stress in the rails is carried due

to the change of rails-inserts of the appropriate length twice a year (in spring and autumn). The similar problem of unloading arises when it is necessary to repair track, when instead of a section, cut out with a defect, a new rail section is inserted which is welded to the section in two joints in points *A* and *B* (Figure 10).

In accordance with the standard documents in Ukraine and other countries for welding in the main tracks only FBW is allowed, providing the real uniform strength with the base metal, as well as according to the values of fatigue strength. In FBW the rails are shortened, and the allowance for flashing is preset by the program. Therefore, to obtain the required allowance for welding of two butts, the welded-in rail is bent in the horizontal or vertical plane to the value which provides the required allowance for welding. The drive of the machine should provide a high accuracy of shortening the rails at the final stage of upsetting.

This technology is used in repair of tracks at the railroads of Ukraine and other countries, that found reflection in the standard documents. In the course of performance of these operations a proposal appeared to carry out welding without bending of the welded-in rail and to obtain the necessary allowance for welding due to tension of both welded sections 2 and 3 (see Figure 10).

When using PF welding technology the allowance for welding is almost twice reduced as compared to the technologies accepted for welding rail in the track. This facilitates solving the task of using allowance during flashing as a parameter for control of tension of sections during welding of closing butts. The new parameters are added to the welding program, defining the movement during flashing, which determine the force and tightness value. As a result the general control algorithm was determined taking into account the conditions of works performance (temperature of laying of continuous track and environment in welding) and, respectively, the necessary parameters of tension. At the same time, the welder-operator introduces only the data on difference in temperature, at which welding is carried out. All the following operations, ending by flash removal, are performed automatically. After welding in the welded sections of rails on the repaired area the required temperature and stressed state are restored.

In the development of FBW technology of rails with tension a more radical technology for renovation of railway tracks was developed, providing their complete renovation. In laying the infinite continuous track the welding of sections of up to 1000 m is performed with tension, creating the permanent tensile stresses in them. Their value is calculated from the
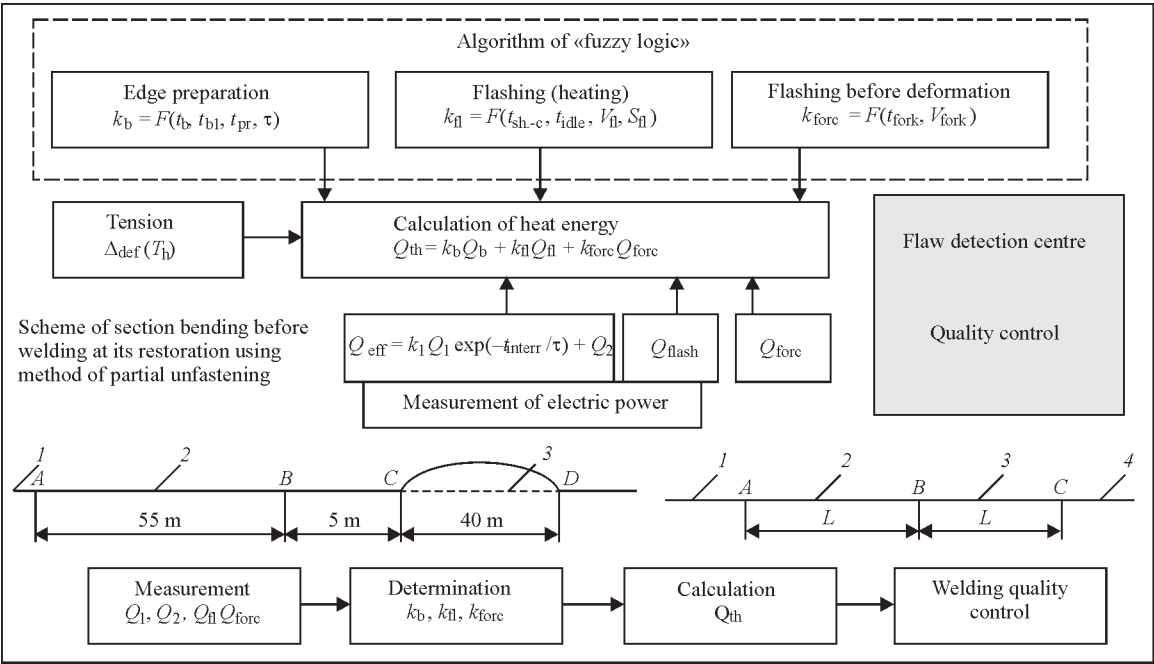
Figure 10. System of automatic multifactor control of welding process parameters in FBW of high-strength rails of steel K76F

condition that during changing the temperature in the range from –5 to 30 °C only tensile stresses will be maintained in the section, the value of which does not exceed 10–15 MPa (for middle latitudes). Such a technology using the welding equipment, designed at PWI (for the first time involving the PWI specialists), was applied by the American «Norfolk Southern Corporation». In the recent years at the railroads of this company the continuous tracks of length of several hundred kilometers (from station to station) are welded.

New generation of equipment for FBW of high-strength rails. To carry out the developed technology for welding high-strength rails, at the PWI a new generation of rail welding machines was developed, the technical characteristics of which are given in Table 3. The serial production of such PWI-developed

equipment is performed by Kakhovka Plant of Electric Welding Equipment. The welding machines are used in the stationary and field conditions. Despite the differences in the design of mechanical components of the machines, they have common elements of automatic control of welding process, energy input, control systems and automatic control algorithms. All these new developments allow fully realizing the advantage of PF welding technology.

They use automatic systems for PF control based on application of high-speed hydraulic drives, adaptive electric systems for control of fast running electric processes. Their development and application allowed largely eliminating the unfavorable change of service conditions on the reproduction stability of preset welding modes. All the machines apply systems for automatic operation control of joints quality

Table 3. Technical characteristics of PWI-developed rail-welding machines

Parameter	Type of machine					
	K355A-1	K900A-1	K920-1	K921	K922-1	K922-2
Rated primary current (duty cycle = 50 %), A	395	395	540	540	540	540
Rated power (duty cycle = 50 %), kV·A	150	170	210	210	210	210
Transmission factor	60	60	54	54	54	54
Rated upsetting force, kN (kgf)	450 (45,000)	500 (50,000)	1000 (100,000)	1500 (150,000)	1200 (120,000)	1200 (120,000)
Rated clamping force, kN (kgf)	1250 (125,000)	1200 (120,000)	2500 (250,000)	3750 (375,000)	2900 (290,000)	2900 (290,000)
Rate of upsetting at idle operation, mm/s, not less than	20	25	35	35	40	50
Machine travel, mm	70	70	90	150	100	150
Mass of welding head, kg, not more than	2375	2500	2900	4200	3450	3500
Mass of delivery set, kg, not more than	4000	4100	4500	6000	5150	5100
Dimensions ($W \times H \times L$), mm	810×1059××1140	1030×1140××1550	1060×1195××1600	1190×1400××2430	1060×1300××1895	1060×1300××2050

11
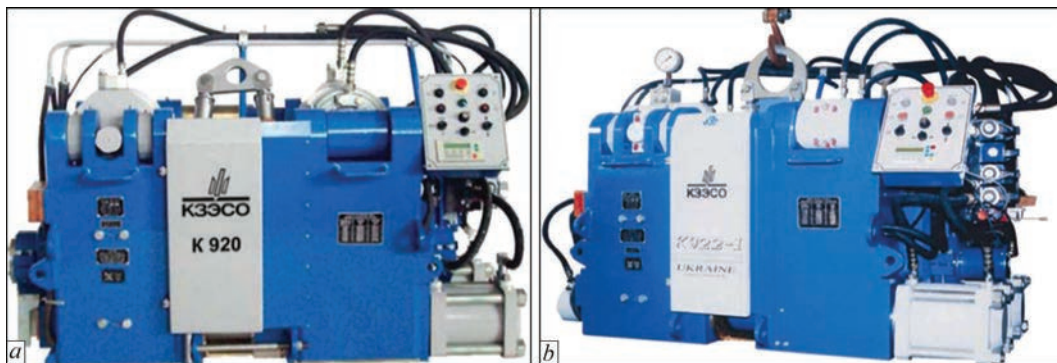
Figure 11. Mobile machines K920 (*a*) and K922-1 (*b*) for welding high-strength rails

on the basis of the recorded deviations from the preset values. The algorithms for quality evaluation in the function of these deviations and their introduction in a common electronic form to the general system in real time were determined.

The new machines (Figure 11) provide the upsetting force 2–2.5 times higher than the values of machines of the previous generation (K355, K900). It allows using PF modes for welding high-strength rails of different manufacturers. In addition, the opportunities for application of technologies of welding with tension were significantly expanded. The hydraulic drive of the machines allows developing force of up to 150 t and tightening the rail sections to distance of 300 mm to perform auxiliary operations during operation with long-length sections.

Conclusions

In welding of all the investigated batches of high-strength rails the required values of mechanical properties of welded joints were obtained at welding modes characterized by a low energy input which is 1.5–2 times lower than in welding of rails of previous generations.

The PF welding technology was developed providing a highly concentrated heating and formation of quality joints of high-strength rails of different production.

The system of multifactor control of flashing process parameters was developed and approbated in the industrial conditions, providing a stable reproduction of the preset energy input in welding of rails of different composition. The admissible limits of deviations from the preset value were determined.

The system of in-process quality control of welded rails was developed and tested under the industrial conditions.

The comprehensive tests of welded joints of different categories of high-strength rails were carried out. According to the basic values, the welded joints meet the requirements of different international standards.

The technology for welding of high-strength rails with tension was developed, providing the optimum level of internal stresses in continuous track during welding process.

A new generation of machines was developed for FBW of high-strength rails in the stationary and field conditions. The manufacture of such machines was mastered by Kakhovka Plant of Electric Welding Equipment (Ukraine).

1. Genkin, I.Z. (1951) Electric resistance welding of rails: Technical reference book of railroader, Vol. 5, 378–390.
2. Kuchuk-Yatsenko, S.I., Lebedev, V.Kh. (1976) *Continuous flash-butt welding*. Kiev: Naukova Dumka.
3. *TU U 27.1-40081293-002:2016*: New welded rails for railroads. Dniptopetrovsk: Ukrzaliznytsya.
4. Genkin, I.Z. (2003) *Welded rails and switches*. Moscow: Intekst.
5. Dotsenko, V.E. (1949) *Resistance welding of rails*. Moscow: Mashgiz.
6. Genkin, I.Z. (1973) Studies, welding experience and service of case-hardened rails. In: *Technology of manufacturing of railroad rails*, 132–136. Kharkov: UkrNIIMet.
7. Kuchuk-Yatsenko, S.I., Khryashcheva, N.K., Shlyapin, V.B. et al. (1973) Continuous flash-butt welding process. *Put i Put. Khozyajstvo*, **2**, 9–10.
8. Kuchuk-Yatsenko, S.I., Krivenko, V.G., Bogorsky, M.V. (1977) Intensification of heating of rails in pulsed flash-butt welding. *Avtomatich. Svarka*, **4**, 45–50.
9. Danilenko, E.I., Karpov, M.I., Kostyuk, M.D. et al. (2002) *Technical recommendations on arrangement, laying, repair and maintenance of continuous rail track on railroads of Ukraine*. Kyiv: Transport Ukrainy.
10. Tokareva, A.E., Vinogorov, N.P. (2002) Repair of defective lengths. *Put i Put. Khozyajstvo*, **4**, 121–141.

STATISTICAL CONTROL OF PROCESS OF FLASH-BUTT WELDING OF RAILS. TWO-LEVEL CONTROL SYSTEM

S.I. KUCHUK-YATSENKO, P.M. RUDENKO, V.S. GAVRISH, A.V. DIDKOVSKY and **E.V. ANTIPIN**

E.O. Paton Electric Welding Institute, NASU

11 Kazimir Malevich Str., 03680, Kiev, Ukraine. E-mail: office@paton.kiev.ua

The article deals with the modern approach to creation of system for control of process of flash-butt welding of rails based on statistical analysis of data collection, characterizing this process. In the received data such an analysis allows detecting a number of previously unknown and useful knowledge interpretations (knowledge discovery in databases), required for making decision on the process control. The analysis of causes was carried out which may lead to deviations in the course of technological process and, as a consequence, to violation of the quality of welded butts. To detect these disturbances, two-level control system was proposed. At the lower level in the system of direct digital control the traditional quality control of welded joints is used for «instantaneous» response to the occurrence of rejection and prevention of its further spreading. At the upper level (at the diagnostic center of Company «Ukrzaliznytsya») the statistical processing of welding rails protocols is carried out to detect disturbances which are difficult to control by direct measurements. The developed algorithms passed an experimental verification and can be recommended for their further introduction into industry. 5 Ref., 1 Table, 4 Figures.

K e y w o r d s : *flash-butt welding, two-level control system, control of process parameters, statistical control, technical state of equipment, allowance control*

The modern control systems of the FBW process of rails, installed in all the PWI-designed welding machines of new generation, allow measuring and calculating the basic parameters of the process, which allow judging about the quality of welded butt with a certain degree of validity. These data in the form of a protocol of welding butt are actually its certificate. The obtained protocols are stored within the whole period of operation of welded joints in the railroad track and form the significant arrays of information, which, except of the acceptance certificate of the product for operation, can be used to reveal disturbances influencing the welding process, but are not subjected to the methods of direct measurement. The similar methods of information processing, so-called data mining, the intellectual data analysis, profound data analysis are used for detection of previously unknown, non-trivial, practically useful and accessible interpretations of knowledge in the data required for making decision in different areas of human activity.

The use of the well-known methods of statistical processing of information by butts, collected during the certain time periods in one and the same machines, the complex of machines of a one rail welding enterprise (RWE) or a branch as a whole, allow optimizing the operating conditions of welding machines and the control of welded rails production in general.

For this aim at the PWI the two-level system was developed. On the lower level in the system of direct digital control the traditional quality control of welded joints for «instantaneous» response in real-time to the occurrence of rejection is used to prevent its further spreading.

Further, the information on welded butts is transferred from the welding machines of RWE to the upper level — diagnostic center. At the diagnostic center the statistical processing of rail welding protocols is carried out to detect disturbances which are difficult to control by direct measurements. For example, unsatisfactory performance of auxiliary operations on preparation of rails before welding, deviation of physical and chemical properties of rails metal, unsatisfactory observing of technological operations by service personnel or unsatisfactory industrial conditions (Figure 1).

Taking into account the capabilities of existing local systems for process control, the developed system, except of direct digital control of welding process, performs the following functions:

● prediction of quality of welded butt according to the process parameters using more advanced algorithms with the possibility of involvement of qualified specialists for prediction in special cases;
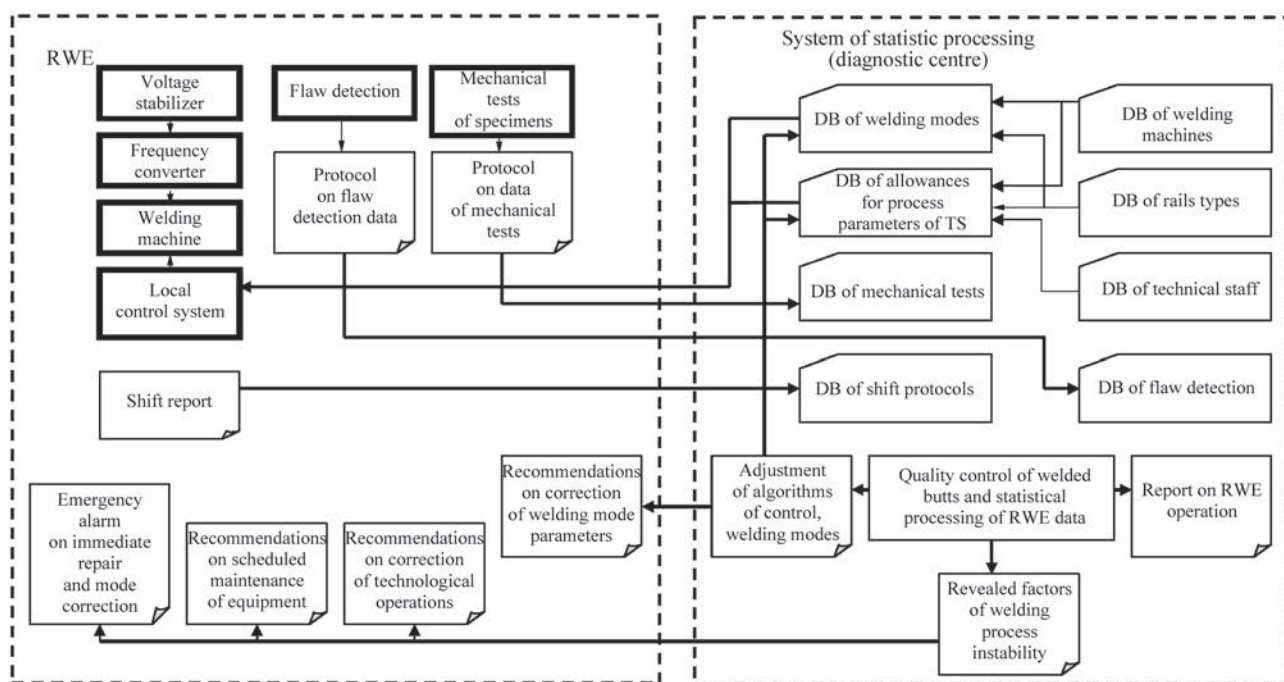
Figure 1. Block diagram of two-level control system

● control of technical state of welding equipment, elaboration of recommendations and planning of its maintenance;

● detection and recognition of emergency situations for immediate intervention into the technological process;

● detection of systematic deviations and trends of process parameters, which may result in deterioration of the quality values of welded joints, elaboration of recommendations on correction of welding parameters.

For FBW of rails in the stationary and mobile welding machines the following causes can be distinguished, which may result in deviations in the course of technological process and, as a consequence, violation of welded butts quality [1–3]:

● unsatisfactory performance of auxiliary operations on preparation of rails before welding: edges preparation, cleaning the rails surface at the places of current supply and postweld treatment of butts — machining of rails surface during flash removal;

● deterioration of technical state of welding equipment, for example, increase in welding circuit resistance of the machine;

● defects in the base metal of rail steel;

● unsatisfactory keeping the technological operations by welder (poor cleaning and alignment of rails before welding);

● unsatisfactory industrial conditions: inadmissible changes of ambient temperature and mains voltage;

● unfavorable combination of process parameters, even when these parameters are in the range of al-lowances, for example, decrease in mains voltage and increase in welding circuit resistance of the machine.

To detect the described disturbances the algorithm of statistical processing of the data of the process parameters was developed, at which the arrays of protocols of welding butts are processed with their separation and grouping according to the relevant characteristics (the Table).

During welding process the following information is formed in real time (Figure 2):

1. In welding of butts according to the measured values of parameters of the welding process x_1–x_{12} using the control algorithm based on «fuzzy» logic [4] the quality value of welded joint, i.e. the probability of its compliance with the requirements of the Technical Specifications, is calculated. The obtained data are formed in the arrays according to the number of machine, surname of welder, serviceman, flaw detection engineer and the team on performance of auxiliary operations (preparation of rails before welding and postweld treatment of butts), by correction of welding mode for displacement of distribution of random values of the mentioned measurements to the center of the allowance interval.

2. According to the data of ultrasonic flaw detection (UFD) the presence of cracks, lacks of penetration, dull spots, etc. is checked in each welded butt, these data are recorded in the UFD databases. The quality of machining of welded butt after flash removal is also visually checked. The information on the presence of defects is immediately provided to the welder and to the shift serviceman. The defective butt is cut out. The mentioned functions are carried out

Separation of welding butts protocols for detecting different disturbances violating the technological process

Cause for arising violation in the technological process for welding rails	Identification parameter	Sampling volume	Parameter of arrays separation	Influence parameter
Auxiliary operations on preparation of rails before welding and postweld butt treatment	$Z_{sh.-c}$, visual data on postweld butts machining	1–2 shifts	Full name of shift serviceman + RWE	Methods and equipment
Technical state of welding equipment	T_w, U_h, U_l, V_{flash}, v_{forc}, V_{ups}, S_{tot}, S_{ups}, $Z_{sh.-c}$	1/3–1 month	Number of welding machine	Maintenance, repair
Physical and chemical properties of rails metal	L_b, F_{fr}, data on flaw detection	Immediately during detection or 1 shift	Number of batch, rails grade, Number of machine	Mode correction
Technological operations of welder	T_w, T between welding and flashing of obliquity, $Z_{sh.-c}$, slipping	Immediately during detection or 1 shift	Full name of welder	Methods (industrial instructions)
Control of the process of welding specimens and UFD	L_b, F_{fr}, UFD data	1 shift	Full name of welder, UFD engineer	Methods and equipment
Industrial conditions	U_h, U_l, v_{flash}, v_{forc}, v_{ups}	1–2 months	RWE	Stabilization of U_{ains} or T_{oil}
Unfavorable combination of process parameters	Fuzzy algorithm of control and monitoring	Immediately during detection or 1 shift	Number of rail section	Correction of welding mode

beyond the control system, the entry of UFD data is carried out manually.

3. At the beginning, in the middle and the end of the shift the welding of rail specimens and mechanical tests are carried out. The tests data, namely bending deflection L_b and fracture force F_{fr} are compared with the preset values. If the obtained values are lower than the preset ones, the welding and testing of additional specimens is carried out to detect the reliability of inadmissible deviation. During confirmation of inadmissible deviation of the process the correction of welding mode is carried out. The obtained data are used to adjust the model of welding quality control. The mentioned functions are carried out beyond the control system, the entry of the results of mechanical tests of specimens is carried out manually.

Beyond the time of technological process the following information is formed:

4. To control the technical state of welding machine, the data on sections of one and the same grade of rails welded in one and the same machine are unified in the protocol of technical state of welding machine. The time of response, and thus, the average time can be significant: from one to several shifts. It is obvious that in case of emergency situation the information on repair is supplied immediately.

5. To control the industrial conditions the statistical evaluations of welding at one and the same modes and in one and the same type of machine of each RWE are combined. According to voltage U_f and Uh the stability of power mains and according to the speeds v_{flash}, v_{forc} and v_{ups} the stable operation of hydraulic drive are determined, which, in its turn, is connected with the temperature of the environment and its influence on

the properties of hydraulic system fluid. The comparison of these evaluations at different RWE can serve as a basis for taking measures to improve the industrial conditions.

6. To specify the allowances for the control of the process the statistical data for all RWE are unified for each grade of rails and the corresponding welding mode.
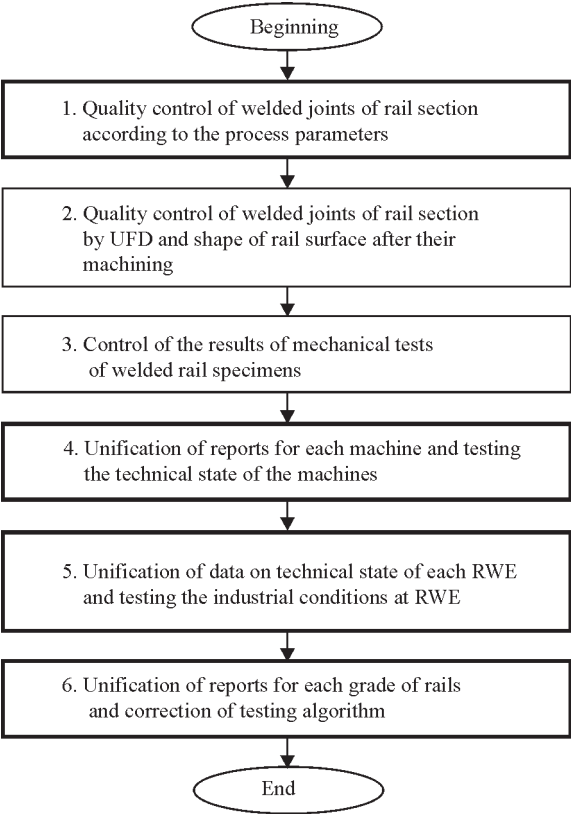
Figure 2. Algorithm for the rail welding process monitoring (operations are distinguished which are automated in the computer control system)
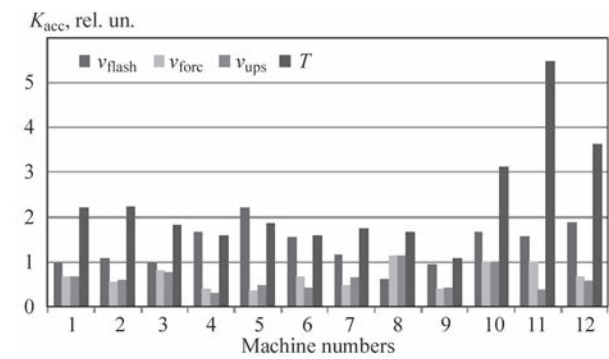
Figure 3. Coefficients of accuracy K_{acc} of parameters grouped according to machines

Figure 4. Coefficients of accuracy K_{acc} of parameters grouped according to RWE

In the statistical analysis the distribution of random values of welding process parameters were evaluated according to their average value and the mean square deviation. For easy comparison of different parameters these values were further considered in the relative units in the form of so-called coefficients of accuracy K_{acc} and adjustment K_{adj} [5]:

$$K_{acc} = 6S_{msd} / \delta; \quad K_{adj} = (X_{av} - X_0) / \delta,$$

where S_{msd}, X_{av} is the mean square deviation and the average value of distribution of values of the welding process parameter; δ is the parameter allowance; X_0 is the middle of the tolerance field or the preset parameter value.

For analysis of deviations it is necessary to take into account that some controlled parameters (e.g. S_{flash}, U_1, U_2, U_3, L_{ups}, P_{ups}, T_{ups1}) are preset by direct method in the control system, and the errors in their reproduction are related to the accuracy of operation of the equipment and, in particular, of the control system.

At the same time, the other parameters (v_{flash}, T_w, v_{forc}, v_{ups}) are preset indirectly. The errors of reproduction of these parameters are connected both with the condition of welding equipment as well as with the coarse of the technological process.

As an example of system operation, let us consider the data on the accuracy coefficient for 12 welding machines of 4 RWE of the branch at number of welded butts of about 30,000.

According to the indirectly preset parameters (Figure 3) it is seen that 3 machines (10, 11 and 12) have a sharp difference in the data on time of welding. These machines belong to one RWE, and it was natural to suggest some general deviation in the process charac-

teristic to this RWE. The additional analysis directly at the enterprise revealed differences in the technology of rails edges preparation before welding as compared to other RWE.

The data on the accuracy coefficient for the parameters, grouped by RWE, revealed that the hydraulic pump stations at different RWE (P_{ups} parameter) differ greatly as to their technical state and require additional checking (Figure 4).

It is obvious that except of the technical problems the described algorithm affects organizational problems of the whole production of welded tracks and should be not only specified as to experimental operation of the control system, but first of all agreed with the management of track facilities service.

Conclusions

The two-level control system was developed and the statistical processing of results of allowance control of quality of rail butts welded during the recent years at the enterprises of «Ukrzaliznytsya» was performed. The obtained results revealed new opportunities for improvement of the quality stability of welded joints.

1. Kuchuk-Yatsenko, S.I. (2008) *Influence of structure heredity of low-alloy and carbon steels on weldability in solid phase*, Vol. 1, 148–165. Kiev: Akademperiodika.
2. Gudkov, A.V., Nikolin, A.I. (2012) Specifics of welding of modern rails. *Put i Put. Khozyajstvo*, **4**, 9–13.
3. (2011*) Improvement of efficiency and reliability of rails*: Transact. of VNIIZhT. Ed. by A.Yu. Abdurashitov. Moskow: Intekst.
4. Kruglov, V.V., Dli, M.I. (2002) *Intelligent information systems: Computer support of fuzzy logic and inference*. Moscow: Fizmatlit.
5. *R 60-601-20–91:* Recommendations on assessment of accuracy and stability of technological processes (equipment). Moscow: VNIIS Gosst. Rossii.

TECHNOLOGY AND EQUIPMENT
FOR RESISTANCE BUTT WELDING
OF LARGE-SECTION PARTS OF DISSIMILAR STEELS

S.I. KUCHUK-YATSENKO, A.A. NAKONECHNY,
I.V. ZYAKHOR, S.V. CHERNOBAJ and **M.S. ZAVERTANNY**
E.O. Paton Electric Welding Institute, NASU
11 Kazimir Malevich Str., 03680, Kiev, Ukraine. E-mail: office@paton.kiev.ua

The resistance butt welding finds new areas of application. The aim of the work is the development of technology for RBW of T-joints of rods and eyelets of hydraulic cylinders of dissimilar steels 45 and 17GS in the range of diameters from 16 to 60 mm. The tasks of investigations were the selection of optimal technological scheme of RBW process of large cross-section parts, testing of technological methods, providing localization of heating and deformation of metal in the contact zone. The RBW process and the structure of joints of these dissimilar steels produced with preliminary preparation of welded edges and using the composite inserts were investigated. It was found that in RBW of T-joints of steels 45 and 17GS with optimum preparation of welded edges and programmable change in welding force at the stage of heating it is succeeded to localize the heat generation in welding zone, to avoid the formation of defects and to provide the high mechanical properties of welded joints. During mechanical tests of welded rods on bending the fracture occurs in the base metal of the rod. The technology for RBW of T-joints of dissimilar steels using the composite inserts was developed. The technology of RBW of rods of hydraulic cylinders of 16–60 mm diameter was realized in specialized welding machine K1040, designed and manufactured at the PWI. 14 Ref., 15 Figures.

K e y w o r d s : resistance butt welding, T-joint, hydraulic cylinder rod, dissimilar steels, welded joint, preparation of edges, composite insert

For the domestic machine building the actual problem is the development and implementation of an effective high-performance technology for welding the rods of hydraulic cylinders. The billets of a rod of high-strength steel 45 of 16–60 mm diameter should be joined with the eyelets of steel 17GS of 20–200 mm diameter with wall thickness of 5–24 mm. A significant volume of production of welded rods of hydraulic cylinders causes a necessity of applying the high-performance technology and equipment providing operations on clamping, alignment, welding, as well as, in some cases, heat treatment of products in automatic or semi-automatic mode.

At the present time in different fields of industry the high-performance methods of pressure welding are used, in particular, friction welding and resistance butt welding. Friction welding meets the majority of the abovementioned requirements, but a rather high cost of the modern equipment is a limiting factor in its use in the domestic machine building.

The carried out analysis showed that from the standpoint of technical and economic efficiency of solving the problem of welding rods of hydraulic cylinders, the application of RBW is the most appropriate. This method is widely used in the industry for dissimilar joint of metal cutting tool, band saws, wires, bars, tubes of steel and non-ferrous metals [1–3]. The RBW found a wide spreading due to a high performance, hygiene of the process, acceptable cost of the equipment necessary for its realization. In welding of high-strength aluminum alloys [4], advanced structural materials, in particular alloys based on titanium aluminides [5, 6] and powder materials [7] the RBW using the intermediate layers is challenging.

However, for the traditional RBW technology some disadvantages are inherent, in particular, decrease in mechanical properties of the joints, especially ductility values [1, 8] which is connected with overheating of metal, formation of coarse-grained structure in the joint area and defects in the form of oxide films and microcracks. To a large extent it is revealed in welding of large-section parts. The problem of providing a stable high quality of welded joints during RBW of large-section products of high-strength steels is relevant over many years.

The aim of the work is the development of technology for RBW of T-joints of rods and eyelets of hydraulic cylinders of dissimilar steels 45 and 17GS in the range of diameters from 16 mm to 60 mm.

The rods of hydraulic cylinders are manufactured of carbon steel 45 which has the following values in as-delivered state: σ_t = 590 MPa, *HB* 2100 MPa, the
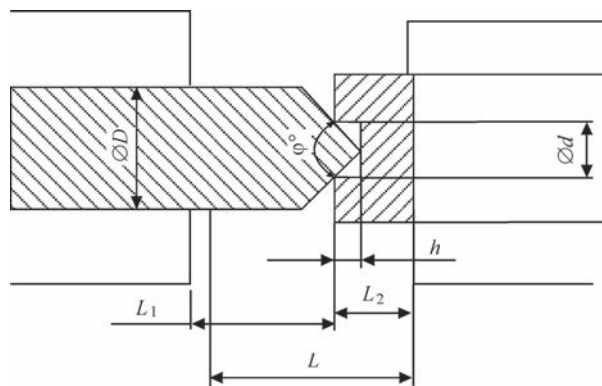
Figure 1. Scheme of preliminary preparation of edges of rod and eyelets for RBW

surface of the rod is coated with chromium of 0.15 mm thickness. The eyelet is manufactured by grinding of steel 17GS, in as-delivered state it has $\sigma_t = 510$ MPa and *HB* 1800 MPa.

During the experiments, welding machine K1040 was used, designed and manufactured at the PWI. Machine K1040 provides the realization of RBW process with continuous or step change in welding force in the range from 600 to 7200 kg. The control system of the machine on the basis of KSU KS02 provides automatic cycle of welding and heat treatment, quality control and registration of welding parameters, as well as control of the frequency converter. In RBW of large-section parts the significant loads to electrical mains with a pulsed increase in current prevail. Therefore, three-phase–one-phase converter [9] was used, providing a uniform three-phase loading of mains.

The initial requirements during the development of technology for RBW of T-joints of rods of hydraulic cylinders were providing the formation of defect-free joints with mechanical properties being at the level of the base metal values, keeping the preset allowances
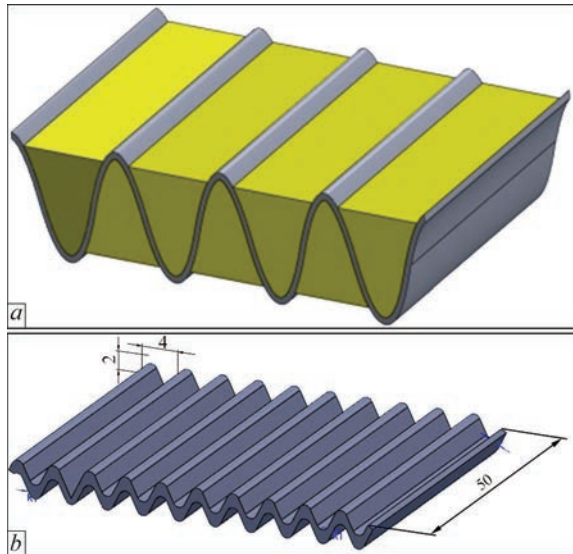
Figure 2. Scheme of CI with activating flux (*a*) and metallic profiled insert (*b*)

for dimensions of the product. It is known that a high quality of joints during RBW is provided at high current densities, minimum heating period, current and pressure cycles (continuous or step), corresponding to a particular section of billets, increased allowances for upsetting [1, 3]. In this case, the formation of a coarse-grained structure is excluded and the removal of contaminants, oxide phases and overheated metal from the welding zone is provided.

For the RBW process of T-joints of dissimilar steels the significant differences in the conditions of heating of part metal volumes adjacent to the butt are typical, which causes the asymmetry of deformation conditions and complicates the ejection of oxide films from the butt and formation of quality joints. Therefore, during development of technology for RBW of rods of hydraulic cylinders the tasks were put to find the ways of localization of processes of heating and deformation of the metal in the contact area and improvement of efficiency of dispersing, dissolving of oxide phases and their ejection from the butt.

While practicing the technology of welding the rods of hydraulic cylinders the following technological schemes were investigated: RBW with preliminary preparation of welded edges — scheme 1 (Figure 1), and RBW using the composite inserts (CI) — scheme 2 [10] (Figures 2 and 3). It was assumed that the preliminary edge preparation and the use of CI would allow expanding the technological capabilities of the process of RBW of large-section billets in producing dissimilar joints of structural steels.

CI (see Figure 2) consists of a metal base and a flux [10] the composition of which is preset so that its melting temperature $T_{melt.f}$ is below the melting temperature of the base metal $T_{melt.BM}$ of parts being welded. The presence of flux allows protecting the metal heated at the contact zone from oxidation and provides quality joints formation in the process of upsetting of parts. Thus, the possibility of producing joints at the heating temperature of metal of near-contact layers below the solidus temperature of the base metal, and to form the joints a lower deformation of ends is required than that in traditional RBW technology.
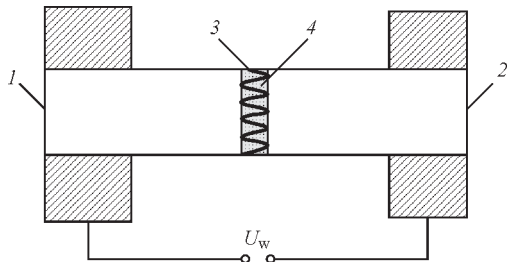
Figure 3. Scheme of RBW process using CI: *1*, *2* — parts; *3* — CI with flux

The base of CI consists of a profiled sheet (Figure 2, *b*), height and pitch of the profile are selected from the calculation of admissible current density and define the intensity of heat generation in the contact. The shape of CI relief influences the intensity of heat generation in the contact area, especially at the initial stage of heating, and the formation of welded joint. The increase in the concentration of heat generation in the contact area is determined by a high current density. The parameters of metal profiled insert were changed in the following range: sheet thickness 0.8–2.0 mm, profile pitch 2–4 mm, and height of peaks was 1–2 mm.

The composition of welding flux is one of the determining factors of RBW technology using CI. The flux protects the welding area from the atmosphere, acts as a heat source in the contact area of parts, cleans the metal surface from oxide films and facilitates the spreading the molten metal over the surface. Moreover, the flux deoxidizes the metal in parts contact and influences crumpling of the profiled insert. To provide a high quality of welded joint, properties of flux should meet the following requirements: react with oxides before the formation of liquid metal phase, wet the metal of parts being welded and the metal of insert, not to cause corrosive effect on the joined parts, not to change its chemical composition during heating due to evaporation of separate components.

In the work the oxide-salt fluxes of $Na_2B_2O_7$–Li_3AlF_6–TiO–KF system and the salt flux of $Na_2B_2O_7$–CaF_2–BaF_2–LiF system were used. The flux was applied in the form of alcohol slurry on the surface of the profiled insert. In the composition of flux as a binder 5 % of nitrovarnishes was added, which prevented shedding of the flux after drying from the profiled insert surface. To form the liquid phase, wetting surfaces of parts being welded and ejection of fluxing remnants from the butt, the depressant elements were included into flux composition, which come into reaction of contact melting with the metal of parts and the profiled insert. In welding of carbon and low-alloy steels these elements are carbon and manganese, which are introduced into the composition of flux in the amount of 15 and 10 %, respectively. This allows producing a liquid metal phase already at 1150 °C.

At the initial stage of the RBW process, welding flux prevents crumpling of the relief of the profiled metal insert. When electric current passes through the butt with CI (see Figure 3), the intensive heating and melting of the insert is observed due to a significant internal resistance. This is accompanied by localization of heating as compared to the traditional method of resistance heating. The value of transition resis-
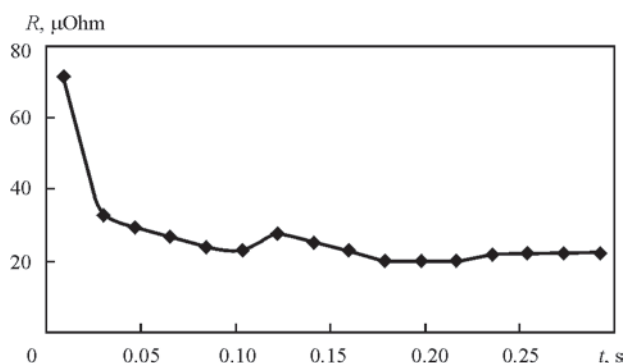
Figure 4. Time change of complete resistance in contact zone during RBW of steels 45 to 17GS specimens with $d = 32$ mm

tance in the contact area then decreases (Figure 4), that is correlated with the data of work [11].

The selection of cyclogram of changes of RBW parameters was carried out on the basis of literature data [1, 3], results of previous investigations of the authors [12] and technical capabilities of welding equipment. In welding machine K1040 the clamping forces are provided by a four-section pneumatic cylinder, that allows realizing the required cyclogram of RBW process by switching the pneumatic valves of each section, controlled by a microprocessor (Figure 5).

The first series of experiments on RBW of rods of hydraulic cylinders of steels 17GS and 45 was carried out with the use of preliminary edge preparation according to scheme 1 (see Figure 1). The parameters of edge preparation were optimized so that the initial contact was near the apex of the cone and the bottom of the groove, and the total allowance for welding was preset depending on the diameter of the billets so that during plastic deformation of billets the remnants of cast metal, oxide films were ejected beyond the welded joint.

The formation of joints during RBW was investigated according to scheme 1. Such a scheme is recommended [13, 14] for welding of T-joints and is called «welding on the sharp edge». The carried out
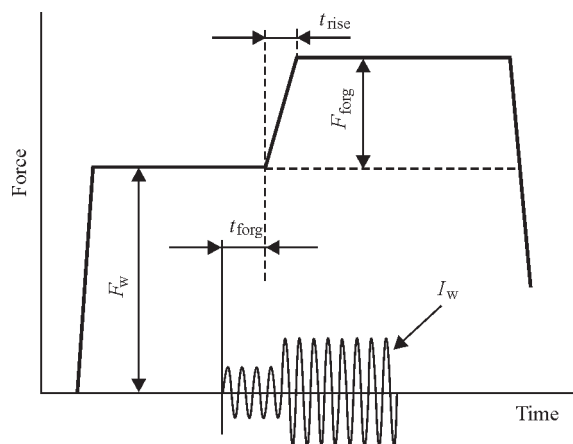
Figure 5. Cyclogram of RBW process with programmable change in welding force
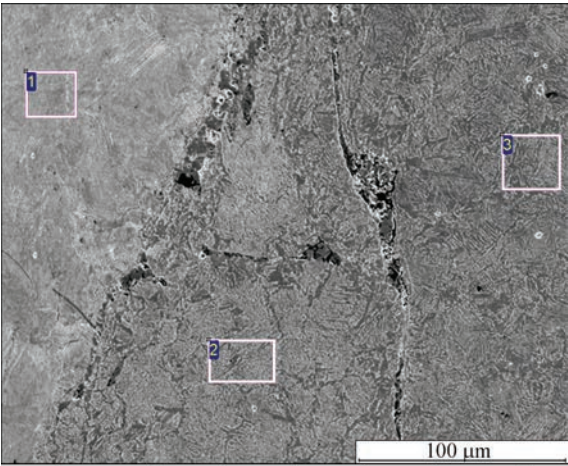
Spectrum	C	O	Si	Mn	Fe
1	2.19	1	0.27	0.73	95.81
2	1.41	0.70	0	1.02	96.87
3	1.47	0.49	0.21	1.43	96.40

Figure 6. Microstructure of steels 45 to 17GS welded joint produced according to scheme 1 in Figure 1 at single-stage cyclogram of force

investigations found that RBW with a single-stage cyclogram of welding force application cannot localize heat generation in the welding area, the remnants of molten metal are found in the butt, and the defects are formed as a result of air pressing-in into the joint (Figure 6). Therefore, the further experiments on RBW were carried out with programmable change in welding force in accordance with the cyclogram presented in Figure 5, and an optimized shape of edge preparation, excluding air pressing-in into the joint zone.

The macrostructure of welded joint of rod with eyelet produced using RBW according to scheme 1 is presented in Figure 7, and the microstructure of metal in different zones of the joint — in Figures 8–10. The optical microscopy and SEM found that in the joining area in different parts of the section, namely central (Figure 8), middle (Figure 9) and peripheral (Figure 10), lacks of penetration, oxide films, cracks
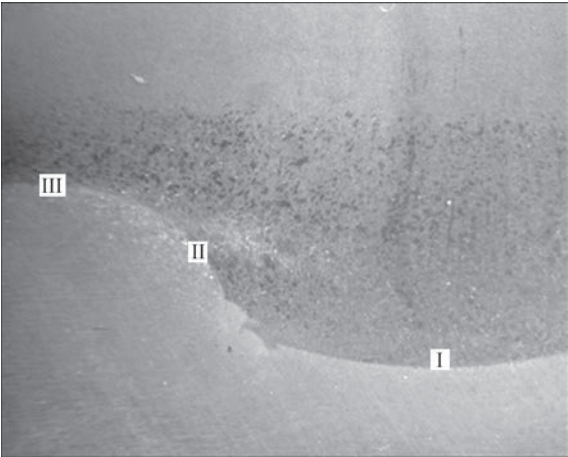
Figure 7. Macrostructure (×4) of steels 45 to 17GS welded joint (for I–III see Figures 8–10, respectively)
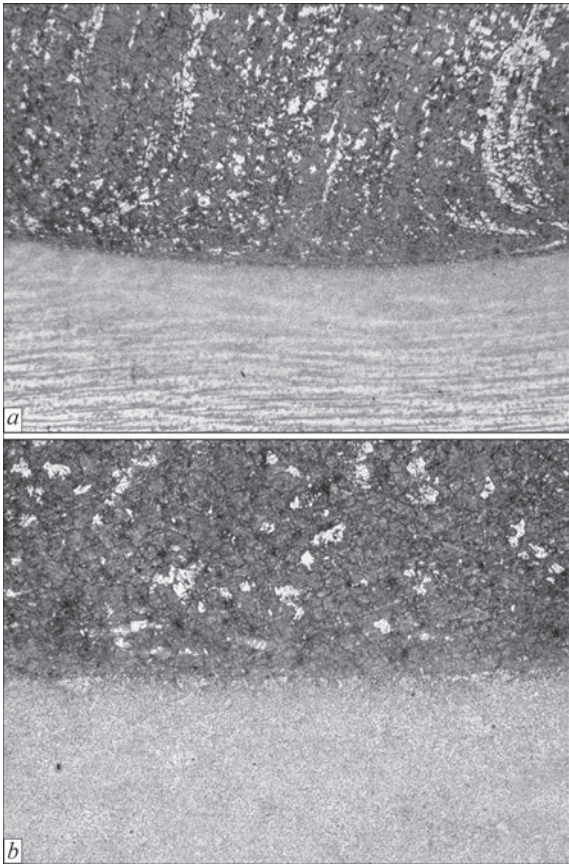
Figure 8. Microstructure of metal of central area I: *a* — ×25; *b* — ×100

caused by the formation of hardening structures are absent. The absence of areas with cast and coarse-grained structure at the boundary, characteristic for overheated metal, evidences that the process of metal solidification in the joining area occurred under the conditions of intense shear deformation during upsetting. The structure in the joint zone and zone of thermomechanical influence is ferrite-pearlite, the areas with martensite structure were not revealed.

It is known that the rate of deformation has a significant influence on the structure and properties of metal of welded billets, namely during its increase a more fine-grained structure is formed in the joining area. This is explained by the fact that solidification process is suppressed by the deformation process, accompanied by refining of grains. Therefore, in the pressure welding methods it is recommended to apply the scheme of comprehensive uneven compression, which allows controlling the volumetric stressed state and character of plastic deformation.

At the developed optimal RBW modes according to scheme 1 the deformation of metal occurs under the conditions of comprehensive non-uniform compression and has a character of viscous flow (the same as during extrusion), which contributes to gripping of welded surfaces, their cleaning from oxide films, «healing» of micro-discontinuities and structural re-

Spectrum	C	O	Si	Mn	Fe
1	0.44	0.95	0.25	0.76	97.80
2	0.32	0.83	0.26	0.98	97.60
3	0.27	0.45	0.23	1.27	97.79
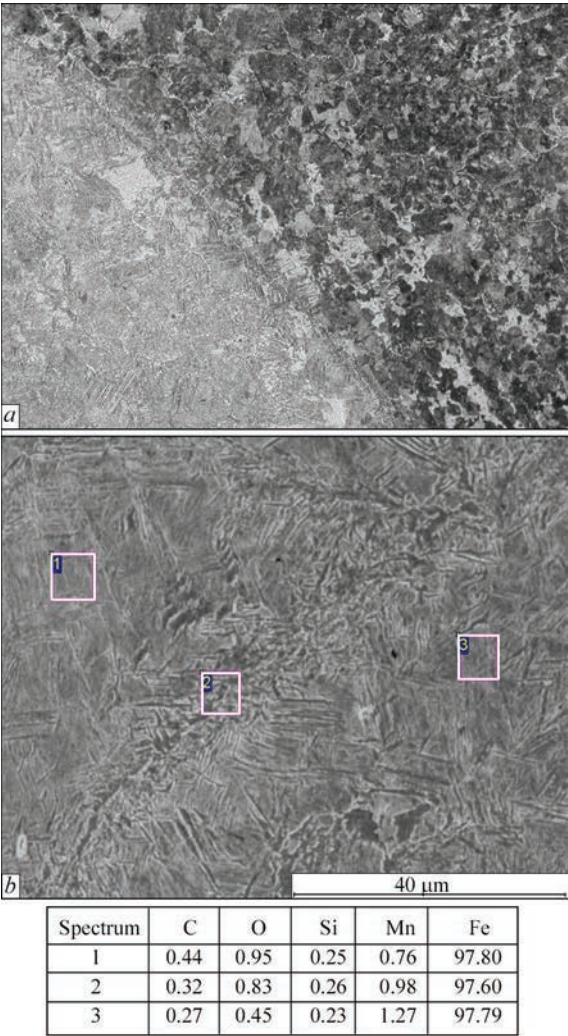
Figure 9. Microstructure of metal of middle area II: *a* — ×100; *b* — SEM

Figure 10. Microstructure of metal of peripheral area III: *a* — ×100; *b* — ×400

finement. At the end of upsetting a large part of metal, heated till switching off the power, is squeezed beyond the welded section, and in the joining area the metal is remained which was not subjected to heating up to high temperatures.

The mechanical tests of welded rods on bending in the welding zone were carried out in hydraulic press with maximum 100 t force. The welded rod was considered qualitative under the conditions of fracture outside the zone of welded joint. Figure 11, *a* presents the welded rod after the tests: localization of fracture occurs along the base metal. Thus, in RBW with optimal preparation of welded edges and programmable change in welding force at the stage of heating it becomes possible to localize heat generation in the welding zone, to avoid defects formation in the joints of rods in the investigated range of diameters and to provide high mechanical characteristics of welded products.

The RB-welded rod produced according to scheme 2 with the use of CI of steel 09G2S with the activating flux is presented in Figure 11, *b*. The microstructure

Figure 11. Rod Sh25 RB-welded according to scheme 1 after tests on bending (*a*), and rod produced according to scheme 2 (*b*) (see Figures 1 and 3, respectively)
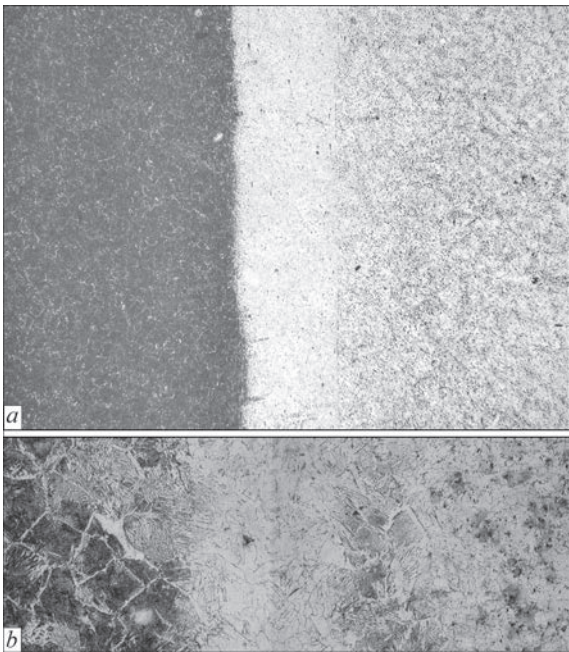
Figure 12. Microstructure of metal in cross-section center in RBW according to scheme 2: *a* — ×50; *b* — ×200

of metal in different zones of the joint is presented in Figures 12 and 13, the distribution of microhardness of metal in the joining area — in Figure 14. During metallographic examinations in the joining area none of the defects (cracks, lacks of penetration, pores, oxide films, remnants of flux) are detected. In order to prevent the formation of hardening structures while
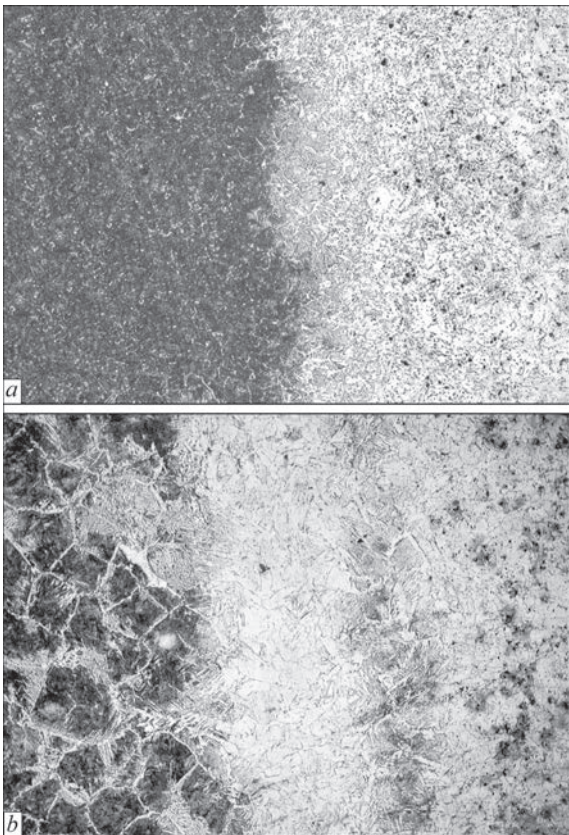
Figure 13. Microstructure of metal in cross-section periphery in RBW according to scheme 2: *a* — ×50; *b* — ×200
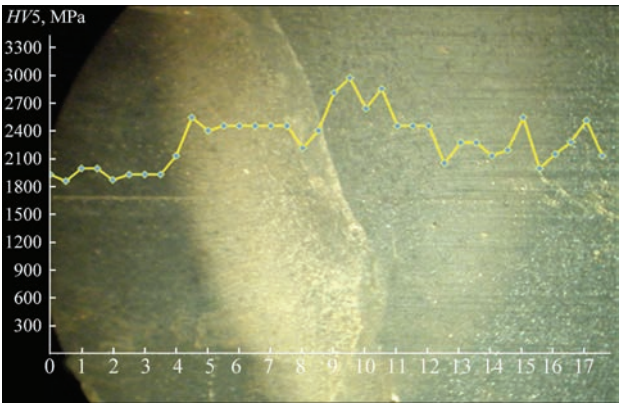
Figure 14. Distribution of microhardness in the area of welded joint after heat treatment in clamps of welding machine

joining the rods of large diameter (more than 32 mm) the postweld heat treatment of rods in the clamps of the welding machine was carried out by passing the current pulses and at the same time the pyrometric control of heating temperature was carried out.

On the basis of investigation results the technology of RBW of rods of hydraulic cylinders of steels 45 and 17GS of diameter from 16 to 60 mm was developed. The technology was realized in specialized welding machine K1040 with welding force from 600 to 7200 kg, at welding current from 15 to 65 kA during joining the rods of different types and sizes, and welding time from 0.8 to 3.5 s.

For the first time for welding machines of such power the three-phase frequency converter was applied, which provides a uniform loading of phases. RBW with postweld heat treatment in the clamps of the machine provides the strength of welded joint of rod and eyelet of hydraulic cylinder at the level of the rod base metal. The welding modes for 96 variants of joints of rods and eyelets were developed. As a result of experiments, the parameters of preliminary edge preparation of different sizes of rod and eyelet were optimized. At the developed technology for RBW of rods in the range of diameters of 16–60 mm the quality joint formation without splashes, with high mechani-

Figure 15. RB-welded rods

cal properties and high geometry precision of welded product is provided, the allowance for the length and diameter does not exceed 0.5 mm (Figure 15). The hydraulic cylinders with rods, welded according to the developed RBW technology, successfully passed the certification tests and are supplied to the EU countries, countries of Eastern Europe and Iran.

Conclusions

In RBW of large-section T-joints the formation of quality joints is complicated due to asymmetry of heating and deformation conditions, which causes the formation of defects and low values of static and cyclic strength.

It was found that in RBW with optimal preparation of welded edges and programmable change in welding force at the heating stage it becomes possible to localize heat generation in the zone of welding rods to egelets in the investigated range of diameters (up to 60 mm), to avoid the defects formation and to provide high mechanical properties of welded joints.

Metallographic examinations revealed that lacks of penetration, oxide films, cracks, caused by the formation of hardening structures, are absent in the joints. The metal structure in the joint zone and the zone of thermomechanical influence is ferrite-pearlite, the areas with martensite structure were not detected. During mechanical tests of welded rods on bending the fracture occurs over the base metal of the rod.

The technology of RBW of T-joints of dissimilar steels 45 and 17GS using the composite inserts was developed.

The technology for RBW of rods of hydraulic cylinders with diameter of 16–60 mm was realized in specialized welding machine K1040, designed and manufactured at the PWI. It uses a three-phase frequency converter, which provides a uniform loading of phases. The welded cylinders successfully passed the certification tests.

1. Sakhatsky, G.P. (1963) Investigation of flash-butt and resistance welding. *Avtomatich. Svarka*, **10**, 26–32.
2. Lebedev, V.K., Besprozvanny, I.A., Mirgorod, Yu.A. (1979) Resistance butt welding and inertia friction welding of billets of end metal-cutting tools. *Ibid.*, **8**, 39–43.
3. Zhang, H., Senkara, J. (2006) *Resistance welding fundamentals and applications*. Boca Raton.
4. Kuchuk-Yatsenko, V.S., Shvets, V.I., Sakhatsky, A.G. et al. (2007) Peculiarities of resistance welding of aluminium alloys using nanostructural and aluminium-nickel and aluminium-copper foils. *Svarochn. Proizvodstvo*, **9**, 12–14.
5. Kuchuk-Yatsenko, V.S., Shvets, V.I., Sakhatsky, A.G. et al. (2009) Features of resistance welding of titanium aluminides using nanolayered aluminium-titanium foils. *The Paton Welding J.*, **3**, 11–14.
6. Kuchuk-Yatsenko, S.I., Zyakhor, I.V., Chernobaj, S.V. et al. (2015) Structure of γ-TiAl joints in resistance butt welding with application of interlayers. *Ibid.*, **9**, 5–12.
7. Kharchenko, G.K., Novomlynets, O.O., Fedorchuk, V.E. et al. (2007) Weldability of new alloys of Al–Cr–Fe–Ti system hardened with nanoquasicrystal particles. *Visnyk ChernigivDTU*, **30**, 55–60.
8. Kuchuk-Yatsenko, S.I., Kharchenko, G.K., Zagadarchuk, V.F. et al. (2004) Formation of structure of joints in resistance and flash-butt welding. *The Paton Welding J.*, **2**, 13–16.
9. Kuchuk-Yatsenko, S.I., Rudenko, P.M., Gavrish, V.S. et al. (2015) Converter of frequency and number of phases for flash-butt welding of rails. *Ibid.*, **7**, 38–40.
10. Kuchuk-Yatsenko, V.S., Nakonechnyi, A.A., Sakhatskiy, A.G. *Method of resistance butt welding corrugated flux-filled metal inserts*. Pat. 8,426,762, B2 US. Publ. 23 April, 2013.
11. Song, Q., Zhang, W., Bay, N. (2005) An experimental study determines the electrical contact resistance in resistance welding. *Welding J.*, 85(**5**), 73–76.
12. Kuchuk-Yatsenko, V.S., Nakonechny, A.A., Gavrish, V.S. et al. (2012) Technology of projection welding of parts of large thicknesses with T-shaped joints. *The Paton Welding J.*, **8**, 42–44.
13. Lipa, M., Golasek, Ya. (1970) Resistance projecion welding. Kiev: Tekhnika.
14. Gilevich, V.A. (1976) *Technology and equipment for projection welding*. Leningrad: Mashinostroenie.

EFFECT OF NON-METALLIC INCLUSIONS OF RAIL STEEL ON WELDED JOINT FORMATION

S.I. KUCHUK-YATSENKO, V.I. SHVETS, A.V. DIDKOVSKY and **E.V. ANTIPIN**
E.O. Paton Electric Welding Institute, NASU
11 Kazimir Malevich Str., 03680, Kiev, Ukraine. E-mail: office@paton.kiev.ua

On the railways of Ukraine since 2012 the laying of high-strength rails of steel grade K76F of Company «MK Azovstal» production, as well as rails produced in Russia, in tracks began. For this purpose at PWI the technology for flash-butt welding of high-strength rails of different production was developed, providing the values of strength and ductility of welded joints required according to the Technical Specifications. In the process of industrial implementation of technology for welding the high-strength rails by the rail welding enterprises of Ukraine a large amount of information was gained on the results of complex application of in-process control with non-destructive and destructive testing methods. It was established that the formation of metal structure in the joint zone alongside with energy input has a significant influence on the composition and distribution of non-metallic inclusions in the base metal of welded rails. The type and the structure of defects are largely determined by the composition of non-metallic inclusions. This effect is manifested in different degrees during changes in energy input in the process of welding. 5 Ref., 3 Tables, 8 Figures.

K e y w o r d s : *flash-butt welding, flashing, rails, high-strength rails, pulsed flashing, defects in rails, non-metallic inclusions, dull spots, quality control, continuous track*

At PWI the technology of flash-butt welding of high-strength rails of different production was developed, providing the values of strength and ductility of welded joints required according to TS. It is based on the method with pulsed flashing (PF) [1], allowing joining the high-strength rails with their minimal softening and preservation of the required ductile properties. As compared to the known technologies for welding rails, the developed technology requires 1.5–2 times lower energy input.

A stable reproduction of technological process requires precise control of energy input, that is provided by the system of automatic control of flashing process using the system for in-process control the welding parameters. At the same time, the maximum admissible deviations from the preset temperature field were established, that provide the optimal conditions for joint formation [2].

In the process of industrial implementation of the technology for welding the high-strength rails by rail welding enterprises (RWE) of Ukraine a large volume of information was gained on the results of complex application of in-process control with non-destructive and destructive testing methods. It was established that the formation of metal structure in the joining area alongside with energy input has a significant influence on the composition and distribution of non-metallic inclusions (NMI) in the base rails metal. This effect is manifested in different degrees during changes in energy input in the process of welding.

The aim of the investigations was to study the effect of NMI in the rail steel on formation of the structure of welds of high-strength rails.

To carry out investigations at the RWE the specimens of high-strength rails of different manufacturers were selected. The selection was carried out mainly from the batches of rails, during welding of which the unstable values of quality of welds were observed.

The chemical composition and mechanical properties of the investigated batches of specimens are shown in Table 1. The content of impurities and alloying elements in them corresponds to the certification documents.

Table 1. Chemical composition of rail steel investigated, wt.%

Steel grade	Chemical composition, %						
	C	Mn	Si	V	P	Al	S
K76F (Ukraine)	0.71–0.82	0.80–1.30	0.25–0.45	0.03–0.07	0.035	0.015	0.045
76F (Russia)	0.71–0.82	0.75–1.05	0.25–0.45	0.03–0.15	0.025	0.02	0.03
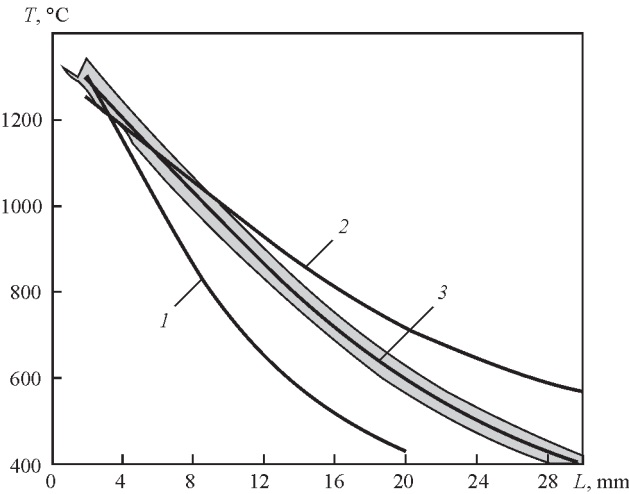
Figure 1. Temperature distribution in HAZ before upsetting during pulsed FBW of rails R65 at extremely low (*1*), extremely high (*2*) and optimal (*3*) heat input: *1* — t_w = 30–40; *2* — 110–120; *3* — 70–80 s

The welding of specimens of high-strength rails was carried out in stationary machine K1000, which is operated at the RWE of Ukraine. The welding programs were used the same as in the industrial conditions. At the same time, the modes with extremely low (Figure 1, mode 1), extremely high (mode 2) and optimal (mode 3) admissible heat inputs were preset.

The welded joints of all the batches were subjected to non-destructive ultrasonic testing and tested also for static bending in accordance with the accepted procedures. A part of the joints was investigated using the methods of metallographic analysis in optical microscope «Neophot-32» and in microanalyzer JAMP-9500F.

In Table 2 the results of tests of welded joints of rails on static transverse bending are shown, as well as the requirements of standard documents are given for comparison. According to the test results it can be said that the best values were obtained in welding at mode 3 and within its limits, and in welding at modes 1 and 2 the stable results were not obtained.

Here in both cases, the lacks of separate values of strength and ductility are recorded. In the fractures of such joints the defects are observed, determined as «dull spots» (DS). They are distinguished by undeveloped relief on the fracture surface and characterized by the grey color. Their total area is regulated by normative documents [3]. According to our investigations, in the microstructure of DS the numerous fused-type inclusions (Figure 2) are present on the background of mostly pit matrix fracture (single cleavage facets are found).

According to the results of X-ray microanalysis the basis of inclusions consists of manganese silicates. At negligible iron content their composition may include such active elements as aluminum, calcium, titani-
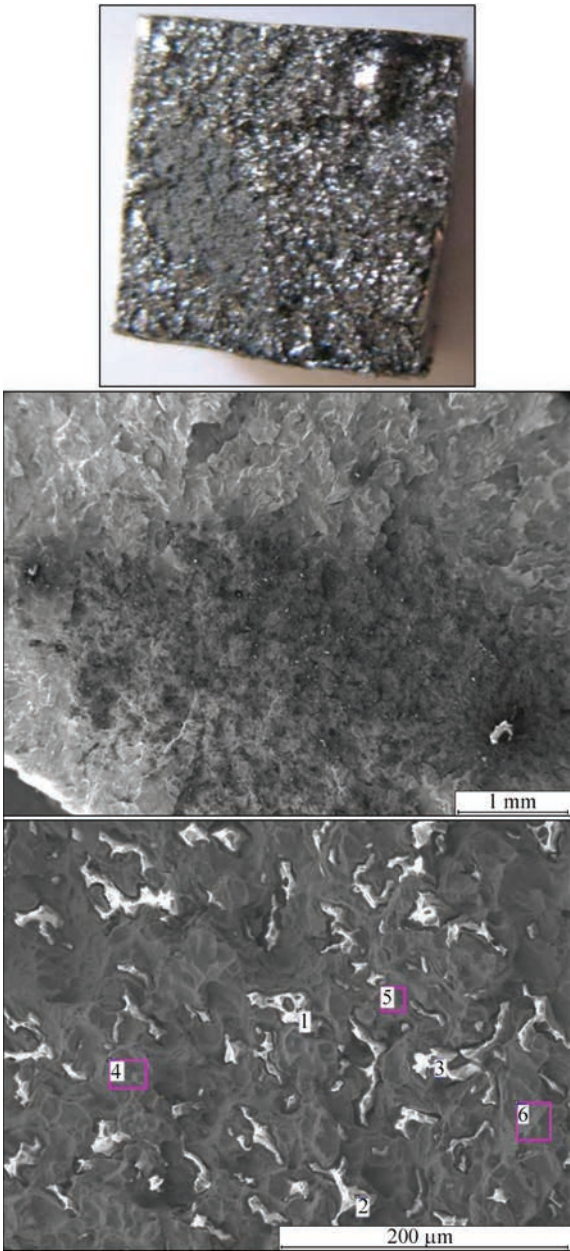
	C	O	F	Al	Si	Mn	Fe
1	3.27	66.66	3.49	1.11	16.48	8.12	0.86
2	1.63	61.08	2.73	2.15	16.70	14.73	0.99
3	2.41	68.91	3.16	1.32	16.39	6.90	0.90
4	4.43	1.57	0	0.11	0	0.80	93.09
5	5.51	0.86	1.88	0	0.18	0.81	90.76
6	4.70	1.50	0	0	0.15	1.11	92.54

Figure 2. Silicate «dull spots» on the fracture of welded joints and results of analysis of rail metal of «Azovstal» production

um and magnesium. The size of inclusions of about 10 μm gives grounds to consider that the observed cluster of silicates is formed as a result of a large inclusion fragmentation during upsetting.

Alongside with the traditional silicate DS in the fractures of rails of steel K76F of «Azovstal» production, fractured during the tests on bending along the base metal and in HAZ, the clearly contoured DS of other nature were observed (Figure 3). In definite cases their area reached tens of square millimeters.

	C	O	Mg	Al	Si	S	Ca	Fe
1	34.38	7.66	–	0.68	3.60	–	4.58	45.64
2	46.57	29.02	–	1.47	4.41	1.53	–	2.40
3	24	23.21	–	1.49	3.27	–	0.74	47.29
4	49.32	33.05	0.23	1.87	6.48	0.30	0.79	6.03
5	55.94	27.26	0.45	2.35	6.54	–	1.81	5.57
6	4.70	1.50	0	0	0.15	1.11	92.54	–

	C	O	Si	Fe
1	13.61	22.79	0.81	62.79
2	16.87	10.99	0.52	71.63
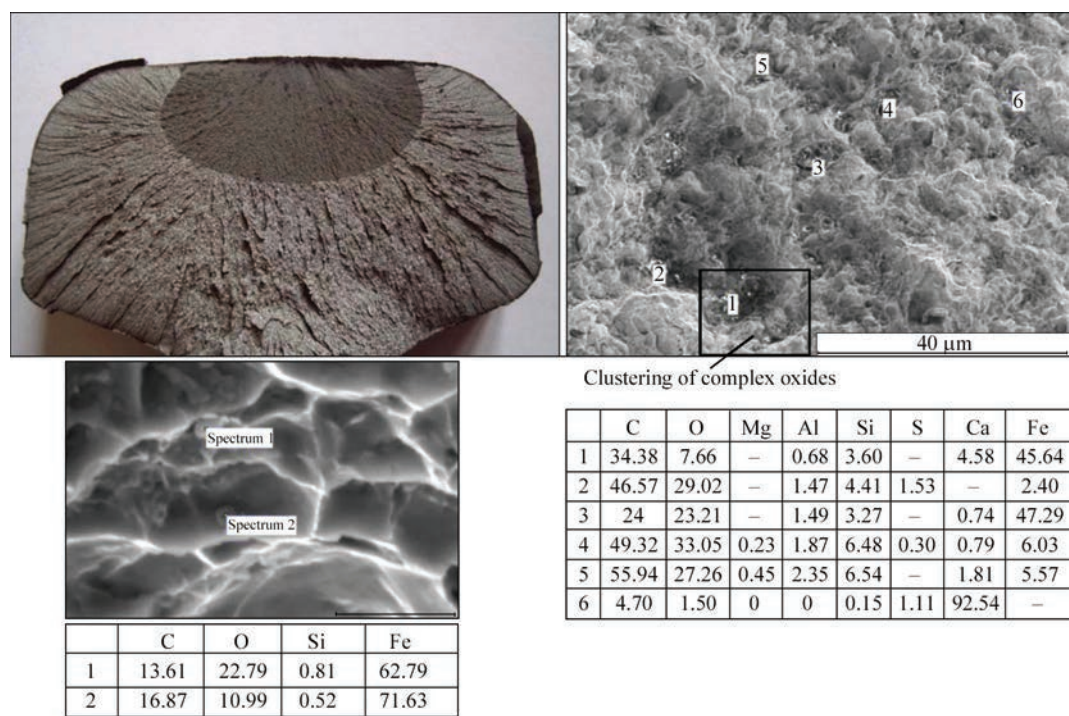
Figure 3. Oxide «dull spots» on the fracture of rails of «Azovstal» production

Table 2. Results of tests of rails of steels K76F and 76F on bending

Number of mode	Standard and steel grade	Fracture load, kN	Bending deflection, mm	Note
	Ukraine	160	≥30	TU U 24.1-40075815-002:2016
	Russia	210	≥27	STO RZhD 1.08.002–2009
1	K76F	1750–2000 1950	25–35 28	PF
1	76F	1750–2300 1950	12–35 28	Same
2	K76F	1800–2000 1900	14–30 19	»
2	76F	1700–2300 2000	12–32 21	»
2	K76F	2000–2300 2150	35–45 38	»
3	76F	2300–2600 2450	30–46 38	»
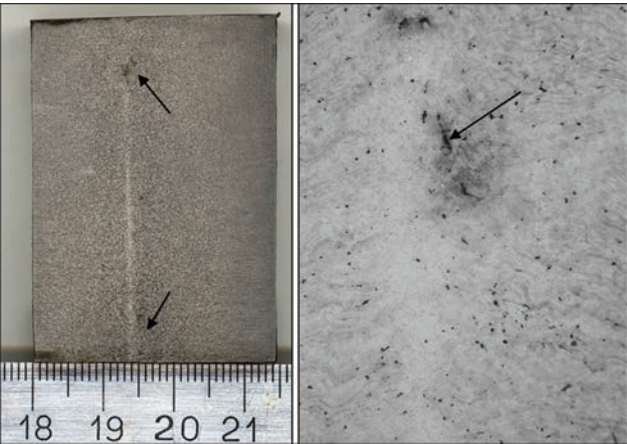
Figure 4. Microcracks in macrostructure (×25) of welded joints of rail steel 76F
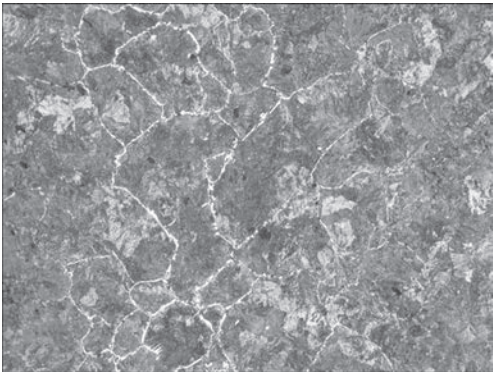
Figure 5. Microstructure (×100) of joint of rails of 76F steel welded at mode 2 with extremely high heat input
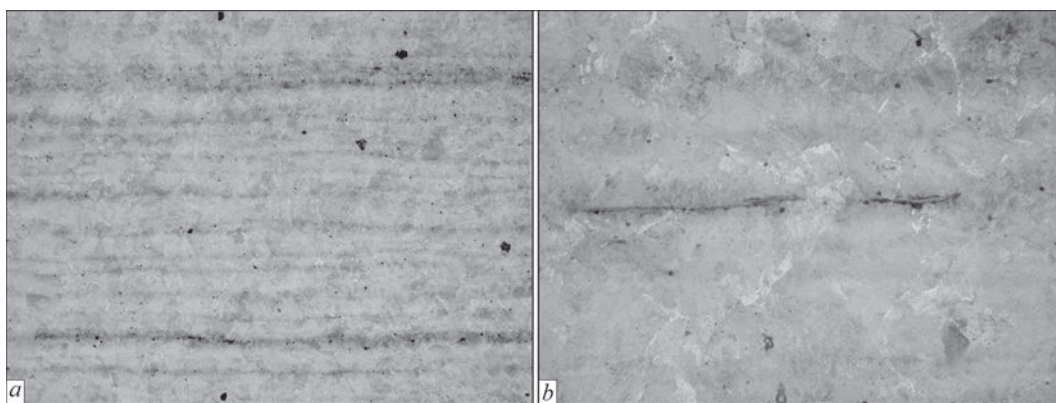
Figure 6. Inclusions of sulfides in the rails metal of steel 76F revealed by etching in sodium picrate: a — ×100; b — ×400

Fine metallographic examinations showed that the nature of fracture in the area of spots is also of pit type. However, in the pits not silicates are present, but iron oxides of the size smaller than several tenths of micron. It should be noted that within the spot the clusters of larger inclusions of complex oxides of aluminum, calcium, silicon of the size of several microns were also observed.

Obviously, these spots are the result of formation of low-melting films in the metal, the base of which is iron oxide. Such spots on the fracture surface, unlike the silicate ones, can be classified as oxide DS. Due to a very small film thickness to detect them in the rail metal using ultrasonic testing is problematic, that complicates the preliminary rejection of rails.

The increase in heat input during welding leads to decrease in test values of investigated steels. This is caused, first of all, by increase in grain size in the middle part of the weld and development of the process of ferrite precipitation along the boundaries of primary austenite grains along the joining line.

In the specimens of rails of steel 76F welded at mode 2, the metal heterogeneity was detected using ultrasonic testing, and the subsequent analysis of macrostructure showed that the observed heterogeneity is the result of crack initiation (Figure 4).

The microstructure of weld metal is homogeneously sorbite (Figure 5). Along the joining line a layer with a ferrite fringing of boundaries of the primary austenitic grains is observed. The width of this layer is about 500 μm. According to ASTM the size of primary austenitic grains corresponds to 1–2. The width of normalization area of welded joint is about 40 mm.

The microstructure of base rail metal is sorbite-pearlite. In the base metal the numerous sulfides (Fe, Mn)S are present in the form of chains of small globules and lenticular inclusions, extended along the direction of rolling (see Figure 5 and Table 2). Separate, randomly scattered large sulfides of irregular shape were also encountered. Lenticular sulfides, as

is known, are enriched with iron, more ductile and are the product of hot deformation during rolling [4].

In the thermal deformation conditions of welding the sulfide inclusions are stretched along the deformation bands. In the near-contact layer the activation of diffusion processes leads to violation of linearity of their location and coagulation (Figures 6 and 7).

The microcracks, detected in the near-contact layer, are adjacent to the sulfide inclusions (Figure 8). The iron content in these sulfides is significantly higher than that in the lenticular inclusions of base metal (80–85 versus 50–60 wt.%), that is the evidence of active interaction with the iron matrix.

In system FeS–MnS the eutectics with melting temperature of 1164 °C exists. At the contact boundary of inclusions of manganese sulfides with iron matrix the formation of the eutectic melt is possible during technological heating. The intensification of this process leads to increase in the melt volume and its spreading along the structural boundaries. In the literature this phenomenon is defined as a tough-brittle transition at the near-solidus temperatures [5], which is not a natural property of steel and is determined by the presence of impurity elements of metallurgical origin, mainly sulfur, phosphorus and oxygen.

Cracking of the joint metal of rails along the eutectic interlayers, forming in the near-contact layer, can occur both during cooling, as well as under the load in the process of operation. It has a risk that the joints of rails, which passed testing, can be fractured being laid in track.

The crack propagation is significantly influenced by metal deformation in the near-contact layer during
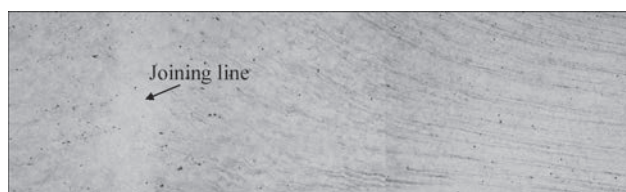
Figure 7. Transformation of microstructure of welded joint of 76F rail steel
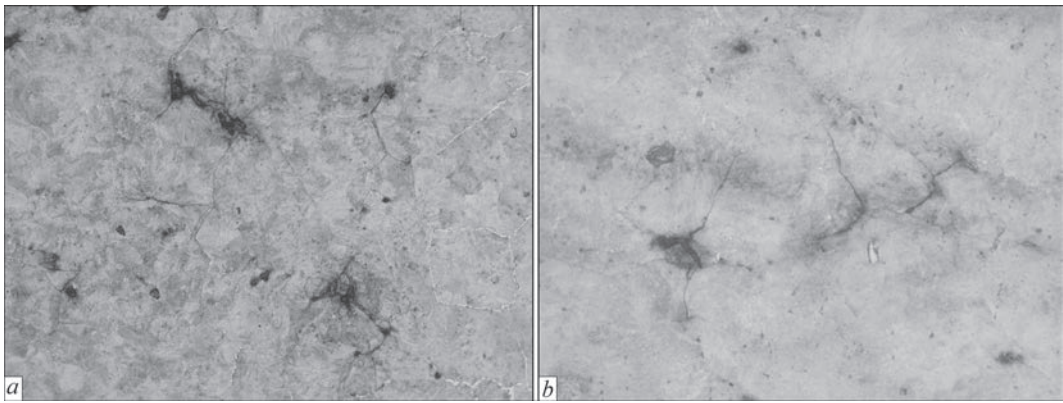
Figure 8. Microcracks in the near-contact layer of welded joints of steel 76F rails: *a* — ×100; *b* — ×400

Table 3. Results of X-ray spectral microanalysis of chemical composition of inclusions in the rail metal

Structural component	Elements, wt. %				
	Al	Si	S	Mn	Fe
Matrix	0.341	0.135	0	0.798	98.726
Inclusions in BM	0.530	0.361	18.511	30.872	49.726
Inclusions in BM	0.321	0.049	15.254	25.738	58.630
Inclusions in BM	0.358	0.209	16.312	27.269	55.852
Inclusions near the joining line	0.729	0.430	3.751	7.657	87.433
Inclusions near the joining line	0.278	0.463	3.211	6.336	89.712

upsetting. The rolled bands enriched with inclusions of sulfides (Table 3) are bent and orient the weakened region into the most unfavorable direction in relation to the loads, to which the rail joint is subjected.

The more severe heating mode results in immunization of the process of sulfides transformation and its retard at the stage of coagulation before spreading of eutectic melt along the grain boundaries. It allowed avoiding the cracking of metal in the joints, welded at modes 1 and 3.

Conclusions

1. The presence of NMI in the rail steel can significantly effect the formation of defects in welding zone. The type and the structure of defects are largely determined by the NMI composition.

2. The oxide inclusions, concentrated in the rolled bands, are carried away to the weld zone, and under the deformation conditions forming clusters, are lined up in the most unfavorable direction in relation to the loads, to which the rail is subjected.

3. The energy input in welding influences the formation of defects. With increased energy input in the near-contact zone on the basis of manganese sulfides the low-melting eutectics are formed, propagating along the grain boundaries and causing danger of microcracks formation.

1. Kuchuk-Yatsenko, S.I., Lebedev, V.Kh. (1976) *Continuous flash-butt welding*. Kiev: Naukova Dumka.
2. Kuchuk-Yatsenko, S.I., Krivenko, V.G., Didkovsky, A.V. et al. (2012) Technology and new generation of equipment for flash butt welding of advanced high-strength rails for construction and reconstruction of high-speed railway lines. *The Paton Welding J.*, **6**, 22–26.
3. *TU U 27.1-40081293-002:2016*: New welded rails for railroads. Dnipropetrovsk: Ukrzaliznytsya.
4. Dementiev, V.P. (2002) Liquation in R65 profile of rail steel. *Izvestiya Vuzov. Chyorn. Metallurgiya*, **10**, 1–9.
5. Zabilsky, V.V., Nikonova, R.M. (2005) Tought-brittle transition in steels at near-solidus temperatures. Mechanism of grain boundary embrittlement. *FMM*, Vol. 99, Issue 3, 1–9.

TECHNOLOGY AND EQUIPMENT FOR PRESS MAGNETICALLY-IMPELLED ARC WELDING OF POSITION JOINTS OF SMALL-DIAMETER PIPES IN SITE AND STATIONARY CONDITIONS

V.S. KACHINSKY, S.I. KUCHUK-YATSENKO, M.P. KOVAL and **E.I. GONCHARENKO**

E.O. Paton Electric Welding Institute, NASU
11 Kazimir Malevich Str., 03680, Kiev, Ukraine. E-mail: office@paton.kiev.ua

Increase in the quality of welding of position butts of pipes in site conditions is a challenging task. The aim of the work was the development of technology and equipment for press magnetically-impelled arc welding (PMAW) of position butts of pipes of 18–64 mm diameter with wall thickness of up to 5 mm, which is used for pipes of air ducts of railway cars, pipelines in the repair and construction of greenhouse complexes and other purposes of industrial application. The adaptive system for automatic control of energy input at PMAW and the pipe welding technology on its basis under the conditions providing a stable quality of joints were developed. The technology of PMAW of pipes of 18–64 mm diameter in the field conditions was developed based on the method of automatic control of gap between the pipe being welded, providing a stable energy input during welding. The new generation of equipment was designed, manufactured and passed the industrial tests for PMAW of pipes of 18–64 mm diameter in the field conditions using the systems of automatic control of main parameters of the process. 8 Ref., 3 Tables, 12 Figures.

K e y w o r d s : press welding with magnetically-impelled arc, induction of controlling magnetic field, pipelines

Welding of position circumferential welds of pipes of 18–64 mm diameter of carbon and low-alloyed steels is applied in different branches of industry, construction, power engineering and greenhouse economy. At the same time, different technologies of manual, automatic orbital gas-electric and gas welding are mainly applied. In the previous years, at the E.O. Paton Electric Welding Institute the technology of welding pipes of small diameter was developed applying press magnetically-impelled arc welding (PMAW). The technology and equipment were successfully implemented and used in the manufacture of different parts of tubular round section in the automobile industry [1]. The installations for PMAW of parts of tubular section are designed and manufactured.

PMAW [2–5] differs from the existing arc methods by high efficiency, quality stability of welded joints, high degree of mechanization and automation of the technological process. Welding is performed in the automatic mode, which significantly reduces the influence of welding operator on the quality of welded joints. In PMAW of steel pipes the welding consumables and shielding gas are not required.

This technology and equipment are used in welding of position pipe butts under stationary conditions. Here, the basic parameters of welding process are preset by the programs, the reproduction of which is possible at a strictly preset value of the arc gap between the ends of pipes being welded. In PMAW in the field conditions and repair works the fulfillment of this condition is not always possible. The experience of PMWA of different pipes, gained at the PWI, shows that to stabilize of the gap is possible by developing the systems of automatic control of its value during welding process.

The aim of the work was the development of technology and equipment for PMAW of position butts of pipes of 18–64 mm diameter with wall thickness of up to 5 mm, which is applied for pipes of air ducts of railway cars, pipelines in the repair and construction of greenhouse complexes and other purposes of industrial use adapted to the conditions of site welding of position butts in the repair of pipelines. To solve the put problem, the following investigations were carried out:

● development of adaptive system of automatic control of the process of metal heating and formation of joints during PMAW of pipes of the specified sizes;

● investigations of deformational processes in PMAW in order to achieve the required reinforcement of the weld by determining the basic parameters of the machine drive;

● investigations of the influence of thermal cycles in welding pipes of specified sizes on the structure and mechanical properties of joints and development of welding technology;

Figure 1. Installation MD101: *1* — welding machine; *2* — control cabinet; *3* — control panel

Figure 2. Installation MD103: *1* — welding machine; *2* — control cabinet; *3* — pump station

● development of mobile equipment for PMAW of small-diameter pipes.

To carry out investigations on welding the steel pipes of 32–51 mm diameter with wall thickness of 2.5–5.0 mm of steels 20 and 09G2S were used. The investigations were carried out in the laboratory machines MD101 and MD103 (Figures 1 and 2). Installation MD101 with a manual lever clamping and a pneumatic upsetting drive is designed for welding pipes of diameter from 12 to 51 mm with maximum cross-section area of 460 mm^2 maximum outer diameter of 51 mm and wall thickness of 3 mm. Power of the installation is not more than 40 kV·A. Weight of the installation is 250 kg. Installation MD103 with a hydraulic drive of clamping and upsetting is designed for welding pipes of diameter from 40 to 120 mm with maximum cross-section area of 2000 mm^2 and outer diameter of up to 120 mm with wall thickness of 5 mm. Power of the installation is not more than 70 kV·A. Weight of the installation is 940 kg. A significant weight of installations MD101 and MD103 does not allow applying them in welding in the site conditions.

The metallurgical examinations were performed in microscopes «Neophot-32» and «Versomet» at different magnifications. The value of microhardness was measured at 100 g load in the LECO microdurometer M-400. The grain size was determined according to the scales of GOST 5639–82. The chemical composition of steels is given in Table 1.

One of the main technological parameters influencing a stable movement of the arc in the magnetic field is the magnetic induction. As the investigations showed, at the low values of magnetic induction the arc burns unstable with short circuits. From the point

of view of power, for a stable arc movement it is desirable to provide the optimal induction in the gap. The optimal parameters of the field were accepted those, which could be realized later for using in the industrial conditions.

A stable arc movement depends also on the gap size, parallelism of ends and bevel angle of edges of pipes to be welded. The size of the arc gap, where the induction of controlling magnetic field is present and the arc is moved, largely determines the quality of welded joints. This parameter is determined from the requirement of stable arc excitation, its stable movement at the maximum possible time of burning, achieving the highest rotation speed. In the investigated range of pipes the value of the gap, as was established by the experiments, is in the range of 1.2–1.8 mm. For the pipes with a small wall thickness (up to 2 mm) this gap is 1.2–1.5 mm, for the pipes with wall thickness of 5 mm it is in the range of 1.6–1.8 mm.

On the basis of the carried out investigations the system for automatic control of the arc gap size during heating using high-speed magnetically-impelled arc was developed, which allows maintaining the optimum value during the whole heating period, regardless of the initial value of the gap. The system allows starting a stable arcing process even in the case of excitation with a short circuit, which greatly simplifies the alignment of pipe edges at the site assembly of butts and also reduces the requirements to the accuracy of cutting of pipe ends before welding. The system for automatic control of heating process of pipes in PMAW was patented in the leading countries and significantly widends the application of this technology in welding in the field conditions [6, 7].

The principle of arc gap regulation is based on the method of processing the feedback signal between the

Table 1. Chemical composition of steels used, wt.%

Grade of steel	C	Si	Mn	P	S	Cu	Ni	Cr	Mo	Al
20	0.20	0.24	0.47	0.015	0.016	0.05	0.05	0.25	0.05	0.01
09G2S	0.11	0.75	1.38	0.035	0.037	0.28	0.29	0.29	0.09	N/D

voltage drop at the welding arc and the subsequent controlling the effect on the device for movement of movable part in the welding machine. The block-diagram of the regulator is shown in Figure 3.

The regulation of arc gap is performed as follows. Before the start of the welding process, the pipes to be welded with the as-abutted ends are clamped into the movable and stationary parts of the welding machine. Before the welding cycle starts the power source is switched on. The voltage on the movable and fixed bodies of the welding machine is equal to zero (short-circuit mode). At a zero signal of input voltage the opening of the movable part of the machine to the preset value of arc voltage occurs. The excitement of welding arc occurs and the process of heating the pipe ends begins. The signal corresponding to the voltage drop at the welding arc is transmitted to the input of a rating amplifier. In the process of pipe heating from the output of the rating amplifier the signal is transmitted to the input of the analog-digital converter and is converted into a sequence of package data corresponding to changes in voltage value at the welding arc moving in the gap between the pipe ends. In the software-hardware complex based on PC the data package is processed by the program of recording the voltage drop at the arc. Carrying out the continuous analysis of these data, the system influences the movable part of the welding installation, maintaining the arc voltage within the preset limits in order to provide a stable movement of the arc at the ends of pipes being welded. The use of the system allowed producing high-quality joints at a lower energy input and, respectively, heating and deformation of pipe ends, as far as heating stabilization allowed narrowing the excessive reserve of energy input envisaged for its reduction at the deviations of parameters.

Figure 4 shows the diagram of temperature distribution in welding of pipes of 42×3 mm using the method of flash-butt welding (FBW) and PMAW, characterizing the temperature distribution in the metal of HAZ and along the line of structure joining.

The investigation of thermal cycles in the period of pipes heating using thermocouples and tests of joints showed that the decisive factor influencing the quality of joints is the temperature of heating pipe ends before their compression allowing producing the sufficient deformation during upsetting. The optimum temperature of heating of the area located at the distance of 1 mm from the pipe end is up to 1000–1100 °C. The heating duration, in case the other parameters are maintained constant, remains in the narrow range. Its value depends on the arc current. The overheating of pipe ends by the moving arc leads to the appearance of molten bridges in the gap and re-
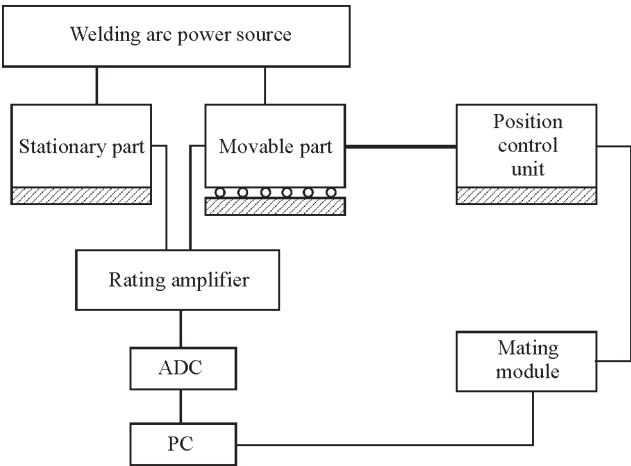
Figure 3. Block-diagram of arc gap regulator

duction in the speed of the stable arc movement. The arc under the influence of magnetic field moves in the gap between the ends of the pipes. A high speed of the arc (up to 140 m/s) on the pipes of small diameter allows obtaining a uniform heating across the pipe ends over the entire welded surface. For welding the machines were equipped with a drive, which allows changing the value of the arc gap between the pipe ends as well as regulating the amount of deformation during upsetting.

Development of welding technology. Figure 5 presents different types of welded joints of pipes of 38×3 mm produced in the field conditions. The application of the system stabilized the gap value and energy input during the whole heating period, that allowed obtaining a stable temperature distribution during heating the pipes with wall thickness from 3 to 5 mm (see Figure 4).

In press welding of pipes the weld reinforcement is formed on the inner and outer pipe surface. Depending on the service conditions of welded joints and pipe structures the reinforcement is removed by machining or retained in the structure. During welding
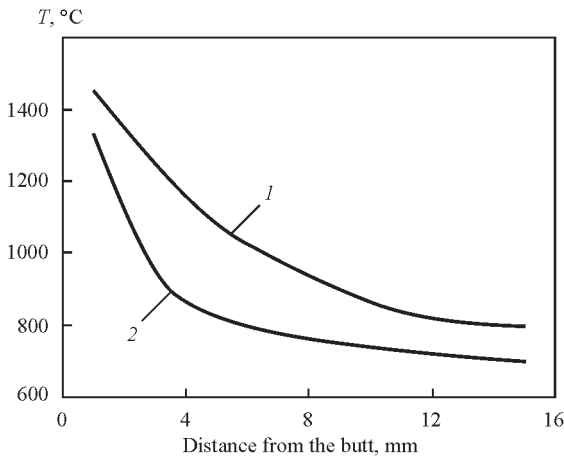
Figure 4. Determination of temperature in welding of pipes of 42 mm diameter with wall thickness of 3 mm: *1* — FBW; *2* — PMAW

Figure 5. Welded joints of pipes of 38×3 mm: *a* — pipe with pipe; *b* — pipe to plug

of position butts of pipes the outer flash, if necessary, is removed and the inner one is admitted on the condition that it does not exceed the preset value. This requirement creates additional tasks in the development and searching of optimal thermal deformation cycles in welding. By controlling the energy input to the heated pipe ends and the allowance for upsetting, it was succeeded to reduce the amount of inner weld reinforcement (Figure 6).

In welding the course of the process is influenced by different factors, which causes the need in testing the quality of welded joints. The main condition for the welded joint formation is a process of a combined plastic deformation of the parts. The process of forming joints is influenced by the following factors:

● state of the pipe ends (surface temperature, presence of microroughness, oxide films and other contaminants);

● temperature distribution in the pipe ends being welded;

● value and character of ends deformation during upsetting.

From the results of the carried out investigations the technology of PMAW of pipes of small diameter of up to 64 mm was developed. The basic parameters of welding are given in Table 2.

Figure 7 shows the microstructure along the line of joining the pipes of 42×4 mm welded using the method of PMAW. The band of joining is quite clearly ex-

Figure 6. Macrosection of welded joint of pipe of 42×3.5 mm

Table 2. Basic technological parameters of welding pipes

Grade of steel	Size, mm	Time of welding, s	Upsetting force, kN	Shortening of pipes, mm
20	38×3	9	24	3.8
20	42×5	14	40	4.7
09Г2С	42×4	12	37	3.7
09Г2С	48×3.5	13	35	3.4

pressed throughout the whole height of the weld, its width is 40–60 μm.

The microstructure of HAZ metal in the area of coarse grains is ferrite-pearlite. Pearlite is precipitated in the form of separate grains in the composition of ferrite-pearlite mixture. The number of the grain in the coarse-grain c area orresponds to 6–5. The hardness amounts to HV1-1930–2210 MPa. At the area of normalization (Figure 8) the structure is fine-grained (number is 9–10 according to GOST 5639–82), and ferrite-pearlite with the predominance of a ferrite component, the width of the area is 1400 μm, the hardness is HV1-1640–1870 MPa. The base metal (Figure 9) represents a ferrite-pearlite mixture with obvious traces of rolling, the number of grains is 8 according to GOST 5639–82. The hardness of the base metal is HV1-1510–1710 MPa. The width of HAZ of welded joint is 6800 μm.

The hardness was measured along the BM–HAZ–joining line–BM–HAZ line at 100 g load and 500, 300, 200 and 100 μm step. The value of hardness is shown in Figure 10. The HV1 hardness of joining band is 2150, 1990, 2280, 2060, 2280 and 2060 MPa. The thermal cycle at PMAW is characterized by a rapid heating and cooling. In general, the metal structure is characterized by finer grain and smaller width of HAZ than in other types of pressure welding of similar products. The cooling rate is much higher in PMAW than in FBW, that leads to increase in hardness along the line of welded joint in PMAW. The microstructure of joint band consists mostly of lamellar ferrite with a
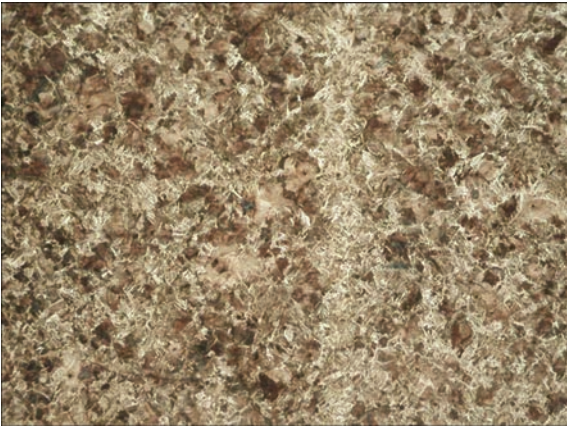
Figure 7. Microstructure (×100) of steel 20 along the joining line of PMA-welded joint

Figure 8. Microstructure (×100) of area of complete recrystallization in PMA-welded joint

Figure 9. Microstructure (×100) of base metal of PMA-welded joint

disordered second phase which has a higher hardness than free ferrite. It causes an increased hardness of the joining band as compared to FBW, where its structure represents mainly a polyhedral ferrite.

The mechanical properties of base metal and welded joints are given in Table 3. The analysis of the results of tests performed at 20 and –20 °C temperature showed that mechanical properties of welded joints are at the level of those of base metal.

According to the results of investigations a mobile machine was designed for press welding of pipes of up to 51 mm diameter using magnetically-impelled arc [8]. For operation under the industrial and field conditions, mobile machine MD1 for press welding pipes of small diameter was manufactured.

Figure 10. Hardness of PMA-welded joint along the BM–HAZ–JL–HAZ–BM line

Main technical characteristics of MD1 installation

Maximum cross-section area of pipes, mm² 450
Maximum diameter of pipes, mm 57
Maximum upsetting force, kN (kgf) 30 (3000)
Maximum clamping force, kN (kgf) 60 (6000)
Supply voltage, V 380
Power consumption, kV·A 50
Weight of machine, kg 90
Dimensions of machine, mm . . . . 800×600×400

The process of PMAW in installation MD1, which consists of the machine, welding rectifier and control cabinet, is performed as follows.

The pipes to be welded are installed in the machine using clamping devices (Figure 11). The pipes are firmly clamped using drives of the machine. The arc is burning in the narrow gap between the pipe ends

Figure 11. Installing of pipes into the clamping devices of designed welding machine MD1

(Figure 12). The welding is performed by heating the pipe ends until the state of plastic deformation. After heating the upsetting is performed.

Developed installation MD1 provides welding of pipes of 57 mm diameter both in the field as well as in the stationary conditions in the range of ambient

Table 3. Mechanical properties of PMA-welded joints of pipes

Grade of steel	Pipe size, mm	σ_t, MPa		KCV_{+20}, J/cm²		KCV_{-20}, J/cm²	
		BM	WJ	BM	WJ	BM	WJ
20	38×3	508–525 / 516.5	512–545 / 528.5	56–58 / 57	54–58 / 56	56–59 / 57.5	54–62 / 58
09G2S	42×5	460–478 / 469	453–484 / 465	57.7–58.1 / 57.9	59–78.1 / 68.5	57.8–58 / 57.9	64–74.5 / 69.3

Figure 12. Process of press welding of 51×4 mm pipes in MD1 machine

temperature from –40 to 40 °C. The manufacture of welding mobile complexes based on this installation is possible.

Conclusions

The adaptive system for automatic control of energy input process at PWMA and the pipe welding technology on its basis were developed at the conditions providing a stable quality of joints.

The comprehensive investigations of pipe joints quality were carried out indicating the equal strength with the base metal according to all values, including the impact toughness.

The possibility of obtaining the limited sizes of flash due to optimization of thermal cycle was established.

The technology of PMAW of pipes of 18–64 mm diameter in the field conditions was developed, based on using the method of automatic control of gap size between the ends of pipes being welded providing a stable energy input, proposed by the authors.

The possibility of producing high-quality PMA-welded joints at minimum energy input and deformation during upsetting was shown in order to reduce the value of flash.

The comprehensive tests of welded joints of pipes of 18–64 mm diameter were carried out at a minimum energy input and indicate their practical equivalence with the base metal, including the values of impact toughness.

A new generation of equipment for PMAW of pipes of 18–64 mm diameter in the field conditions using the systems for automatic control of the basic process parameters was developed, manufactured and passed the industrial tests. The possibility of significant simplification of operations of alignment and assembly of pipes with the systems for automatic control was established.

The metallographic examinations showed absence of pores along the welded joint line. The measurement of hardness along the BM–HAZ–joining line–HAZ–BM line showed 10–15 % increase in the hardness, that is acceptable according to standard documents.

The technology for welding of pipes at the car repair enterprises of railway, construction and repair of greenhouse complexes was developed.

Mobile machine MD1 was designed for PMAW of small-diameter pipes under the stationary and field conditions.

1. Kuchuk-Yatsenko, S.I., Kachinsky, V.S., Ignatenko, V.Yu. et al. (2010) Magnetically-impelled arc butt welding of automobile parts. *Austral. Welding J.*, 55(2nd Quart.), 40–48.
2. Ganovski, F.J. (1974) The magnetarc welding process. *Welding Metal Fabr.*, **5**, 206–213.
3. Edson, D.A. (1982) Magnetically impelled arc butt welding of thick wall tubes: *IIW Doc. 726–82*, July, 726.
4. Takagi, K., Arakida, F. (1982) Magnetically impelled arc butt welding of gas pipeline. *Metal Constr.*, **10**, 542–548.
5. Kuchuk-Yatsenko, S.I., Kachinsky, V.S., Ignatenko, V.Yu. et al. (2010) Magnetically-impelled arc butt welding of pipes of steel X70. *Austral. Welding J.*, 55(2nd Quart.), 20–22.
6. Kuchuk-Yatsenko, S.I., Kachinskiy, V.S., Ignatenko, V.Yu. et al. *Method of magnetically impelled arc butt welding*. Pat. 6.211.489 BI US. Pat. 03.04.2001.
7. Kuchuk-Yatsenko, S.I., Kachinsky, V.S., Koval, M.P. *Method of press welding*. Pat. 100278 Ukraine. Reg. 10.12.2012.
8. Kuchuk-Yatsenko, S.I., Kachinsky, V.S., Galakhov, M.V. et al. *Machine for pressure welding of pipes with heating by magnetically-impelled arc*. Pat. 95360 Ukraine. Reg. 25.12.2014.

TECHNOLOGY AND EQUIPMENT FOR ELECTRON BEAM WELDING OF STRUCTURES IN AEROSPACE INDUSTRY

V.M. NESTERENKOV and **K.S. KHRIPKO**

E.O. Paton Electric Welding Institute, NASU

11 Kazimir Malevich Str., 03680, Kiev, Ukraine. E-mail: office@paton.kiev.ua

Electron beam welding is one of the leading technological processes used in development of structures for aerospace industry. For many years PWI has taken leading positions in development of specialized equipment for EBW. The paper provides description of different types of developed units, differing by overall dimensions of welding chamber, as well as variants of chambers and configurations of vacuum systems, displacement mechanisms of the EB gun or item being welded. All the units are fitted with modern systems of control of equipment included into them. Samples of aerospace products manufactured by EBW are given. 6 Ref., 16 Figures.

K e y w o r d s : *electron beam welding, aerospace industry products, units, welding chambers, chamber overall dimensions, vacuum system, displacement mechanisms, control systems, welded components*

Aviation and space industries occupy a leading position as to application of light and strong alloys of non-ferrous metals. Considering the priority of these directions, PWI paid a lot of attention to development of technologies of welding such materials by different processes, including EBW [1, 2].

Application of computer numerical control (CNC) tools for EBW brought this technology into the category of leading processes, owing to the capabilities of precision control of both electron beam movement trajectory in welding and its energy, including regulation of the total value of power and shape of this power distribution in space [3, 4]. This ultimately led to an essential expansion of EBW technological capabilities and to improvement of repeatability of the process of welding batch-produced parts in the programmed mode.

Main characteristics of PWI developed units are as follows [5]:

1. *«Small» (small-sized) units* have up to 0.26 m^3 volume of welding (vacuum) chamber (Figure 1).

Working pressure in EB gun is less than $5 \cdot 10^{-5}$ Torr, and not higher than $(2.5–3.0) \cdot 10^{-4}$ Torr in the welding chamber. Typical time of pumping down the welding chamber and gun is equal to not more than 5 min (depends on vacuum system components).

The units are of a comparatively simple design with permanently fixed outside welding gun. Welding movement is realized by miniature CNC mechanism of displacement of the part being welded: one- and two-coordinate work table and welding manipulator (rotator), mounted in one of the two positions — either with vertical axis of rotation of the faceplate or

with horizontal axis. Moreover, the unit can be fitted with, for instance, miniature tailstock (for horizontal orientation of the axis of rotation of the welded part), small lathe chuck, additional center, etc.).

This type of units is fitted with a comparatively low-power high-voltage welding power unit of 6–15 kW (at fixed accelerating voltage of 60 kV).

These are versatile units, typical purpose of which is welding small-sized parts with linear and circumferential welds from different structural metals, including aluminium, magnesium and titanium alloys, usually of less than 30 mm maximum thickness.

2. *«Medium» (midsized) units* have welding (vacuum) chamber of 2.7–5.7 m^3 volume.

Working pressure in EB gun is less than $5 \cdot 10^{-5}$ Torr, and not higher than $(2.5–3.0) \cdot 10^{-4}$ Torr in welding chamber. Typical time of pumping down the welding chamber and the gun is not more than 12–15 min.

**Figure 1.** Small-sized unit for EBW

Figure 2. Medium-sized unit with stationary EB gun and two-co-ordinate work table

Such units have external permanently fixed (vertical) welding gun (Figure 2).

Welding displacement (CNC) is here realized by precision two-coordinate work table and welding manipulator (rotator), mounted on work table top, either in the position with vertical axis of faceplate rotation, or with horizontal axis (Figure 3). Displacement of the entire moving base of the work table (on rails) from vacuum chamber onto loading-unloading platform and back into the chamber, with smooth approach to the parking position in the chamber proper, is additionally realized.

The unit can be fitted with tailstock with rotating or non-rotating center paired with the main welding manipulator (at horizontal orientation of its axis of rotation), as well as lathe chuck and additional center for this welding manipulator, etc. In addition, the units are usually fitted with paired set of special cabinets-stands for welding manipulator and tailstock, respectively (see Figure 3). Stands for the same manipulator, but for the case of vertical orientation of the axis of its rotation can be additionally supplied. In the general case, presence, quantity and height of stands
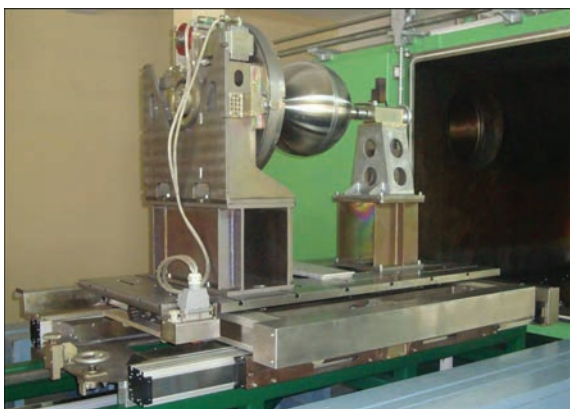
Figure 3. Two-coordinate work table of medium-sized unit with welding manipulator (rotator) mounted on special stands and tailstock

Figure 4. Medium-sized unit with mobile welding gun and one-coordinate work table

are selected, proceeding from the maximum admissible value of working distance from EB gun to outer surface of parts of a specific typesize.

In some cases, by customer request, combined schematic of linear welding displacement is used in mid-sized units (Figure 4): mobile EB gun module, moving along welding chamber roof along one axis (usually, Y axis) and one-coordinate work table, moving along the other — transverse axis (axis X, respectively).

Irrespective of the above-mentioned schematic of welding displacement, typical linear working travel of such units is about 500 mm along both axes X and Y. Such working travel along axis X is due to sufficiently large length of work table top, capable of accommodating welding manipulator and tailstock along its length, with welded item fixed between them.

Units of this type are usually fitted with high-voltage welding power unit of 15 or 30 kW (at fixed accelerating voltage of 60 kV).

Such units, similar to «small» ones, can be used for welding all kinds of small-sized parts with linear and circumferential welds from any structural metals, including also aluminium, magnesium and titanium alloys of up to 60 mm maximum thickness. Nonetheless, their main purpose is welding cylindrical and spherical parts of up to 700 mm diameter. So, in particular, these units perform welding of billets of hemispheres of spherical tanks of various typesizes from structural titanium alloy Ti–6Al–4V and their subsequent final joining by through-thickness circumferential weld (see Figure 3).

3. *«Large» (large-sized) units* (Figure 5) have welding (vacuum) chamber of 19 to 42 m^3 volume.

Working pressure in EB gun is less than $5 \cdot 10^{-5}$ Torr, and in the welding chamber it is not higher than $(2.5-4.0) \cdot 10^{-4}$ Torr. Time of complete pumping down (i.e. both welding chamber and gun) is not more than 20–40 min, depending on vacuum system components.

Unit configuration envisages mobile in-chamber welding gun, precision CNC displacement mechanism of which ensures linear movement along three

Figure 5. Large-sized unit with mobile in-chamber welding gun and work table (roll-out carriage)

coordinate axes (along the chamber — X, across the chamber — Y, and vertically — Z), as well as gun inclination up to 90° in Z–X plane (from gun «vertical» orientation to its «horizontal» orientation).

Unlike earlier described smaller units, work table in «large» units does not participate in the movement and is a loading-unloading carriage, with upper mounting plate with T-shaped slots, designed for placing and fixing various types of welding manipulators and additional accessories to them, as well as for all kinds of specialized welding fixtures for non-rotating parts and components. Naturally, there is the respective mechanism of work table movement on rails from the chamber to external loading-unloading platform, and back into the welding chamber with smooth approach to parking position.

A feature of «large» unit design is the fact that the above-mentioned gun rotation is realized through rotation of the base of cantilever beam, carrying the mechanism of displacement along axis Y (Figure 6). Here, this rotation assembly proper can move freely within the greater part of welding chamber in Z–X plane.

Depending on the unit purpose, the welding gun module can have an additional degree of freedom: CNC-axis of gun rotation by ±45° in a plane parallel to axis Y.

Rotation of the part being welded is usually ensured by one of three standard welding manipulators: welding manipulator with horizontal axis of rotation (it is usually supplied with tailstock of respective height), welding manipulator with vertical axis of rotation (both the manipulators can be replaced by one all-purpose manipulator, designed for both the orientations (horizontal and vertical), and welding manipulator with inclined axis of rotation. The latter

allows inclination of the axis of faceplate rotation in the range from –30 up to +90° (from the vertical), that enables handling, for instance, complex sections of aircraft engines (Figure 7), or other aircraft components, for instance, aircraft wing pylon (Figure 8).

To expand production capabilities, welding chambers in «large» units can have not one, but a pair of «sliding» working doors and a pair of mobile work tables, respectively.

This type of units is fitted high-voltage welding power unit of 15, 30 or 60 kW (at fixed accelerating voltage of 60 kV), depending on specific materials being welded and their thicknesses.

Such units can be called «conditionally all-purpose» as they, in principle, can be used for welding most of the components fitting into in-chamber di-
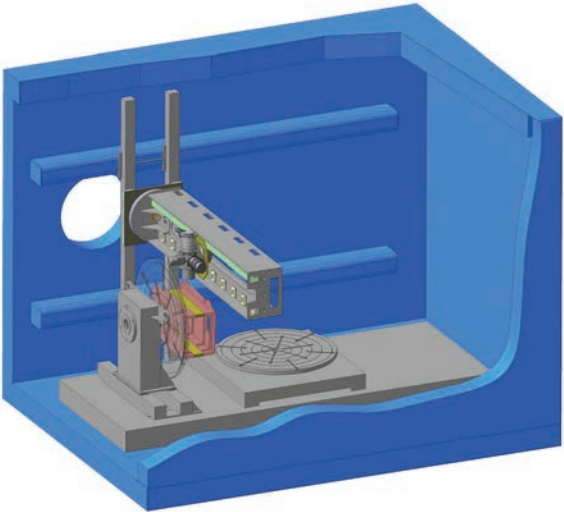
Figure 6. Model of in-chamber mechanisms of typical large-sized unit for EBW
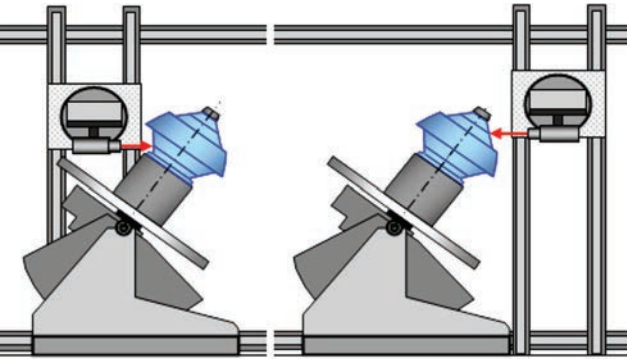
Figure 7. Example of EBW schematic of rotating parts of complex shape using welding manipulator with inclined axis of rotation

mensions, welded thicknesses of which are within the capabilities of the supplied power unit. However, their typical purpose is welding components of aircraft engines and other comparatively compact parts and components [6] (Figures 9–12).

4. *«Superlarge» (particularly large-sized) units* have welding (vacuum) chamber volume of 80 to 100 m³.

As to their purpose, such units (Figure 13) do not, in principle, differ from «large» ones and can also be regarded as «conditionally all-purpose», but they are designed for components of much larger dimensions, respectively. The range of thicknesses being welded still is within the limits of capabilities of similar welding power units of 15, 30 or 60 kW (at fixed accelerating voltage of 60 kV).

Thus, the purpose of such units is welding large-sized components of aircraft engines and other large-sized and long parts.

Working pressure in EB gun is below $5 \cdot 10^{-5}$ Torr, and not higher than $(2.5-4.0) \cdot 10^{-4}$ Torr in the welding chamber. Time of pumping down the welding chamber and the gun is not more than 20–40 min (it also depends on the set of vacuum system components and on required working vacuum).

To ensure such comparatively short time of pumping down, this type of units are fitted with efficient vacuum systems (Figure 14).

Figure 9. Billet of section of aircraft engine from titanium alloy

Configuration of such units further incorporates mobile in-chamber welding gun, precision CNC displacement mechanism of which ensures similar linear motion along three coordinate axes (along the chamber — *X*, across the chamber — *Y*, and vertically — *Z*), as well as gun inclination up to 90° in *Z–X* plane. This gun inclination is also realized through rotation of the entire mechanism of displacement along *Y* axis. However, unlike «large» units, in «superlarge» units gantry design is usually used instead of cantilever design. Here, the parts of rotating mechanism of the beam of *Y* axis (i.e. angle of gun inclination in *Z–X* plane) are fixed between two symmetrical gantries, which ensure free movement of the gun in greater part of welding chamber in *Z–X* coordinate plane. Depending on the unit purpose, it can additionally be fitted with CNC-axis of gun rotation through ±45° in the plane parallel to *Y* axis.

Similar to «large» units, welded component rotation is ensured by one of three standard welding ma-

Figure 8. Pylon of aircraft wing on welding manipulator with inclined axis of rotation

Figure 10. Billet of aircraft component of titanium alloy butt welded from several sections
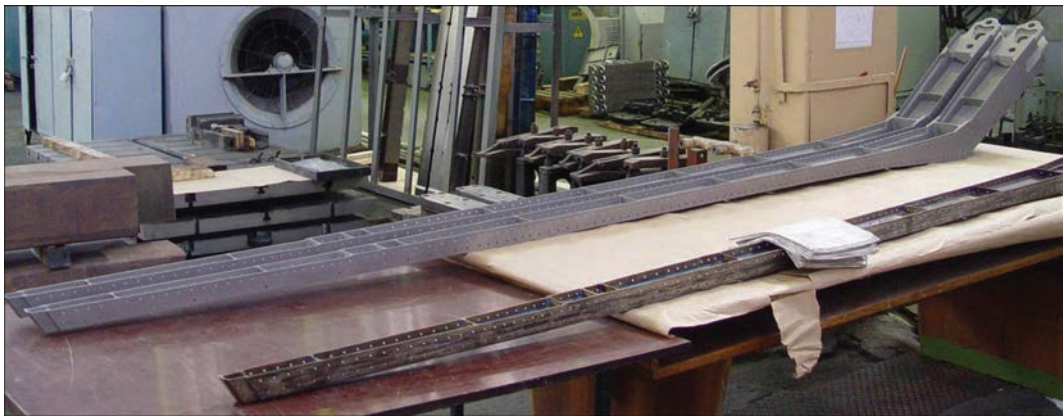
Figure 11. Long aircraft structures welded by electron beam
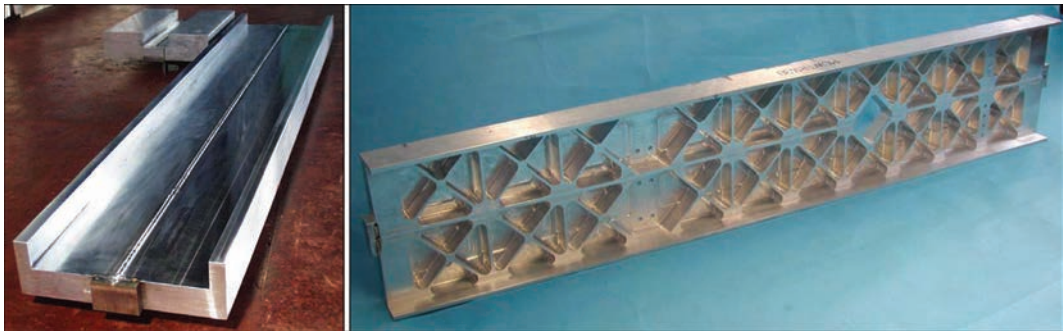
Figure 12. Welded blank (*left*) of aircraft wing beam from high-strength aluminium alloy (*right* — beam after machining)

nipulators: welding manipulator with horizontal axis of rotation (usually paired with the respective tailstock), welding manipulator with vertical axis of rotation, and welding manipulator with inclined axis of rotation.

All types of units are fitted with modern high-voltage inverter welding sources of respective power (set up for fixed accelerating voltage of 60 kV). The source was specially developed for highly efficient and reliable EBW: minimum response time of control circuits

of accelerating voltage and welding current (electron beam current) has markedly improved their stability.

High-voltage inverter power unit is used as the source of 60 kV accelerating voltage. The other part of welding source, including filament and bias modules, as well as stabilizer crate, incorporates all the recent PWI developments in the field of EBW control. As a result, all key channels (accelerating voltage channel, channels of filament and bombardment of

Figure 13. Appearance of superlarge unit fitted with mobile in-chamber welding gun and two work tables (loading-unloading carriages). Chamber is fitted with two doors

Figure 14. Vacuum system of welding chamber of 100 m³ volume

welding cathode) have high-frequency power, formed on the basis of signals of individual microcontroller, operating by the respective algorithm. In terms of design all the high-voltage parts of the source are located in a special oil tank (Figure 15, position *a*), and low-voltage boards are in stabilizer crate (position *b*) and in the module (modules) of high voltage control (position *c*). Differing «earth» levels are galvanically decoupled and have separate power sources. Setting and feedback connection of different levels is performed through fiberoptic lines.

Welding source is quite compact in size and at up to 30 kW power inclusive, it usually fits into one power cabinet, to which power and interface cables are connected, and from which just the power cable comes out (usually through the roof), which powers the gun. In the case of 60 kW power the welding source usually consists of two parts.

Welding source is a hardware complex, all interaction with which proceeds through industrial interface (CAN bus). The only exception is special modulation signal from RASTR system, fed in the initial form. This is realized due to external connections being provided by respective microcontroller modules, connected to CAN bus and designed for control and diagnostics of all the welding source channels. These modules, in their turn, directly interact with actuator elements of the welding source, including the commercially manufactured accelerating voltage source.

Together with the welding source, all the units are fitted with RASTR-6 system of secondary-emission electron imaging, integrated into this source. Such integration is due to the fact that functioning of this system is directly related to formation of the electron source. The integration results in the welding source momentarily forming, on the base of modulation signal generated by RASTR-6 system, an electron scan pattern on the welded part surface by a low-power («probing») electron beam, controlled by microcontroller of welding current channel by a special law.

At passing of «probing» electron beam along the scan pattern lines, secondary electrons are emitted in
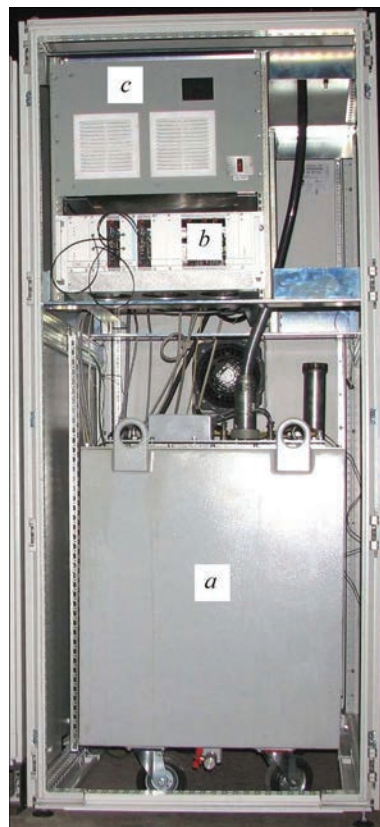
Figure 15. Cabinet of welding source of 15 kW power

the site of point bombardment of the part surface by beam electrons (primary). These electrons are captured by special passive sensor (Figure 16, *a*) usually located on welding gun end face, which can be of different design (usually depending on application area, i.e. it can be adapted to suit the configuration of welded parts). Located directly near this sensor, is a compact module of preamplifier, which forms and enhances the useful signal, the voltage of which is proportional to current value read from the sensor. This, already amplified signal, is taken out of the chamber through a shielded line and comes to the system main video amplifier. Ultimately, the signal is digitized by specialized computer board WLCA and is output to the interface in the form of an image (Figure 16, *b*) used both for visual observation and for manual guidance to the butt being welded, and for operation of special program algorithms helping the user (welding operator) to make new welding programs and reproduce the already existing programs in welding of recurring typical parts. The system allows forming a quite stable image of the welding zone, both before the start of welding and after its completion, and directly during performance of welding proper.

RASTR-6 system design incorporates microcontroller module of forming process scan patterns, controlled by CAN bus, as is the entire welding source. As a result, scan signals generated by this module in both the channels (deflecting coil poles) are enhanced
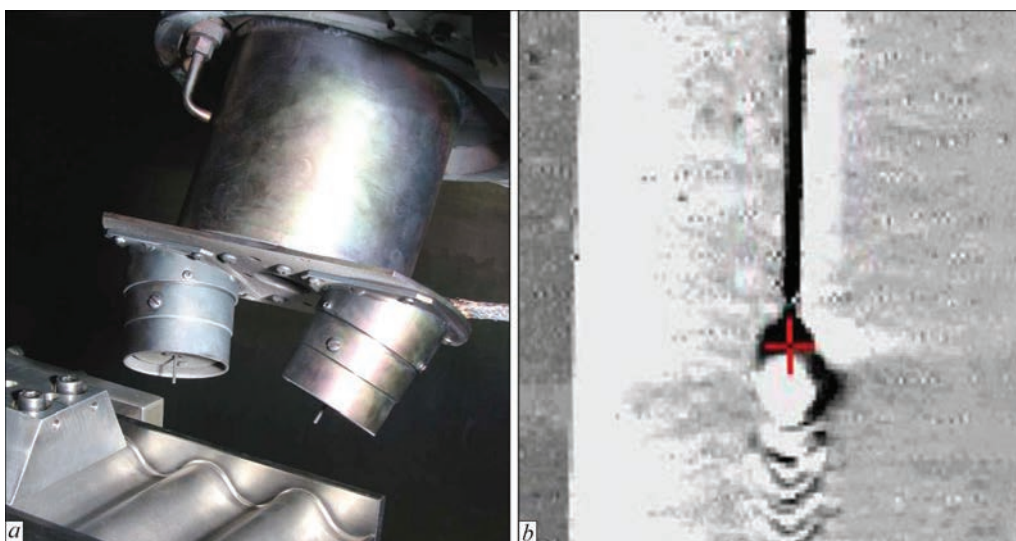
Figure 16. Sensor of secondary electrons of RASTR-6 system (*a*), and welding zone image formed by it (*b*)

by standard amplifiers of line and frame scanning of RASTR-6 system.

All EBW units, developed and manufactured at PWI, have modern system of controlling all the equipment included into their structure. The main part of the equipment, on which the welding process proper depends, is under continuous program control, providing both fully automated and manual mode of this equipment functioning. Here, the concept of high-level program control is used. User interacts with the equipment solely through Windows-oriented graphic interface (GUI), which is operated using standard tools: keyboard and mouse-type manipulator. Interface was developed so as to be intuitively clear to any person, who has already used software in Windows OE, and requires absolutely no special qualifications for operating low-level machine programming (G-codes, etc.). Each of equipment subsystems has the respective window graphic tools with the required checking of input data and locks, primarily, to ensure the safety of the user himself and of equipment operated by him. The program has all the tools for controlling the vacuum system, manual displacement of welding gun and part, manual control of welding parameters, compiling automatic welding programs (welding by a program), their storage and fulfillment, as well as tools for acquisition and storage of diagnostic information on operation of key subsystems of the unit, administrative tools, etc.

Hierarchical control system was divided into two hardware levels. Upper level includes all the tools for interaction with the user, including graphic interface, tools for welding program compiling and storage, diagnostic data acquisition and storage, administering, etc. Lower level directly supports fulfillment of all the procedures by commands from the upper level.

At present PWI uses two basic configurations of the system of EBW unit program control. The first envisages application of Siemens complete industrial system (CNC + PLC) Sinumeric 840D, and the second one — application of trimmed industrial system Synamics S120, also of Siemens company.

In the case of application of complete Sinumeric 840D system, the main user interaction program is installed in standard upper level industrial computer Sinumeric PCU-50, operating in Windows environment.

Profinet system is used to transmit data from its upper level to lower software and hardware level, which includes: machine control panels Sinumeric MCP, Sinumeric NCU, connecting module Basic PN, to which mobile manual terminal Sinumeric HT 2 is connected (it is used as remote panel to control manual movement of the gun/part). In its turn, NCU, through network connection DRIVE-CLiQ, interacts with the modules of servomotors of welding displacement axes and their encoder modules, and through ProfiBUS bus it interacts with analog and digital input/output station Simatic ET 200M.

Computer servicing RASTR-6 system is an additional element of the lower level. Control program of this system is in constant interaction with upper level main program (in PCU-50), using Ethernet-connection. As a result, upper level program can at any moment display the secondary emission image of welded part surface, formed and transmitted by RASTR-6 system. More over, at operation of specialized automated algorithms of «searching» for the butt being welded (when making the program of the trajectory of welding a new part and for correction of the existing trajectory in welding typical recurring parts) both the control programs of the upper level and of RASTR system operate inseparably.

Welding displacement (gun/part) is CNC controlled (Sinumeric NCU), both in manual displacement mode, and in automatic welding. In the latter case, the text script prepared on the upper level of

welding program is transmitted to NCU, where CNC, by its own algorithms, performs complete calculation of the trajectory, interpolations, velocities and accelerations along each of the axes. In automatic welding, CNC provides complete synchronization of all the axes, both mechanical, and virtual, for which channels of welding and focusing currents, as well as of process scanning of the electron beam, are used. Here, control tasks of these virtual axes are read from DMP module of high-speed outputs of Simatic ET 200M station, and are converted to the protocol of CAN bus (from which high-voltage welding source is controlled).

Control of welding parameters in the manual mode is performed from upper level computer, for which it has the respective CAN bus adapter.

NCU programmable logic controller (PLC) controls the vacuum system, using analog inputs, as well as digital inputs and outputs of Simatic ET 200M station. In the automatic mode the user just issues (from upper level) the commands for switching the respective operation mode of vacuum system («Pumping down», «Air», «Waiting» or «Stop»), the other decisions being taken by PLC, in keeping with the algorithm entered into it. Contrarily, in the manual mode, the user can control each vacuum system element directly (through the respective functions of the same PLC algorithm). Such a mode is designed exclusively for adjustment or repair operations, as all the locks of automatic algorithm are switched off, and the user takes up full responsibility for correct operation of the system that is always potentially dangerous.

The described control system has been actually introduced into standard modern machine CNC complex, the reliability of operation of which is ensured by many-year stepped evolution of the entire complex. Here, it should be noted that as a control complex for a welding unit with high-level control, it is somewhat redundant in its functionality (particularly, as regards CNC capabilities) and is not quite rational in terms of structure. In the latter case, we mean that stationary control panel Sinumeric MCP is not used at all, and high-speed analog outputs are actually used for other purposes. More over, an additional computer is required to control RASTR-6 system.

The above considerations led to control system based on «complete» Sinumeric 840D complex being used only by special customer request. In all the other cases, in EBW units (developed at PWI) a specialized two-level control system is applied, which is based on two simple standard single-board industrial computers, using «trimmed» Synamics S120 complex as the actuating mechanism to control multiaxial welding displacement and vacuum system. One of the computers is designed for functioning of Windows program of upper level control, with which the user interacts,

and the second operates as the lower level — as CNC and PLC simultaneously. Modern computer capability is quite sufficient for performance of both high-priority tasks, characteristic for CNC, and for low-priority tasks, characteristic for PLC. Ultimately, one lower level program runs in the computer under control of real-time operating system QNIX. This program is responsible for control of multiaxial welding displacement and welding source (and for synchronizing their simultaneous operation), as well as control of vacuum system and RASTR-6 system.

Both the industrial computers have respective Ethernet-adapters for exchanging the data of upper and lower level programs, as well as respective CAN bus adapters. In addition, lower level computer has Profi-BUS bus communications board (adapter).

As a result, interaction of all the system elements is almost completely performed through industrial CAN and ProfiBUS buses. Lower level program, via ProfiBUS bus, controls the vacuum system through Simatic ET 200M station, and controls welding displacements through the main part of Synamics S120. Here, in the case of automatic welding (by a program) it synchronizes the movement with the change of welding parameters via CAN bus. Manual movement tasks are transmitted to lower level either from upper level program, or from remote panel via CAN bus. Otherwise, control of both the welding source and RASTR-6 system is similar to the first considered variant.

PWI is in the process of continuous improvement of EBW equipment control system, enhancing the convenience and functionality of the developed equipment, taking into account the steadfast evolution of the hardware and component base, as well as accumulated many-year experience of development of the technology and equipment for EBW of diverse materials and their thicknesses.

1. Nazarenko, O.K., Kajdalov, A.A., Kovbasenko, S.N. et al. (1987) *Electron beam welding*. Ed. by B.E. Paton. Kiev: Naukova Dumka.
2. Ilyushenko, R., Nesterenkov, V. (2006) Novel technique for joining of thick section difficult-to-weld aluminium alloys. In: *Proc. of 10th Int. Conf. on Aluminium Alloys* (Vancouver, Canada, July 9–13, 2006), Vol. 519–521, 1125–1130.
3. Paton, B.E., Nazarenko, O.K., Nesterenkov, V.M. et al. (2004) Computer control of electron beam welding with multi-coordinate displacements of the gun and workpiece. *The Paton Welding J.*, **5**, 2–5.
4. Akopiants, K.S., Nesterenkov, V.M., Nazarenko, O.K. (2002) Electron beam welding of 60 mm thick steels using longitudinal oscillations of beam. *Ibid.*, **9**, 2–4.
5. Nazarenko, O.K. (2008) Up-to-date equipment of the E.O. Paton Electric Welding Institute for electron beam welding. *Ibid.*, **10**, 31–35.
6. Bondarev, A.A., Nesterenkov, V.M. (2013) Examination of weldability of MA2 magnesium alloy by electron beam in vacuum. *Kompres. Mashinostroenie*, **2**, 21–28.

ELECTRON BEAM WELDING
OF CENTRIFUGAL COMPRESSOR IMPELLERS

V.M. NESTERENKOV, L.A. KRAVCHUK and **Yu.A. ARKHANGELSKY**

E.O. Paton Electric Welding Institute, NASU

11 Kazimir Malevich Str., 03680, Kiev, Ukraine. E-mail: office@paton.kiev.ua

Nowadays the impellers of centrifugal machines are manufactured by vacuum brazing, arc welding and braze welding. In order to achieve a more perfect production of impellers the technology of electron beam welding of T-joints of the «disc–blade» type as-applied to impellers of centrifugal machines was developed. The investigations on the development of technology for EBW of high-alloy corrosion-resistant steel X3CrNiMo13-4 of austenitic-martensitic class were carried out to create an impeller of the centrifugal compressor with wall thickness of the covering disc of 12, 15, 20 mm and 6 mm thickness of the blade. The optimal power, time and spatial parameters of the electron beam were obtained providing the formation of high-quality welds of a slot type of the required penetration depth. To produce fillets of 2–3 mm radius the joining method between the blade and the covering disc was proposed by melting metallic inserts which were fastened on the both sides of the blade. The impeller of centrifugal compressor, welded according to the developed technology, passed static and dynamic balancing with the subsequent acceleration tests. The developed technology of EBW of impellers can be used in the structures intended for service under the vibration loads. 6 Ref., 14 Figures.

K e y w o r d s : electron beam welding, centrifugal compressor, blades, discs, high-alloy steel, T-joint, high-temperature brazing alloys, fillet, acceleration tests

EBW refers to the methods of welding using highly-concentrated power sources, allowing joining the metal of up to 300 mm thickness in one pass. The high levels of ductility of welded joints provide a successful application of EBW in the production of parts made of heat-hardened materials, when the postweld heat treatment is not possible.

The technological prospects of EBW give opportunity to design and create the new high-performance designs of gas-turbine engines. For example, the new challenging task of the power engineering is the manufacture of impellers of the centrifugal compressor with improved operational characteristics, as well as the improvement of reliability of the input and reverse guiding devices [1].

An impeller of the centrifugal compressor consists of the main and the covering disc with the blades located between them forming inter-blade channels. During operation of the impeller under the action of inertial forces a dust is deposited on the main disc and is pushed out to the perimeter of the impeller under the action of centrifugal forces. Considering the high speeds of impeller rotation, the movement of dust along the inter-blade channels is accompanied by a wear of the blades. To the most intensive wear the places of mating the blades with the main and the covering disc of the impellers are subjected. Therefore, to increase the life of operating impellers of centrifugal compressors it is necessary to produce mating places with radius of 2–3 mm. The development of technological process for joining the covering disc with the blades providing the mating radius of 2–3 mm is the aim of this work.

For manufacture of compressor impellers, steel 1.4313 (according to DIN — X3CrNiMo13-4) is widely used, which refers to the corrosion-resistant steels of austenitic-martensitic class. The chemical composition of steel 1.4313 according to standard EN 10088-3 is the following: wt.%: $\leq$0.05 C; $\leq$0.7 Si; $\leq$1.5 Mn; 12–14 Cr; 0.3–0.7 Mo; $\geq$0.02 N; $\leq$0.04 P; $\leq$0.015 S; 3.5–4.5 Ni. The mechanical properties of steel are the following: $\sigma_{0.2} \geq$ 800 MPa; $\sigma_t \geq$ 900 MPa; $\delta \geq$ 12 %; $\psi \geq$ 40 %; $KCV \geq$ 70 J/cm^2.

The investigation of characteristics of EBW of steel X3CrNiMo13-4 in vacuum was carried out in installation UL-209M with the computer control of all the parameters and systems. Installation UL-209M is equipped with power complex ELA-60/60 and EB gun moved inside the vacuum chamber along linear coordinates X, Y, Z, and also rotated around axis Y–Y along coordinate QG at angle of 0–90°. Additionally, the installation is modified with a rotator having a horizontal rotation axis (Figure 1).

The vacuum chamber of the installation with inner dimensions of 3850×2500×2500 mm and volume of 24 m^3 is pumped out in the automatic control mode to operating vacuum of $2.66 \cdot 10^{-2}$ Pa ($2 \cdot 10^{-4}$ Hg mm) for 25 min.

Figure 1. General view of EB installation UL-209M

During accelerating voltage $U_{acc} = 60$ kV the EB gun with of tungsten cathode together with power complex ELA-60/60 provides the range of EB current of 0–500 mA and the formation of technological beam scans in the process of EBW (circle, ellipse, dash line, triangle) with amplitude of 0–4 mm. The positioning accuracy of the EB gun along the coordinates was not less than 0.1 mm. The image of welding place in the secondary emission electrons and also centering the electron beam with the butt at accuracy of not less than 0.1 mm was performed using RASTR-6 system.

During practicing the technology of EBW of steel X3CrNiMo13-4 the control of electron beam focusing was carried out according to the definition of beam trace image on the specimen surface displayed on the monitor of RASTR-6 system and in parallel according to the brightness of illumination of the circular beam scan of diameter $d_c = 5$ mm with $I_b \sim 10$ mA on the copper plate. The discrepancy of the compared focusing current values at operating distance from the

Figure 2. Scheme of T-joint of «disc–blade» type: H — weld depth; $H1$ — height of weld reinforcement; S — thickness of covering disc; $B1$ and $B2$ — weld width in its upper part and in the contact plane of covering disc with blade, respectively

gun cut to the plates to be welded in the range of $L_{op} = 150$–250 mm amounted to ±1 mA at the level of $I_f = 620$–650 mA, that is quite acceptable for practical application.

At the first stage of investigations the technology for joining the covering disc with the blade was practiced using slot welds. Taking into account the design features of the impeller, the most optimal EBW parameters were selected providing the formation of welds of 16, 19 and 25 mm depth. The system of simultaneous movement of the gun of installation UL-209M along coordinates X–X, Y–Y and Z–Z together with RASTR-6 system provides positioning of the electron beam along the surface of the covering disc at accuracy of 0.1 mm. At the same time, on the produced T-joints the weld root is located exactly in the center of the blade (Figure 2).

Before the assembly of T-joints the surfaces of the blade and the disc were degreased with a solvent or alcohol. The assembly for EBW was carried out applying spot tacks using argon arc welding along the ends of the billets at $l_{op} = 150$ mm and $I_f = 665$ mA.

At 12 mm thickness of the covering disc the required weld formation was achieved at the following mode: $I_w = 110$ mA, $I_f = 658$ mA, $v_w = 4.2$ mm/s, amplitude of the transverse scanning $A = 4$ mm. The obtained weld geometry was the following: $B1 = 7.5$ mm, $B2 = 3.5$ mm with penetration depth $H = 16$ mm and height of face bead $H1 = 1.7$ mm.

With the growth in thickness of the covering disc to 15 mm the EBW parameters were changed to the following values: $I_w = 120$ mA, $I_f = 655$ mA, $v_w = 3.5$ mm/s at $A = 4$ mm. Under such modes a good formation of the face weld with $B1 = 8$ mm, $B2 = 3.7$ mm, $H = 19.5$ mm and $H1 = 1.7$ mm was obtained.

For welding of T-joints of the covering discs of 20 mm thickness the following EBW parameters were used: $I_w = 130$ mA, $I_f = 652$ mA, $v_w = 2.8$ mm/s, $A = 4$ mm, and good formation of face bead with $B1 = 9.0$ mm, $B2 = 3.5$ mm, $H = 24.5$ mm and $H1 = 1.9$ mm was obtained.

The general view of the EB-welded upper beads of the covering discs of 12, 15 and 20 mm thickness is shown in Figure 3, and their cross-section — in Figure 4.

The carried out quality control of welded joints showed the absence of any defects in them.

To produce fillet of 2–3 mm radius between the blade and the covering disc the possibility of applying brazing alloys and additional metal inserts in the mating places was investigated. Such technological processes are known and their results are published in the literature [2–6].

In the work the brazing alloys were used, widely applied in the industry of Ukraine. First of all, they in-
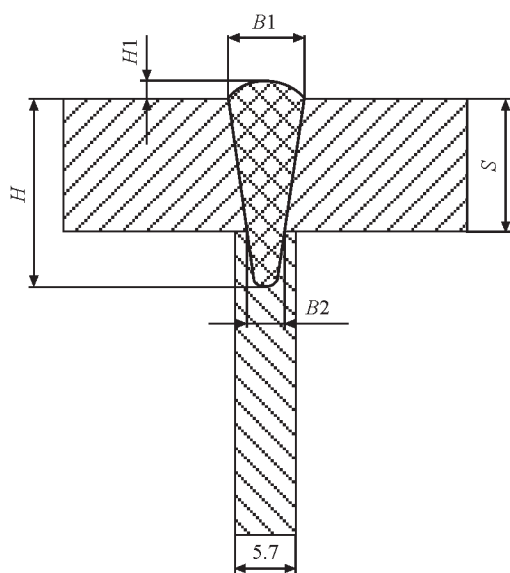
Figure 3. Appearance of EB-welded «disc–blade» T-joints of 12, 15 and 20 mm thickness

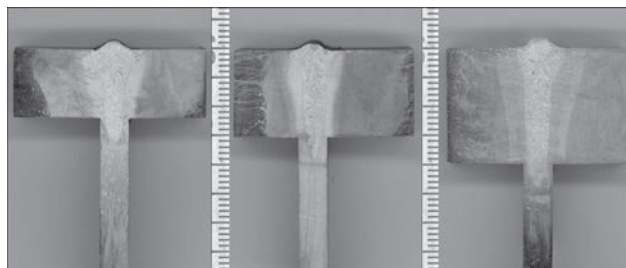**Figure 4.** Cross sections of welds produced in EBW «disc–blade» joints of 12, 15 and 20 mm thickness

clude high-temperature brazing alloys VPr2, Vpr2M, PMFS 6-0.15 and powdered brazing alloys based on Cr, Ni, Si and B. In the proposed technological scheme it was supposed to produce melting of brazing alloy and formation of fillets due to the heat from heating of metal during EBW.

Brazing alloy VPr2 (PM20ML) refers to the copper brazing alloys, providing high quality of brazed joints. The joints brazed with VPr2 have a significantly higher strength than those brazed with silver brazing alloys. These brazing alloys are not characterized by the ability to selective penetration along the grain boundaries of stainless steels and, therefore, can be applied for brazing of thin-walled structures. In non-aggressive environments the corrosion resistance of the joints brazed using these brazing alloys almost does not differ from the corrosion resistance of the joints brazed with silver brazing alloys.

Also, brazing alloy PMFS 6-0.15 alloyed with silicon or silicon and silver with decreased content of phosphorus has good properties. The limits of the alloying elements content in the brazing alloy are the following, wt.%: 5–8 P; 0.1–1.5 Si; Cu is the rest. The brazing alloy of this composition is recommended for brazing of products of copper and brass operating without the exposure to significant impact loads. Melting point of brazing alloy is 725 °C, brazing temperature was 750–780 °C. For the products with an increased impact toughness of brazed joints the brazing alloy with the following composition was proposed, wt.%: 5–6 P; 3 Ag; 0.15 Si; Cu is the rest; brazing temperature was 750–780 °C.

To apply the brazing alloy into the blade-covering disc T-joint, the mixture based on acrylic resin BMK-5, powdered brazing alloy and solvent was prepared. This dough-like mixture was applied to the T-joint as is shown in Figure 5. After solidifying of the mixture in the air the specimens were loaded to the vacuum chamber and welding was performed at the already selected modes.

Unfortunately, this technological method did not give a positive result. Regardless of grade of brazing alloys a reliable formation of mating after EBW failed to be produced.

In the further developments the brazing alloys in the form of foil were applied:
- Cu-based brazing alloy 1.5 mm thick;
- brazing alloy based on brass 1.5 mm thick;
- steel brazing alloy without copper 1.5 mm thick;
- steel brazing alloy with low mixture of copper 1.5 mm thick;
- steel foil 0.1 mm thick;
- brass foil 0.1 mm thick.

For brazing alloys in the form of foil the scheme of assembly of welded joint was used shown in Figure 6. The upper edge of the blade was inserted into the milled groove on the covering disc of 1 mm depth. Between the walls of blade and the side surface of groove a gap was provided, into which the brazing alloy of a rectangular cross section was tightly laid. Thus, the width of groove was changed depending on the thickness of the applied brazing alloy.

The plates of brazing alloy, which were pressed into the groove, had a thickness from 0.1 to 1.5 mm. After pressing and fixing the T-joint in the vacuum chamber, welding was performed according to the selected modes. But, as a result, none of the applied brazing alloys allowed obtaining the uniform formation of fillet between the blade and the disc. The best formation was obtained when applying brazing alloy based on brass and copper, however, the confident wetting of brazing alloy with the surface of the disc was also absent (Figure 7). The macrosection of welded joints with the copper brazing alloy is shown in Figure 8.

To provide a reliable formation of fillets the method of joining the blades with the covering disc with additional passes and melting of steel additives X3CrNiMo13-4 using electron beam was proposed. The scheme of the process is shown in Figure 9.
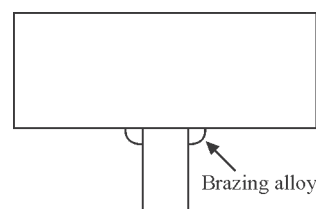
Figure 5. Scheme of brazing alloy embedding into T-joint
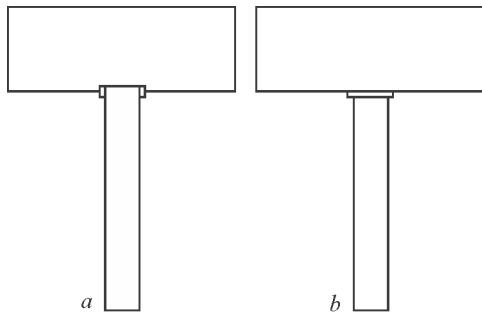
Figure 6. Scheme of embedding brazing alloy into «blade–covering disc» joint: *a* — using groove in covering disc; *b* — without groove

The additive was attached on the both sides of the blade (Figure 9) and EBW of the «disc–blade» joint was performed by vertical beam at the modes mentioned above. After that the specimen was turned over 90° and fixed on the desktop. The EB gun was posi-

Figure 7. Formation of mating using brazing alloy based on brass (*a*) and copper (*b*)

Figure 8. Macrosection of welded «blade–disc» joint produced using copper brazing alloy

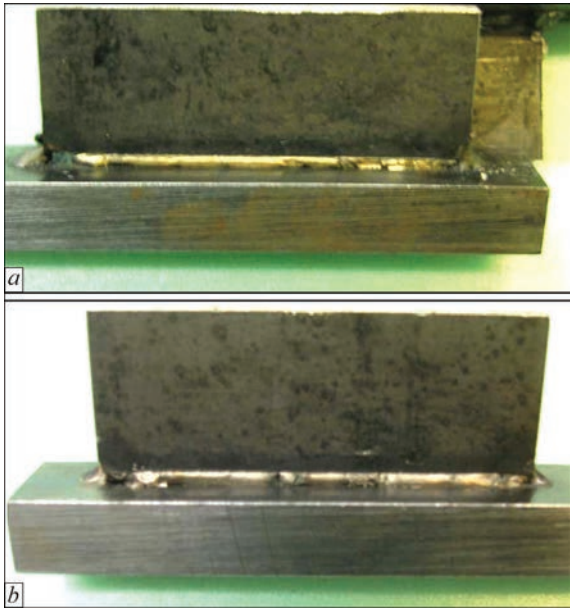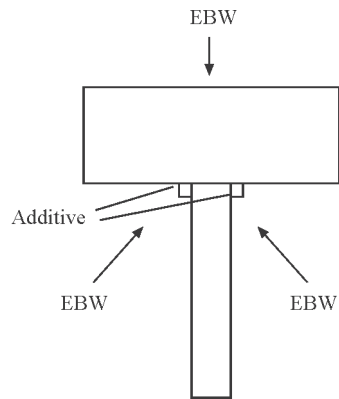**Figure 9.** Scheme of welding «blade–disc» T-joint using electron beam for melting additive of steel X3CrNiMo13-4

tioned at angle of 5° to the horizontal, allowing the beam to penetrate into the gap of the impeller for the whole length of the blade, to melt the additive and form a fillet. As a result a reliable weld and a perfect fillet formation of the «disc–blade» joint were produced (Figures 10 and 11).

The obtained results of EBW of models of the «blade–disc» joints of the impeller allowed us to design, manufacture and weld a model similar to real impellers produced at Company «Sumy Frunze NPO».

The gun fixed at a certain angle was moved along the coordinates *Z–Z* and *Y–Y*. Simultaneously with the movement of the gun the rotation of the mock-up was carried out using a precision rotator. Working out of the program of changing the coordinates of gun and mock-up movement in time was carried out using monitoring system RASTR-6. The uniformity of fillet formation between the disc and the blades is shown in Figure 12. The ultrasonic quality control of joints along the entire length of the blades did not reveal any deviations.

At the final stage of the investigations the impeller of centrifugal compressor of steel X3CrNiMo13-4 was prepared and welded (Figure 13). After the cleaning, assembly and coupling of the main and the covering discs the impeller was mounted on the rotator and

Figure 10. Formation of transition «blade–disc» joint during melting of additive with electron beam

Figure 11. Macrosection of produced «blade–disc» joint

Figure 12. Formation of fillets on the impeller model

Figure 13. General view of main and covering discs of impeller before assembly and welding

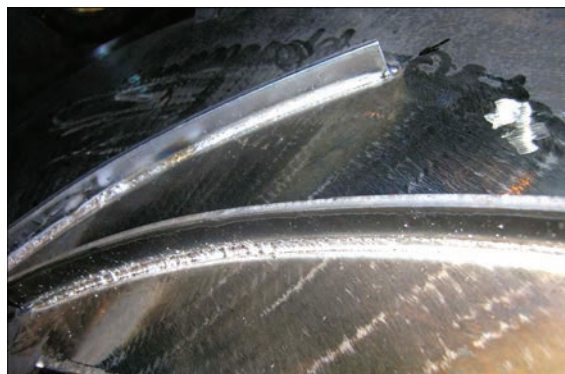placed into the vacuum chamber. Using the worked out technological process, the fillets were welded first on the side of convex part of the blades, and then on the side of aconcave one.

The movement of the gun was carried out along the two coordinates: X–X and Y–Y, and the workpiece rotation during welding was provided by a high-precision rotator. EBW was carried out at the following mode: $U_{acc} = 60$ kV, bombardment current of 65 mA, $L_{op} = 300$ mm, $I_w = 65$ mA, current of focusing lens of 615 mA, and $v_w = 4$ mm/s. General view of the welded impeller is presented in Figure 14.

After the final machining the impeller passed static and dynamic balancing with the subsequent acceleration tests at rotation speed of 11,295 rpm. After acceleration tests the reference sizes of the impeller were measured, which were preserved and equal to the corresponding sizes before the acceleration tests.

Thus, the possibility of manufacturing the centrifugal machine impellers was confirmed applying EBW, which provides the formation of fillets between the disc and the blades of 3 mm radius. The results of the work allow recommending the EBW technology for manufacture of standard impellers of the centrifugal machines.
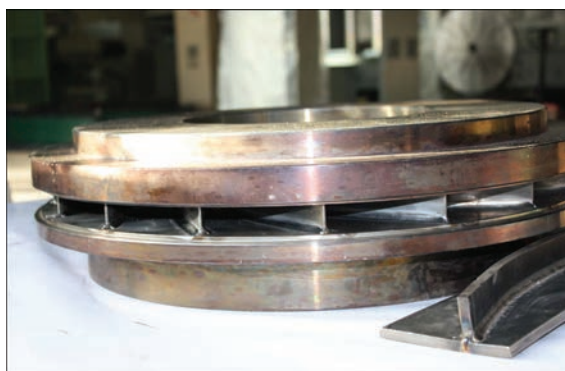
Figure 14. General view of welded impeller with fillets of 3 mm radius between blades and covering disc

1. Belousov, A.N., Musatkin, N.F., Radko, V.M. (2003) *Theory and calculation of aircraft impeller machines*. Samara: Samarsky Dom Pechati.
2. Laflamme, G., Rugh, J., MacWilliams, S. et al. (2006) Hybrid EBW process joins heavy-duty impellers. *Welding J.*, **1**, 44–47.
3. Myers, L., Laflamme, G. (2000) Electron beam braze welding of compressor impellers. *The Paton Welding J.*, **8**, 53–57.
4. *C7.1M/C7.1:2004*: Recommended practices for electron beam welding. Miami: AWS.
5. Radzievsky, V.N., Gartsunov, Yu.Yu., Tkachenko, G.G. et al. (2001) Specifics of formation of thick-wall T-joint using brazing and fusion welding. *Svarochn. Proizvodstvo*, **4**, 42–46.
6. Radzievsky, V.N., Rymar, V.I., Bespalov, V.K. (1991) Vacuum brazing of T-joints with large fillet from metallic powder. *Ibid.*, **8**, 5–6.

NEW ELECTRON BEAM EQUIPMENT AND TECHNOLOGIES FOR PRODUCING OF ADVANCED MATERIALS USING VACUUM MELTING AND EVAPORATION METHODS DEVELOPED AT SPE «ELTEKHMASH»

N.I. GRECHANYUK, P.P. KUCHERENKO, A.G. MELNIK, I.N. GRECHANYUK,
Yu.A. SMASHNYUK and **V.G. GRECHANYUK**
SPE «Eltekhmash»
25 Vatutin Str., 21011, Vinitsa, Ukraine. E-mail: vin25ebt@ukr.net

The paper presents the designs of laboratory and production electron beam equipment, developed at SPE «Eltekhmash». Recent achievements of the Company in the following fields are briefly considered: development of industrial technologies for producing heat-resistant alloys and items from them for coating deposition by electron beam and ion-plasma methods; powders for plasma deposition of coatings, and special titanium alloys for medicinal purposes. 11 Ref., 6 Tables, 10 Figures.

At present it is difficult to visualize development of many industrial sectors without application of modern electron beam technologies. Electron beam equipment and technologies are the object of numerous multidisciplinary research and development. Scientists from US, Germany, France, Great Britain, Japan and Ukraine made significant contribution into its progress.

Work [1] presents the results of development of electron beam equipment and technologies for producing materials and coatings, performed at scientific-production enterprise «Eltekhmash» (Ukraine) in the period from 2005 to 2015.

This review is devoted to analysis of the results of development of new generation of electron beam equipment and technologies in this company over the last 10 years. The company is intensively developing several directions of electron beam technology, including:

● development of laboratory and industrial equipment for melting metals and alloys, deposition of protective coatings, producing composite materials condensed from the vapour phase;

● producing high-purity Ni–W alloys, used as seeds in growing single-crystal blades;

● production of special titanium alloys for biomedical purposes;

● master alloy production;

● production of quality ingots from scrap of high-temperature alloys JS26-VI and JS32;

● manufacturing tubular billets-cathodes from Ni–Cr–Al–Y, Ni–Co–Cr–Al–Y heat-resistant alloys for ion-plasma coating deposition;

● producing special metal powders for plasma deposition of coatings;

● production of electric contacts;

● deposition of protective coatings on gas turbine blades.

Development of versatile laboratory and pilot-production electron beam equipment with different functional capabilities, which are currently realized in specialized units, allows saving time and funds for development of new technological processes. L-2 unit belongs to this type of equipment. Figure 1 gives the general view of the unit.

Specification of EB unit L-2

Dimensions of evaporated billets (ingots), mm:
    diameter 70
    length . . . . not more than 400
Dimensions of billets melted from upper mechanism, mm:
    diameter 80
    length . . . . not more than 390
Dimensions of condensation surfaces, mm, not more than:
    rectangular . . . . 350×350
    round Ø400
    cylindrical:
        diameter 200
        length 350
Distance from evaporation surface to condensation
surface, mm 200–325
Number of crucibles, pcs 3
Speed of evaporated ingot displacement, mm/min 1– 350

Figure 1. Appearance of EB unit L-2

Speed of displacement of billets melted from
the top, mm/min 5–350
Speed of item rotation on horizontal shaft, rpm 3–25
Speed of item rotation on vertical shaft, rpm 5–70
Number and power (kW) of electron beam guns
(thermal cathode guns with strip cathode):
    for material evaporation from the crucibles . . . . 3×60
    for heating from above . . . . 2×60
    for heating from below . . . . 1×60
Consumed power, kW, not more than:
    high-voltage power source 250
    power source of ion cleaning device 30
Rated accelerating voltage, kV 20
Working vacuum in the chambers, Pa (mm Hg). . . $6 \cdot 10^{-3}$–$1 \cdot 10^{-2}$
. . . .($5 \cdot 10^{-3}$–$1 \cdot 10^{-4}$)
Overall dimensions of the unit, mm, not more than:
    length 4300
    width 6200
    height 3300
Unit weight, t 16.5

The unit allows realization of four types of different technological processes.

The first of them is coating deposition on various items, in particular turbine blades (Figure 2). Three independent copper water-cooled crucibles of 70 mm diameter allow, simultaneously or independently, performing evaporation of three different materials by a set program, and forming heat-resistant, metal, ceramic or metal-ceramic, single-layer and multilayer graded coatings. Modern requirements to vacuum hy-

giene at coating deposition are satisfied due to design features of the unit (two-chamber variant). Loading and unloading of initial (uncoated) and coated blades (items) are performed in reloading chamber without breaking the vacuum in the main working chamber, where the actual technological process of deposition is conducted.

Second technological task solved in this unit is producing condensed from the vapour phase composite materials of dispersion-strengthened, microlaminate or microporous type. At evaporation from three independent crucibles the vapour flow is deposited on a stationary or rotating substrate from steel of St.3 grade of 500 mm diameter and up to 20 mm thickness (Figure 3). For easy separation of condensed material from the substrate a thin separating layer is applied on the deposition surface. Composite sheet blanks of 500 mm diameter and 0.1 to 7 mm thickness are produced.

A new technological direction of L-2 unit application is producing dispersed metal, ceramic and composite powders (Figure 4). A feature of producing powders is vapour flow condensation on a rotating substrate cooled to room temperature. An enamel coating is first applied onto the substrate surface. The above technique practically eliminates interaction of the deposited material with the substrate. The loose residue is scraped off the substrate surface and is fed
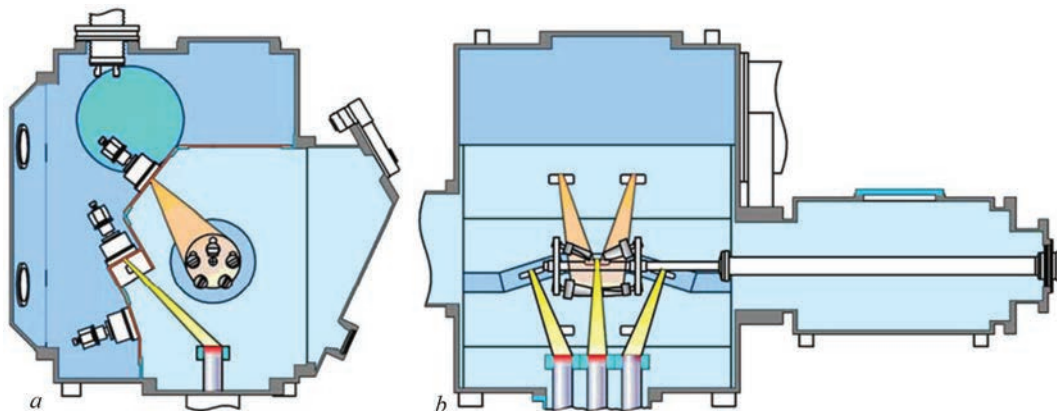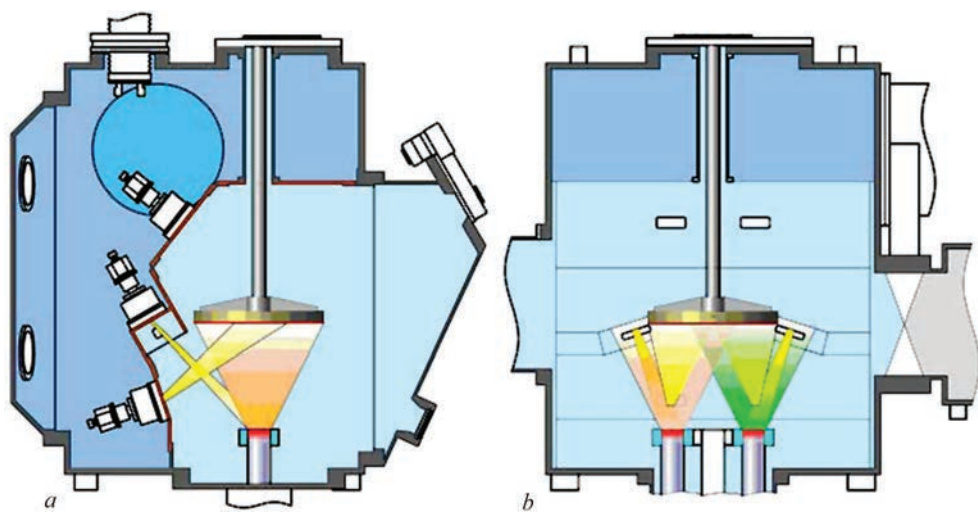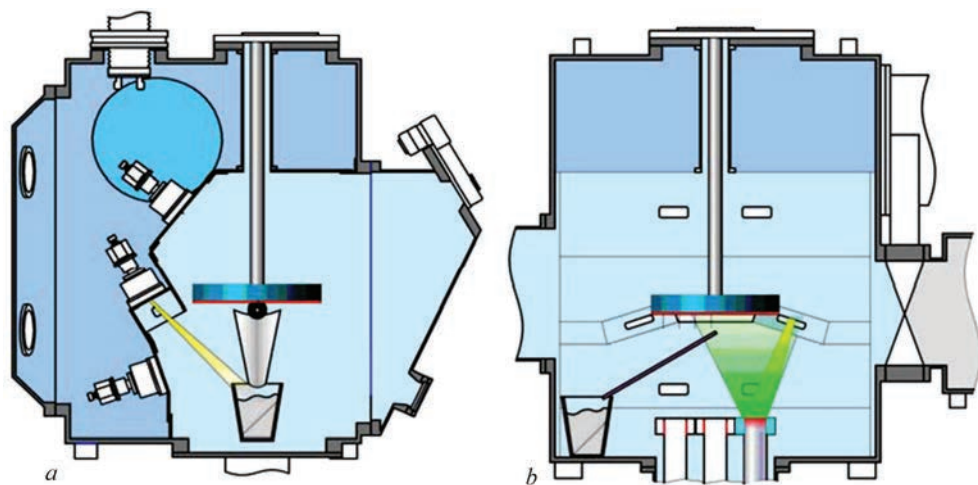

Figure 2. Schematic of coating deposition on gas turbine blades: *a* — side view; *b* — front view

Figure 3. Schematic of producing composite materials condensed from the vapour phase: *a* — top view; *b* — front view

Figure 4. Schematic of producing powders from the vapour phase: *a* — side view; *b* — front view

into powder collection tank through vibrating feeder. Produced powders are of a round shape, their diameter varying from 0.4 to 5 μm.

The fourth technological process which is realized in the unit is producing ingots of pure metals and alloys (Figure 5).

Variant given in Figure 5, *a* is used mainly to produce ingots of refractory metals and alloys. Here, the consumed (remelted) billet is suspended from the upper rotation mechanism. A certain speed of billet rotation is set and the first electron beam gun is used to perform melting of its end face. Liquid metal pen-
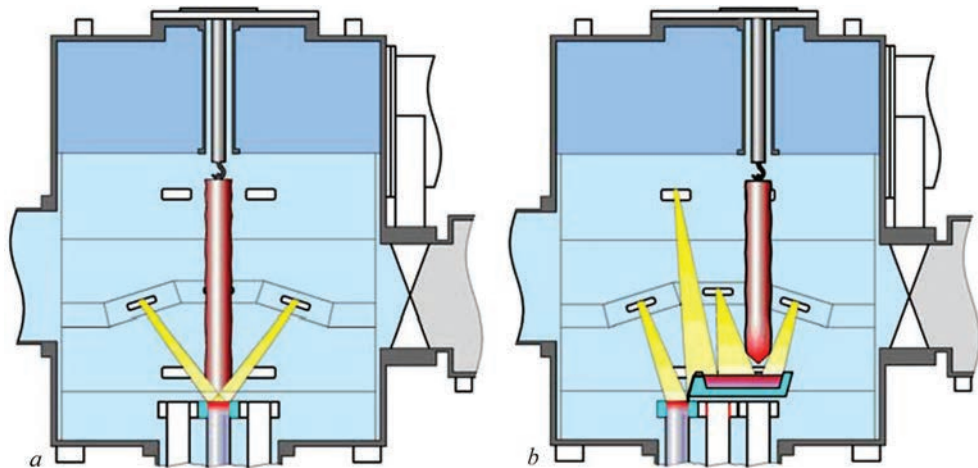
Figure 5. Process chart of producing ingots (alloys) in L-2 unit: *a* — remelting directly into the mould; *b* — remelting through intermediate crucible into the mould

etrates directly into the copper water-cooled crucible, where the electron beam of the second gun forms the ingot. Melting through the intermediate crucible is the most extensively applied (Figure 5, *b*). Such technological process provides maximum refining of remelted material from interstitial impurities and nonmetallic impurities.

At present special attention is given to development of specialized electron beam equipment for deposition of thermal barrier coatings (TBC) on blades. Leading world manufacturers include ALD Vacuum Technologies, Von Ardenne, Pratt and Whitney, and PWI.

SPE «Eltekhmash» developed new generation production electron beam unit L-8 for deposition of TBC on turbine blades [2]. Unit appearance is shown in Figure 6. Schematic of technological process of coating deposition in the unit working chamber is given in Figure 7.

Specification of EB unit L-8

Dimensions of cylindrical cassette with parts, mm, not more than:
    diameter 250
    length 500
Speed of item rotation on horizontal shaft, rpm 0.5–50
Number of evaporators, pcs 4
Crucible inner diameter, mm 70
Length of evaporated ingots, mm . . . . not more than 500
Ingot feed rate, mm/min 0.5–350
Distance from upper edge to cassette rotation axis
or condensation plane, mm 350
Number and nominal power (kW) of electron beam guns:
    for material evaporation from crucibles . . . . 4×100
    for item heating . . . . 2×60
Type of electron beam guns — axial guns with cold cathode
(based on high-voltage glowing discharge)
Consumed power, kW, not more than:
    high-voltage power sources 520
    auxiliary equipment 80

Figure 6. Appearance of EB unit L-8

Rated accelerating voltage, kV 30
Working vacuum in the chambers, Pa (mm Hg):
. . . . $6 \cdot 10^{-3}$–$6 \cdot 10^{-2}$
. . . . ($5 \cdot 10^{-3}$–$5 \cdot 10^{-4}$)
Unit overall dimensions, mm, not more than:
    length 10500
    width 9500
    height 4300
Weight of the unit (with power source), t . . . . not more than 25

A feature of L-8 unit is application of gas-discharge guns with up to 1000 h operating life and deposition of all types and structures of protective coatings: metal, ceramic, composite, single-layer, multilayer, graded, etc. TBC of complex composition and structure on turbine blades can be formed in one process cycle.

Two reloading (lock) chambers of the unit accommodate devices, providing ion cleaning of blades before coating deposition, blade preheating, and formation of barrier microlayers on the boundaries: blade — inner heat-resistant layer; inner heat-resistant layer — outer ceramic layer for slowing down the diffusion processes on interfaces.
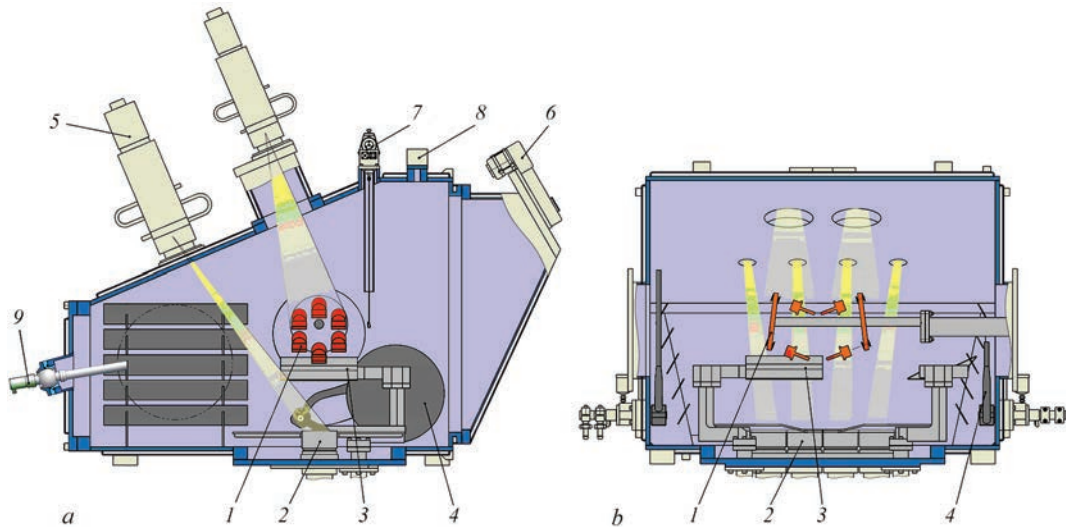

Figure 7. Schematic of technological process of coating deposition in unit working chamber: *a* — cross-sectional view; *b* — longitudinal view; *1* — cassette with blades; *2* — crucibles; *3* — evaporator gate valves; *4* — lock gates valves; *5* — electron beam gun; *6* — viewing system; *7* — load cell; *8* — process gas leak valve; *9* — ball lead-in for pyrometer mounting

Figure 8. Appearance of EB unit L-4

Sensor for controlling deposited coating thickness is mounted on working chamber upper wall, and ball lead-in with sighting tube and viewing window for contactless measurement of item temperature, using high-technology infrared pyrometer and special software, are mounted on working chamber rear wall.

The unit also supports the possibility of partial ionization of technological gas and metal vapour by applying negative bias to the item (up to 2 kV). Ionization promotes improvement of coating quality and their adhesion to the item being protected.

Advantages of electron beam remelting, compared to other methods (vacuum-arc and vacuum-induction) are the highest quality of material refining under vacuum, as well as high degree of production purity. Possibility of controlling the process allows reproducing the parameters to ensure the required alloy composition.

SPE «Eltekhmash» developed and put into commercial operation production electron beam unit L-4 for refining and melting of metals and alloys with application of cold-cathode (gas discharge) guns as the heat source [3]. General view of the unit is shown in Figure 8. Schematic of process chamber, in which meting and refining of metals and alloys are performed, is given in Figure 9.

Specification of EB unit L-4

Maximum size of remelted billet, mm . . . . 200×200×150
Maximum size of melted ingot, mm. . . . . Ø300×1900
Maximum size of melted slab, mm . . . . 200×300×1900
Diameters of moulds in the unit set, mm Ø70, 100, 130
Overall dimensions, mm . . . . 200×300
Dimensions of metal liquid pool surface in intermediate
crucible, mm . . . . 300×300
Number and maximum power (kW) of electron
heaters . . . . 4×100
Maximum gun current, A 3.3
Rated accelerating voltage, kV 30
Consumed power, kW, not more than:
    electron beam gun power sources. 400
    auxiliary equipment 60
Vacuum in working chamber, Pa (mm Hg) . . . $1.3 \cdot 10^{-2}$–$1.3 \cdot 10^{-1}$
. . . . ($1.3 \cdot 10^{-4}$–$1.3 \cdot 10^{-3}$)
Cooling water pressure, Pa (kg/cm^2). . . . . $3 \cdot 10^{5}$–$4 \cdot 10^{5}$ (3–4)
Unit overall dimensions, mm:
    length 7000
    width 6000
    height 5000

Equipment allows producing high-quality ingots and slabs of the required chemical composition from such traditional metals as iron, nickel, cobalt, copper, highly-reactive refractory metals as titanium, niobium, zirconium, tungsten, hafnium, high-temperature and heat-resistant alloys, Ti_3Al, $TiAl$, Ni_3Al, $NiAl$ and other intermetallics.

Producing ingots and tubular billets from Me–Cr–Al–Y alloys for electron beam and ion-plasma coating deposition. The Company has mastered commercial production of a range of ingots for electron beam coating deposition, in accordance with TU U 27.4-20113410.002–2001 (version 3) [4]. Ingot composition is given in Table 1.
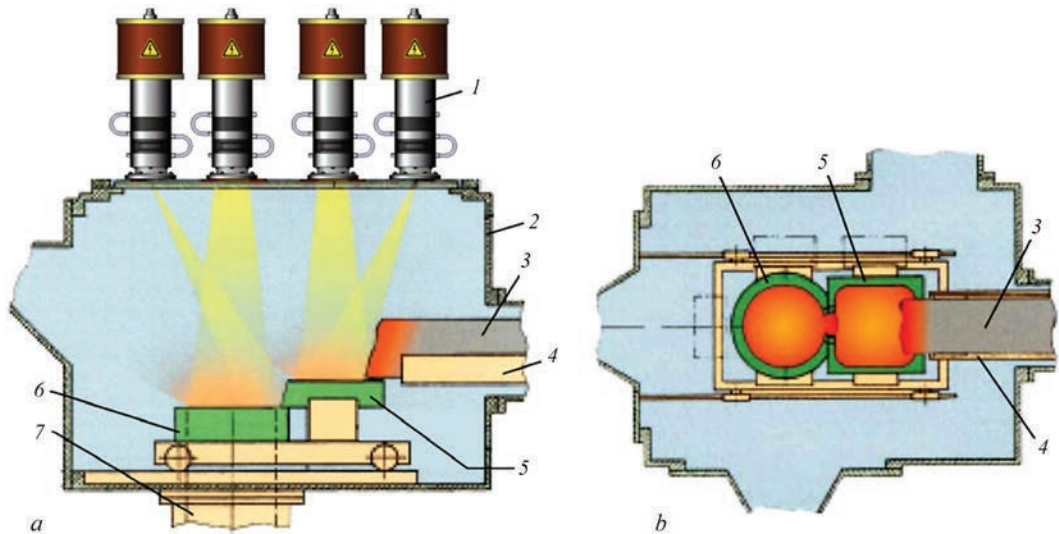

Figure 9. L-4 unit process chamber: *a* — front view; *b* — top view; *1* — electron bean gun; *2* — working chamber; *3* — remelted material; *4* — pullout tray; *5* — intermediate crucible; *6* — mould; *7* — ingot drawing mechanism

More than 10 t of ingots of different chemical composition have been manufactured. At present M3P-6 ingots are supplied to Company «Zorya-Mashproekt» (Nikolaev), as well as to People's Republic of China.

Commercial production of tubular billets-cathodes from M3P-1 alloy for ion-plasma deposition of high-temperature coatings in MAP-1, MAP-2, MAP-3 units was started. Cathode appearance is shown in Figure 10.

Electron beam technology of tubular billet casting allows an essential improvement of cathode quality and, eventually, of the quality of coatings deposited from them, as well as refusing to purchase them from RF.

Production of quality ingots for casting blades from high-temperature alloy wastes. Wastes of high-temperature alloys in casting production are technologically unavoidable remains of the initial alloy, not included into quality ingot weight. The importance of the problem of refining high-temperature alloy wastes consists in that a considerable quantity of wastes, caused by casting rejects, mould defects, presence of crop, etc., accumulate at GTE manufacturing enterprises in the process of producing blades from initial materials. High cost of primary high-temperature alloys led to appearance of a tendency of application of casting

Figure 10. Appearance of tubular cathodes for ion-plasma coating deposition: *a* — in initial state; *b* — after machining

production wastes in blending melts for blade casting that allows lowering product cost [5].

«Eltekhmash» developed an original commercial electron beam technology of processing high-temperature alloy JS26-VI. Results of chemical analysis of produced ingots after machining, 95–97 mm in diameter and of 300–320 mm length, is given in Table 2.

Data given in the Table confirm the complete correspondence of ingot composition to requirements of TU-92-177–91. Electron beam remelting (EBR) leads

Table 1. Composition of ingots for electron beam coating deposition

Designation	Elements, wt.%					Impurities, wt.%, up to					
	Co	Ni	Cr	Al	Y	Hf	Zr	Si	Fe	Cu	C
M3P-1	Base	0–2	20–24	10–13	0.4–1	0.2	0.4	0.5	0.3	0.06	0.06
M3P-2	Same	8–12	18–24	10–13	0.4–1	0.2	0.4	0.5	0.3	0.06	0.06
M3P-3	»	0–2	21–25	10–13	0.4–1	0.2	0.4	0.5	0.3	0.06	0.06
M3P-4	»	8–12	18–24	10–13	0.4–1	0.2	0.4	0.5	0.3	0.06	0.06
M3P-5	18–22	Base	18–24	10–13	0.4–1	0.2	0.4	0.5	0.3	0.06	0.06
M3P-6	–	Same	18–24	10–13	0.4–1	0.2	0.4	0.5	0.3	0.06	0.06
M3P-7	–	»	18–24	10–13	0.4–1	0.2	0.4	0.5	0.3	0.06	0.06
M3P-8	8–10	»	18–24	10–13	0.4–1	0.2	0.4	0.5	0.3	0.06	0.06
M3P-9	–	–	18–24	10–13	0.4–1	0.2	0.4	0.5	Base	0.06	0.06

Table 2. Composition of billet-casting of 97 mm diameter produced from recycled alloy JS26-VI by EBR

Sampling location	Element content, wt.%									
	C	Cr	Co	W	Al	Ti	Mo	Fe	Nb	V
Top	0.137	4.70	8.96	11.50	6.10	1.02	1	0.06	1.43	0.90
Middle	0.129	4.94	9.03	11.53	5.74	0.90	1	0.06	1.64	0.91
Bottom	0.132	4.94	9.03	11.53	5.74	0.90	1	0.06	1.64	0.91
TU 1-92-177–91	0.12–0.17	4.3–5.3	8.7–9.3	11.2–12.0	5.6–6.1	0.8–1.2	0.8–1.2	≤0.5	1.4–1.8	0.8–0.2

Table 2 (cont.)

Sampling location	Element content, wt.%						
	Ni	Si	Mn	S	P	O_2	N_2
Top	Base	<0.2	<0.3	0.003	0.003	0.00068	0.00109
Middle	Base	<0.2	<0.4	0.003	0.003	0.00070	0.00106
Bottom	Base	<0.2	<0.3	0.003	0.003	0.00074	0.00105
TU 1-92-177–91	Base	≤0.2	≤0.3	≤0.005	≤0.010	≤0.002	≤0.002

Table 3. Chemical composition of titanium alloys of Ti–Nb–Zr–Si system

Alloy number	Nb	Si	Zr
1	11–13	0.9–1.1	1.9–2.2
2	11–13	0.9–1.1	3.9–4.2
3	11–13	0.9–1.1	5.9–6.2
4	11–13	0.9–1.1	9.9–10.2
5	11–13	0.9–1.1	14.8–15.2
6	18–20	0.9–1.1	1.9–2.2
7	18–20	0.9–1.1	3.9–4.2
8	18–20	0.9–1.1	5.9–6.2
9	18–20	0.9–1.1	9.9–10.2
10	18–20	0.9–1.1	14.8–15.2

to essential reduction of the content of such impurities as sulphur, phosphorus, oxygen and nitrogen. As to their quality, the ingots after EBR exceed the initial material (billets of Ø80) produced by OJSC «CM Kompaniya» (Stupino, RF) in vacuum furnace by equiaxed crystallization.

Ingots of JS26-VI alloy after EBR, produced from recyclable wastes, have passed the full testing cycle at Company «Motor-Sich» (Zaporozhie) and are now used as initial materials in casting gas turbine blades. First batch of ingots of JS-32 alloy in the quantity of 300 kg was also produced by EBR of the respective wastes.

Master alloy production. Commercial production of Ni–Y master alloys is performed in keeping with TU 48-0531-464–93. Experimental batches of master alloys Al–Mo, Al–Ni, Al–Zr are produced.

Titanium alloy production. Experimental batches of Ti–Nb–Zr–Si system alloys are produced for Ukrainian and US users. Alloy composition is given in Table 3.

As is seen from the Table, titanium-based alloys are produced in a quite narrow range of alloying component concentrations. Here, repeatability in the melts reaches 95–98 %. Ti–Nb–Zr–Si system alloys are designed for medical purposes.

Production of metal powders of Co–Cr–Al–Y–Si system for plasma deposition of coatings. Production of powders of Co–Cr–Al–Y–Si system for plasma deposition of coatings has been mastered recently [4, 6, 7]. Tables 4 and 5 give chemical composition of ingots and powders made from them.

Ingots for powder manufacture were produced by EBR of pure initial components. Powders of 40–100 μm fractions are made by the method of chemical fragmentation of respective ingots. Production batches of powders of Co–Cr–Al–Y system are supplied to Company «Zorya-Mashproekt» and PRC.

Table 4. Chemical composition of alloys for Co-based powder manufacturing

Designation	Elements, wt.%					Impurities, wt.%, up to				
	Ni	Cr	Al	Y	Si	Hf	Zr	Fe	Cu	C
M3P-10	0–2	26–0	6–9	0.8–1.2	1.5–4.0	0.2	0.4	0.3	0.06	0.06
M3P-11	0–2	20–25	10–13	0.4–0.1	1.5–4.0	0.2	0.4	0.3	0.06	0.06

Note. Total content of Nb + Mo + W + Ti of not more than 1 % is allowed in M3P-10 and M3P-11 alloys.

Table 5. Chemical composition of Co-based powders for plasma deposition of coatings

Designation	Elements, wt.%					Impurities, wt.%, up to				
	Ni	Cr	Al	Y	Si	Hf	Zr	Fe	Cu	C
M3P-10	0–2	26–30	6–9	0.8–1.2	1.5–4.0	0.2	0.4	0.6	0.06	0.1
M3P-11	0–2	20–25	10–13	0.4–0.1	1.5–4.0	0.2	0.4	0.6	0.06	0.1

Note. Total Nb + Mo + W + Ti content of not more than 1 % is allowed in polycrystalline powders M3P-10 and M3P-11.

Table 6. Electron beam equipment supplied by Company «Eltekhmash» in 2005–2014

Description	Purpose	Year	Customer
Electron beam unit L-1	Deposition of protective coatings from vapour phase in vacuum	2005	Ukraine
Electron beam unit L-4	Refining and remelting of metals and alloys in vacuum	2006	Armenia
2 power units with HVGD-based guns of 220 kW each	Commercial production of «solar silicon» from metallurgical silicon	2007	Japan
Power unit with HVGD-based guns of 30 kW power	Coating deposition	2008	Taiwan
2 power units with HVGD-based guns of 30 and 100 kW power	Upgrading of units for refining metallurgical silicon	2008	Russia
Power unit with HVGD-based gun of 100 kW power	Upgrading of unit for refining and remelting of noble metals	2010	Russia
Electron beam unit L-2	Deposition of protective coatings from the vapour phase in vacuum	2012 2013	Ukraine China
Electron beam unit L-8	Deposition of protective coatings on GTE parts	2014	Russia

Production of electric contracts. The most recent achievements in the field of manufacture of materials for electric contacts and products from them are given in [8–10].

Commercial production of new materials for electric contacts Cu(0.05–0.1)(ZrY)–W and Cu–(0.05–0.1(ZrY)–Cr has been mastered.

More than 15 composite materials have been produced, from which more than 1.6 mln pieces of electric contacts and electrodes for various national economy applications have been manufactured.

Coating deposition on gas turbine blades. Company «Eltekhmash» realized a closed cycle of coating deposition on turbine blades, including melting of all types of Ni and Co-based ingots [4], manufacture of ZrO_2–Y_2O_3 ceramic ingots [11], and deposition of TBC from the above initial materials of customized design and chemical composition in user equipment [1, 4].

Manufacture of industrial electron beam equipment. Table 6 gives the data on enterprise supplies of laboratory and production electron beam equipment for material melting and evaporation in 2005–2014.

Enterprise supplies both individual components of equipment, and laboratory and production electron beam units with complete set of components for realization of technological processes of melting metals and alloys, protective coating deposition, and producing composite materials from the vapour phase.

1. Grechanyuk, N.I., Kucherenko, P.P., Grechanyuk, I.N. (2007) New electron beam equipment and technologies of producing advanced materials and coatings. *The Paton Welding J.*, **5**, 25–29.
2. Grechanyuk, N.I., Kucherenko, P.P., Melnik, A.G. et al. (2014) Industrial electron beam installation L-8 for deposition of heat protective coatings on turbine blades. *Ibid.*, **10**, 45–50.
3. Grechanyuk, N.I., Kucherenko, P.P., Melnik, A.G. et al. (2016) Industrial electron beam installation L-4 for vacuum remelting and refining of metals and alloys. *Poroshk. Metallurgiya*, **7/8**, 140–149.
4. *TU 27.4-201134.10.002–2001:* Materials in ingots and powders for protective coatings. Modification No. 3 to KTU. Version 3 of 03.09.2015.
5. (2007) *Electron beam melting in foundry.* Ed. by S.V. Ladokhin. Kiev: Stal.
6. Grechanyuk, N.I., Gogaev, K.A., Zatovsky, V.G. (2012) Peculiarities of producing powder alloy Co–Cr–Al–Y–Si. *Poroshk. Metallurgiya*, **11/12**, 18–25.
7. Gogaev, K.O., Grechanyuk, M.I., Grybkov, V.K. et al. *Method for producing of complex-alloyed powders on cobalt base.* Pat. 99557 Ukraine. Publ. 27.08.2012.
8. Grechanyuk, N.I., Grechanyuk, V.G., Khomenko, E.V. et al. (2016) Modern composite materials for switching and welding equipment. Inf. 2. Application of high-rate vacuum evaporation methods for manufacturing electric contacts and electrodes. *The Paton Welding J.*, **2**, 34–39.
9. Grechanyuk, M.I., Grechanyuk, V.G., Bukhanovsky, V.V. et al. *Composite material for electric contacts and method of its manufacturing.* Pat. 104673 Ukraine. Publ. 25.02.2014.
10. Grechanyuk, M.I., Grechanyuk, I.M., Grechanyuk, V.G. et al. *Composite material for electric contacts and method of its manufacturing.* Pat. 86434 Ukraine. Publ. 27.04.2009.
11. *TU.U-13.2-201134.10-004–2003*: Ceramic materials for thermal protection coatings.

NEW OPTICAL OBSERVING SYSTEM IN SERIES ELECTRON BEAM GUNS

V.A. KRAMARENKO, V.M. NESTERENKOV and **V.I. ZAGORNIKOV**

E.O. Paton Electric Welding Institute, NASU

11 Kazimir Malevich Str., 03680, Kiev, Ukraine. E-mail: office@paton.kiev.ua

Different approaches were studied for welded butt observing in the vacuum chambers under conditions of intensive deposition. The results of development of new optical system suitable for application in industrially applied guns of ELA 60/60 type are given. The system differs by simplicity and possibility of wide application of standard assemblies. The system will find commercial application due to completeness of set, high functionality and simplicity. 3 Ref., 6 Figures.

A process of EBW takes place at large rates that requires high accuracy of alignment of electron beam and butt being welded. The latter is assembled with a gap close to zero. An operator is located out of a vacuum chamber at some distance from a place of welding, therefore the issues of beam-to-butt combining, alignment of mutual location of beam and part are very relevant for the whole technological process [1, 2].

Currently, three types of view systems are developed in the commercial EB systems, i.e. viewports, optical and TV systems or their combinations. It is a well-known system RASTR [3] used for observing the welding place in secondary emission electrons and beam to butt alignment with 0.1 mm accuracy. A principle of RASTR equipment operation is based on measurement of current of the secondary emission electrons forming in cyclic (with 300 ms period) scanning of working zone of the part with low power fine-focused beam in short-term moments (to 5 ms) of interruption of EBW process. An image of part surface is formed based on the signals from secondary emission electrons probe installed on the EB gun in the vicinity to welding place. Measured and digitized by observing equipment brightness levels in areas of scanned surface are recorded in computer memory in form of shot (matrix) of the image and displayed in the separate window of RASTR monitor after special software processing.

Low power fine-focused electron beams are used for welding of small-size precision parts, and the parts of 1–3 mm thickness are assembled with increased accuracy. Combined optical-TV systems with direct observing the welded butt through gun optical system can be useful for such parts.

This paper provides for the results of development of a new optical system suitable for application in widely applied in industry guns of ELA 60/60 type. Taking into account that the main drawback of the optical systems is deposition of mirrors with metal evaporating in welding, the work pays great attention to optics protection from deposition. It is a well-known fact that the protective devices based on stroboscopic effect are used under conditions of intensive deposition. Such systems are characterized by decrease of object illumination. It is possible to increase their efficiency by stabilizing rotation of a drum with up to 1 Hz accuracy on frequencies divisible by shot frequency (50, 1250, 2500 Hz etc.) that is highly sophisticated.

Tape transporting mechanisms, changeable glasses, including protective rotating and shifting glasses [1] are widely used. They shall have compact structure, work in wide range of operating distances with sufficient supply of protective tape, which should not be deformed and stuck. Application of such mechanisms is possible only at sufficient distance from the beam. Removal of the optics from the electron beam results in significant distortions of the image on video camera, elimination of which requires thorough production (polishing of mirrors etc.) and complication of structure of view device, that resulted in refusal from this direction in development of the observing systems.

Proposed system differs from the earlier developed by simplicity and high level of assembly unity. The whole package does not require drastic changes in the structure of EB gun (Figure 1). A view optical system is set in a body of gun anode block with ap-
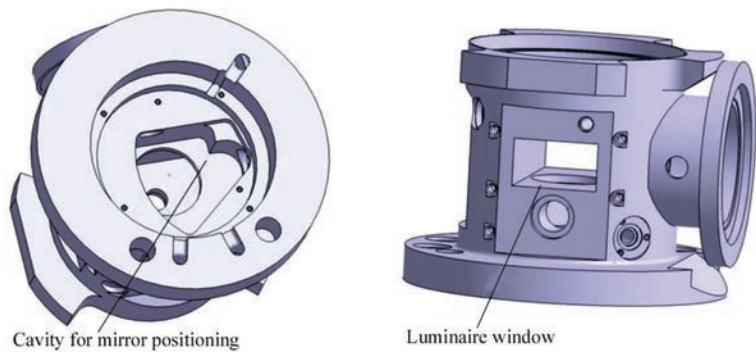
**Figure 1.** Improvement of body of anode block in EB gun ELA 60/60

proximated to the maximum coaxial alignment of the axis of electron beam to the optical system axis.

The body has a milled-out cavity for positioning mirror mechanism and a hole for axis of external electric motor of mirrors drive. Few threaded holes were added outside of the body for fixing mounted blocks of video monitoring unit. Mirror mechanisms board *1* has axis *3* relatively to which mirror holder *2* is rotated (Figure 2). In welding mode the mirrors are removed from a beam channel of the gun and do not effect the welding parameters. The image is absent in this case and access of mirror-deposition vapours from the materials being welded is blocked. In a set-up mode the mirrors are positioned across the optical axis of luminaire *6* and objective lens *7* by means of pinion shaft *5* of electric drive and gear sector *4* of mirror holder *2*. Light from the luminaire is directed by own mirror on part section being welded and via reflection from another mirror is directed along the optical axis of objective lens and CCD-camera. Mirror holder design prevents direct entering of the luminaire beams in CCD-camera objective lens.

This mode assumes turning on of electron beam with 0.8–1.5 mA current intensity, which flows through the hole between the mirrors and allows observing brightened point in a place of beam entering into billet being welded. Deposition of the mirrors was not virtually observed at such a current. In order to prevent mirrors' deposition the program for welding mode regulation blocks beam current rise, if the mirrors are not removed from the beam channel. Miniature electric drive *3* (see Figure 2) with rotating moment of around 10 kg/cm is used for mirror holder rotation. Requirements on absence of magnetic field in inactive mode and good heat-sink in vacuum are made to it. Besides, scheme of its regulation should stipulate current limitation at 120–150 % level from nominal at mechanism stopping in lock and further power shut down. The video system is made in from of removable unit, in which objective lenses can be replaced depending on set requirements. The objective

lenses have an electro-mechanical drive for regulation of focus and diaphragm, that allows easy adjustment of image quality. The CCD-camera itself is located in a hermetic enclosure (Figure 3) which is mounted to objective lens body with the help of coupling nut. Air in a CCD-camera box provides for sufficient heat exchange of electronic circuit with body. Further, heat is dissipated over the parts of objective lens body and EB gun.

Figures 4 and 5 show the video-monitoring unit in section. Observing position of the mirrors opens the channels in the mirror holder for luminous flux from luminaire to objective lens. The luminous flux of source (*white arrows*) comes to mirror 1 and being directed to welding zone area. The image of this zone (*grey arrows*) is reflected from mirror 2 and guided to the objective lens. The angles of mirror positioning are set and calculated for showing the welding zone in 50–500 mm range from EB gun edge. Flow of electrons from the cathode passes through the hole between mirrors of 5 mm diameter and in this case a
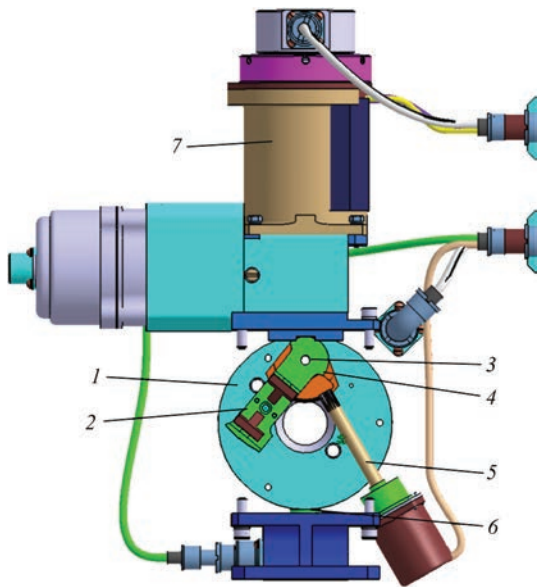
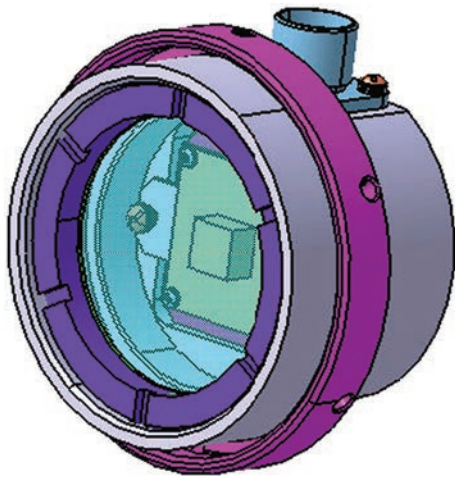**Figure 2.** View of mechanism of mirror drive (see designations in the text)
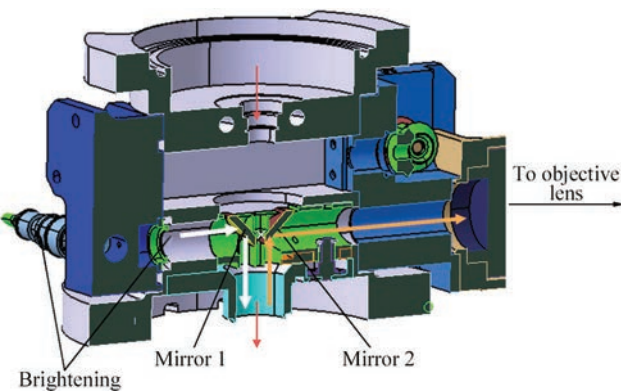
Figure 3. View of CCD-camera body

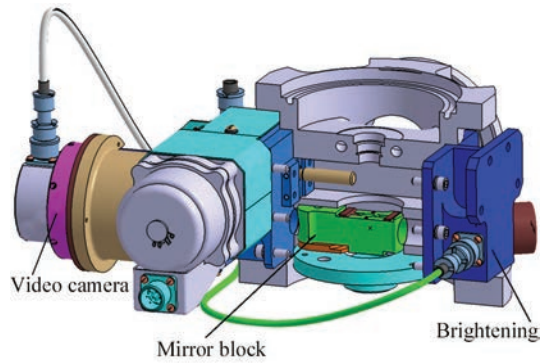**Figure 4.** Cross section of optical observing system

Figure 5. View of observing system with mirror rotation mechanism
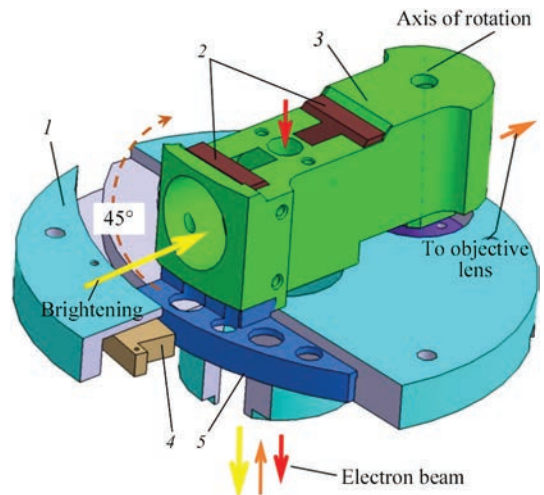

Figure 6. View of running mirror block: *1* — video block body; *2* — mirrors, *3* — rotating body of mirrors; *4* — piezocartridge; *5* — piezodrive surface

brightened point of contact of beam with metal surface can be observed in the image.

Before welding the mirrors are removed sideways from the beam channel (mirror holder is turned to 40°). At that for preventing metal evaporation the objective lens is closed by half-round backside of the mirror holder, and a special pivoting spring-loaded shutter is used for lens of the luminaire. Two light emitting diodes indicate position on control panel, namely red — beam channel is closed, beam current is limited by 0.8–1.2 mA value, and green — mirrors are removed, the system is ready for welding on operating current.

Two V-positioned mirrors are located under gun beam deflector in the proposed device. One of these mirrors directs the light beam from luminaire to part being welded, and another directs the light reflected from the surface of part with butt being welded (see Figure 4) into eyelens. Polished copper plates were used as mirrors since application of glass mirrors is complicated due to formation on glass of a static electron discharge, distorting electron beam, as well as flares deteriorating visibility.

A running block of mirrors mounted on an arm (Figure 6) is located on a flange embedded in the gun body. Balance wheel of the block, having radial movement with the help of reversible piezomotor, allows quick switch from tracking to welding mode. Advantage of the piezodrive lies in absence of magnetic fields during its operation. Photolens and TV-camera, image from which is displayed on the computer monitor, provide for five-fold magnification of the image at controlled area to 100 mm² depending on operating distance.

Proposed observing system allowed realizing welding in difficult-to-reach places, working through EBW procedure for critical thin-walled parts with circumferential welds, some of which are deepened in the part body to 200 mm.

1. Chvertko, A.I., Nazarenko, O.K., Svyatsky, A.M. et al. (1973) *Equipment for electron beam welding*. Kiev: Naukova Dumka.
2. Schiller, S., Heisig, U., Panzer, S. (1980) *Electron beam technology*. Moscow: Energiya.
3. Nazarenko, O.K., Shapoval, V.I., Loskutov, G.A. et al. (1993) Supervision of electron beam welding process and automatic joint tracking. *Avtomatich. Svarka*, **5**, 35–38.

SYSTEMS FOR VISUALIZATION OF WELDING PROCESSES IN REAL-TIME MODE USING NOISE-PROOF CHANNEL FOR TRANSFER OF SECONDARY ELECTRON EMISSION SIGNAL

V.A. MATVEJCHUK

E.O. Paton Electric Welding Institute, NASU
11 Kazimir Malevich Str., 03680, Kiev, Ukraine. E-mail: office@paton.kiev.ua

Noise-proof digital systems were developed for processing, transfer and input into computer of a secondary electron emission signal with visualization of welding processes in real-time mode. The equipment was developed for conversion, transfer and processing of the secondary electron emission signal, namely block of processing, conversion and transfer of the secondary electron emission signal; block of input and decoding of the digital electron secondary emission signal; block of processing, conversion and transfer of the secondary electron emission signal via Ethernet. Video monitoring systems using the equipment for conversion and transfer of the signal and equipment for conversion and information transfer into computer were developed and tested. Software was designed. The investigations of developed video monitoring system were carried out, their comparative analysis with video monitoring system RASTR, widely used in the units for electron beam welding, were performed. 6 Figures.

K e y w o r d s : electron beam welding, interference immunity, electron beam, secondary electron emission, video monitoring, image

EBW is widely used in industry for producing the parts of critical designation, first of all, in aerospace and power branches due to vacuum protection of molten metal from gas saturation, small welding deformations and possibility to achieve high weld depth-to-width ratio. Image of a weld and butt of the edges can be received simultaneously with welding processes using electron beam in a mode of low current scanning of metal surface.

Computer technologies allow accurate guiding of electron beam in the butt, but only at sufficiently high ratio, desirably more than 20 dB, of useful and noise signals of the secondary electron emission (SEE). Usually, this ratio makes from 12 to 14 dB.

Parasitic noises are formed in a cable transmitting analog signal of the SEE from preamplifier to device of information input into computer. A noise signal is imposed on useful one, at that it has wide amplitude and frequency spectrum. It is extremely difficult to select and eliminate the noise signal, therefore, it is necessary to minimize its effect on the useful signal.

It is possible to eliminate or significantly reduce the effect of noises on the SEE signal by means of its conversion into digital form and transfer by noise-proof digital channel.

Currently, the units for EBW widely use RASTR video monitoring system designed for displaying the welding processes in real-time mode on a screen. RASTR block-diagram is shown in Figure 1.

Scanning field, created by focused electron beam of EB gun (EBG), is formed in a control and scan block. Scan control signals are fed to a deflection system (DS) of EBG. Electron scanning beam is directed on the surface of examined object. A flow of electrons, reflected from examined area, comes to a secondary electron probe (SEP), in which an electric
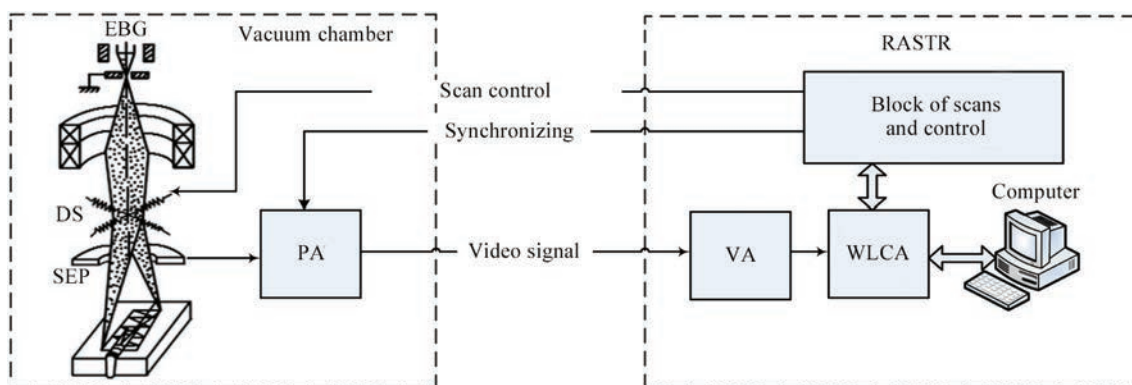

Figure 1. Block-diagram of video monitoring system RASTR (see designations in the text)

© V.A. MATVEJCHUK, 2016

signal of the SEE is formed. This signal is transferred to a preamplifier (PA), located in vacuum chamber. The signal from the preamplifier is fed to a video-amplifier (VA) of RASTR system. After VA the signal comes to WLCA block, in which an analogue signal of the SEE is converted into digital code. The data from WLCA block come to control computer. In the computer received information is processed by a program and video image of welding process is formed in real-time mode.

Analogue signal of the SEE in RASTR system is transmitted from PA to VA using long coaxial cable. The PA is located in a unit vacuum chamber, the VA is in a control cabinet out of the vacuum chamber. The coaxial cable is laid in the cable channels close to power and signal cables of a drive control system, high-voltage cable of the EBG and cables of the executive and control devices. The electric motors of drives are regulated by alternating current, waveform of which is different from sine one. This current develops high-frequency electromagnetic interferences in a wide spectrum of frequencies and amplitudes.

Interferences are overlaid on useful signal of the SEE. Effect of the interferences results in distortion of image of welding processes and depression of performance of a system for automatic butt tracking.

Application of a digital channel for information transfer is proposed as an efficient method preventing the effect of interferences on a signal of the SEE. An analogue signal of the SEE in the direct vicinity from the PA should be converted into digital code and obtained information is transmitted through noise-proof digital channel.

Systems for processing, transfer and signal input into computer was developed for realizing the given task by the PWI specialists together with International Center «Institute of Applied Optics» of the NAS of Ukraine.

The following equipment was developed:

● block of processing, conversion and transfer of signal (BPS), in which an analogue signal of the SEE is converted into digital code;

● block of input and decoding of digital signal (BDS), in which information on signal of the secondary electron emission is converted from digital code to analogue signal;

● block of processing, conversion and transfer of signal via Ethernet (BPSE), in which an analogue signal of the SEE is converted into digital code and in accordance with TCP/IP protocol is transferred into computer via Ethernet.

Systems for imagining the welding processes in real-time mode were developed by PWI specialists using equipment indicated above:

● video monitoring system using the equipment for conversion and transfer of signal (ECTS), and

● video monitoring system using the equipment for conversion and information transfer into computer (EITC).

Software allowing processing the information on SEE signal and forming an image of welding process in real-time mode was developed for EITC. Investigations of the video monitoring system were carried out and their comparative analysis with RASTR visual system was performed.

Description of the developed systems is given below.

Block-diagram of video monitoring system using ECTS is presented in Figure 2.

Scanning field, developed by focused electron beam of the EBG, is formed in a block of control and scans of RASTR system. Scan control signals are fed to deflection system of the EBG. Scanning beam of electrons is directed on a surface of examined object. A flow of electrons, reflected from examined surface, is fed to SEP, in which an electric signal is formed. This signal is transferred to BPS of ECTS system. In BPS a signal of the SEE is amplified, synchronized with control signals and converted into digital code. Data are transferred by wire noise-proof cable outside the vacuum chamber to a control cabinet, where BDS is located. BDS converts the signal into analogue signal, which is transmitted to VA of RASTR system, where an image of examined object is formed in real-time mode.

In ECTS system the signal of the SEE is transferred in a digital form through wire shielded twisted pair cable.

Information transfer in the digital form provides for high interference immunity of a transferred signal.
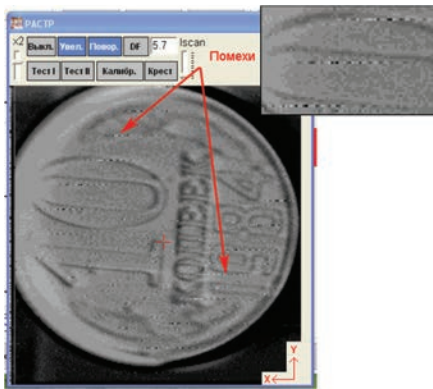
Block-diagram of system of video monitoring using EITC is given in Figure 3.

Scanning field, developed by focused electron beam of the EBG, is formed in a block of control and scans. Scan control signals are fed to DS of EBG. Scanning beam of electrons is directed on a surface of examined object. A flow of electrons, reflected from examined surface, is fed to SEP, in which an electric signal is formed. This signal is transferred to BPSE. In BPSE the signal of the secondary electron emission is amplified, synchronized with control signals and transformed into digital code. Obtained data in digital form are transferred outside the unit vacuum chamber. The information comes to Ethernet port of computer for program processing. Image of the examined object is displayed on the screen in real-time mode.
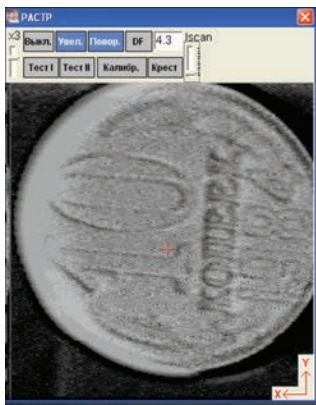
Data are transferred in a digital form through wire Ethernet cable in accordance with network protocol TCP/IP, that provides for high interference immunity of a transferred signal.

Experimental results and discussion. Operation efficiency of the video monitoring systems ECTS and

Figure 2. Block-diagram of EITC system (see designations in the text)

Figure 3. Block-diagram of EITC system (see designations in the text)

EITC was evaluated using a method of comparative analysis with the video monitoring system RASTR.

Quality of imagining of welds and reference objects as well as presence of interferences caused by process equipment was compared.

Tests were carried out on a test bench and industrial unit for EBW.

Investigation of video monitoring system using test bench. A test bench is developed based on EBW small-size unit of SV-112 type.

Quality of image of the investigated objects was tested visually.

Images, received using different imagining systems, are given in Figure 4. Quality of the image made by RASTR system is acceptable for performance of process works on EBW equipment.

The image made by ECTS system is acceptable for performance of welding and process works, but is inferior in image quality of the objects made by RASTR system. It is necessary to note lower image detailing, that is caused by loss of information at double transformation of a signal of the SEE from analogue to digital and back.

The principle difference of ECTS system from RASTR system lies in the method of transfer of the SEE signal from secondary electron probe to information imagining block. Information in ECTS is transferred in digital form, that provides for interference immunity of data transfer. This makes an advantage of ECTS system.

Images in Figure 4, *c*, *f* were made by EITC imagining system. It is necessary to note higher image quality of examined objects, better detailing in comparisons with image made using RASTR system. Information on SEE signal in EITC system is transferred in a digital form, that provides for interference immunity of data transfer. Effect of the interferences on the SEE signal is minimum. It makes an advantage of EITC system in comparison with RASTR system.

An advantage of EITC system in comparison with ECTS system is an absence of multiple conversion of

Figure 4. Image of objects made using imaging systems RASTR (*a*, *d*), ECTS (*b*, *e*) and EITC (*c*, *f*)

Figure 5. Interferences on investigated object image form by RASTR system

Figure 6. Image made using ECTS system

signal, which results in information loss and, as a consequently, deterioration of quality of object imaging.

However, application of EITC system in existing EBW units with preinstalled RASTR system will provoke change of hardware and software parts of the equipment, that is not always acceptable.

Application of ECTS system for modernizing does not require introduction of changes in hardware part of the equipment. This is an advantage of ECTS system in comparison with EITC system. Preferred application of EITC in comparison with RASTR and ECTS is obvious in newly developed equipment as well as in units requiring substantial modernizing.

Investigation of video monitoring system using EBW commercial unit. Investigation of the system was carried out on commercial unit of KL-181 type. Effect of the industrial interferences on image quality was investigated as a result.

Figure 5 shows an image of tested object formed by RASTR system on KL-181 unit. The interferences in form of horizontal bands displaced in diagonal can be observed on the image. The interferences were caused by an effect of drive control signals on analogue signal of the SEE.

Optimum location of the cables inside the unit is used in practice for interference control. It allows reducing of effect interferences, but does not eliminate them. Transfer of signals of the SEE in a digital form allowed significant improvement of the interference immunity. Figure 6 shows an image of tested object made using ECTS system.

The image has no interferences in form of diagonal bands, that verifies necessity of application of digital noise-proof channels for transfer of a signal of the SEE.

Conclusions

1. Signal of the SEE for elimination of the interferences is proposed to convert from analogue form to digital one and transfer through noise-proof digital channel. A signal converter shall be located in the direct vicinity to the secondary electron probe.

2. New equipment was developed for conversion, transfer and processing of the signals of the SEE, namely block of processing, conversion and transfer of the secondary electron emission signal; block of input and decoding of the digital electron SEE signal; and block of processing, conversion and transfer of the SEE signal via Ethernet channel.

3. The systems were developed for imagining the welding processes in real-time mode using noise-proof digital channel for transfer of the SEE signal, namely video monitoring system using the equipment for conversion and transfer of the signal; video monitoring system using the equipment for conversion and information transfer into computer.

4. Software was developed for a video monitoring system using the equipment for conversion and information transfer into computer.

5. Investigations of the developed video monitoring systems ECTS and EITC, and their comparative analysis with widely used in present time imagining system RASTR were carried out. Video monitoring systems are applicable for further operation. They provide for high interference immunity of transfer the SEE signal, acceptable quality of imagining of objects and welding processes in real-time mode.

6. ECTS system is designed for modernizing the EBW units having installed RASTR video monitoring systems. EITC system is designed for application with newly developed EBW equipment as well as for substantial modernization of the equipment with RASTR video monitoring system.

ELECTRON BEAM WELDING
OF COMPLEX-ALLOYED HIGH-STRENGTH TITANIUM ALLOY

S.V. AKHONIN, S.G. GRIGORENKO, V.Yu. BELOUS,
T.G. TARANOVA, R.V. SELIN and **E.L. VRZHIZHEVSKY**

E.O. Paton Electric Welding Institute, NASU
11 Kazimir Malevich Str., 03680, Kiev, Ukraine. E-mail: office@paton.kiev.ua

The paper deals with features of joint formation in complex high-strength (α + β)-titanium alloy in vacuum electron beam welding. Investigations were performed on samples of alloy of Ti–Al–Mo–V–Nb–Cr–Zr system produced by electron beam remelting. Influence of thermal cycle of welding and subsequent heat treatment on structural-phase transformations in the metal of weld and welded joint HAZ has been studied. A structure with prevalence of metastable β-phase forms in the metal of weld and HAZ, which promotes lowering of ductility and impact toughness values. Post-weld heat treatment is required to improve the structure and properties of EB-welded joints. The best combination of strength and ductility of studied welded joints was achieved after performance of furnace heat treatment (annealing at T = 900 °C for 1 h and cooling in the furnace), which promotes producing a practically uniform structure and metastable phase decomposition in the weld and HAZ. 8 Ref., 2 Tables, 8 Figures.

K e y w o r d s : EBW, titanium alloys, heat treatment, welded joint, structure, mechanical properties

Development of modern competitive equipment usually requires improvement of performance of metal structures and parts. These requirements also apply to high-strength Ti-based alloys, which have become widely accepted as structural material. Leading materials science centers of the USA, EU, Russia and China perform intensive work on upgrading the currently available titanium alloys. More over, possibility of creating new alloys with a large amount of alloying elements is studied [1].

Modern two-phase high-alloyed Ti-based alloys are characterized by high specific strength. At present ever more attention is paid to fabrication of welded structures and components from titanium alloys with ultimate tensile strength $\sigma_t \geq 1100$ MPa [2]. Alloys with (α + β)-structure are widely applied as structural materials. They feature the best combination of technological and mechanical properties — they are stronger than single-phase alloys, can be easily forged, stamped, and heat-treated and have satisfactory weldability. Welded structures from these alloys are applied in aircraft engineering, rocket production, nuclear engineering, shipbuilding and chemical engineering [3, 4].

Weldability of two-phase high-alloyed titanium alloys, application of which can yield the greatest reduction of structure weight, is much worse than that of low alloys, and by this characteristic, they are inferior even to some high-strength steels. EBW is widely applied in fabrication of structures from high-alloyed titanium alloys, including also heat-hardenable two-phase alloys. High cooling rates at EBW and increased sensitivity of complex-alloyed titanium alloys to welding thermal cycle in a number of cases lead to lower ductility of the welded joint [5]. Therefore, two-phase titanium alloys require mandatory PWHT [6]. In development of new alloys, considerable attention is given to the possibility of producing welded joints with the strength of not less than 0.90–0.95 of base metal strength.

The objective of the work is studying the influence of thermal cycle of welding and PWHT on structural-phase transformations in the metal of weld and HAZ in EB-welded joints of complex-alloyed high-strength titanium alloy.

Table 1. Mechanical properties of complex-alloyed high-strength titanium alloy 8 mm thick

| Metal condition	Tensile strength σ_t, MPa	Yield point σ_y, MPa	Relative elongation δ_s, %	Reduction in area ψ, %	Impact toughness KCV, J/cm^2
As-rolled	1259.9	1179.5	1.7	6.2	5.0
As-annealed at 850 °C for 1 h	1214.9	1089.2	10.0	18.5	9.0
As-annealed at 900 °C for 1 h	1186.0	1123.6	13.3	19.0	13.5
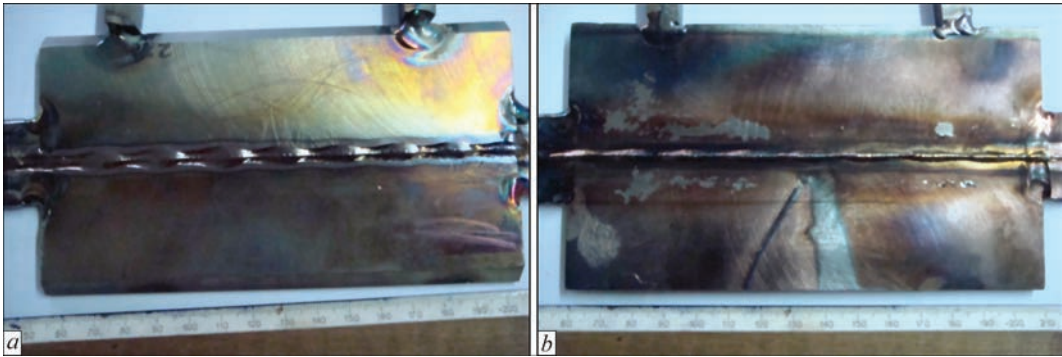
Figure 1. Appearance of EB-welded joint of complex-alloyed high-strength titanium alloy: *a* — face; *b* — root side

Materials and methods of investigations. We used 8 mm thick plates produced from ingots of test titanium alloy as research material [7]. After melting the ingots were subjected to thermodeformational treatment. Samples prepared for investigations had the following composition, wt.%: Ti–6.5Al–3Mo–2.5V–4Nb–1Cr–1Fe–2.5Zr. Mechanical properties of the studied alloy are given in Table 1.

EBW was performed in UL-144 unit, fitted with ELA 60/60 power source, in the following mode: accelerating voltage of 60 kV; beam current of 120 mA; circular scan diameter of 2 mm; welding speed of 25 m/h.

One of the advantages of EBW technology as regards titanium and alloys on its base, in addition to providing reliable protection of welded joints, is the possibility to perform local preheating and PWHT in the vacuum chamber [8]. Preheating of welded joints is a quite efficient technique, used in welding to prevent formation of cold cracks. However, as the studied alloy is not prone to cold cracking, preheating of surfaces being welded was not performed.

Figure 1 gives the general view of EB-welded joint.

To perform local PWHT the joint was heated by the electron beam developed into a rectangular scan. Heat treatment mode was selected, allowing for beam power and width of heated region (i.e. scan width). Electron beam power during local heat treatment was equal to about 3 kW and was corrected to maintain the required temperature in the treatment zone on the level of 850 °C. Treatment time was 5 min. Figure 2 gives the schematic of electron beam scanning at local PWHT of titanium alloy samples.

Postweld annealing of welded joints was performed in the furnace at 900 °C for 1 h.

Samples were cut up in «Isomet» unit of BUEHLER, using diamond disks. Chemical composition of test alloys was determined by spectral and chemical analyses. Metallographic examination and filming were performed in light microscope «Neophot-32» fitted with PC, digital camera OLYMPUS and archiving system. Sample hardness was determined in M-400 hardness meter (LECO) at 100 g and 1 kg load. Investigation of fracture surfaces of base metal and welded joints was conducted in high-performance multifunctional modern instrument — field emission Auger microprobe JAMP 9500F (JEOL). Testing for static tension and impact bending was performed to determine welded joint mechanical properties (according to GOST 1497–84).

Investigations were performed on the following samples of complex-alloyed high-strength titanium alloy:

● sample 1 — EB-welded joint;

● sample 2 — EB-welded joint with local PWHT (850 °C, 5 min);

● sample 3 — EB-welded joint with PWHT (furnace annealing at 900 °C, 1 h).

Investigation results. Local nature and intensity of EBW process provide a deep and narrow weld and small HAZ.

Metallographic investigations of sample 1 (Figure 3) revealed in welded joint metal cast crystallites
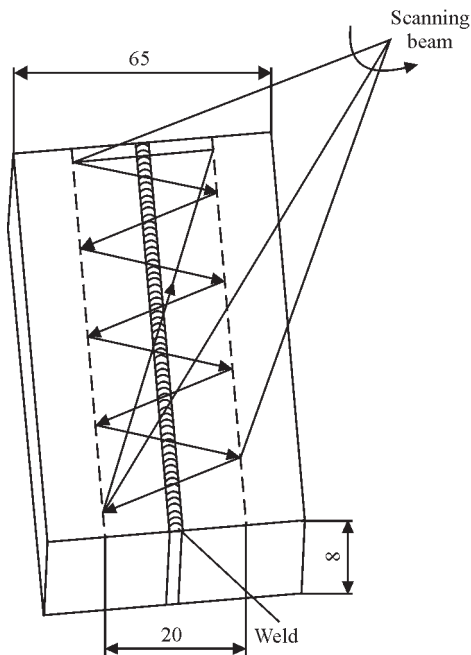
Figure 1. Schematic of EB-welded joint of complex-alloyed high-strength titanium alloy: *a* — face; *b* — root side
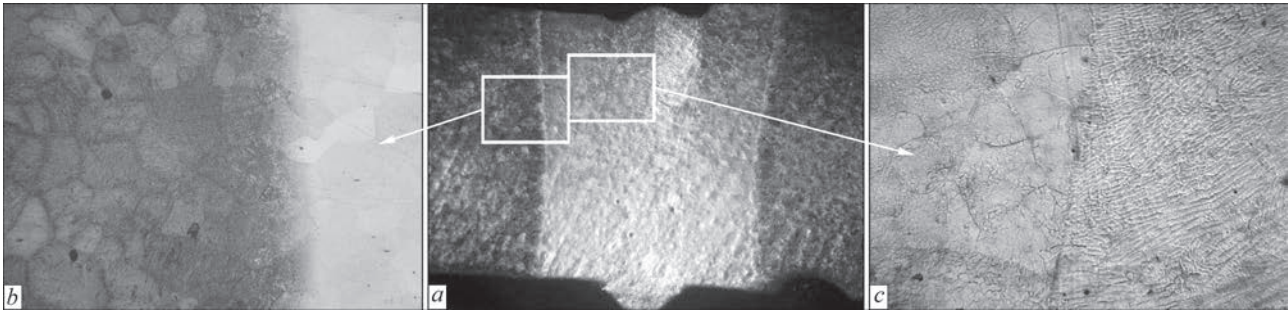
**Figure 3.** Structure of EB-welded joint of sample 1: *a* — general view (×10); *b* — BM microstructure (×50); *c* — microstructure of weld and HAZ (×100)
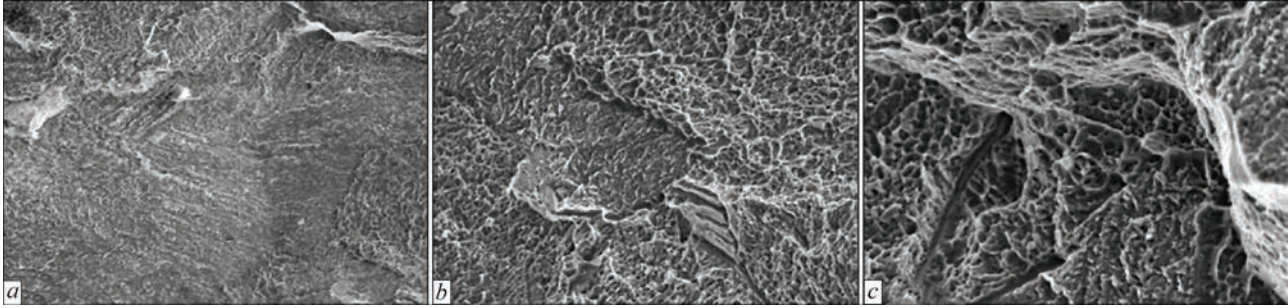
Figure 4. Fragments of fracture surface of sample 1: *a* — intergranular (×300); *b* — intragranular with separation (×500); *c* — pit type with separation and secondary cracks (×1000)

disoriented in the center, and oriented in the direction of heat removal along the edges, with clearcut dendritic structure. Weld metal microstructure is practically single-phase and consists of β-phase. Partial decomposition of β-phase with precipitation of fine particles of α-phase is observed in individual grains and along their boundaries. Hardness of weld metal is 2790–3210 MPa, weld width is 3–4 mm. In the HAZ, near the weld, the structure consists of large polyhedral grains of β-phase, with precipitates of fine-needled α-phase in the grain body. Individual grains with a substructure are also observed on weld–HAZ boundary. When getting closer to base metal, the size of β-phase grains becomes smaller. HAZ metal hardness is equal to 2690–3300 MPa, HAZ width being approximately 2–3 mm. Base metal structure consists of packs of parallel plates of (α + β)-phase. Grain size is 0.088–0.125 mm, base metal hardness being 3340–3430 MPa.

Fractographic studies of sample fracture surface after mechanical testing (Figure 4) showed that surface relief is weakly pronounced and fracture mode is of mixed type. Brittle fracture mode is 65 % quasi-cleavage, and that of ductile fracture is 35 % pit structure.

Metallographic investigation of sample 2 (Figure 5) showed that after local PWHT structural uniformity of welded joint becomes higher. Weld and fusion line are not as clearcut as after welding. The weld is a mixture of elongated and polyhedral β-grains with disoriented precipitates of α-phase plates. Weld metal hardness is equal to 3220–3450 MPa. HAZ consists of coarse polyhedral β-grains with precipitates of disperse α-phase. Hardness is equal to 3250–
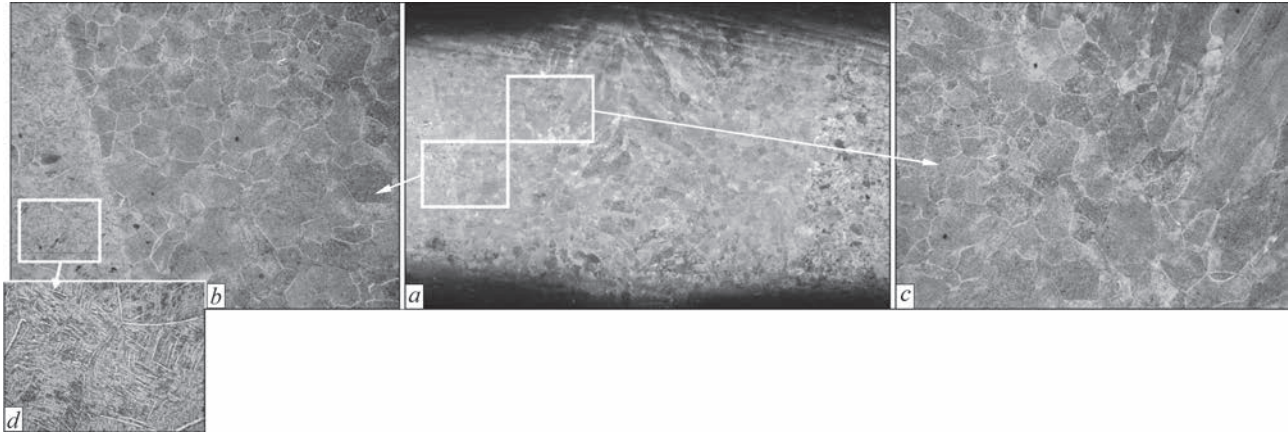
Figure 5. Structure of EB-welded joint of sample 2 after local PWHT (850 °C, 5 min): *a* — general view (×10); *b* — microstructure of HAZ–BM boundary (×50); *c* — microstructure of weld and HAZ (×50); *d* — microstructure of BM (×500)
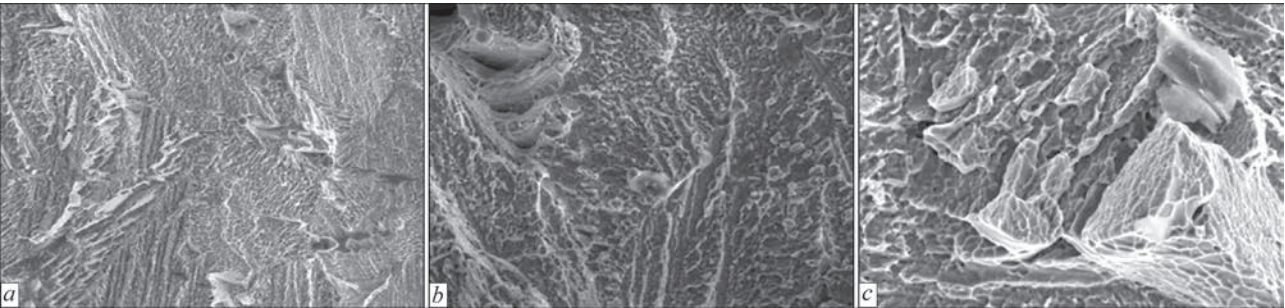
Figure 6. Fragments of fracture surface of sample 2: *a* — intergranular (×300); *b* — intragranular in combination with separation (×500); *c* — pit type with separation (×1000)
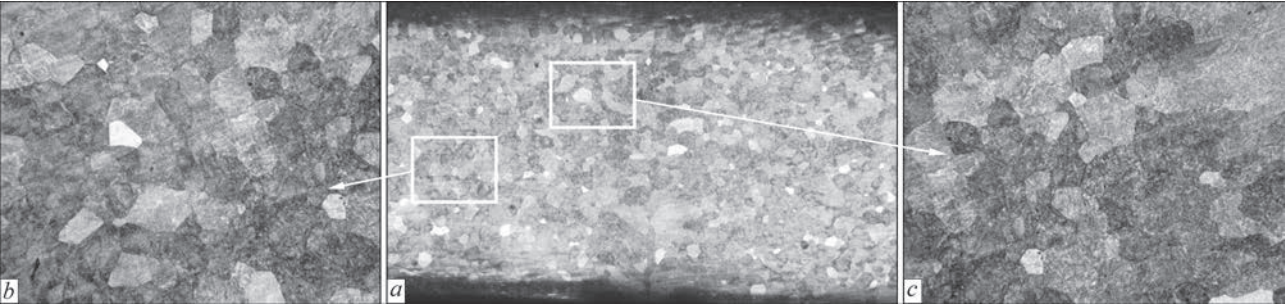
Figure 7. Structure of EB-welded joint of sample 3 after postweld furnace annealing (900 °C, 1 h): *a* — general view (×10); *b* — microstructure of HAZ–BM area (×50): *c* — weld and HAZ microstructure (×50)
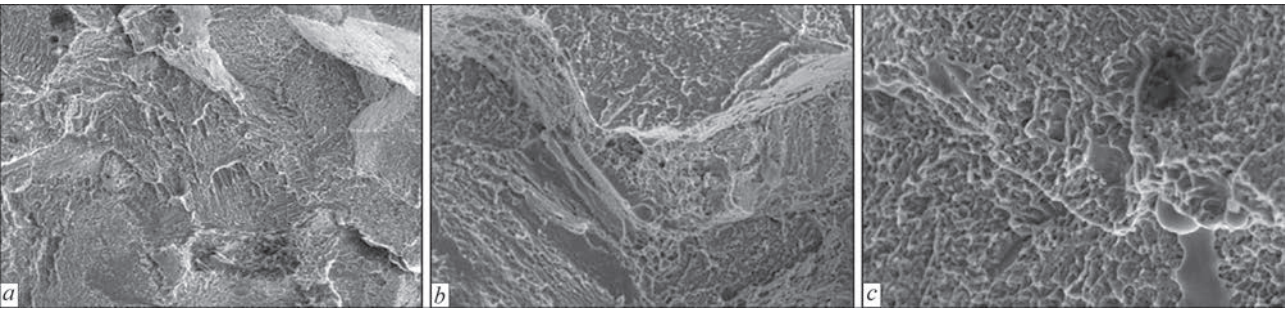
Figure 8. Fragments of fracture surface of sample 3: *a* — intergranular (×300); *b* — intragranular in combination with separation (×500); *c* — pit type (×1000)

3450 MPa. Base metal structure is presented by finer polyhedral grains with plate-like (α + β)-phase and hardness from 3420 to 3600 MPa.

Fractographic studies of the sample showed that fracture surface has a complex microrelief (Figure 6). The crack runs along the interfaces of β-phase matrix and disperse needle-like α-phase. Fracture surface contains cleavage facets against the background of intergranular fracture (separation sections). Fracture surface has many elevations in the form of steps.

Metallographic investigations of sample 3 (Figure 7) showed that after furnace heat treatment the studied sample structure becomes practically uni-

form, and no boundaries between the weld, HAZ and base metal are detected. The structure over the entire studied surface has different grains with plates of (α + β)-phase of different size. Hardness (from weld center into base metal) is equal to 3340–3440 MPa.

Fractographic studies showed that sample fracture is of a mixed nature (Figure 8). Fracture contains 30 % of brittle component and 70 % of ductile component. The crack propagated strictly perpendicular to the applied load. Brittle fracture proceeds in the mode of intragranular cleavage, and ductile fracture results from micropore coalescence. The observed cleavage facets are divided by separation sections. Separation

Table 2. Mechanical properties of EB-welded joints of complex-alloyed high-strength titanium alloy

Sample number	Sample condition	σ_t, MPa	σ_y, MPa	δ_5, %	ψ, %	KCV, J/cm²	
						Weld	HAZ
1	As-welded	1415	1380	2.0	6.6	7.2	6.0
2	Local PWHT (850 °C for 5 min)	1258	1216	4.3	9.2	7.3	14.4
3	Furnace PWHT (900 °C for 1 h)	1131	1089	12.0	24.5	12.4	12.7

occurs in those cases, when material has sufficiently high ductility.

Table 2 gives the results of mechanical testing of the studied samples.

Analysis of the Table leads to the conclusion that PWHT increases the values of ductility and impact toughness of welded joint of complex-alloyed high-strength titanium alloy. Particularly effective is furnace treatment (annealing at 900 °C for 1 h), which leads to significant increase of ductility and impact toughness in combination with a slight lowering of strength characteristics.

Conclusions

1. Structure and properties of welded joints of complex-alloyed high-strength (α + β)-titanium alloy produced by EBW were studied. It is found that the alloy has satisfactory weldability, but the structure in the metal of the weld and HAZ is not uniform and metastable phases are observed that leads to lowering of strength and ductility values.

2. Heat treatment of EB-welded joints of complex-alloyed high-strength (α + β)-titanium alloy, improves structural uniformity, lowers the probability of cracking in them and promotes improvement of mechanical property values.

3. After local PWHT of welded joints, toughness values increase only slightly, that is attributable to incomplete decomposition of metastable structures, resulting from short-time thermal impact (heating at 850 °C for 5 min).

4. The best combination of strength and ductility of the studied welded joints was achieved after furnace PWHT (annealing at 900 °C for 1 h and cooling with the furnace). Such treatment promoted formation practically uniform structure, decomposition of metastable phases in the weld and HAZ, that lead to significant improvement of ductility and impact toughness values.

1. Khorev, A.I. (2007) Theory and practice of titanium alloys development for advanced structures. *Tekhnologiya Mashinostroeniya*, **12**, 5–13.
2. Kablov, E.N. (2012) Strategy of development of materials and technologies of their treatment for period up to 2030. *Aviats. Materialy i Tekhnologii*, **5**, 7–17.
3. Grabin, V.F. (1982) *Metals science of fusion welding*. Kiev: Naukova Dumka.
4. Shorshorov, M.Kh. (1965) *Metals science of welding of titanium and titanium alloys*. Moscow: Nauka.
5. Gurevich, S.M., Zamkov, V.N., Blashchuk, V.E. et al. (1986) *Metallurgy and technology of welding of titanium and its alloys*. Kiev: Naukova Dumka.
6. Khorev, M.A., Gusev, Yu.V., Gribova, N.K. (1983) Heat treatment of welded joints of titanium alloys OT4 and VT20. *Avtomatich. Svarka*, **7**, 19–23.
7. (2007) *Electron beam melting in foundry*. Ed. by S.V. Ladokhin. Kiev: Stal.
8. Nazarenko, O.K., Kajdalov, A.A., Kovbasenko, S.N. et. al. (1987) *Electron beam welding*. Ed. by B.E. Paton. Kiev: Naukova Dumka.

APPLICATION OF FRICTION STIR METHOD FOR WELDING OF MAGNESIUM ALLOYS AND OF THEIR STRUCTURE MODIFYING

A.L. MAJSTRENKO[1], **V.A. LUKASH**[1], **S.D. ZABOLOTNY**[1] and **R.V. STRASHKO**[2]

[1]V.N. Bakul Institute for Superhard Materials, NASU

2 Avtozavodskaya Str., Kiev, 04074, Ukraine. E-mail:3ab@ukr.net

[2]E.O. Paton Electric Welding Institute, NASU

11 Kazimir Malevich Str., 03680, Kiev, Ukraine. E-mail: office@paton.kiev.ua

A technological process was developed for friction stir processing of surfaces of parts from magnesium and aluminum alloys for structure modification directed on formation of layer of fine-grain alloy structure (grain size 1.2–4.5 μm) that is 16–63 times less than the initial metal grain size (75.8 μm). It is determined that the maximum temperature of alloy heating in zone of contact interaction of a tool with FS-processed layers of the samples from researched alloys has reached 340–380 °C. Analysis of effect of kinetic parameters of the tool on change of microstructure of modified surface layers of the parts and welded joints was carried out. 18 Ref., 11 Figures, 3 Tables.

Regardless the fact that all the processes for joining structure metallic parts using electric arc, plasma, laser or electron beam and their combinations differ by separate process and economic advantages, but all of them have one common thing, i.e. presence of liquid phase in the joining zone, using which they are connected. This fundamental and important peculiarity of the process provides for a change of metal structure after its recrystallization, in particular, increase of grain size, phase transformations as well as formation of residual welding stresses, which have negative effect on welded joint strength. Therefore, during the whole history of metal fusion welding, the scientists from all over the world tried to develop the alternative methods of joining, in particular, solid-phase ones, which allow, at least partial, reduction of effect of mentioned phenomena.

Bevington (USA, 1891) [1] was one of the first who proposed solid-phase friction welding of pipes and rods, and then Khrenov and Sakhatsky (PWI, 1953) carried out «cold» friction welding [2]. Chudikov (1957) [3] can also be referred to the first developers of friction welding and surfacing. Method of rotation friction welding of metals developed by Kabanov and Averin (1960) [4] is one of the solid-phase friction welding methods, which has received wide distribution. However, this approach can not be used for butt and lap welding of the flat sheet structures as well as surfacing of other metals and alloys.

Application of the principle of solid-phase friction butt and lap welding of flat or curved sheet parts was proposed in 1991 in patent of Thomas et al. [5]. They proposed the method of welding of parts using active non-consumable tool. This technology, which authors called friction stir welding (FSW), provides for very simple method of tool and workpiece interaction.

Designs and materials of FSW tools. The method of dissimilar parts joining by FSW, proposed by Thomas and his colleagues, can be referred to the most significant technological achievements for the last thirty years. It provided for the possibility to join the parts from the materials which earlier couldn't be welded at all by traditional arc welding or was difficult-to-weld, i.e. different aluminum, magnesium and titanium alloys. Application of new technology expanded the possibilities of reconstruction and repair of complex equipment by means of deposition of new layer of metal over part surfaces.

However, regardless the success of FSW, there are a lot of problems which should be solved for expansion of industrial application of this technology. Among them the main problem is providing the process with safe, reliable and wear-resistant tool. In the process of welding the tool is simultaneously subjected to the effect of torque moment, alternating-sign cyclic bending forces as well as effect of high temperatures. Absence of reliable answers to these questions in the world scientific resources makes difficult application of new advanced technology, i.e. FSW, in

a broad-scale. Figure 1 shows a schematic diagram of operation of the tool, which is used in FSW of different metals [5].

For a long time the E.O. Paton Electric Welding Institute has been carrying out the experimental works in «cold welding» [6], and in course of several years V.N. Bakul Institute for Superhard Materials has been performing the works on development and application of the tools for FSW of different metals and alloys [7–10]. Analysis of available sources on manufacture of such type tools gives an idea of the materials which should be used at that [11–14].

These materials should keep high hardness and strength at high temperatures. At that their properties should significantly exceed mechanical characteristics of the materials being welded or surfaced. Besides, the tool, in particular, its working part, should have high wear and heat resistance. These properties are, first of all, determined by significant temperatures and forces on the tool, which appear in welding or surfacing.

The working tips of FSW tools are made in form of cylinders with rounded edges, cones or cylinders. On the surfaces of the latter a complex-shape groove with shiftable step is cut, which should promote better metal movement within the weld. As a rule the groove has a direction opposite to tool rotary motion. Probably, in order to provide better weld formation and reduce forces on the tool, the latter is set not vertically to surface plane, but at small angle 2–5° to the side opposite to advance direction.

The complex shape of pins are necessary to provide the best metal stirring as possible in order to increase welding process efficiency. The results of multiple investigations showed the relationship between heat, which is generated depending on process kinematic parameters, and weld static strength [10]. Also a change was observed in the microstructure of HAZ as well as stirring zone in comparison with base material.

Analysis of data, received on tools for FS surfacing and welding, for the first stage allowed making a conclusion on producing the tool samples from high-strength tool steel. These samples were manufactured from high-speed steel R18, quenched at 1270 °C. After quenching the tool was subjected to 1 hour tempering at 550–570 °C for transformation of residual austenite into martensite and dispersion quenching (secondary hardening). Steel hardness of the part reached *HRC* 65 as a result of heat treatment. The tools with higher hardness can be produced by application of powder steels, developed for replacement of R18 and R9 steels, namely ROM2F 3-MP, M6F 1-MP and M6F 3-MP.
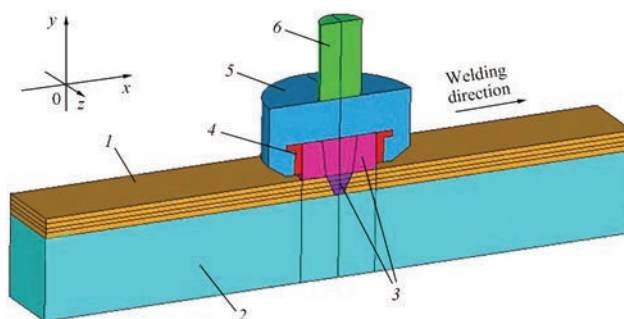
Figure 1. Schematic of FSW process: *1*, *2* — part being welded; *3* — tool with shoulder; *4* — hard alloy casing; *5* — steel holder; *6* — drive steel shaft

Application of steel in tool manufacture allows having the pin of complex shape, which is not always possible in use of ultra-hard materials. Besides, price of the tool will be significantly less, that makes its application economically effective in series of cases.

There are steel grades, physical-chemical properties of which can be used for the FSW tool. At that, tungsten-alloyed tool steels, namely R18 and R9M4 K8, such called highs speed steels [7, 8], have the largest strength. However, their heat resistance is in the range of 600–650 °C, that states these steels application only for welding of parts from fusible alloys. Austenite class steels 20Kh23N18 and 12Kh25N-16G7AR have somewhat lower strength indices, but their heat resistance is significantly larger and reaches 1000 °C. Analysis of known properties of alloys based on chromium, nickel and cobalt indicates the necessity in the tools from heat- and wear-resistant materials, design of which was developed in scope of «Resurs» program (Figure 2) [7, 8] for FSW of these alloys.

Thus, the tools for FSW of relatively fusible aluminum and magnesium alloys, shown in general in Figure 2, *a*, were developed and manufactured. At the same time, the attempts to use steel tool for surfacing of nickel or cobalt on copper substrate didn't give positive results due to relatively high temperature in FSW zone. Therefore, the tools from hard alloy VK8 (Figure 2, *b*) were manufactured for FS welding and surfacing of copper and its alloys, and the tools from polycrystal cubic boron nitride (CBN)-based ultra-hard material (Figure 2, *c*) (Table 1) [7] were used for FSW of steels, nickel, cobalt and other refractory metals and alloys.

However, even application of powder metallurgy does not always provide for radical increase of strength of steel tool for FSW and dramatically increases its costs and terms of production. Thus, a decision was made on application of the tools from hard alloy or polycrystal ultra-hard materials (PUHM) (Table 1) [7, 8] for welding of materials with higher strength and
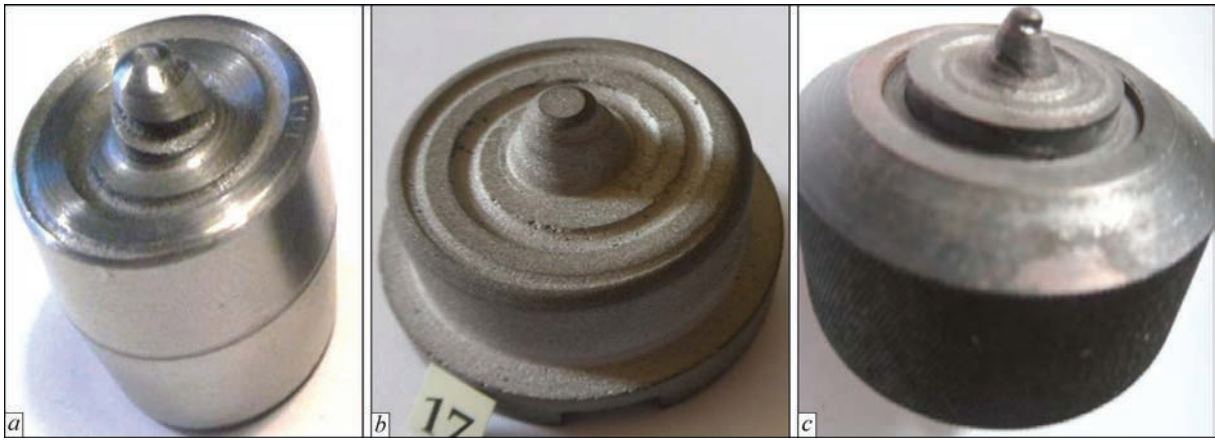
Figure 2. View of tools for welding, surfacing and modification of metal by friction stir process [7, 8]; *a* — from steel R18 for FSW and modification of structure of aluminum and magnesium alloys; *b* — from hard alloy VK8 for surfacing of copper; *c* — from CBN for surfacing of nickel and cobalt

larger melting temperature, such as copper and nickel. Such high physical-mechanical properties, respectively, gives rise to complex and laborious machining of tools from CBN.

The investigations show that very thin and homogeneous grain structure [9, 10] is formed during FSW in the zone of tool proceeding. Also, it should be noted that hardness of material being processed to significant extent depends on rotation and forward speeds of the tool and is widely varied in processing area. They determine distribution of material deformation rates in the processed zone, correlating with deformation rate distribution and average size of grain microstructure, bound by Zener–Hollomon parameter.

Grant and Weil [15] investigated the process of solid-phase FSW. They showed that tool immersing the subsurface layer of metal, as a result of friction work and plastic deformation, provides for metal heating to the temperature sufficient for reduction of yield point and hardness to visco-plastic state. At that, the authors have proposed to divide FS-welded joint cross-section on conventional zones, namely fine-grain «core» of weld stirred metal (SM) consisting of re-crystallization zone with changed microstructure, thermomechanical-affected zone (TMAZ), HAZ and base metal.

This work pays main attention to the peculiarities of structure in weld SM zone and TMAZ, formed in stir friction.

Research of heat generation in zone of FS-welded processing of magnesium alloys. Investigation of the process of heat generation at interaction of the

tool with processed surface layer of metal is carried out by setting the compound parameters of tool loading and measurement of distribution of tool heating temperature. However, structure of metal and parameters of this zone will depend on shape and size of the tool, physical-mechanical characteristics of processed material and kinematic parameters of tool movement. Therefore, one of the priority tasks in development of FSW tool is to determine the temperature distribution in different points of zone of its interaction and, thus, study the thermal-physical conditions of operation, and, based on that, create more well-grounded boundary conditions for solution of the problem on thermo-stressed state of FSW tool depending on kinematic parameters of its movement [10].

It is a well-known fact that a heat source of large intensity is formed in the FS process due to friction between tool rotating surface and metal of the part as well as deformation work of this metal. Therefore, the process of heat generation in stir zone during FSW or modification of structure of surface layers of metals and alloys depending on kinematics and force parameters of tool interaction with metal of the part [16] was studied for determination of main factors of effect of stir or welding process on change of metal structure in this zone.

Magnesium alloy ML10, which is widely used in aircraft and space technologies, was taken as an object for investigation of effect of FS process on change of metal structure state. Let's consider some reference properties of this alloy related with heat-resistant cast magnesium alloys [17, 18]. ML10 alloy is

Table 1. Physical-mechanical properties of some materials used for FSW tool manufacture [7, 8]

Material	*HRC*	*HV*, GPa	σ_{bend}, ГПа	σ_{comp}, ГПа	Heat resistance, K	CTE $\alpha \cdot 10^{-6}$ K^{-1}
High-speed steel	62–67	–	2–6	2.5–4.0	900–1000	9–12
Hard alloy	88–89	13–14	0.75–2.60	3.5–5.9	1100–1300	3.0–7.5
PUHM–CBN	–	30–40	0.4–1.5	2.0–6.5	1200	4.9–7.9
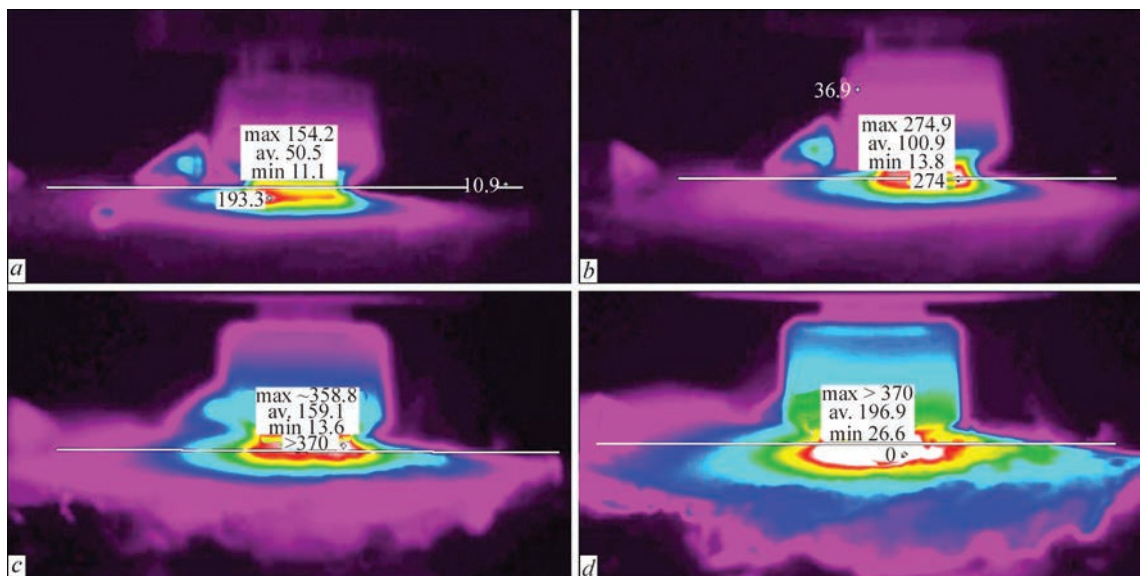
Figure 3. Change of Fluker-ir25-measured temperature distribution on surface of ML10 sample at tool movement over sample of 5 (*a*), 10 (*b*), 15 (*c*) and 20 (*d*) s

referred to Mg–Nd–Zr system. The structure of this alloy represent itself a solid solution of Nd, Zr and Zn in Mg and their eutectics along the grain boundaries, which includes Mg9Nd compound. The average size of grains of initial alloy ML10 reaches 75–100 μm. The mechanical properties of alloy at room temperature are sufficiently high, but the main peculiarity of its properties is the fact that they are kept at elevated (up to 250 °C) temperatures.

Processing the surface layers of samples of alloy ML10 was carried out using steel tool to 6 mm depth with six modes of tool rotation: v_w = 20–40 mm/min and tool rotation rate ω = 600–800 rpm [9]. Temperature measurements and determination of temperature field distribution in zone of ML10 alloy modification were registered with the help of infra-red imager Fluke-ir25 at different moments of tool movement over the sample (with 5 s increment) (Figure 3). Table 2 shows the average values of temperature in zone of FS processing on surface of ML10 samples at different kinematic parameters of tool movement in their surface layer. It is noted that the maximum temperature of ML10 alloy heating in the zone of contact interaction of the tool with processed layer of the sample reached 380 °C.

Figure 4 shows in-time variation of temperature distribution in the section across the width of tool in-

teraction zone. At that, it should be noted that temperature in zone of tool effect shall reach (0.4–0.6) T_m for realization of FSW (FS) process. The results of carried measurements allowed determining not only the average temperature values on the surface of contact zone, but also time which is spent before the beginning of tool immersion in the metal up to reaching a thermal balance of heat flows which are formed directly in the processing zone, and heat flow which is emitted from the surface of sample and tool. Thus, thermal balance in the processing zone is stabilized in 15–20 s (see Figure 4) [9, 16].

Obtained result can be considered from technological point of view, which lies in the necessity of receiving similar conditions of tool operation with part metal. Therefore, it should be considered that before tool entering in the zone of part processing, the metal reaches necessary temperature only in 15 s, i.e. the process of part processing shall be done only using artificial support.

Modifying the structure of surface layer of magnesium alloys. Modifying the alloy structure is

Table 2. Change of maximum temperature in zone of processing of ML10 samples at different kinematic parameters of tool movement in sample surface layer

v_w, mm/min	T_{max}, °C, at ω, rpm	
	630	800
20	360	350
31.5	350	360
40	340	380
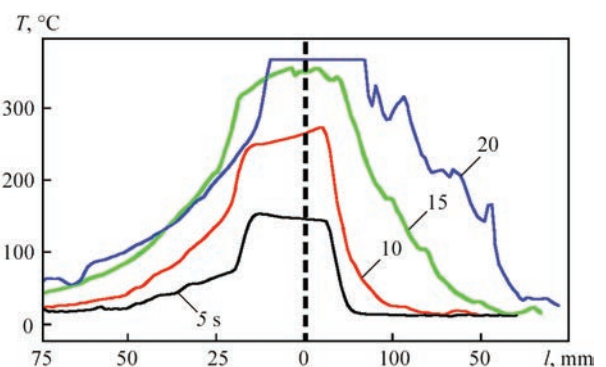
Figure 4. In-time change of temperature distribution in contact zone of tool with surface layer of ML10 sample from the beginning of its horizontal movement
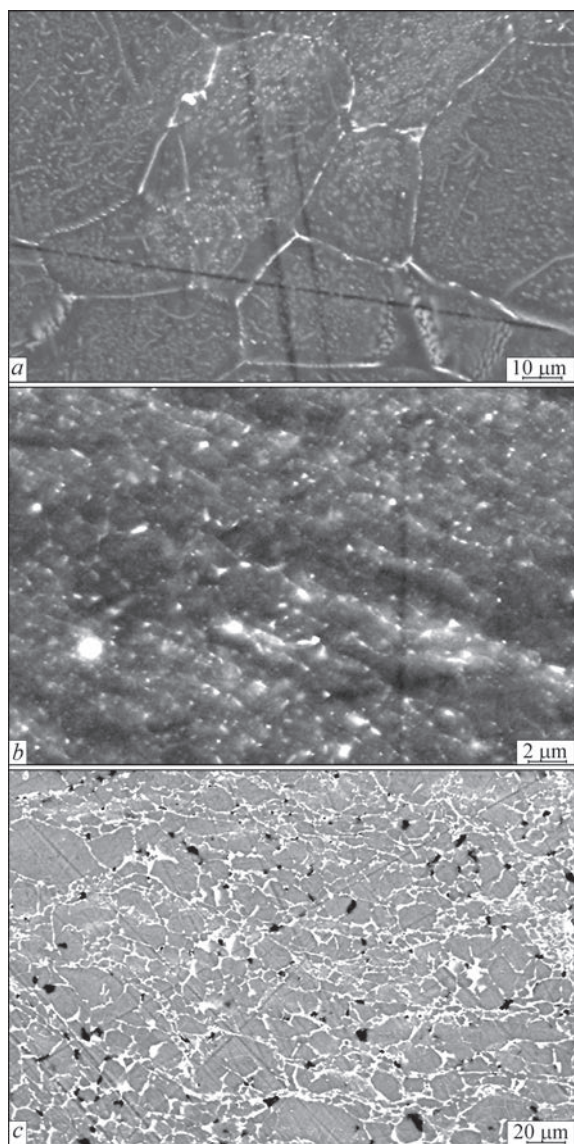
Figure 5. Size of grains of ML10 alloy in FS processing zones: *a* — base metal (d_{av} = 75.8 μm); *b* — SM zone (1.2–4.5 μm); *c* — intermediate TMAZ zone between SM and base metal (7.8 μm)
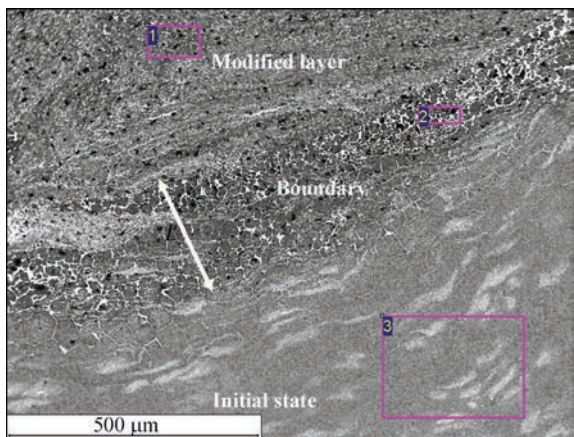
Figure 6. Microstructure of modified surface layer of ML10 sample at FS processing mode 1 (here and in Figures 7–11 mode parameters see in Table 3)
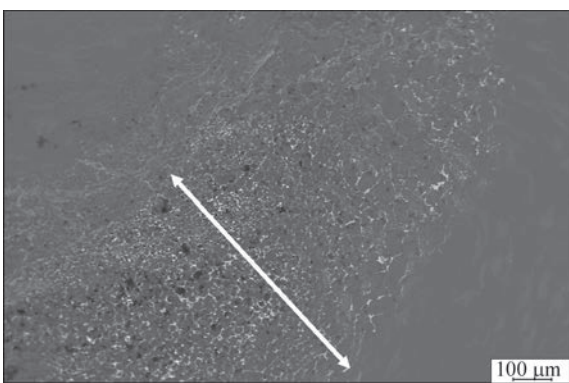
Figure 7. Microstructure of modified surface layer of ML10 sample at FS processing mode 2

the process of change of its structure similar to that which takes place in metal structuring in hot rolling or forging, i.e. structuring and refining of grain structure under the effect of intensive plastic deformations. Researches on FSP of the surface layers of parts from magnesium alloys are directed on determination of the effect of kinematic and force parameters on change of structure and properties.

Modification of the structure of surface layers of alloy ML10 was carried out with steel tool to 6 mm depth. As it was mentioned above, the tool in FSW forms SM zone and TMAZ, which later on determines the strength of joining of stirred metal with base metal, and HAZ (Figure 5). Structures of the base ML10 metal and different SM zones and TMAZ were analyzed using standard stereology methods. It made a basis for determination of the values of average alloy grain size in these zones in comparison with the value of alloy grains in the initial condition (d_{av} = 75.8 μm).

Thus, the distribution of average values of grain size in the zones of technological ML10 alloy processing was determined as a result of carried investigation, namely in ML10 base metal d_{av} = 75.8, in TMAZ — 7.8, in SM zone — 1.2–4.5 μm.

Effect of kinematic parameters of tool movement on formation of intermediate TMAZ in FSW of ML10 alloy. Let's consider the effect of kinematic parameters of tool movement at different processing modes on formation of structure and thickness *L* of the intermediate TMAZ in FSW of magnesium alloy (Table 3; Figures 6–11). As it was mentioned above,

Table 3. Effect of FSW parameters on thickness of transition zone of TMAZ with base ML10 metal mating

Mode number	v_w, mm/min	ω, rpm	*L*, μm
1	20	630	250
2	31.5	630	800
3	40	630	1200
4	20	800	1100
5	31.5	800	800
6	40	800	300
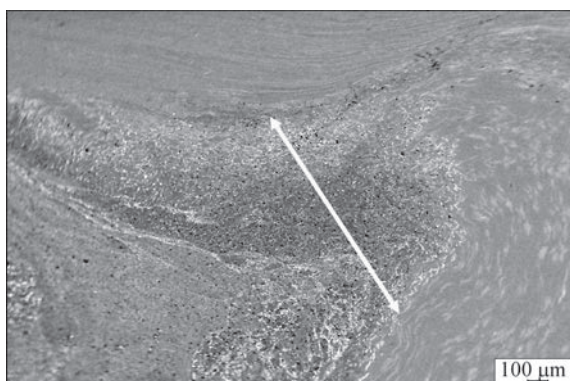
Figure 8. Structure of modified surface layer of ML10 sample at FS processing mode 3

Figure 10. Structure of modified surface layer of ML10 sample at FS processing mode 5

the structure of SM zone and TMAZ was formed at set kinematic parameters and depth of tool immersion in the surface layer to 6 mm.

Analysis of images of metal structure in FSW zones at different kinematic modes of surface layer modification was performed. It allowed making a conclusion that FSW at v_w = 40 mm/min and ω = 630 rpm approaches to the optimum for ML10 alloy because at that the thickness of TMAZ achieves the maximum size L = 1200 μm. Meeting this particular condition at the boundary of TMAZ and base metal eliminates formation of lamination and cracks, that provides for maximum strength of the joint.

The following conclusions can be made based on carried analysis of structure of magnesium alloy ML10 after FSP.

Fundamental changes of the structure are observed in FS zone and HAZ in contrast to base metal. This is a consequence of refinement of the initial metal grains (to 1.2–4.5 μm), that is 16–63 times less than the size of grains in the base metal (75.8 μm). This effect is characteristic for all FS-welded joints independent on technological parameters of welding.

Weld metal structure in the cross section is virtually uniform, except for the zone of its mating with the base metal and subsurface area of weld face, which was formed at contact with rotating tool. Formation

of fundamentally other structure, namely fine and close to equilibrium one, takes place due to base metal grain refining as a result of plastic deformation in FSW process. It allows obtaining higher properties of weld metal strength and ductility. TMAZ metal structure of near-weld zone in joint can be compared with the initial one, but in contrast to texture of base metal it virtually has 10 times difference on grain size (d_{av} = 7.8 μm), orientation as well as shape of grains.

The zone of weld to base metal mating is the zone which represent itself TMAZ of 250–1200 μm width with adjacent to it metal volumes from the side of weld and base metal. TMAZ metal as well as weld metal is the zone of maximum metal heating, which is subjected to intensive mechanical impact of rotating welding tool. The width of TMAZ in ML10 alloy welded joint has direct dependence on heat effect in welding. TMAZ metal structure is a transfer one from fine-grain (in weld SM) to re-solidified, which partially preserves the base metal texture. Fine equiaxed disordered grains are observed from the side of base metal along the boundaries of coarse grain. Such change of structure is a consequence of effect on near-weld zone metal of significant plastic deformations which take place in process of welded joint formation as well as of processes of re-crystallization under conditions of heating in FSW.
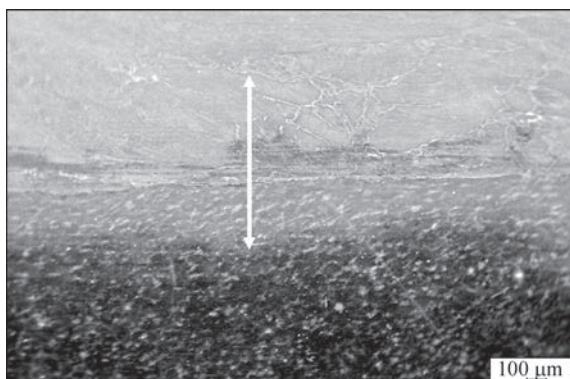
Figure 9. Structure of modified surface layer of ML10 sample at FS processing mode 4

Figure 11. Structure of modified surface layer of ML10 sample at FS processing mode 6

The average size of grains in TMAZ makes 7.85 μm that is 10 times less the size of base metal grains. The maximum thickness of TMAZ with re-solidified structure reaches 1200 μm, at that the maximum values of temperature of metal heating on weld surface for investigated FSW modes (v_w = 40 mm/min and ω = 630 rpm) do not exceed 340–350°C. The results of metallographic investigations showed that TMAZ near-weld metal can be the weakest chain between base and weld metal. Thus, welding is reasonable to be performed using modes with limited heat generation for reduction of softening thermal effect of FSW.

Fracture and disorienting of crystallites of initial metal, appearing in formation of fine-grain structure (grain size 1.2–4.5 μm), that is 16–63 times less than the initial grain size (75.8 μm), was determined in FS zone of magnesium and aluminum alloys using reflection electron diffraction method on SEM with energy-dispersive analyzer.

1. Bevington, J.H. *Spinning tubes*. Pat. 444721 US. Pat. 13.01.1891.
2. Khrenov, K.K., Sakhatsky, G.P. *Method of cold butt welding of metal products*. USSR author's cert. 97024. Fill. 20.07.53.
3. Chudikov, A.I. *Method of butt welding*. USSR author's cert. 106270. Int. Cl. B23k 20/12. Publ. 1957.
4. Kabanov, N.N., Averin, I.V. *Method of friction butt welding of dissimilar metals*. USSR author's cert. 126732. Fill. 03.06.59. Publ. 01.01.60.
5. Thomas, W.M., Nicholas, E.D., Needham, J.C. et al. *Friction stir butt welding*. Pat. 9125978.8 GB; 5460317 USA. PCT/92/02203.
6. Poklyatsky, A.G., Ishchenko, A.Ya., Yavorskaya, M.R. (2007) Strength of joints on sheet aluminium alloys produced by friction stir welding. *The Paton Welding J.*, **9**, 42–45.
7. Zelenin, V.I., Poleshchuk, M.A., Zelenin, E.V. et al. (2010) Repair of plates of continuous casting copper molds by friction stir surfacing. In: *Rock cutting and metal-working tool — technique and technology of its manufacturing and application*, Issue 13, 476–479.
8. (2013) *Development of design and manufacturing technology of tool for friction stir welding of alloys based on Cr, Ni, Co. Manufacturing of tool prototypes and realization of laboratory experiments on nature of their wear and fracture during operation*: Report of works on agreement P7.5.2. Kyiv: ISM.
9. (2014) *Development of friction stir welding tools from superhard materials designed for manufacturing and restoration of life of aluminium and magnesium alloys:* Report of works on agreement P8.6.1. Kyiv: ISM.
10. Majstrenko, A.L., Nesterenkov, V.M., Dutka, V.A. et al. (2015) Modeling of heat processes for improvement of structure of metals and alloys by friction stir method. *The Paton Welding J.*, **1**, 2–10.
11. Rai, R., De, A., Bhadeshia, H.K.D.H. (2011) Review: Friction stir welding tools. *Sci. and Tech. of Welding and Joining*, Vol. 16, 325–342.
12. Mironov, S.Yu. (2014) Formation of grain structure in friction stir welding. *Fizich. Mezomekhanika*, Issue 17, 103–113.
13. Lee, J.A., Carter, R.W., Ding, J. (1999) *Friction stir welding for aluminium metal matrix composites (MMC's)*: MSFC Center Director's Discret Fund. Final Report TM-1999-209876. NASA.
14. Shtrickman, M.M. (2007) State and development of friction welding process of linear joints (Review). *Svarochn. Proizvodstvo*, **10**, 25–32.
15. Grant, G., Weil, S. (2011) Joining technologies for coal power applications. In: *Advanced Res. Materials Program:* Ann. Rev. Meet. Proc. (Portland, Apr. 26–28, 2011).
16. Nesterenkov, V.M., Majstrenko, A.L., Lukash, V.A. et al. (2013) Possibilities of modification of light alloys structure by stir friction. In: *Proc. of Int. Sci.-Techn. Conf. on New and Unconventional Technologies in Resource and Energy Savings* (22–24 May 2013, Odessa, Ukraine), 117–120.
17. Kolobnev, I.F., Krymov, V.V., Melnikov, A.V. (1974) *Reference book of founder. Nonferrous castings*. 2nd ed. Moscow: Mashinostroenie.
18. Portnoj, K.I., Lebedev, A.A. (1952) *Magnesium alloys*: Refer. Book. Moscow: Metallurgizdat.

PECULIARITIES OF STRUCTURE OF Cu–Cu, NI–Cu AND STEEL–Cu JOINTS PRODUCED BY OVERLAP FRICTION STIR WELDING METHOD

G.M. GRIGORENKO, M.A. POLESHCHUK, L.I. ADEEVA,
A.Yu. TUNIK, E.V. ZELENIN and **S.N. STEPANYUK**
E.O. Paton Electric Welding Institute, NASU
11 Kazimir Malevich Str., 03680, Kiev, Ukraine. E-mail: office@paton.kiev.ua

The work is dedicuted to investigation of overlap friction stir welded joints of sheet billets of homogeneous (Cu–Cu) and dissimilar metals with unlimited (Ni–Cu) and limited solubility (Cu–St.3, Kh18N10–Cu) of the components in solid state. The FSW process is performed due to plastic deformation of metal being heated to recrystallization temperature without melting. The leading role in this process plays mechanical stirring of metals in plastic state. The role of diffusion processes is insignificant. The quality joints are received at optimum welding modes. Plasticization and dynamic recrystallization in FSW of Cu–Cu plates promote for grain refinement (5–30 μm) in the stir zone and develop dense weld microstructure, comparable with the base metal. The weld microhardness reaches 80–107 % of the base metal microhardness. FSW of Cu and Ni resulted in the quality welded joint with mutual penetration of one metal into another at up to 3 mm depth. Interdiffusion of Cu and Ni along the grain boundaries takes place at up to 20 μm depth with formation of solid solution interlayers of these metals. Examination of Cu–St.3 and Kh18N10–Cu joints demonstrated significant grain refining in the recrystallization zone as well as in the HAZ. St.3 and Kh18N10 steels plung in copper at 1000 and 2000 μm depth in form of bands and strips. Large amount of Fe-based inclusions, embedded in form of separate bands and particles, is noted in the stir zone. Thus, applying the welds at specific distance from each other allows producing quality solid welding-up of upper thinner plate to massive lower plate (as in deposition) with overlapping of recrystallization zones at minimum heating and distortion of the parts. The carried investigations allow recommending this method for reconstruction of initial dimensions and development of protective layer (Ni, Kh18N10 steel) on copper plates of CCM mold. 11 Ref., 1 Table, 8 Figures.

K e y w o r d s : friction stir welding, lap joint, mechanical stirring of metals, diffusion, solubility in solid phase, microstructure, X-ray spectrum microanalysis, chemical composition, microhardness

FSW is the variation of pressure welding when a welded joint is formed as a result of mutual plastic deformation of parts being joined in solid phase [1–3]. From other types of pressure welding it differs by heating method, namely, by the method of heat input in the parts being welded. Kinetic energy in FSW is transformed into the heat energy, moreover, heat generation is strictly localized in the thin sub-surface layers of metal. Most of the researchers indicate the following advantages of FSW in comparison with other methods for production of permanent joints [4, 5]. This is, to a great degree, retaining of the properties of the base metal in the welding zone in comparison with fusion welding methods; possibility of producing defect-free welds on alloys which tend to formation of hot cracks and porosity in weld metal during fusion welding etc. Currently the possibility of FSW application for producing the dissimilar metal joints [6–9] is of large interest.

The FSW process involves the following: rotating tool in form of a rod, consisting of two main parts, i.e. shoulder and projecting from it pin, which plunges

the material in such a way that the pin should enters to a depth below interface of two plates being joined. The shoulder presses the plates with significant force and serves as a main heat source. The tool is moved at determined rate and carries out welding of two plates (Figure 1). The FSW process generates sufficient amount of energy, necessary for plasticization, stirring and formation of quality joint. Deformation and stirring of the metal in solid phase develops denser, fine microstructure of the joint zone in comparison with the base metal [10, 11].

One of the main problems restraining wider application of FSW is resistance (life) of working tool, basic diagram of which and variants of manufacture are given in work [4].

The tool itself and, in particular, the working rod (pin) are subjected to high thermal-mechanical loadings. Torque moment and alternating cyclic bending force simultaneously effect the heated working rod. The material of surfacing tool shall be heat-resistant and high-temperature that allows operating in 800–1200 °C temperature range, at which plasticization of
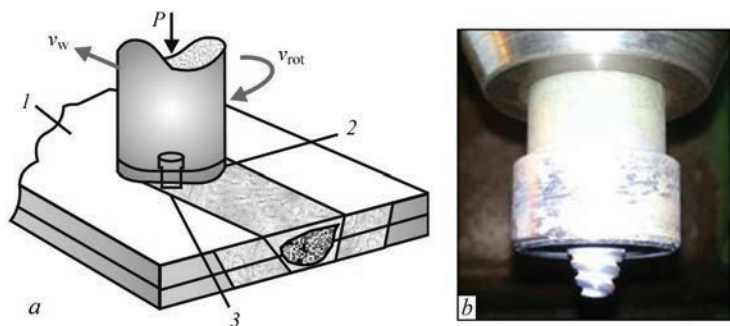
Figure 1. Scheme of FSW process (*a*), and working tool (*b*): *1* — part; *2* — shoulder; *3* — tool with special profile

copper, nickel, iron and their alloys takes place. An important requirement is also sufficiently high bending strength of the tool under these conditions.

For this work the V.N. Bakul Institute for Superhard Materials has developed and proposed the new materials based on vanadium carbides and boron nitrides. The technology was developed for sintering the tools from mixture of cubic boron nitride and aluminum with addition of refractory compounds of titanium and zirconium.

The tool's shape plays an important role in the FSW process. Thus, the best results were obtained at application of the tool with cone pin (Figure 1, *b*). In this case the bending loadings come along a tangent to main body of the tool, that is very important in use of tool of increased brittleness. Size and shape of the tools were developed based on number of experiments on surfacing of copper, nickel and other materials carried out between PWI, ISM and SPC «VISP».

Cu–Cu, Ni–Cu, Cu–St.3 and Kh18N10–Cu lap joints were examined for investigation of the processes taking place in FSW of homogeneous and dissimilar metals. Copper and nickel form continuous series of solid solutions, and copper with carbon and stainless steels have limited solubility of elements in solid state. FSW modes and characteristic of materials being welded are given in the Table. A complex procedure including optical metallography, X-ray spectrum microanalysis, scanning electron microscopy and durometry was used for examination of obtained joints.

Cu–Cu joint. Lap joints of copper plates were produced by FSW, the relationships were determined between structural changes, microhardness of samples and modes on which welding was carried out (see the Table). The copper plates were joined by sin-

gle-pass (Figure 2, *a*) and multi-pass weld by overlaying of single-run parallel welds at specific distance from each other (Figure 2, *b*). As can be seen from Figure 2, the received joints are sound, without pore, defects and cracks.

In all the cases, tool passing provokes for a dynamic recrystallization in the upper plate, and fine-grain structure with equiaxed grains from 20 to 100 μm size (Figure 2, *c*) is registered. The depth of this zone makes 3–5 mm. A zone of oval-shape nucleus with insufficiently determined, interrupting growth rings of not less than 5 mm depth is formed under the recrystallized metal of upper layer. Size of grains in it is comparable with recrystallized grains of the upper plate.

Welding-up of copper plates between themselves is provided during their lap FSW at 16–19 mm distance between the welds (shoulder diameter 31 mm). The stirring zones of weld metals overlap each other. Sufficient amount of heat was generated at given modes of welding (v_w = 56–160 mm/min, v_{rot} = 1400 rpm) which is necessary for plasticization and stirring of material of plates being welded and formation of quality joint as in deposition. FSW provides for high quality of welding. Denser microstructure of the joint zone comparable with the base metal is developed during metal deformation and stirring in solid phase. The weld microhardness achieves 80–90 % of the base metal microhardness and sometimes even more due to grain refinement. Thus, microhardness of the weld zones, i.e. the metal of upper plate and nucleus in relation to the base metal, makes 98 and 107 %, respectively (Figure 3) at v_w = 110 mm/min and v_{rot} = 1400 rpm.

In practice, the FSW method is used for lap welding (as in deposition) by parallel welds of copper

Modes of FSW and characteristics of materials to be welded

Material of upper/ lower plate	Grade of material of upper/lower plate	Thickness of upper/ lower plate, mm	Depth of pin plunge, mm	Welding speed, mm/min	Rate of pin rolation, rpm	Microhardness of upper/lower plate, MPa
Cu/Cu	M0/M0	2.5–5.0/16–22	3.5–5.5	56–160	1200–1400	1145/1195
Ni/Cu	M1/M0	4/10	5.0	40	1250	2312/1160
Cu/St.3	M0/St.3	7/8	8.0	60	1250	1160/2160
Kh18N10/Cu	Kh18N10T/M1	3/18	4.5	56–160	1400	1430/470
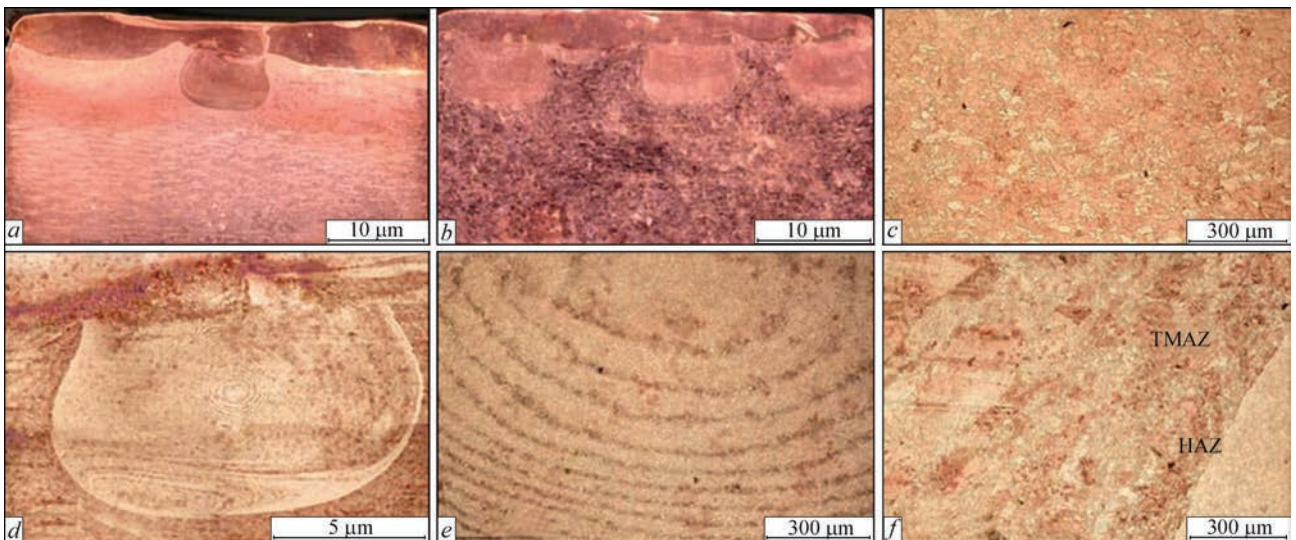
Figure 2. Structure of single- (*a*) and multipass (*b*) joints at lap FSW of copper plates; *c* — metal of upper plate; *d*, *e* — nucleus; *f* — HAZ and TMAZ

sheet to copper plate in CCM mold for the purpose of reconstruction of its initial size.

Ni–Cu joints. The joints of Ni–Cu dissimilar metals were produced by FSW using the modes indicated in the Table. Welding was carried out through nickel plate of 4 mm thickness. Longitudinal and cross metallographic sections of this joint (Figure 4) were investigated. The welded joint has no defects, i.e. lack of penetration, cracks and pores. A nucleus of rounded shape of 4×6 mm size located in copper and representing itself concentric deformation rings with nickel particles inclusions (nickel content makes approximately 10 vol.%) was formed in the joint zone cross-section. A region of nickel-to-copper mass transfer was formed in the nucleus upper part due to immersion of pin (Figure 4, *a*).

Examination of longitudinal section of the joint in Ni-to-Cu contact zone shows mutual penetration of these metals at up to 3 mm depth. Stirring of metals is observed in form of mutually penetrating alternating strips, directed to the side of pin movement (Figure 4, *b*). Structure refinement takes place due to recrystallization in these strips. Grain size in copper varies from 5 to 20 and that in nickel is from 5 to 40 μm. Microhardness of nickel bands makes 1270±40 and that
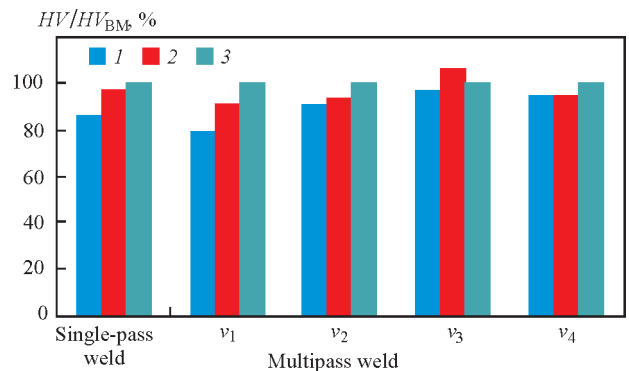
Figure 3. Relationship of microhardness of different weld regions to base metal microhardness HV_{BM} at different speeds of FSW: v_1 = 56; v_2 = 80; v_3 = 110; v_4 = 160 mm/min: *1* — region of upper place over nucleus; *2* — nucleus; *3* — BM

of copper is 1140±50 MPa. The thermomechanically affected zone (TMAZ) of up to 3 mm thickness with directed deformation strips and 20–70 μm grain size is registered in nickel over the area of metals stirring. The border region of nickel — HAZ located over the thermomechanically affect zone TMAZ — has coarser grains. The regions of thermal and thermomechanical effect of 0.6 and 0.1 mm width, respectively, are found in copper under nucleus zone. Edges of the strips and regions of nickel, in direct contact with cop-
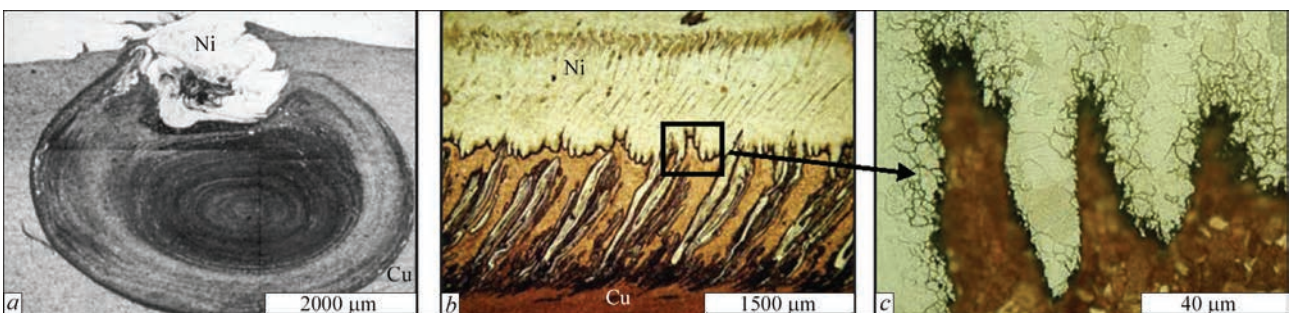
Figure 4. Microstructure of FS-welded Ni–Cu joint: *a* — cross section; *b* — longitudinal section; *c* — Ni and Cu mutual diffusion region
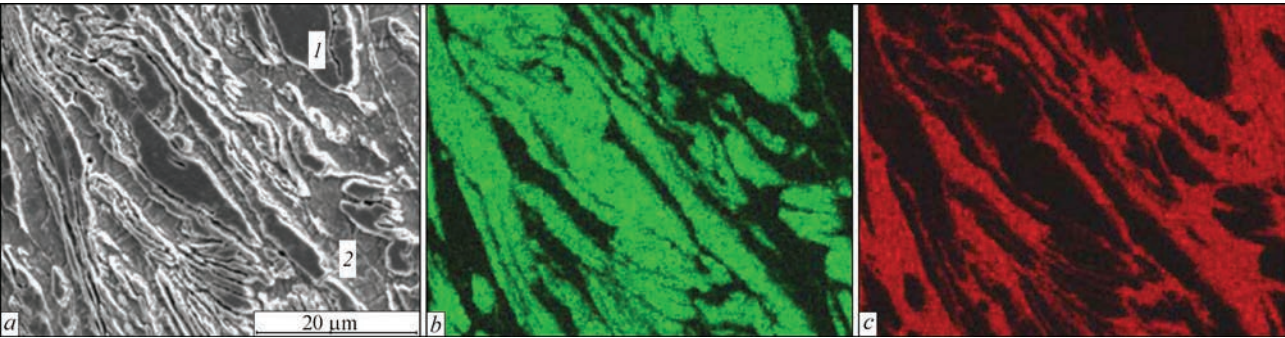
Figure 5. Image of Ni to Cu stir zone in secondary electrons (*a*), Ni (*b*) and Cu (*c*) in characteristic radiation (chemical composition of examined regions, wt./at.%: *1* — 99.23/99.29 Ni, 0.77/0.71 Cu; *2* — 4.03/4.35 Ni, 95.97/95.65 Cu)

per, have larger lamination and lower microhardness (1100±60 MPa). It can be explained by mutual diffusion of copper and nickel along grain boundaries with formation of solid solution interlayers of these metals at 10–20 μm depth (Figure 4, *c*).

The XSMA of the stir zone in characteristic radiation shows insignificant mutual diffusion of elements deep down the alternating strips of nickel and copper. Figure 5 represents the results of mapping of a zone of mechanical stirring of metals in Ni–Cu joint. The results of examination outline the fact that the mechanical stirring of metals in plastic state plays the leading role in FSW and to smaller extent their mutual diffusion.

Cu–St.3 joint. A copper-to-carbon steel joint was produced by FSW by means of action of the pin through a copper plate of 7 mm thickness. Examination of longitudinal and cross section of joint showed that it is dense and has no defects (Figure 6). Since the steel hardness is much more than the copper hardness, then formation of classical oval nucleus (Figure 6, *a*) in welded joint cross-section did not take place. The joint zone in the upper part consists of recrystallized copper, and lower one is a mixture of steel particles of different size in copper matrix. Wedge-like steel implantations in copper to 700–1000 μm depth limit the joint nucleus. These wedge-like implantations have ferrite-pearlite structure and virtually do not contain copper. The stir zone was formed in the copper-to-steel joint zone. Large number of iron inclusions, implanted in copper in form of the separate bands and particles (Figure 6, *b*) is noted.

Joint longitudinal section has a tooth nature. The wedge-like implantations inclined in welding direction are observed in copper (Figure 6, *c*). This region consists of implanted in wrought copper the finest steel particles of 1–10 μm size, microhardness of these regions is 2740–3020 MPa. Upper weld section, i.e. recrystallized copper of 7–30 μm size, is located above the wedge-like implantations. HAZ width in steel achieves 4.5 mm. Regions of complete and partial recrystallization are clearly observed. In the contact zone the size of steel grain is an order lower than in the base metal, its microhardness makes 2290±120, when that of ferrite-pearlite steel is 2160±100 MPa.

Figure 7 shows the results of mapping of the stir zone in Cu–St.3 joint, which represents itself mechanical mixture of copper (base) and steel particles of different size. The disperse inclusions of copper are observed in the largest steel particles. The examination of copper and iron in characteristic radiation does not show mutual diffusion of elements, however, can not be excluded in the near-boundary regions. It is also determined that FSW of these metals provokes for significant grain refinement in the stir zone as well as in HAZ metal. It follows from carried investigations that stirring of metals in plastic state plays the leading role in production of copper-to-steel welded joint using FSW, and role of diffusion processes is insignificant.

Kh18N10–Cu joint. Joining of Kh18N10 stainless steel with copper was produced by FSW at modes, given in the Table. This experiment was carried out
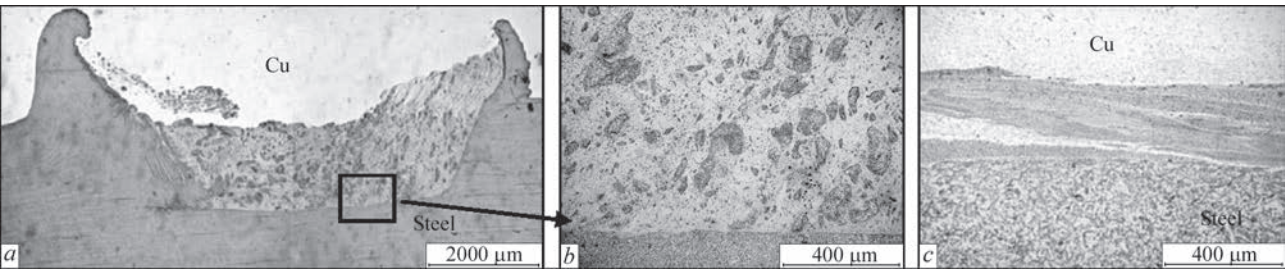
Figure 6. Microstructure of FS-welded Cu–St.3 joint: *a* — cross section; *b* — stir zone; *c* — longitudinal section
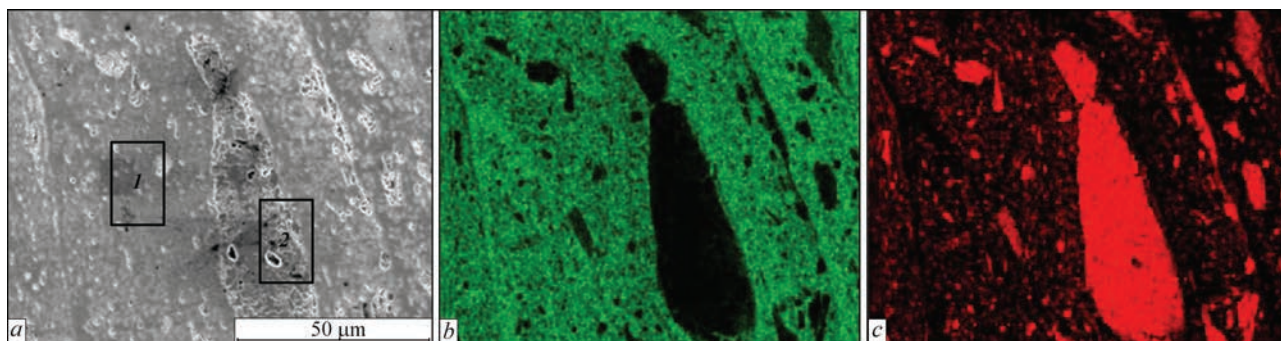
Figure 7. Image of Cu to St.3 stir zone in secondary electrons (*a*), Cu (*b*) and Fe (*c*) in characteristic radiation (chemical composition of examined regions, wt./at.%: *1* — 21.47/23.72 Fe, 78.27/75.99 Cu, 0.26/0.29 Mn; *2* — 97.60/97.44 Fe, 0.99/0.87 Cu, 1.14/1.16 Mn)

for creation of protective layer of stainless steel (as in deposition) on copper plate of CCM mold.

The steels of this class have pronounced tendency to air quenching and formation of cracks in welding. The heat conductance and expansion coefficient of this steel is considerably lower than carbon one.

Longitudinal and cross sections of steel-to-copper lap joints (Figure 8) were investigated. Stainless steel plunges into copper at up to 2 mm depth in form of strips and bands at pin height 4.5 mm. Simultaneously, dragging and stirring of the small regions of copper into stainless steel take place. Weld consists of two parts, i.e. one is located in steel, and another is in copper (Figure 8, *a*). In the weld steel part the pin promotes for deformation of metal with 20–30 % reduction of its thickness, appearance of deformation bands and structure recrystallization with formation of equiaxial grain of 5–25 μm size. Microhardness of this zone makes 1450–1700 MPa. Part of the weld located in copper is virtually a stir zone. Recrystallization of the both metals with fine grain formation,

namely 10 μm (Figure 8, *b*) takes place in this region. HAZ with fine grain of 200–300 μm width is located around the stir zone in copper. Behind it the TMAZ with coarse, somewhat wrought grain, is located, along the boundaries of which incomplete recrystallization with formation of fine (20–30 μm) grain took place (Figure 8, *c*).

Examination of the weld cross-section showed that metal stirring takes place with steel implantation into copper in form of alternating bands and inclined strips at 4.4–5.2 mm gap (Figure 8, *d*). Their high and extension increases with welding speed rise. The maximum depth of steel implantation into copper makes 2 mm, and thickness of bands is varied from 30 to 100 μm at welding speed increase from 10 to 110 mm/min.

Macrostructure of the examined specimens, produced at different speeds of welding (see the Table) have common peculiarities. Investigation of cross and longitudinal section of the joints showed that the mass transfer of steel into copper takes place in form of bands, separate strips and particles (Figure 8, *e*, *f*). It is
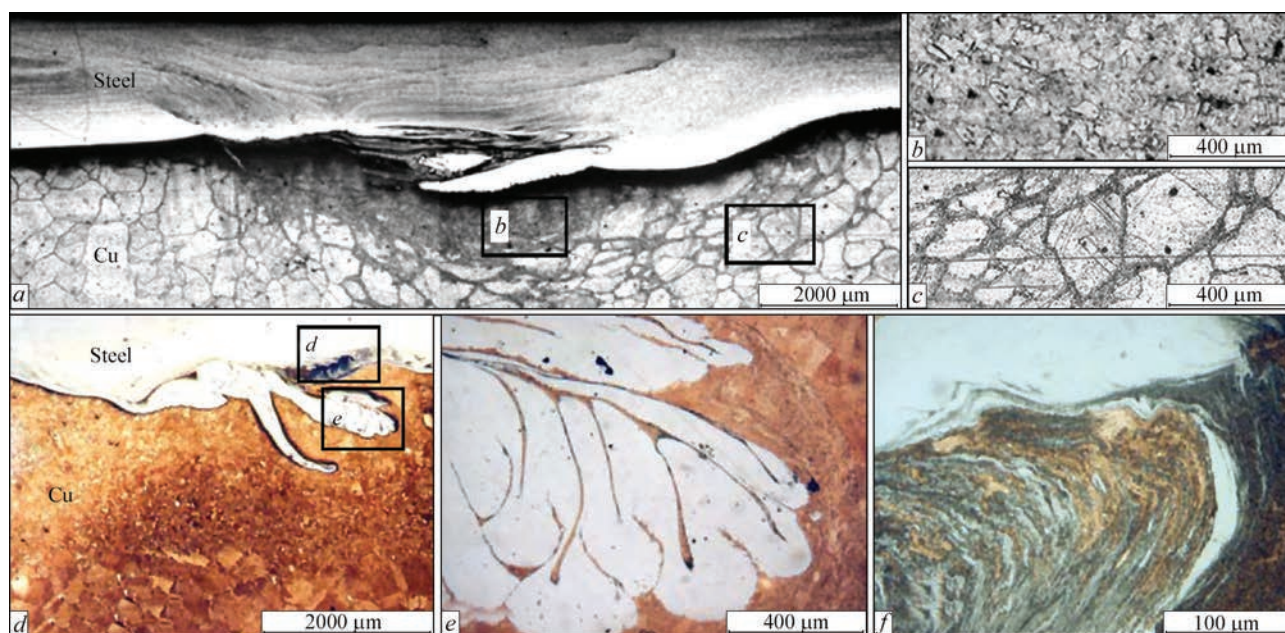
Figure 8. Microstructure of FS-welded Kh18N10–Cu joint: *a* – cross section; *b* — HAZ; *c* — TMAZ, *d* — longitudinal section; *e*, *f* — stir regions

found that formation of such stir regions occurs with certain sequence, and distance between them increases with welding speed rise. The most often defects of the joints are pores and cracks which are formed in stainless steel. The cracks are observed from the side of tool advancing in zone of copper-to-steel contact at small welding speeds (to 20 mm/min). Welded joints of the highest quality are produced at v_w = 20–50 mm/min.

Conclusions

1. FSW process, which is performed without base metal melting due to plastic deformation of metal heated to recrystallization temperature at optimum modes of welding, allows producing high-quality lap welded joint of homogeneous (Cu–Cu) as well as dissimilar (Ni–Cu, steel–Cu) metals.

2. Mechanical stirring of metals in plastic state plays the leading role in FSW. The role of diffusion processes is insignificant. Processes of recrystallization in the zones of metal plastic stirring promote for grain refinement and development of dense microstructure of weld comparable with base metal.

3. Carried investigations allow recommending this method for lap welding of dissimilar metals, having different solubility in solid state. Weld deposition at specific distance from each other helps to receive quality solid welding-up of upper (thinner) plate to massive lower one (by deposition type) with overlapping of recrystallization zones at minimum heating and distortion of the parts.

1. Thomas, W.M. *Friction stir butt welding.* Pat. 9125978.8 G.B. Int. Cl. PCTrGB92. Publ. 01.12.91.
2. Lebedev, V.K., Chernenko, I.A., Mikhalsky, R. et al. (1987) *Friction welding*: Refer. Book. Leningrad: Mashinostroenie.
3. Ericsson, L.G., Larsson, R. (2003) Rotational friction welding: Researches and new fields of application. *Tekhnologiya Mashinostroeniya*, **6**, 81–84.
4. Mishraa, R.S., Ma, Z.Y. (2005) Friction stir welding and processing. *Materials Sci. and Eng.*, **50**, 1–78.
5. Arbegast, W.J. (2006) Friction stir welding. After a decade of development. *Welding J.*, 85(**3**), 28–35.
6. Grigorenko, G.M., Adeeva, L.I., Tunik, A.Yu. et al. (2014) Structural features of FSW joints of metals with different element solubility in the solid phase. *The Paton Welding J.*, **4**, 6–16.
7. Xue, P., Ni, D.R., Wang, D. et al. (2011) Effect of friction stir welding parameters on the microstructure and mechanical properties of the dissimilar Al–Cu joints. *Materials Sci. and Eng.*, **528**, 4683–4689.
8. Saeida, T., Abdollah-Zadehb, A., Sazgarib, B. (2010) Weldability and mechanical properties of dissimilar aluminum-copper lap joints made by friction stir welding. *J. Alloys and Compounds*, **490**, 652–655.
9. Kosta, A., Coelho, R.S., dos Santos, J. et al. (2000) Microstructure of friction stir welding of aluminium alloy to magnesium alloy. *Ibid.*, **66**, 953–956.
10. Karmanov, V.V., Kameneva, A.L. (2013) *Friction stir welding of aluminium alloys: Matter and specifics of process*. Kiev: Naukova Dumka.
11. Graf, E.V., Shevchuk, M.V. (2008) Friction stir welding of nonferrous metals and their alloys. In: *Proc. of 12th Regional Sci.-Pract. Conf. of Students on Advanced Technologies and Economy in Machine-Building*, 17–19. Yurga: TPU.

EFFECT OF STRUCTURE AND PROPERTIES OF ALUMINIUM-LITHIUM ALLOY WELDED JOINTS PRODUCED BY ARGON-ARC AND FRICTION STIR WELDING METHODS

L.I. MARKASHOVA, A.G. POKLYATSKY and **O.S. KUSHNARYOVA**

E.O. Paton Electric Welding Institute, NASU

11 Kazimir Malevich Str., 03680, Kiev, Ukraine. E-mail: office@paton.kiev.ua

An essential difference in formation of structural-phase state at application of different welding conditions — friction stir welding compared to argon-arc welding — is considered in the case of welded joints of complex aluminium-lithium alloys. The urgency of comprehensive experimental-analytical assessment of interrelation of welded joint structure and properties is also shown. Assessments of specific contribution of structural-phase state (chemical composition, phase dimensions, grain, subgrain and dislocation structure) into the change of the main service properties of welded joints made by argon-arc welding and friction stir welding are considered, as well as the influence of welded joint structural state on the nature of distribution, level of growing internal stresses and their relaxation mechanisms under specific welding conditions. 10 Ref., 5 Figures.

Welded joints of complex aluminium alloys, extensively applied in aircraft and aerospace engineering and operating, as a rule, under complex operation conditions, should provide reliable mechanical properties of welded structures, that is mainly determined by structural-phase state of welding zone, formed during the applied technological operations, namely alloying, welding conditions, etc. [1]. In this respect, the issue of structure influence on properties is extremely urgent, particularly for welded joints of complex aluminium alloys. These alloys are characterized by an abrupt change not only of structures, but also of phase precipitates (PP) during various technological operations, including the influence of welding processes.

To assess the role of technological modes used in friction stir welding (FSW), in the change of welded material properties, namely strength, ductility and crack resistance characteristics [2–6], it appears appropriate to compare the dependencies of welding modes ↔ joint properties with similar interconnections studied (and in sufficient detail) for the regularly used processes of aluminium alloy welding, to which TIG welding belongs.

Material and procedures. To compare the influence of different welding modes on welded joint properties, investigations were performed on welded joints of complex Al–Li alloys 1460 (%: Al–3Cu–2Li–0.08Sc) produced by TIG welding in MW-450 unit (Fronius, Austria) under the following condi-

tions: 20 m/h speed and 140 A current at application of Sv1201 and Sv1201 + 0.5 % Sc fillers. Structure-phase state of welded joints made by FSW without the filler in laboratory unit designed at PWI was studied in parallels. In the latter case a special tool with a conical tip and 12 mm diameter shoulder was used to produce butt joints, tool rotation speed here being equal to 1420 rpm, and linear speed of its movement along the butt being 14 m/h.

Complete experimental data on structural-phase state of welded joint metal was derived with application of the methods of light, analytical scanning (SEM-515, Philips, The Netherlands), as well as microdiffraction transmission electron microscopy (JEM-200CX, JEOL, Japan) with accelerating voltage of 200 kV.

Proceeding from the complex of investigations, analytical assessments of specific (differentiated) contribution of different structural factors and their parameters (chemical composition, volume fraction and phase precipitate dimensions, grain, subgrain and dislocation structure) into the change of service characteristics of welded joints were performed on all structural levels.

Analytical assessment of the total (integral) value of yield point $\Sigma\sigma_y$ was performed using the known dependence [7–10]:

$$\Sigma\sigma_y = \Delta\sigma_0 + \Delta\sigma_{s.s} + \Delta\sigma_{gr} + \Delta\sigma_s + \Delta\sigma_d + \Delta\sigma_{d.h},$$
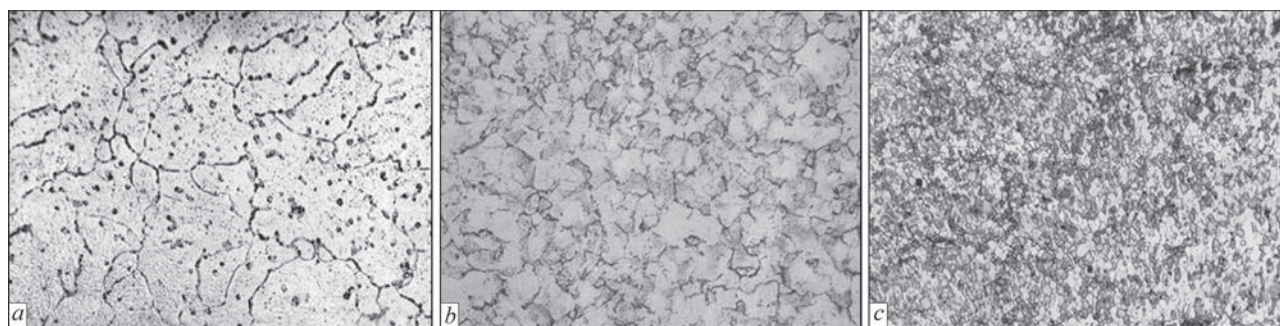
Figure 1. Microstructure (×500) of metal of Al–Li alloy 1460 welds produced by TIG welding with application of Sv1201 (*a*) and Sv1201 + 0.5Sc (*b*) filler wire and by FSW (*c*)

including $\Delta\sigma_0$ — metal lattice resistance to free dislocation movement (lattice friction stress or Peierls–Nabarro stress); $\Delta\sigma_{s.s}$ — solid solution strengthening by alloying elements and impurities (solid-solution strengthening); $\Delta\sigma_{gr}$, $\Delta\sigma_s$ — strengthening due to the change of the size of grain and subgrain (Hall–Petch dependencies — grain-boundary and subgrain strengthening); $\Delta\sigma_d$ — dislocation strengthening due to interdislocation interaction; $\Delta\sigma_{d.h}$ — strengthening due to phase formation particles, according to Orowan (dispersion hardening).

Features of formation of local internal stresses $\tau_{l.in}$ — internal stress concentrators (their level, extent, interrelation with structural features of welded joint metal) were determined by dependence [6]:

$$\tau_{l.in} = Gbh\rho / [\pi(1 - \nu)],$$

where G is the shear modulus; b is the Burger's vector; $h = 2 \cdot 10^{-5}$ cm is the foil thickness; ν is the Poisson's ratio; ρ is the dislocation density.
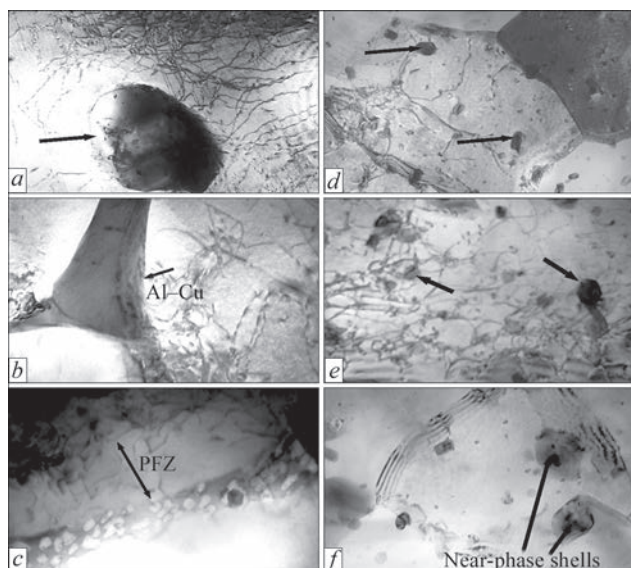
Figure 2. Phase distribution in grain volumes of metal of 1460 alloy weld produced by TIG welding (*a* — PP on grain inner volumes (×2000); *b* — extended grain-boundary eutectics (×30000); *c* — near-boundary PFZ (×3000)) and by FSW (*d*, *e* — PP in grain volumes (×30000); *f* — PP in grain-boundary zones of weld metal (×30000))

Investigation results. The following was established as a result of investigation of aluminium alloy TIG-welded joints produced without scandium alloying and those alloyed with scandium (Figure 1, *a*, *b*). Weld metal of joints of Al–Li alloy 1460 at application of Sv1201 filler (without scandium alloying) is primarily characterized by coarse-grained structure which is quite clearly revealed at investigation by optical microscopy method (Figure 1, *a*). More over, the TEM method reveals formation of coarse globular intragranular phase precipitates with d_{PP} of up to ~3.5 μm, extended massive intergranular eutectics of thickness h_{eut} of up to ~5 μm, as well as presence of precipitation-free zones (PFZ) along the grain boundaries. As is known, lowering of mechanical characteristics of welded joints is associated with the latter. Non-uniformity of dislocations distribution in weld metal of this type of joints is noted, particularly along extended near-boundary PFZ, where dislocation density decreases practically by an order (to $\rho = 3 \cdot 10^8$ cm^{-2}), compared to intragranular dislocation density, where $\rho \sim (2-6) \cdot 10^9$ cm^2 (Figure 2, *a*–*c*).

Now, under the conditions of weld metal alloying by scandium (up to 0.5 %), which is known to be the structure modifier after welding, certain changes are observed in the structure of welding zone metal, compared to respective structures in welded joints unalloyed by scandium. Such changes include, mainly, refinement of grain structure (see Figure 1, *b*), grain-boundary eutectics, dispersion of phase precipitates in grain volumes in combination with certain increase of dislocation density to $\rho \sim (4-9) \cdot 10^9$ cm^{-2}.

Investigations of the features of structural changes at FSW revealed the following. Unlike significant grain coarsening by collective recrystallization mechanism, characteristic for fusion welding, considerable structure refinement (see Figure 1, *c*) is observed in FSW weld metal, which is associated with actively running processes of dynamic recrystallization, i.e. recrystallization by nucleation mechanism.

More over, structure of weld metal in FS-welded joints features an increase of overall dislocation den-

sity up to $\rho \sim (3{-}6) \cdot 10^{10}$ cm^{-2}, that is by an order of magnitude higher than volume dislocation density of weld metal in fusion welding (Figure 2, *d*, *e*). Here, increase of intragranular dislocation density is accompanied by active redistribution of dislocations, that is indicated by formation of substructural elements, namely blocks, fragments, etc.

Apparently, structure refinement and activation of dislocation redistribution under the conditions of friction welding are due to intensive deformation of weld metal heated up to the plastic state and prevalence of dynamic recrystallization over collective one, respectively.

The next feature of structural state of weld metal produced under FSW conditions (compared to weld metal, produced by fusion welding) is an essential refining of PP (by 2.5 to 5 times) and an essential increase of their quantity at uniform distribution, being observed in all the weld metal zones — both in intragranular, and grain boundary volumes (see Figure 2, *d*, *e*).

Fragmentation of such problematic for aluminium alloys formations as grain-boundary eutectics also takes place. All these structural changes in the welding zone are provided by prevalence of thermodeformational processes in formation of structural-phase state of weld metal at FSW.

Complete range of investigations on different structural levels, which provides information about all structural factors formed in the welding zone and their parameters (size of grains, subgrains, chemical composition, dimensions, distribution and volume
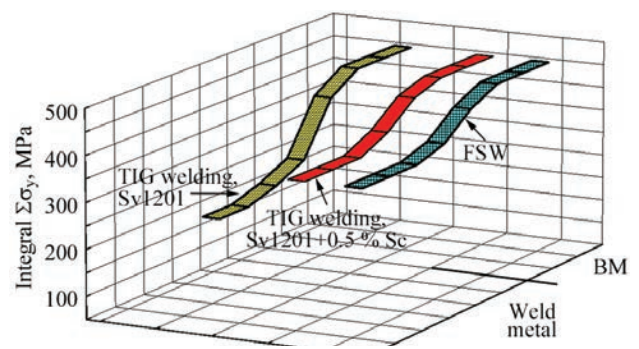
Figure 3. Change of integral $\Sigma\sigma_y$ at base-to-weld metal transition in aluminium alloy 1460 TIG-welded joints with Sv1201 and Sv1201 + 0.5Sc fillers and in FS-welded joint

fraction of strengthening phases, as well as dislocation structure), enables performing analytical evaluation of specific contribution of various structures in the studied zones, into the change of the most important service properties of welded joints, depending on the used welding modes.

Structure contribution into strength characteristics of Al–Li welded joints. As a result of performed assessment of strength properties of studied joints with Sc and without it after TIG welding, the highest values are found in Sc-alloyed joints (Figure 3). Here, grain ($\Delta\sigma_{gr} \sim 29$ %) and solid solution ($\Delta\sigma_{s.s} \sim 25$ %) strengthening make the greatest contribution into total (integral) value of yield point of metal of Sc-containing weld (Figure 4). And in the case without Sc alloying, the greatest contribution to total value of yield point is made, mainly, by solid solution strengthening ($\Delta\sigma_{s.s} \sim 28$ %) (see Figure 4).
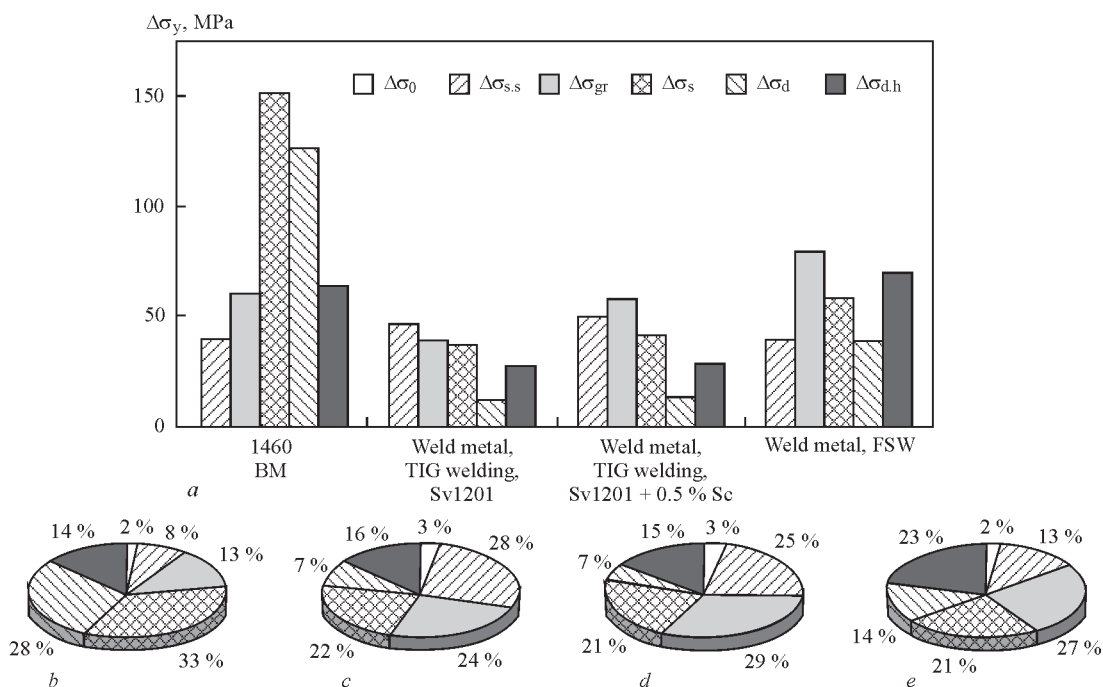
Figure 4. Histogram of differentiated contribution of structural constituents into the calculated value of $\Delta\sigma_y$ (*a*), and pie charts (*b*–*e*) showing percentage of structure contribution into total (integral) change of $\Sigma\sigma_y$ in different studied zones: in base metal (*b*), in weld metal after TIG welding with Sv1201 (*c*) and Sv1201 + 0.5Sc (*d*) and after FSW (*e*)
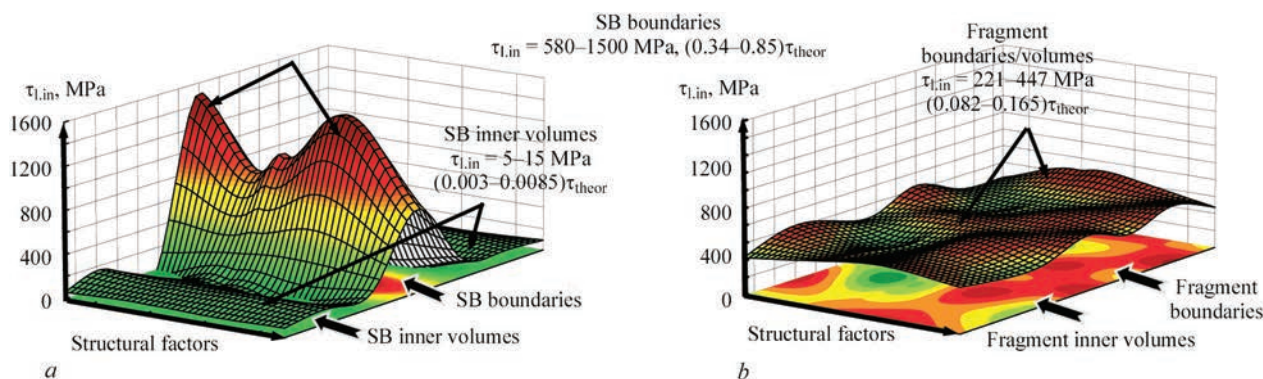
Figure 5. Distribution of $\tau_{l.in}$ in 1460 alloy weld metal: a — TIG welding (weld metal without scandium); b — FSW

Under FSW conditions, assessment of total (integral) value, $\Sigma\sigma_y$ showed overall increase of strength values by 40 %, compared to those for conditions of TIG welding in the case without scandium (see Figure 3), that is ensured, mainly, by refinement of grain (up to 27 %) and subgrain (up to 21 %) structures and PP dispersion (up to 23 %) (see Figure 4).

Assessment of welded joint crack resistance. Comprehensive structural studies in combination with analytical evaluation also allowed clarifying the nature of structural factors influence on cracking processes in the welding zone of studied joints, which are due to the features of development of deformation localization zones, and local internal stresses ($\Delta\tau_{l.in}$). This kind of investigations allows, first of all, determination of structures, influencing formation of $\tau_{l.in}$ to varying degrees.

Specific results of investigations and, primarily, nature of dislocation structure distribution in the studied samples, allowed assessment of $\tau_{l.in}$, determination of their level and extent. More over, respective investigations allow establishing structural factors, provoking growth of $\tau_{l.in}$ concentrators (i.e. processes of crack initiation and propagation), and determining which structural factors block such processes, negative in terms of metal properties, as cracking.

Analytical evaluations showed that under TIG welding conditions extended raisers of $\tau_{l.in}$ of up to 1500 MPa $((0.34-0.85)\tau_{theor})$ form in the metal without Sc, which exactly are the zones of crack initiation and propagation; and boundaries of powerful shear bands (SB) also belong to such zones (Figure 5, a). Contrarily, in SB inner volumes, $\tau_{l.in}$ values drop markedly (practically by 2 orders of magnitude) to ~5–15 MPa $((0.0016-0.0055)\tau_{theor}))$ that eventually creates a marked extended gradient of local internal stresses ($\Delta\tau_{l.in}$), and, therefore, zone of crack initiation and propagation along SB boundaries (Figure 5, a).

Under FSW conditions, an essential lowering (by 3.5 times) of the $\tau_{l.in}$ (to 221–447 MPa) is observed in weld metal microstructure at uniform (without gra-

dients) distribution of this type of local stresses over the entire volume of weld metal (Figure 5, b), that is exactly what ensures an increase of welded joint crack resistance.

Thus, to improve strength characteristics and crack resistance of welded joints of complex aluminium alloys, it is necessary to try to achieve formation of optimum structure that is provided by FSW, as shown by investigations of interrelation of structure and properties.

Conclusions

1. Comprehensive methods of investigation of welded joints of complex aluminium alloy 1460 enabled establishing the changes in key structural-phase parameters, influencing mechanical characteristics of welded joints at variation of the conditions of technological welding modes — from TIG (fusion) welding to FSW (solid-phase).

2. Under TIG welding conditions, weld metal is characterized by coarsening of grain structure, lowering of total volume density of dislocations, formation of globular intragranular and extended grain-boundary phase precipitates of eutectic type.

3. It is found that under the conditions of fusion welding, weld metal alloying by scandium leads to an essential change of structural-phase state of welded joints, namely, dispersion of grain and subgrain structure phase; increase of dislocation density at their uniform distribution; activation of phase formation processes in grain inner volumes, as well as fragmentation and reduction of volume fraction of grain-boundary eutectics.

4. Under FSW conditions, a marked refinement of grain and subgrain structure is observed, that is due to activation of fragmentation and nucleation processes, overall increase of dislocation density, as well as an essential dispersion of phase precipitates at their uniform distribution in intragrain and grain-boundary volumes.

5. For weld metal of aluminium alloy FS-welded joints, investigations with subsequent analytical as-

sessment revealed that the considerable contribution (up to 40 %) to total strengthening of welded joints is provided by refinement of grain (up to 27 %) and sub-grain (up to 21 %) structure, and dispersion of phase precipitates (up to 23 %), that significantly lowers the gradient of strength properties between base metal and weld metal and promotes a more uniform distribution of growing local internal stresses, and improvement of welded joint crack resistance, respectively.

6. Investigation of TIG welding modes showed that overall lowering of yield point values of weld metal is associated with coarsening of grain structure and reduction of overall dislocation density, that promotes an increase of gradient of strength characteristics between base metal and weld metal and lowering of welded joint crack resistance.

1. Fridlyander, I.N. (2000) Aluminium alloys in flying vehicles for periods of 1970–1999 and 2000–2015. In: *Proc. of 5th Session of Sci. Council on New Materials on Problems of Modern Materials Science*, 15–19. Kiev: Naukova Dumka.

2. Goldshtejn, M.I., Litvinov, V.S., Bronfin, B.M. (1986) *Metallophysics of high-strength alloys*. Moscow: Metallurgiya.

3. Markashova, L.I., Alekseenko, T.A., Kushnaryova, O.S. et al. (2011) Role of structure in optimization of strength, ductility, crack resistance properties of welded joints. In: *Building, Materials Science, Machine-Building:* Transact., Issue 58, 446–452. Dnepropetrovsk: GVUZ PGASA.

4. Markashova, L., Kushnareva, O. (2014) Effect of structure on the mechanical properties of the metal of welded joints of aluminum alloys of the Al–Cu–Li system. *Materials Sci.*, Vol. 49, Issue 5, 681–687.

5. Ashby, M.F. (1972) On the orowan stress. In: *Physics of strength and plasticity*, 88–107. Moscow: Metallurgiya.

6. Markashova, L.I., Ishchenko, A.Ya., Kushnaryova, O.S. et al. (2012) Effect of structural-phase transformations in aluminium-lithium alloy 1460 joints on physical-mechanical properties. *The Paton Welding J.*, **5**, 17–25.

7. Markashova, L.I., Poklyatsky, A.G., Kushnaryova, O.S. (2015) Role of structural-phase state in change of service properties of complexly-doped alloy welded joints. In: *Building, Materials Science, Machine-Building:* Transact., Issue 80, 191–195. Dnepropetrovsk: GVUZ PGASA.

8. Conrad, H. (1973) Model of strain hardening for explication of grain size effect on metal flow stress. In: *Superfine grain in metals*, 206–219. Moscow: Metallurgiya.

9. Petch, N.J. (1953) The cleavage strength of polycrystalline. *J. Iron and Steel Inst.*, 173(**1**), 25–28.

10. Orowan, E. (1954) *Dislocation in metals*. New York: AIME.

FEATURES AND ADVANTAGES OF THE PROCESS OF FRICTION STIR WELDING OF BUTT JOINTS OF SHEET ALUMINIUM-LITHIUM ALLOYS

A.G. POKLYATSKY, V.V. KNYSH, I.N. KLOCHKOV and **S.I. MOTRUNICH**

E.O. Paton Electric Welding Institute, NASU

11 Kazimir Malevich Str., 03680, Kiev, Ukraine. E-mail: office@paton.kiev.ua

The paper analyzes the structural features, strength and fatigue life properties of sheet joints of Al–Li alloys 1420 and 1460, produced by nonconsumable-electrode argon-arc welding and friction stir welding. It is shown that application of FSW provides formation of permanent joints with minimum level of stress concentration in the points of weld transition to base material and allows avoiding defects in welds in the form of pores, oxide film macroinclusions or hot cracks due to melting and solidification of metal in fusion welding. Here, intensive plastic deformation of metal under the tool shoulder and in weld nugget results in formation of fine-crystalline (3–4 μm) uniform disoriented structure, and grain elongation and distortion in the direction of plasticized metal displacement proceed in adjacent sections. This leads to increase of hardness and ultimate strength of joint weld metal. Lowering of the temperature of heating of the edges being welded provides reduction of maximum level of tensile residual longitudinal stresses in welded joints, compared to TIG welding. It is found that fatigue resistance characteristics of butt welded joints, made by FSW, are superior to those of the joints, made by TIG welding. 10 Ref., 9 Figures.

K e y w o r d s : Al–Li alloys, friction stir welding, defects, microstructure, ultimate strength, fatigue resistance

Application of high-strength corrosion-resistant Al–Li alloys, characterized by lower density and high modulus of elasticity, allows reducing fuel consumption and improving tactico-technical characteristics of aerospace engineering products. Developed in 1968 by a team led by I.N. Fridlyander, 1420 alloy (density of 2.4 g/cm³) of Al–Mg–Li alloying system containing 4.5–6.0 % Mg and 1.8–2.3 % Li, has by 12 % lower specific weight and 8 % higher modulus of elasticity than D16 alloy, extensively applied in aircraft construction. Its application in riveted structure of fuselage of vertical takeoff aircraft Yak-36 provided a weight gain of 16 %. In 1980 the alloy was recommended for creation of world's first welded aircraft MiG-29 [1, 2].

The strongest ($\sigma_t > 500$ MPa at 2.6 g/cm³ density) is 1460 alloy of Al–Cu–Li system (nominal composition of 3 % Cu and 2 % Li) with zirconium and scandium additives. High values of strength and ductility of this alloy at superlow temperatures are indicative of the good prospects for its application in manufacture of welded cryogenic tanks [3].

To produce permanent joints of aluminium alloys, various fusion welding processes are applied in the majority of cases, in which the weld forms as a result of melting of a certain volume of materials being joined and filler wire in a common weld pool with their subsequent solidification in shielding inert gas. However, in fusion welding of semi-finished products from Li-containing aluminium alloy, structural trans-

formations proceed in weld metal and adjacent sections with formation of characteristic defects in the form of pores at application of base material strips as filler wire, and of extended filamentous macroinclusions of oxide film when filler wire is used. This necessitates application of technological measures, aimed at improving the quality of preparation of surfaces being welded and promoting intensification of weld pool metal stirring and activation of the processes of oxide film breaking up. Here, welded joint strength does not exceed 70–75 %, and weld metal strength — 65 % of this value for base material [4, 5].

Application of FSW allows avoiding metal melting in the zone of weld formation and maximally preserving in welded components the properties of semi-finished products applied in their manufacture. In such welding weld formation proceeds in the solid phase, as a result of heating of a small metal volume to plastic state through friction, its stirring across the entire thickness of edges being welded and deformation in a closed space. Due to this, FSW process has several essential advantages, compared to fusion welding. Formation of fine-crystalline weld structure, lowering of the level of softening of materials being joined, preservation of alloying elements, absence of characteristic defects and improvement of joint mechanical properties are among them [6–9].

The objective of this work is establishing the advantages of FSW process, compared to TIG welding, when producing butt joints of Al–Li alloys 1420 and 1460.

Sheets of Al–Li alloys 1420 1.8 mm thick and 1460 2 mm thick were used for investigations. Butt joints were produced by TIG welding in MW-450 unit («Fronius», Austria) at the speed of 20 m/h and current of 140–150 A, using strips from the respective base material as filler wire (for preservation of weld metal composition similar to base material), and respective filler wires SvAMg63 and Sv1201 of 1.6 mm diameter. FSW process was implemented in a laboratory unit, developed at PWI, using a special tool [10] with rotation speed of 1420 rpm and linear displacement speed of 13–14 m/h.

Sections were cut out of the produced welded joints to study the structure, and samples with 15 mm width of the working part were prepared to determine the ultimate strength at uniaxial tension in keeping with GOST 699–66. Width of sample working part for determination of fatigue resistance was 25 mm. Mechanical testing of samples was conducted in MTS 318.25 versatile servohydraulic complex. Cyclic testing was performed at axial regular loading with coefficient of stress cycle asymmetry $R_\sigma = 0.1$ and frequency of 15 Hz up to complete fracture of samples. A series of 5–7 similar samples was tested at the same conditions. Experimental data of fatigue testing were processed by the methods of linear regression analysis, generally accepted for this type of testing. Results of performed testing were used to plot for each sample series, proceeding from limited endurance limits, the appropriate fatigue curve — a line of regression of experimental data in $2\sigma_a - \lg N$ coordinates.

Metal hardness was measured on face surface of scraped joints. Degree of metal softening in the welding zone was assessed in Rockwell instrument at the load $P = 600$ N. Assessment of structural features of welded joints was performed with application of optical electron microscope MIM-8. Residual longitudinal stresses in welded joints were determined experimentally by cutting method.

As a result of conducted investigations it was found that the mechanism of permanent joint formation in FSW differs essentially from the processes, occurring in fusion welding.

During FSW the weld forms as a result of heating due to friction up to plastic state, stirring and intensive deformation of a small volume of metal of the parts being joined by a special tool in a closed space, without application of shielding gas or filler material. At the initial stage of the welding process, the rotating tool tip gradually plunging into the butt ousts a certain volume of plasticized metal. This metal can move only around the tip or rise upwards, as its movement is limited by backing from below, and by non-plasticized base material from the side. Further immersion of the

tool leads to full contact of working end face of its shoulder with the material being welded and creates completely confined space, which is where plasticized metal displacement occurs by a complex trajectory, determined by the configuration of working surfaces of the tool tip and shoulder. Now, when the instrument starts performing also translational motion, in addition to rotational motion, a zone of excess pressure forms ahead of its tip from the tool advancing side (where directions of vectors of rotation and linear displacement of the tool coincide), from which this pressure ousts a thin interlayer of plasticized metal towards the retreating side (opposite side, where the above vectors have different directions). Then, heated metal under pressure is pressed between the metal being welded and tool side surface from the retreating side into the space, vacated behind it, which forms as a result of the tool linear displacement. This leads to formation of a specific structure of welded joints (Figure 1) with a pronounced nugget (D), which is the result of dynamic recrystallization. Adjacent to it is the zone of thermomechanical impact (C), in which the metal was subjected to plastic deformation. Next comes the HAZ (B), where structural changes of base metal (A) are caused just by temperature rise.

Weld dimensions at FSW are smaller, and its shape differs advantageously from that produced by TIG welding: there is no weld reinforcement, which in fusion welding forms due to filler wire, and no through-thickness penetration, which is due to application of a backing with forming groove (Figure 2). This allows avoiding any significant stress concentration in the points of weld transition to base material, negatively affecting the operational and life characteristics of the joints. More over, formation of permanent joints in the solid phase will allow avoiding defects characteristic for these alloys: pores and macroinclusions of oxide film, formed in fusion welding. Absence of molten metal, in which hydrogen solubility rises abruptly, prevents additional saturation of
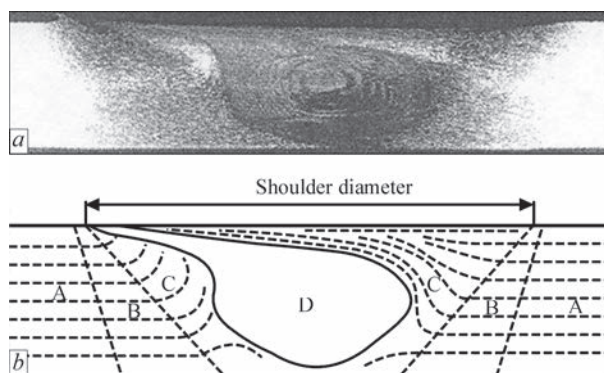
Figure 1. Transverse macrosections of FS-welded joint (*a*), and schematic image of its characteristic zones (*b*) (for zone description see the text)
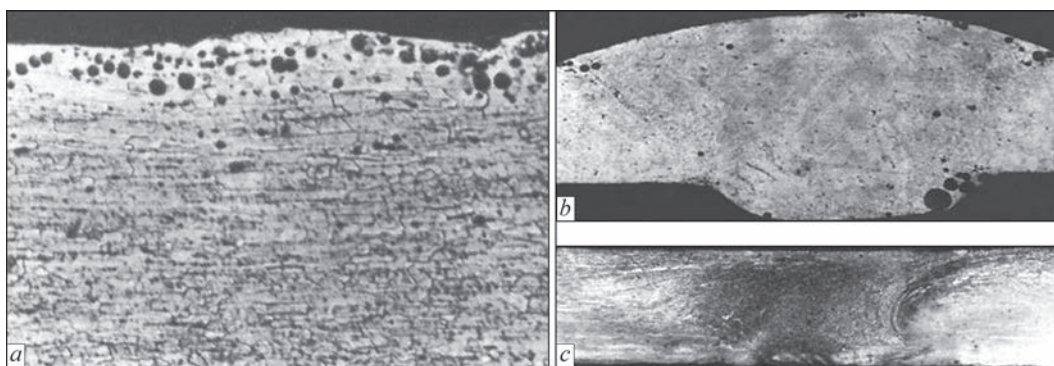
Figure 2. Microstructure (×250) of subsurface layer of the sheet (*a*) and cross-section of welds of 1420 alloy 1.8 mm thick produced by TIG welding (*b*) and FSW (*c*)

welding zone by it due to migration of this gas from the adjacent gas-saturated surface layers of metal.

Intensive deformation and stirring of plasticized metal over the entire thickness of edges being welded promotes breaking up of oxide films present on them. Absence of molten metal in the zone of joint formation allows avoiding its oxidation during welding. Therefore, FS-welds do not have any defects in the form of either isolated or extended macroinclusions of oxide film, characteristic for welds made by TIG welding on Al–Li alloys (Figure 3).

Analysis of microstructure of Al–Li alloys welded joints showed that at TIG welding of 1460 alloy overheating and recrystallization regions are found in the HAZ near the fusion line (Figure 4). Extent of the zone of melting of the structure constituents is equal to about 2.25 mm from the fusion line. In the HAZ grains directly adjacent to this boundary have the largest size. Weld metal is characterized mainly by fine-crystalline structure. However, individual fragments of the central crystallite are observed in some of its sections. Near the boundary of fusion with the

Figure 3. Longitudinal fractures of welds of 1460 alloy 2 mm thick, produced by FSW (*a*) and TIG welding, with isolated (*b*) and extended (*c*) oxide film macroinclusions

base material, an interlayer of fine subdendritic structure is visible in the weld (Figure 4, *b–d*).

In FSW of this alloy, the metal smoothly changes its grain orientation in thermomechanical impact zone in the direction of tool working surfaces displacement. It results in formation in this zone of extended elongated grains, oriented along the path of tool displacement, and fine equiaxed grains. In the weld central part (nugget), fine (3–5 μm) equiaxed grains form as a result of considerable plastic deformation (Figure 4, *e–g*).

In FSW the degree of metal softening is smaller than in TIG welding, owing to lowering of edge heating temperature and formation of fine-crystalline weld structure. So, for 1420 alloy minimum hardness in the weld and zones of its transition to base metal is on the level of *HRB* 86–87. On the other hand, in TIG welding of 1420 alloy with filler wire SvAMg63, minimum metal hardness in the weld central part is just *HRB* 81, and in fusion zones it is *HRB* 89 (Figure 5). Therefore, at tension of samples of joints with weld reinforcement, produced by fusion welding, fracture is localized in the zone of weld fusion with base material, and ultimate strength is equal to 373 MPa. Similar samples with removed reinforcement fail in weld center and have the ultimate strength of about 319 MPa. Ultimate strength of FS-welded joints, in which weld reinforcement is absent and which fail in the region of weld transition to base metal, is equal to 343 MPa. The same strength level is observed for joints with weld reinforcement, produced by TIG welding using a strip from 1420 base material as filler wire.

Measurements of metal hardness in the zone of permanent joint formation showed that in FSW of 1460 alloy hardness is also much higher than in TIG welding. In the weld and zones of weld to base metal transition, hardness is on the level of *HRB* 85–86, whereas in TIG welding with Sv1201 filler wire, minimum weld hardness in weld central part is *HRB* 71 and in the zones of weld fusion with base material it is *HRB* 82–83 (Figure 6).

Therefore, at uniaxial static tension, samples of such TIG-welded joints without weld reinforcement
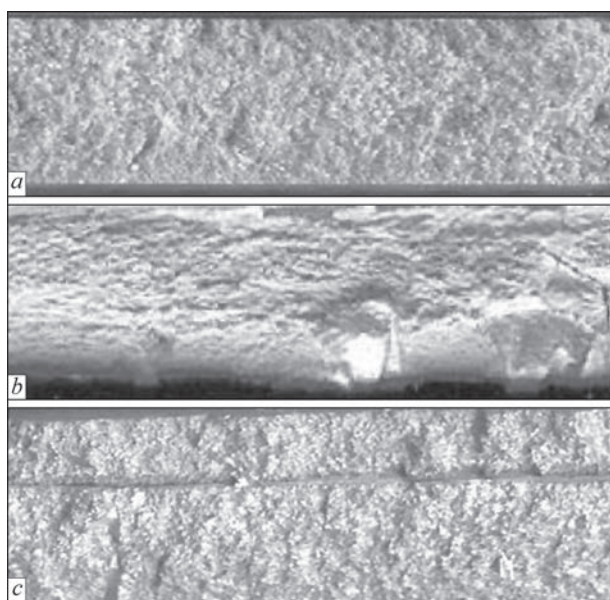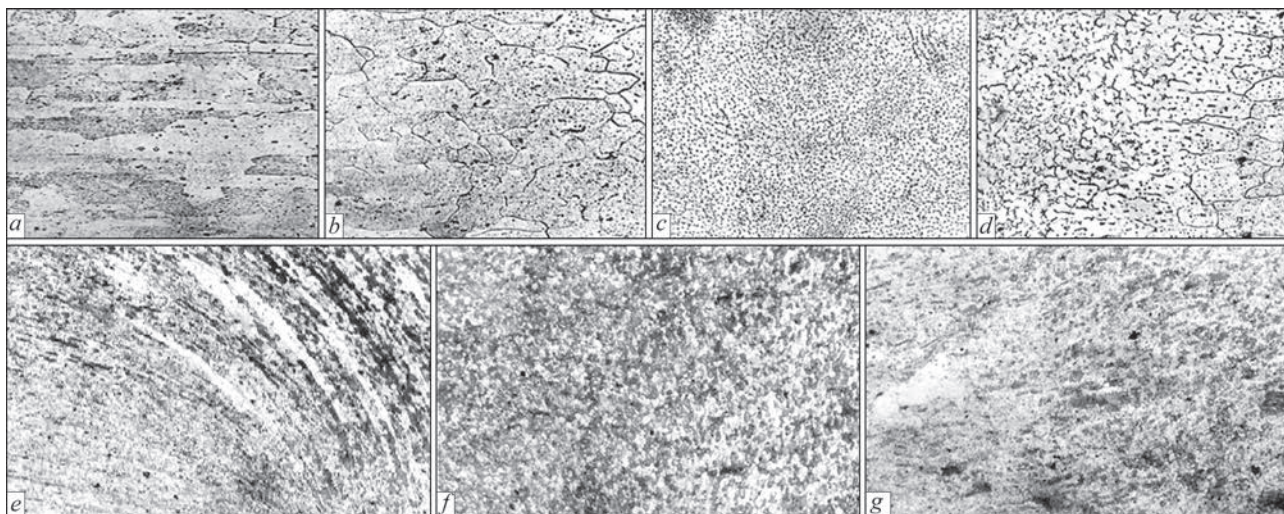
Figure 4. Microstructure (×400) of base metal (*a*) and welded joints of 1460 alloy 2 mm thick, produced by TIG welding with application of Sv1201 filler wire (*b*, *d* — zone of weld fusion with base metal; *c* — weld) and by FSW (*d* — thermomechanical impact zone from the tool advancing side; *f* — weld nugget; *g* — thermomechanical impact zone from the tool retreating side)

fail in the weld metal and have minimum ultimate strength of 257 MPa. Fracture of samples with weld reinforcement proceeds in the zone of weld fusion with base material. Samples of FS-welded joints fail in the zone of thermomechanical impact. Here, their ultimate strength is on the level of 310 MPa, similar to samples with weld reinforcement made by TIG welding with Sv1201 wire. At application of a strip of 1460 base material as filler wire, ultimate strength of samples with weld reinforcement is equal to 297 MPa on average.

Lowering of metal heating temperature in the zone of permanent joint formation at FSW has a positive effect on the level of residual stresses. In TIG welding of 1420 alloy the maximum value of residual longitudinal stresses is on the level of 99 MPa (Figure 7). At about 16 mm distance from weld axis, they drop to zero, and further on compressive stresses develop with maximum value of 29 MPa at 35 mm distance. In FS-welded joints, maximum value of tensile stresses is equal to just 64 MPa. Maximum value of residu-

al compressive stresses at 35 mm distance from weld axis decreases to 22 MPa, respectively.

Experimentally established fatigue curves of butt FS-welded joints of 1420 and 1460 aluminium alloys demonstrate high values of fatigue resistance. Limited endurance limit of FS-welded joints of 1420 alloy is lower by 10–15 % than the respective values for base metal in the entire range of fatigue life of 10^5–$2 \cdot 10^6$ cycles of stress reversal (Figure 8). For 1460 alloy the respective values of limited endurance limit are by
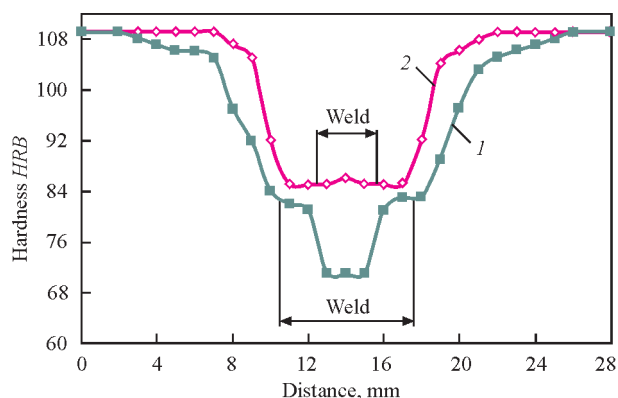
Figure 6. Hardness distribution on the surface of welded joints of 1460 alloy 2 mm thick
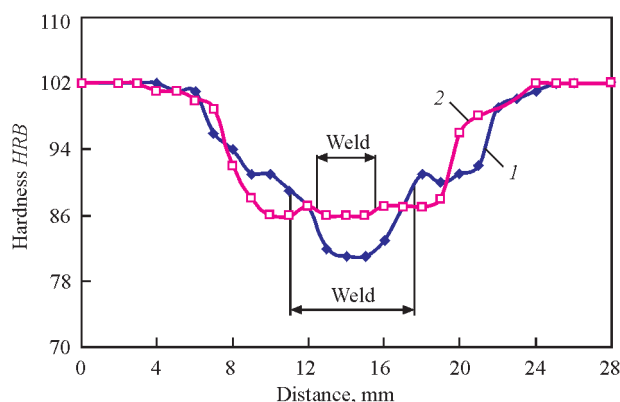
Figure 5. Hardness distribution on the surface of welded joints of 1420 alloy 1.8 mm thick (here and in Figures 6 and 7: *1* — TIG-welded; *2* — FS-welded joint)
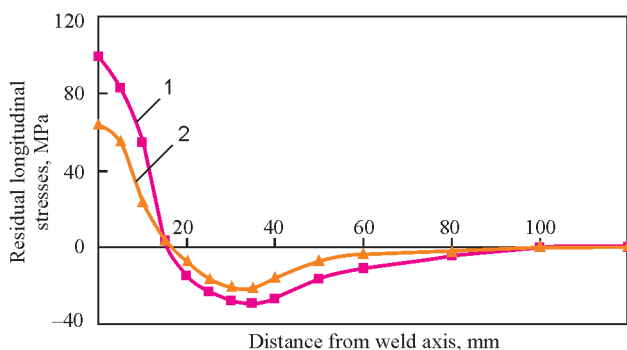
Figure 7. Distribution of residual longitudinal stresses in welded joints of 1420 alloy 1.8 mm thick
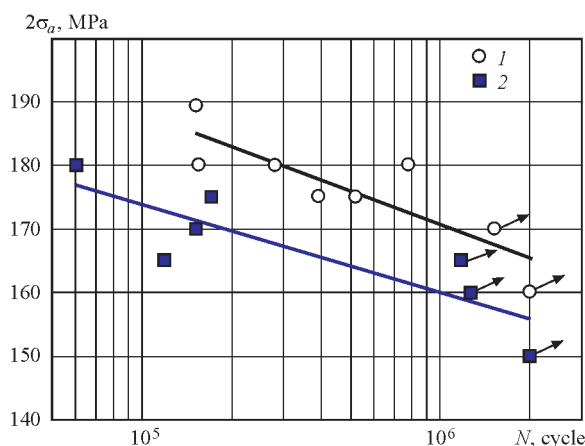
Figure 8. Fatigue curves of base metal (*1*) and FS-welded joints (*2*) of alloy 1420 1.8 mm thick at stress cycle asymmetry $R_\sigma = 0.1$

Figure 9. Fatigue curves of base metal (*1*), FS- (*2*) and TIG-welded (*3*) joints of 1460 alloy 2 mm thick at stress cycle asymmetry $R_\sigma = 0.1$

20–25 % lower than those of base metal (Figure 9). For FS-welded joints of 1420 and 1460 alloys the values of limit ranges of stresses on the base of $2 \cdot 10^6$ cycles are equal to 155 and 120 MPa, respectively. Limit range values for TIG-welded joints of 1460 alloy on the base of $2 \cdot 10^6$ cycles of stress reversal are equal to 85 MPa that is by 30 % lower than the respective value for joints, made by FSW.

Conclusions

1. FSW application provides a permanent joint with minimum level of stress concentration in the points of transition from the weld to base material, and allows avoiding defects in welds in the form of pores and macroinclusions of oxide film due to metal melting and solidification in fusion welding.

2. Formation of permanent joint in the solid phase at FSW allows avoiding coarse-dendrite structure of welds characteristic for fusion welding. Here, refinement of base metal grains and formation of new homogeneous disoriented structure with 3–4 μm grain size and dispersed (≤1 μm) phase precipitates occur around the tool tip, where the metal is the most exposed to thermomechanical impact. Near the weld nugget in the thermomechanical impact zone, a combined structure forms, which consists of fine equiaxed and deformed thin elongated grains, oriented along the direction of tool displacement.

3. At FSW of heat-hardenable Al–Li alloys 1420 and 1460 the thermomechanical impact, in addition to grain refinement in the welding zone, promoting increase of metal hardness, results in simultaneous partial precipitation of excess phases from oversaturated solid solution and their coagulation, that leads to a certain lowering of joint hardness. However, the degree of metal softening in solid-phase welding of 1420 and 1460 alloys is much smaller than in fusion welding. Therefore, ultimate strength of FS-welded
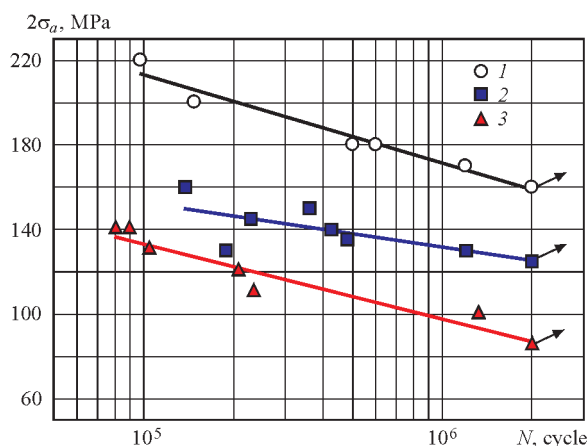
joints of these alloys is higher than that of TIG-welded joints without weld reinforcement.

4. As a result of weld formation in the solid phase at lower temperatures, compared to fusion welding, the maximum level of tensile residual longitudinal stresses in welded joints of 1420 alloy, produced by FSW, is by 35 % lower than that in TIG welding.

5. Proceeding from experimental data of fatigue testing, the rationality of application of FSW process instead of TIG welding in fabrication of structures with Al–Li alloys 1420 and 1460, operating under alternating loading conditions, was substantiated. It is established that fatigue resistance characteristics of butt welded joints, made by FSW technology, are higher than the respective values of TIG-welded joints. Values of limit stress ranges based on $2 \cdot 10^6$ cycles of stress reversal for FS-welded joints are just by 10–20 % lower than those of base material.

1. Beletsky, V.M., Krivov, G.A. (2005) *Aluminium alloys (composition, properties, technology, application)*n: Refer. Book. Ed. by I.N. Fridlyander. Kiev: KOMINTEKh.
2. (2002) *Aircraft materials*: Transact. of VIAM 1932–2002, 424. Moscow: MISIS VIAM.
3. Bratukhin, A.G. (2003) *Modern aircraft materials: Technological and functional peculiarities*. Moscow: Aviatekhinform.
4. Rabkin, D.M., Lozovskaya, A.V., Sklabinskaya, I.E. (1992) *Metals science of aluminium and its alloys*. Kiev: Naukova Dumka.
5. Mashin, V.S., Poklyatsky, A.G., Fedorchuk, V.E. (2005) Mechanical properties of aluminium alloys in consumable and nonconsumable electrode arc welding. *The Paton Welding J.*, **9**, 39–45.
6. Thomas, W.M., Nicholas, E.D., Needham, J.C. et al. *Friction stir butt welding*. Int. Pat. Appl. PCT/GB 92/02203; GB Pat. Appl. 9125978.8. Publ. 1991.
7. Defalco, J. (2006) Friction stir welding vs. fusion welding. *Welding J.*, **3**, 42–44.
8. Ericsson, M., Sandstrom, R. (2003) Influence of melting speed on the fatigue of friction stir welds and comparison with MIG and TIG. *Int. J. Fatigue*, **25**, 1379–1387.
9. Enomoto, M. (2003) Friction stir welding: Research and industrial applications. *Welding Int.*, **5**, 341–345.
10. Ishchenko, A.Ya., Poklyatsky, A.G. *Tool for friction stir welding of aluminium alloys*. Pat. 54096 Ukraine. Int. Cl. B23K 20/12. Fil. 30.04.2010. Publ. 25.10.2010.

HYBRID TECHNOLOGY COMBINING ELECTRON BEAM WELDING AND FRICTION STIR WELDING IN THE PROCESSES OF REPAIR OF AIRCRAFT STRUCTURE ELEMENTS OF MAGNESIUM ALLOYS

A.L. MAJSTRENKO[1], **V.M. NESTERENKOV**[2], **R.V. STRASHKO**[2], **S.D. ZABOLOTNY**[1] and **V.N. TKACH**[1]

[1]V.N. Bakul Institute for Superhard Materials, NASU
2 Avtozavodskaya Str., 04074, Kiev, Ukraine. E-mail:alcon@ism.kiev.ua
[2]E.O. Paton Electric Welding Institute, NASU
11 Kazimir Malevich Str., 03680, Kiev, Ukraine. E-mail: office@paton.kiev.ua

A technological process is developed for friction stir processing of surface layers of the parts from magnesium and aluminum alloys for the purpose of their modifying aimed at formation of a layer of fine-grain structure (of 1.2–4.5 μm) that is 16–63 times lower a grain size of base metal (75.8 μm). Formation of microcracks is shown at the interface of EB-weld metal and base metal of magnesium alloy ML10 as well as their absence in welding through intermediate zone with FS-modified fine-grain structure. It provided for the possibility of increase of strength of EB-welded joints from ML10 alloy. 8 Ref., 1 Table, 13 Figures.

K e y w o r d s : electron beam welding, friction stir welding, modified fine-grain structure, microstructure grain size

Magnesium alloys are particularly important in aircraft and space engineering due to the fact that they differ by relatively high strength at low specific weight [1–4]. Structural magnesium alloys are divided on wrought and cast ones. The main alloying elements in the cast alloys are aluminum, zinc, manganese, silicon, cerium, zirconium and thorium. However, at all positive characteristics and properties these alloys refer to difficult-to-weld materials. These difficulties are caused, first of all, by formation of defect of pore and cavity type in the welds due to appearance in a zone of electric arc effect the local temperatures exceeding not only zinc melting temperature (419.5 °C), but its evaporation temperature (907 °C). Therefore, all the investigations aimed at producing solid, homogeneous and strong welded joint of the parts from wrought and cast magnesium alloys are still relevant. One of the most perspective method in this case is vacuum EBW.

The investigations on vacuum weldability of magnesium alloys ML using electron beam were carried out on UL-209M unit with computer regulation of all parameters and systems [5] developed at PWI (Figure 1). The unit is equipped with power complex based on ELA-60/60 and EB gun moving inside the vacuum chamber along X, Y, Z linear coordinates as well as turning about the axis Y–Y in coordinate QC through 0–90° angle. Air from vacuum chamber of internal dimension 3850×2500×2500 mm and volume 24.1 m³ is pumped in automatic mode to working vacuum $2.66 \cdot 10^{-2}$ Pa for less than 30 min. At $U_{acc} = 60$ kV the EB gun with tungsten cathode together with power complex ELA-60/60 provides for electron beam current range $I_b = 0$–500 mA as well as performance of different technological beam scan in process of EBW. An accuracy of EB gun positioning in the coordinates is not less than 0.1 mm. An image of welding place is visualized in the secondary emission electrons, and combining of electron beam with butt is provided by RASTR system with the accuracy not worth than 0.1 mm [6].

Formation of a keyhole in molten metal is caused by the following factors, namely material evaporation, displacement of liquid metal by pressure of beam electrons, displacement of liquid metal by evaporation

Figure 1. UL-209M unit for vacuum EBW
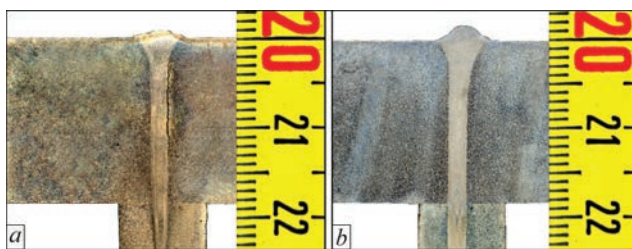
Figure 2. Macrostructure of welded joint of magnesium alloy ML10 of 18.5 mm thickness in downhand EBW with run-on plate without preliminary FSP (*a*) and with FSP (*b*)

recoil pressure, surface tension force and hydrostatic pressure of liquid metal. Molten metal pressure has significant impact on the weld and defect formation. This pressure is in particular obvious in welding of metals of 20 mm thickness. In this connection, task solution for welding of medium and large thickness metals required a change of position of electron beam and weld pool to horizontal one. It provided for more favorable conditions of liquid metal transfer in a crater. Horizontal positioning of a pool also facilitates liquid metal degassing and its refining.

Welding of cast magnesium alloy ML10 of $\delta = 6$ mm was also carried out by vertical welds without run-on plate using horizontal electron beam on upward and downward schemes. The specimens of $150 \times 100 \times 6$ mm size were subjected to preliminary friction stir processing (FSP). Analysis of carried experiments showed that the vertical welds produced with horizontal electron beam have satisfactory formation using both schemes. Figure 2 shows that width of the weld rises in a root part according to both schemes at increase of welding current at $v_w = 20$ mm/s, refocusing $+ \Delta I_f = 30$ mA, diameter of circular technological scan of electron beam $d_{cir} = 1$ mm and working distance $l_{work} = 200$ mm. No defects in form of undercuts, depressions and cracks were found along the fusion line and in HAZ.

Since the weld metal dendrites start growing from the base metal grains on fusion line, the size of crystallites depends on these grain dimensions. Chemical inhomogeneity has negative effect on the final physical-chemical properties of welded joints, and during weld pool solidification promotes for formation of the weld defects. i.e. solidification cracks. Increase of solidification rate and, respectively, reduction of size of dendrites and inter-dendrite areas can be referred to the main measures, aimed at elimination of microchemical inhomogeneity. Therefore, preliminary refinements of the base metal grains promotes for certain decrease of size of weld crystallites. It is well known fact that HAZ in non-ferrous metal and alloys, including magnesium ones, consists of structural areas similar to areas in steel, i.e. area of partial melting — narrow transition band from weld metal to base metal, including submelted and solidified grains of the base metal. The weld crystallites coalescence with the coarse grains of base metal in this solid–liquid state area. A liquation of additives is possible in this case, therefore, this area has significant effect on welded joint quality. Formation of the liquid interlayers at grain boundaries results in reduction of the mechanical properties of welded joints and, quite often, crack appearance.

A fractographic examination of specimen fracture surfaces carried out on «Neophot-32» and «Versamet» microscopes showed that the metal fracture, reflecting overheating condition in the weld to base metal fusion zone, takes place parallel to the axis of applied load. Thickening of grain boundaries takes place in the weld zone structure in arc methods of welding as well as presence of triple compounds and significant amount of eutectics can be observed. In contrast to mentioned above, EBW promotes for mainly polyhedral structure and formation of eutectic reduces, that has positive effect on metal hardness level.

The weld has a fine-disperse, cast structure consisting of α-solid solution of complex composition and uniformly distributed phase precipitates, apparently, Mg_4Al_3 (Figure 3). Besides, presence of round precipitates of light colour (Figure 4) should be noted. Weld hardness reaches $HV01$-658–782 MPa.

Amount of fine grains in the structure increases in withdrawal from the fusion line, the structural constituents remain the same. The structure of base metal consists of alternating bands of different size grains (Figure 5). Lower amount of inclusions and non-dissolved phase (probably Mg_4Al_3) is noted in the structure in comparison with HAZ structure. Hardness at specimen edge makes $HV01$-762–772 MPa.

Hybrid FSW + EBW technology. EBW in comparison with known methods of fusion welding is characterized by high specific concentration of energy, ideal conditions of vacuum shield of molten metal,
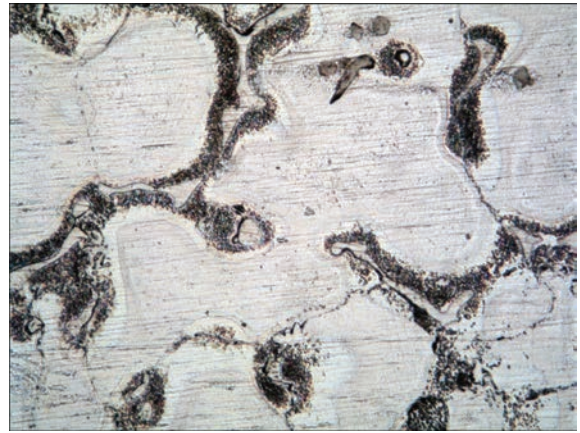

Figure 3. Microstructure (×1000) of weld of magnesium alloy ML10 made with EBW
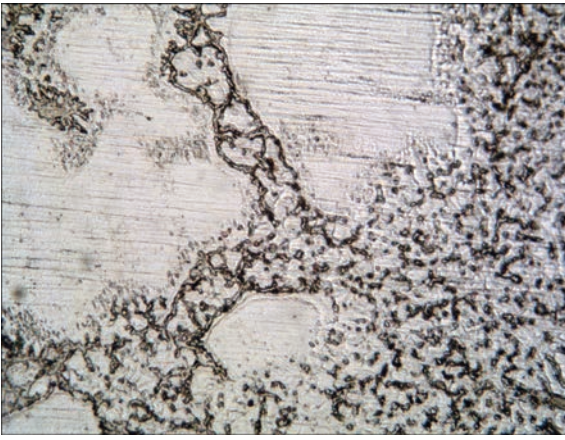
Figure 4. Microstructure (×500) of ML10 alloy along the fusion line in EBW

Figure 5. Microstructure (×500) of base ML10 metal

high welding speed, low values of energy input rate, small width of HAZ, narrow penetration zone and small volume of weld liquid-phase pool, insignificant heat deformations of parts being welded, high flexibility and large range of process capabilities. This sets it apart from other fusion arc welding methods. Nevertheless, fusion welding of magnesium alloys provokes for structural transformations in the weld metal and near-weld zone. Such areas acquire different mechanical properties, due to what a welded joint strength in comparison with a base metal is reduced in some cases to 50–60 %, and formation of cracks (Figure 6) is observed along the fusion line and in the near-weld zones.

Therefore, it is relevant to develop a hybrid technology, which would join high technological effectiveness of EBW and possibility of production of high-strength joints using FSW in order to apply it during manufacture and renewal of life of structures of aircraft and space engineering from aluminum and magnesium alloys. The received process capabilities were also used for modifying a structure of cast magnesium alloy ML10 due to effect of friction stir process on change of a structure of parts' surface layer, which are thereupon being welded using EBW. The idea of structure modifying lied in purposeful refinement of grain size in the processed layer of base metal to 6–8 mm depth.

Influence of preliminary FSP of surface layers of welded parts. FSW proposed in 1991 by TWI [7] refers to the methods of solid-phase joining and differs from traditional friction welding methods. The tool with small diameter pin and shoulder (Figures 7 and 8) pressed in metal being welded at rotation and generating heat emission due to friction work between the tool surfaces and metal being welded, and work of plastic deformations. This results in metal local heating to temperature sufficient for reduction of its hardness and plasticization to ductile-plastic state, after what the tool starts proceed-

ing along parts' interface, provoking plastic stirring of metal of adjacent surface layers in mating parts, by this forming a permanent joint. Thus, formation of the welded joint took place at temperatures significantly lower than in liquid-phase fusion welding, that has vital effect on the structure of formed weld and its strength, but also minimizes residual stresses in HAZ and temperature deformations. It is very attractive for aircraft and automotive industry. Currently, these branches realize number of examples of FSW of metals of 1–10 mm thickness.

It is well know fact that FSW has a number of advantages in comparison with fusion welding. In particular, there is a possibility of joint formation in solid phase, high efficiency and quality (absence of porosity, inclusions, cavities), wide range of welded similar and dissimilar metals with different physical-chemi-
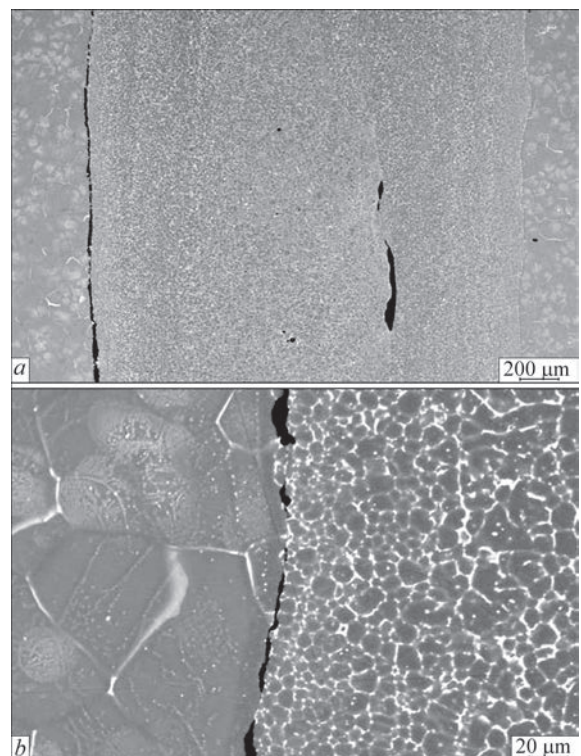
Figure 6. Delamiantion of weld metal from base metal in EB-welded specimen of magnesium alloy ML10
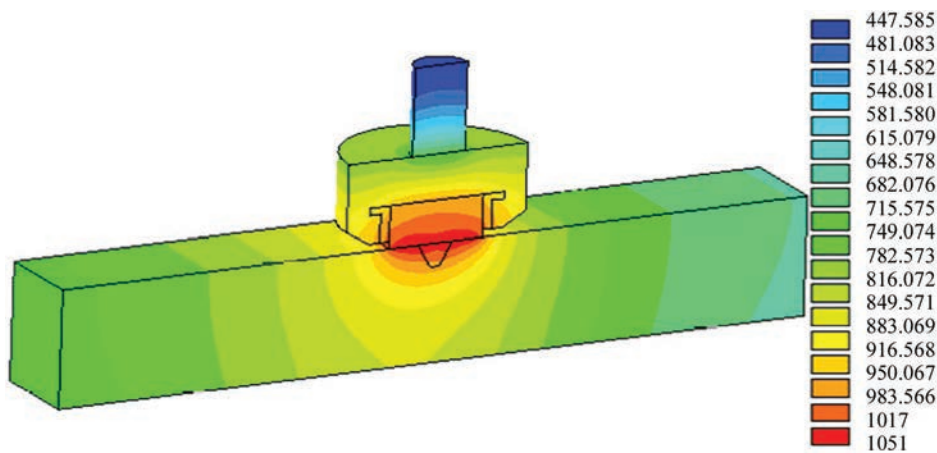
Figure 7. Scheme of FSW

cal properties, absence of auxiliary welding consumables and possibility of performance of operations in any spatial positions.

As it was shown in work [8] FSW provokes for transformation of initial coarse-grain structure of the base metal into fine-grain one in the stir zone. Besides, crystalline particles, formed in the processes of primary solidification (after alloy casting), are fractured in the surface layers of metals being welded, rolling-oriented grains are eliminated and their size is significantly reduced (Figure 9).

Hybrid FSW + EBW technology was tested in welding of magnesium alloy ML10 of 20 mm thickness using downhand scheme with vertical electron beam and run-on plate from the same alloy. The surface layers of specimens were preliminary FS-pro-

Figure 8. View of tool made from steel P18 (*a*), and FSP of surface layer of ML10 alloy block (*b*)

cessed on vertical knee-and-column type milling machine of 6L12P model to 6 mm depth at tool rotation rate 800 rpm and linear rate of tool movement 31.5 mm/min. After FSP the surfaces of edges to be welded were milled. EBW of butt specimens was carried out in a special device from non-magnetic materials. Penetration geometry of the formed welded joints differ by fusion walls virtually parallel base metal on depth. Carried investigations on ML alloys 5–30 mm thick mastering of hybrid welding technology showed welded joints' stable formation.

Thus, it is determined that hybrid welding by vertical electron beam in downhand position and horizontal electron beam using vertical upward and downward schemes provided for satisfactory formation of the welded joints and elimination of defects of ML alloys at through penetration of specimens to $\delta \leq 10$ mm even without use of the run-on plates. There is a necessity in application of the run-on plates in welding of ML alloy specimens of $\delta > 10$ mm due to formation of undercuts and depressions in a weld root part, which take place in all considered schemes at through penetration.

Metallographic examinations of ML10 alloy welded joints were divided in the following way. A hybrid-welded joint is located on the first specimen. Such a sequence (FSW + EBW) of metal effecting assumes preliminary change of the initial structure of surface layers of alloy subjected to FSP with their further EBW. A welded joint made using simple EBW without FSW application was performed on the second specimen. A structure was developed by means of chemical etching in 10 % aqueous solution of citric acid.

A microstructure of weld in examined specimens represent itself a mixture of δ-phase (solution based on magnesium) and intermetallics (see Figures 4 and 5). The weld structure is cast and fine dispersed, weld metal hardness of specimen 1 was *HV*05-779–
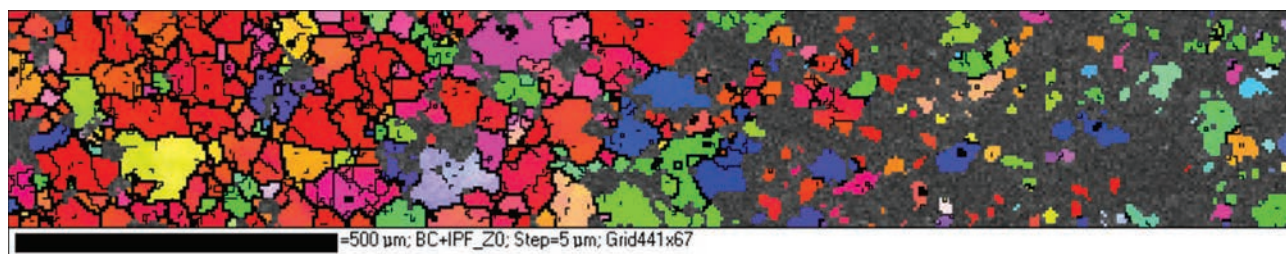
Figure 9. Backscattered electron diffraction image of microstructure of ML10 alloy at interface of initial metal and modified layer after FSP to 6 mm depth
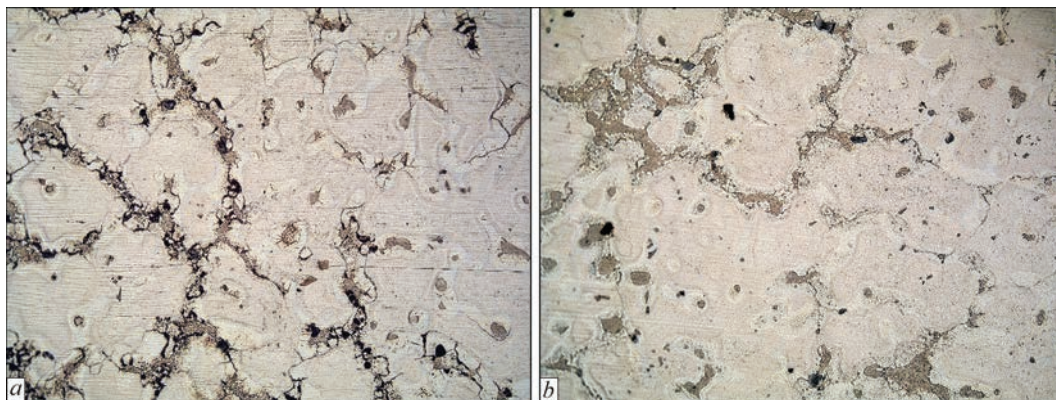
Figure 10. Microstructure (×200) of HAZ areas of hybrid-welded specimens 1 (*a*) and 2 (*b*)

906 MPa and that of specimen 2 HV05-826–934 MPa. The microstructure of weld metal of investigated specimens included the different shape particles (see Figure 4). The precipitates of the same type are present in HAZ (Figure 10) and base metal of examined specimens (see Figures 4 and 5). The structures of weld metal of specimens 1 and 2 differ by somewhat coarser size of the structural constituents in specimen 2 in comparison with specimen 1. The structure of HAZ metal in specimens 1 and 2 represent itself coarse grains of solid solution of alloying elements in magnesium. Compressing them harder eutectic mixture of solid solution (δ-solution) and intermetallic compound are located along the grain boundaries, and it should be noted that the eutectic mixture continues weld structure (see Figure 4). Eutectic amount is reduced in a direction from the fusion line, and eutectic mixture is located only by small fragments along the grain boundaries of δ-solid solution at 500 (specimen 1) and 700 μm distance (specimen 2). HAZ extension in specimen 1 reached 1200 μm and that in specimen 2 was 1500 μm.

A microstructure of base metal (see Figure 5) consists of grains of δ-solid solution (hardness HV01-612–665 MPa), eutectic (HV01-946 MPa) is precipitated along the boundaries and light phase with HV01-1400 and 1330 MPa is precipitated in the center of eutectic. Hardness of grains of δ-solid solution close to eutectic reaches HV01-707 MPa.

Mechanical properties of EB-welded joints. The mechanical tests were carried out for testing a qual-

ity of welded joints of magnesium alloy ML10. The results of pulling tests allow determining the other parameters of welded joint strength, i.e. $\sigma_{0.2}$, δ and ψ (see the Table), in addition to σ_t value. The specimens of welded joints were tested in as-delivered condition, after EBW as well as after hybrid FSW + EBW. The pulling tests of welded joints were carried out using cylinder specimens of 3 mm test portion diameter.

As it follows from Figure 11, failure of specimens after EBW takes place mainly along the fusion line and HAZ, and after FSW + EBW it takes place in a distance from the weld and out of the HAZ (Figure 12). Ductility of the welded joints (δ, ψ) rises insignificantly in comparison with ductility of the base metal, and toughness a_n increases by 30 % and more. Strength of the hybrid-welded joints, increases in comparison with welded joint strength produced without FSP, and reaches $\sigma_{t\,wj}/\sigma_{t\,bm}$ = 94 %.
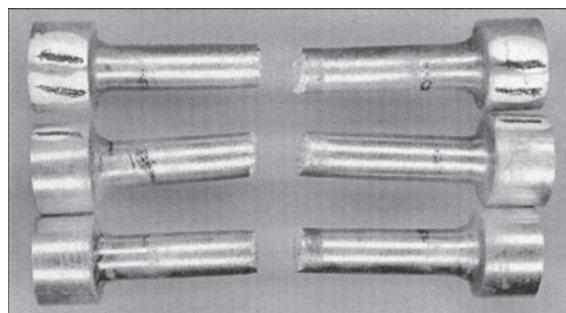
Figure 11. EB-welded specimens of magnesium alloy ML10 after mechanical pulling tests
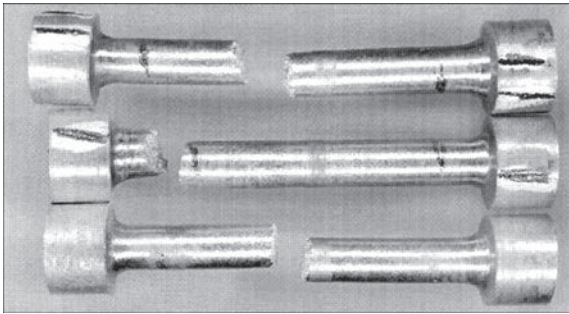
Figure 12. View of specimens of magnesium alloy ML10 with FS-modified structure of alloy layers adjacent to butt and then EB-welded at U_{acc} = 60 kV, I_b = 50 mA, v_{EBW} = 20 mm/s, ΔI_f = = 5 mA and l_{work} = 200 mm after uniaxial tension tests

Figure 13. View of joint structure of parts from ML10 alloy with preliminary modified surface layers (v_{FSW} = 31.5 mm/min; ω = = 800 rpm) and further EBW (dashed lines — conditional EB-weld, FSP-weld and base metal interfaces)

It should be noted that formation of cracks (see Figure 6) is observed after EBW at the interface of weld metal recrystallization zone through liquid phase and base ML10 metal. This phenomenon is considered in more details and approximate evaluation of the reasons of its formation will be carried out.

It is known fact that the volumetric compression modulus of magnesium alloy ML10 equals 41.2 GPa, coefficient of thermal expansion α = 0.0000225 K^{-1} at room temperature and α = 0. 000102 K^{-1} [3, 4] at liquid phase temperature 650 °C, i.e. their ratio reaches 4.53. Thus, we can evaluate the value of temperature stresses, which appear in the weld metal produced by EBW, due to thermoelastic variance to the characteristics of base ML10 metal at cooling after welding from liquid phase temperature (650 °C) to room temperature, i.e. $\sigma_{t.s} \approx K\Delta\alpha\Delta T \approx 41200 \cdot 0.00008 \cdot 600 = 1997$ MPa. Formed thermal stresses reach 2 GPa level and tensile ultimate strength of this alloy (at room temperature) equals only σ_t = 226 MPa. Therefore, it is obvious that formation of microcracks along the interface of these zones is caused by effect of supercritical tensile stresses. Apparently, that reduction of strength of the EB-welded ML10 alloy joint is caused by appearance of microcracks along the weld body to base metal interface (see Figure 6). Thus, it can be concluded that the proposed hybrid technology (FSW + EBW) allows significant change of the situation in comparison with traditional EBW by increase of the strength characteristics of magnesium alloy welded joint at that preserving its ductility (see the Table). In this connection, it is proposed to carry out preliminary change of base metal structure, i.e. its modification, before EBW. It lies in directed refinement of metal grains in surface layers of the parts being welded.

As it was mentioned above, essence of the process of structure modification during FSW lies in grain refinement of the processed layer to 6–8 mm depth in comparison with the base metal [6] (see Figures 6 and 9). Such a refinement by Hall–Petch law can result in increase of metal strength in this zone. Besides, a conclusion on state of crystallites in the FSW and EBW deformed zones can be done based on analysis of image in Figure 9.

Thus, fracture and disorientation of crystallites of the initial metal can be observed in the FSP zone using a method of backscattered electrons on ZEISS EVO SEM, equipped with energy-dispersion analyzer INCA PENTA Fetx3. It results in formation of fine-grain alloy structure (grain size 1.2–4.5 μm), that is 16–63 times less the grain size (75.8 μm) in the initial metal. At that it should be noted that initial orientation of the crystallines (in the base metal) in the modified layer is completely disoriented (see Figure 9).

Change of parameters of the structure of ML10 alloy modified specimens depends on parameters of tool movement (tool rotation rate and speed of welding). SEM-images of grain boundaries of mating modified layer and base ML10 metal (see Figure 9) indicate high level of effect of modification process on change of alloy structure state in form of significant refinement of base metal grains.

Exactly this peculiarity of structure change of ML10 alloy, received as a result of preliminary FS modification of the surface layer (to 6 mm depth), was used for further joining the parts by vacuum EBW for the purpose of increase of weld strength. Figure 13 shows the structure of ML10 alloy, received as a result

Mechanical properties of welded joints of magnesium alloy ML10

Specimen type	σ_t, MPa	$\sigma_{0.2}$, MPa	δ, %	ψ, %
Base metal	230.6	140.0	5.9	11.1
EB-welded joint	197.9	134.3	6.5	12.0
After EBW of parts with FS-modified surface layers	216.8	153.9	6.6	12.5

of EBW its parts after preliminary FSP of the surface layers. At the same time, formation of an intermediate structured fine-grain area, having no observable hot cracks (see Figure 6), is noted after EBW between re-crystallization zone and base metal. The fractographic examination of structure state of the welded joint with modified layer (after FSP to 6 mm depth) showed that the preliminary processing of the surface layers of part edges results in the fact that further EB joining takes place already not over the alloy in the initial state with 75.8 μm grain size (see Figure 13), but on metal with FS-formed fine-grain structure of 1–4 μm size. Moreover, in the zone of weld metal recrystallization through liquid phase the alloy grain size increases only to 9.3–9.8 μm, that is 1.5 times more the size of grain in FS processing zone, but 7–8 times less than in the base metal.

But the most important lies in formation of the intermediate fine-grain area (grain size 6.4 μm), in which microcracks are already observed (see Figure 13), between the recrystallization zone and base metal. This Figure shows the structure state of ML10 alloy in the modified layer as well as conditional interfaces of layers after FSP.

The experiments show that the temperature in processing zone does not exceed $(0.5–0.7)T_m$ but melting temperature of magnesium alloys is in the range from 650 to 680 °C, i.e. temperature in the zone of tool with metal interaction in the process of its structure modification is possible in 270–320 °C limits [8]. The temperature in FSP zone was measured using digital contact-free infrared thermometer DT-8833. Mechanical pulling tests of welded joints of ML10 alloys showed (see the Table) that fracture after EBW with preliminary FSP takes place mainly out of the HAZ (see Figure 12).

Conclusions

1. The optimum modes were determined for EBW of ML magnesium alloy 5–30 mm thick providing set penetration geometry in different spatial positions.

2. Formation of the microcracks at a mating interface of recrystallization zone through weld metal liquid phase and ML10 base metal in EBW as well as their absence in welding through intermediate zone with FS-modified fine-grain structure is shown for the first time.

3. The tools were developed for preliminary FSP of the surface layers of edges of plates of cast magnesium alloy ML10 for modification of their structure, directed on formation of alloy fine-grain structure (grain size 1.2–4.5 μm) which 16–63 times less the size of initial grains (75.8 μm).

4. Metallographic examinations of alloy ML welded joints were carried out, which verified formation of finer structural constituents in the case of FSP application.

5. For the first time it is determined that in EBW over modified layers of specimens of ML10 alloy the zone of FS-modified fine-grain structure with grain size 11.8 times less than that in the initial one, i.e. 6.4 μm, is formed. It lies between the recrystallization zone through liquid phase of weld metal, made by EBW, with alloy grain size 7–8 times less than that of the base metal (75.8 μm), i.e. 9.3–9.8 μm. In addition, for the first time it was found that the average size of grains increases to 6.4 μm from metal recrystallization zone to EBW zone in FS-modified layer (grain size 1.2–4.5 μm) during its heating and cooling.

6. The technology was developed for hybrid FSW + EBW welding of magnesium alloys MA and ML of up to 30 mm thickness which allows eliminating crack formation and increasing strength characteristics of the welded joints.

1. *GOST 14957–76:* Magnesium wrought alloys. Grades.
2. *GOST 2856–79:* Magnesium cast alloys. Grades.
3. Krymov, V.V. (1960) Magnesium cast alloys and their application in engineering. In: *Magnesium alloys*. Moscow.
4. Portnoj, K.I., Lebedev, A.A. (1952) *Magnesium alloys*: Refer. Book. Moscow.
5. Nazarenko, O.K., Nesterenkov, V.M., Neporozhny, Yu.V. (2001) Design and electron beam welding of vacuum chambers. *The Paton Welding J.*, **6**, 40–42.
6. Paton, B.E., Nazarenko, O.K., Nesterenkov, V.M. et al. (2004) Computer control of electron beam welding with multi-coordinate displacements of the gun and workpiece. *Ibid.*, **5**, 2–5.
7. Thomas, W.M., Nicholas, E.D., Needham, J.C. et al. *Friction stir butt welding*. Int. pat. appl. PCT/GB92/02203; GB pat. appl. 9125978.8; US pat. appl. 5,460,317. Publ. Dec. 1991.
8. *Report on R&D*: Development of tools from superhard materials for friction stir welding designed for producing and restoration of structures of aeronautical and space engineering from aluminium and magnesium alloys in the frame of program RES URS R 8.6.1. Kyiv: INM.

HYBRID TECHNOLOGIES OF WELDING ALUMINIUM ALLOYS BASED ON CONSUMABLE ELECTRODE ARC AND CONSTRICTED ARC*

A.A. GRINYUK[2, 3], **V.N. KORZHIK**[1, 2], **V.E. SHEVCHENKO**[1, 2], **A.A. BABICH**[2] and **S.I. PELESHENKO**[4]

[1] Chinese-Ukrainian E.O. Paton Institute of Welding (Guangdong General Research Institute of Industrial Technology, Guangzhou Research Institute of Non-Ferrous Metals
Changxing Str., Tianhe, 510650, Guangzhou, PRC. E-mail: vnkorzhyk@gmail.com
[2] E.O. Paton Electric Welding Institute, NASU
11 Kazimir Malevich Str., 03680, Kiev, Ukraine. E-mail: office@paton.kiev.ua
[3] NTUU «Kiev Polytechnic Institute»
6/2 Dashavskaya Str., 03056, Kiev, Ukraine. E-mail: andrey_grinyuk@ukr.net
[4] South China University of Technology
510641, Guangzhou, PRC. E-mail: sviatoslav@qq.com

Main stages of development of equipment and technology of hybrid consumable-electrode plasma-arc (plasma-MIG) welding of aluminium alloys are analyzed. Main design solutions at development of torches for hybrid plasma-MIG welding are shown, i.e. transition from rod anode in hybrid torch plasma part to ring anode. Application of ring anode simplifies the design of hybrid torch for plasma-MIG welding and improves arc contact. The paper presents the advantages of the process of hybrid plasma-MIG welding with coaxial wire feed compared to traditional inert-gas consumable-electrode welding. 23 Ref., 15 Figures.

Intensive development of high-speed ground-, air- and water-based transport leads to creation of efficient and economically substantiated technologies of producing aluminium alloy welded joints. In the recent decade hybrid technologies of arc welding, combining the energy of nonconsumable electrode constricted arc and consumable electrode arc in one weld pool have been developing intensively. This technology is called hybrid consumable-electrode plasma-arc welding. This process was called Plasma-MIG technology abroad.

Philips Corporation owns the patents for the first hybrid plasmatron with simultaneous application of nonconsumable electrode constricted arc and consumable electrode arc in one pool [1]. Consumable electrode arc runs inside the nonconsumable electrode constricted arc. Schematic of hybrid plasmatron developed by Philips Corporation is shown in Figure 1. Electrode wire was fed coaxially with constricted arc. Welding was performed at direct current of reverse polarity (DCRP) with tungsten electrode located laterally relative to plasma-forming nozzle axis, used as the cathode. Over the next years, the efforts of Philips

Corporation staff were directed at improvement of the design of hybrid plasmatron with lateral position of tungsten electrode [3].

To ensure compact dimensions of hybrid plasmatron, its cathode and electrode wire were shifted to different sides from the axis of plasmatron proper (Figure 2) [4].

Application of not only transferred, but also nontransferred arc was considered. Different variants of producing nontransferred constricted arc were proposed: between tungsten electrode and compression nozzle; between two tungsten electrodes located side by side; between two tungsten electrodes located at equal distance from electrode wire [5].

Applicability of nontransferred arc was considered not only for constricted arc, but also for consumable electrode arc [6]. Furtheron, application of either nontransferred nonconsumable electrode constricted arc, or nontransferred consumable electrode arc did not become widely accepted, and they are mentioned only in patent publications.

Application of two electrode wires for the process of hybrid plasma-MIG welding was tried out [7].
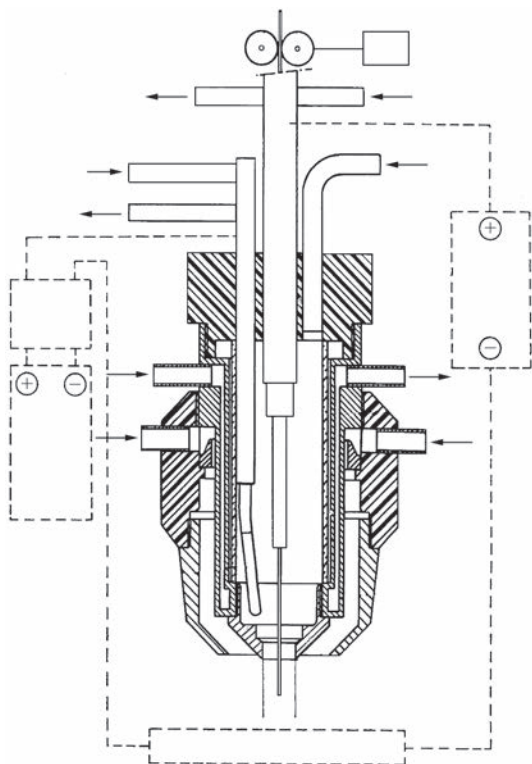
Figure 1. Plasmatron for hybrid plasma-MIG welding developed by Philips Corporation [2]

Designs with lateral position of tungsten anode and current supply to two electrode wires from two different DC power sources, with lateral position of tungsten cathode and coaxial position of split consumable electrode with its powering from one DC source, with tungsten cathode position between the wires of split consumable electrode, as well as application of split consumable electrode and hollow copper cathode operating in the mode of regular DCRP arc generation,
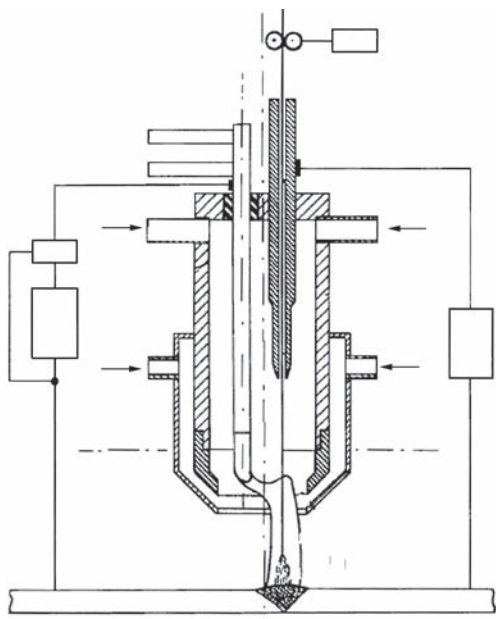
Figure 2. Plasmatron for hybrid plasma-MIG welding with tungsten cathode and electrode wire which are shifted relative to plasmatron axis
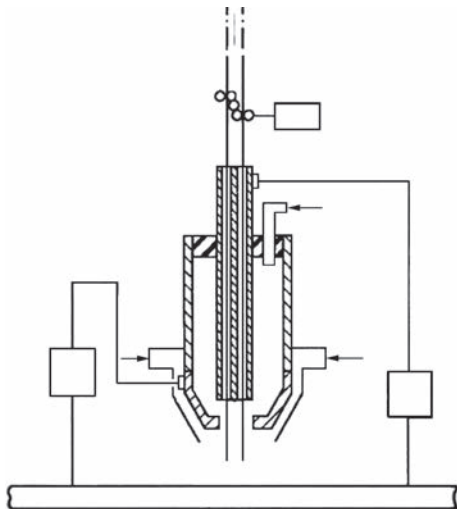
Figure 3. Plasmatron for hybrid plasma-MIG welding with coaxial feed of split electrode through hollow copper cathode operating in the mode of regular nonconstricted arc

were proposed (Figure 3). Such schematics of electrode arrangement were not developed any further.

Variants of simultaneous running into a common pool of regular consumable and nonconsumable electrode arcs with coaxial wire position and hollow anode were proposed [8, 9]. Figure 4 shows the schematic of a hybrid torch for consumable and nonconsumable-electrode welding. Such a schematic of realization of hybrid process of consumable-electrode welding of aluminium alloys did not become widely accepted.

For realization of the process of hybrid plasma-MIG welding, Philips Corporation developed and batch-produced PZ 4302/10 system (Figure 5). The system consists of power source for DCSP and DCRP
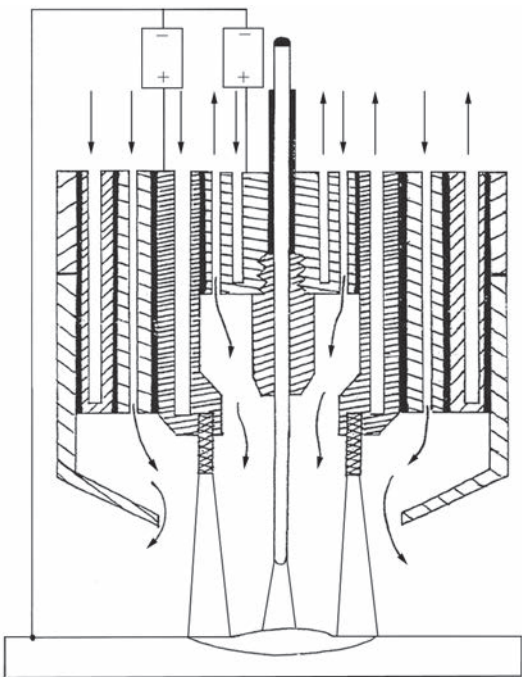
Figure 4. Hybrid torch for consumable and nonconsumable-electrode welding with coaxial wire feed through circular cathode

Figure 5. PZ 4302/10 system for hybrid plasma-MIG welding developed by Philips Corporation

plasma-arc welding, DC power source for consumable-electrode welding (both the power sources are installed in one case), electrode wire feed mechanism and control system. This system provided maximum current of 400 A for DC plasma-arc welding and 630 A for consumable-electrode welding. There is no information about the hybrid plasmatron, with which this system was fitted.

The issue of simultaneous running of nonconsumable electrode constricted arc and consumable-electrode arc positioned in sequence one after the other was also considered [10, 11]. Plasma Laser Technologies Ltd. is the main developer of equipment for hybrid plasma-MIG welding with serial arrangement of nonconsumable electrode constricted arc and consum-

Figure 6. Plasma Laser Technologies hybrid torch for plasma-MIG welding of aluminium alloys

able electrode arc. The process of hybrid plasma-MIG welding developed by this company received patented name of Super-MIG. Consumable electrode torch and plasmatron are located in one case and have one common protective nozzle. To weld materials, having no oxides on their surface with melting temperature above that of base metal, DCSP nonconsumable electrode constricted arc and DCRP consumable electrode arc are used. So-called electromagnetic shield is additionally incorporated into the hybrid plasmatron design to prevent electromagnetic interaction of the arcs. A special torch was developed for hybrid welding of aluminium alloys. It supports plasma-arc welding by different polarity asymmetrical current of up to 200 A and consumable-electrode welding at up to 550 A DCRP current (Figure 6). Equipment complex Super-MIG for hybrid plasma-MIG welding also includes plasma module with equipment complex control system. Control system allows connection to welding robot controllers.

Super-MIG process allows simplifying the hybrid plasmatron design, compared to schematic of coaxial feed of electrode wire, but here the consumable electrode arc is not additionally constricted by nonconsumable electrode constricted arc that causes stronger metal spatter and lower penetrability. Further development of hybrid torches for plasma-MIG welding went along the path of hollow anode introduction [12–15]. The anode was of composite design with refractory material insert.

Hybrid plasmatron of Merkle Company (Germany) is also designed by the schematic of application of ring hollow anode and coaxial feed of electrode wire [16]. Merkle serial power sources for consumable-electrode welding were used as power sources for generation of plasma and consumable electrode arc. A feature of Merkle hybrid torch for plasma-MIG welding is bimetal composite anode (Figure 7). The anode lower part is made from refractory material and is brazed to copper water-cooled part.

Chemnitz Technical University (Germany) developed a device, providing switching on and simultaneous operation of power sources for DCRP nonconsumable-electrode plasma-arc welding and power source for DCRP consumable-electrode welding [17]. Research in the same direction is performed also at SLV Muenchen (Germany). Similar research is performed at Perm State University (Russia) [18, 19]. In Ukraine plasma-MIG welding was studied at Priazovsky Technical University [20]. Features of plasma-MIG welding process were also studied in China and Brazil [21, 22].

TBI Company (Germany) produces customized PLM 500 and PLM 600 torches with ring anode for

Figure 7. Composite anode of Merkle hybrid torch for plasma-MIG welding with coaxial wire feed

hybrid plasma-MIG welding, which can stand total current load from 500 up to 600 A DCRP, respectively (Figure 8). Solid copper anode is the feature of the design of the torch for hybrid plasma-MIG welding of TBI Company. Plasma-forming nozzle and protective gas nozzle in this design are made as one solid part, making the design more complicated and increasing the part cost.

Hybrid 8000 MR system (AMT Maschinen- und Geraetetechnik GmbH, Germany) provides simultaneous generation of DCRP for nonconsumable electrode constricted arc and for consumable electrode arc (Figure 9). Welding current adjustment for each of the arcs is performed individually in the range from 15 up to 400 A. This system can be also used as regular power source for consumable-electrode welding. When this system is applied, nonconsumable electrode constricted arc is excited without using the pilot arc. Application of this system for DC nonconsumable-electrode plasma-arc welding is somewhat difficult, as availability of pilot arc and oscillator for igniting it is not envisaged.

DigiPlus A7PM system (ICM Soldagem, Brazil) provides a similar range of welding functions as AMT Company system. This system also cannot be used for regular nonconsumable-electrode plasma-arc welding for the reason of absence of the module of pilot arc ignition and generation.

A number of all-purpose equipment complexes for plasma-arc, combined and hybrid welding have been developed within the framework of PWI co-operation under a project of Chinese-Ukrainian Welding Institute, and produced by «Science-Production Center «PLAZER Ltd.» (Ukraine). The basic concept of these complexes development is upgrading and adaptation of batch-produced power sources for nonconsumable and consumable-electrode welding. These equipment complexes allow implementation of a wide range of plasma and arc processes: performing DCSP plasma-arc welding with filler wire and welding by asymmetrical current of different polarity, hybrid plasma-MIG welding with plasmatron ring anode
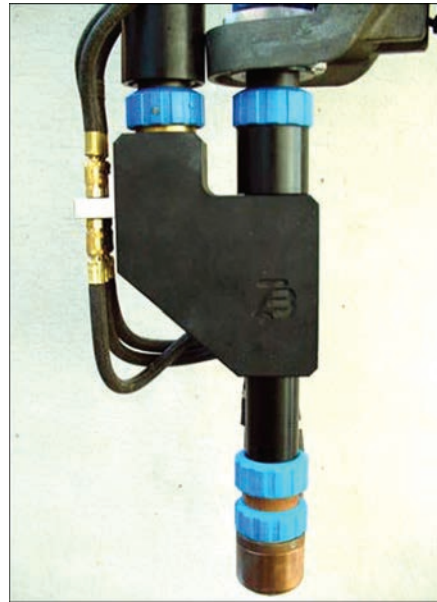
Figure 8. PLM 500 torch of TBI Company for hybrid plasma-MIG welding

and axial feed of electrode wire, combined constricted arc and consumable-electrode welding in «soft plasma» mode, automatic consumable and nonconsumable-electrode welding [23]. This equipment is made of modular design to enable realization of such a set of technological capabilities.

In addition, this equipment supports operation in a complex both with different types of welding manipulators (system for longitudinal welding, columns, rotators, etc.), and with welding robots. For this purpose, the control system has an interface for connection to a robot, with communications protocols, applied for welding robots of leading manufacturers.

Equipment complex PLAZER PW-HYBRID TC (Figure 10) allows performing welding in the downhand position, vertical and horizontal welds on vertical and inclined planes. Availability of rotary welding
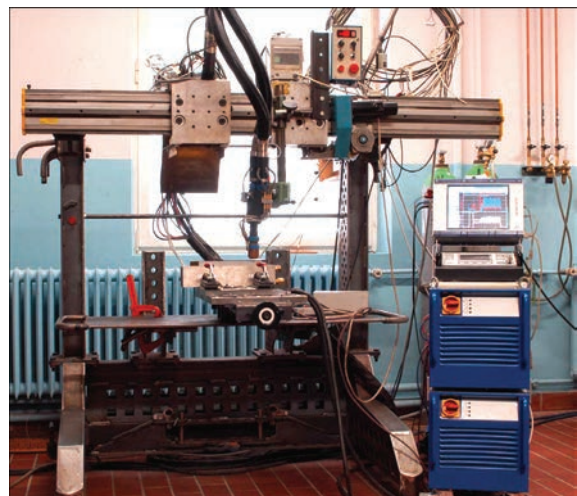
Figure 9. Hybrid 8000 MR system for hybrid plasma-MIG welding with axial feed of electrode wire of AMT Company

Figure 10. All-purpose equipment complex PLAZER PW-HY-BRID TC for nonconsumable-electrode plasma-arc welding, combined and hybrid plasma-arc welding in different spatial positions

Figure 11. PLAZER all-purpose assembly-welding table for welding downhand welds, vertical and horizontal welds on vertical and inclined planes

positioner in its composition, allows performing circumferential welds.

For fitting a welding research section, SPC «PLAZ-ER», developed an all-purpose assembly-welding table by PWI technical assignment. A feature of this table design is movement of the part proper, and not of welding torches. This eliminates the factor of torch oscillation,
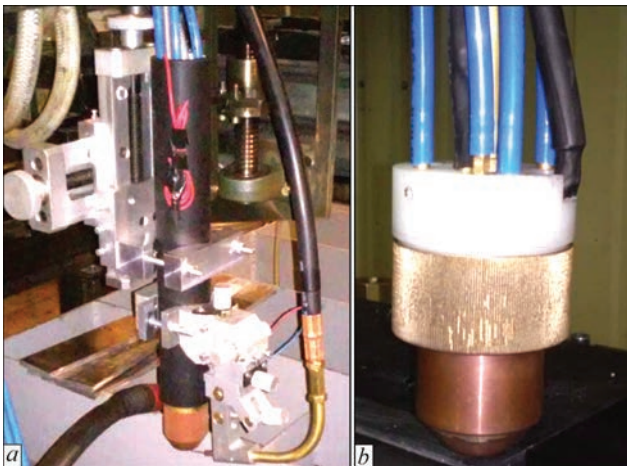
Figure 12. Plasmatrons developed by PWI for nonconsumable-electrode plasma-arc (*a*) and hybrid plasma-MIG welding (*b*)
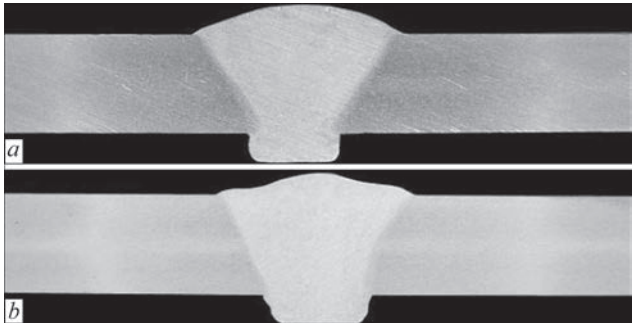
Figure 13. Transverse macrosections of welded joints of aluminium alloy 5083 8 mm thick made by consumable-electrode welding at 5 mm/s speed (*a*) and by hybrid plasma-MIG welding (*b*)

that allows a more accurate evaluation of electrical parameters influence on arcing. Special mechanisms provide the possibility of moving the table into different spatial positions to perform vertical and horizontal welds on vertical and inclined planes (Figure 11).

All-purpose equipment complexes for nonconsumable and consumable-electrode plasma-arc welding developed at PWI are fitted with control system based on PLC controller and respective software. This solution enables development of welding complexes based on serial power sources for consumable and nonconsumable-electrode arc welding. Application of a wide range of controllers, both with digital and with analog inputs-outputs enables application of welding equipment of different manufacturers fitted with connectors for data exchange by digital protocols or having only analog inputs-outputs.

All the all-purpose equipment complexes are fitted with plasmatrons for nonconsumable and consumable-electrode welding developed by PWI (Figure 12).

Application of hybrid plasma-MIG welding for joining aluminium alloy 5083, compared to regular consumable-electrode welding, enabled reducing welding consumables consumption for weld for-
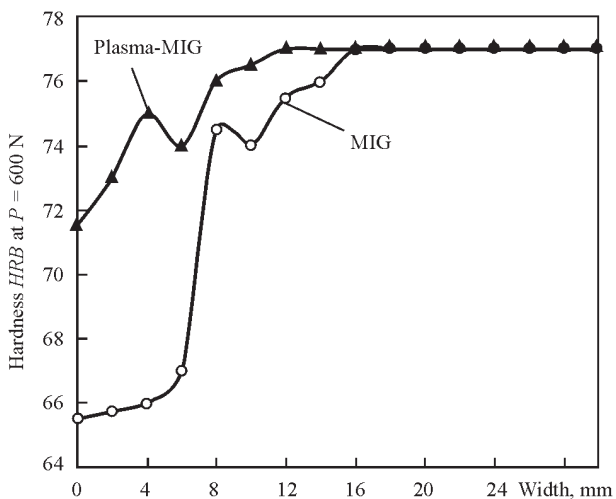
Figure 14. Transverse hardness distribution of MIG-welded joints of aluminium alloy 5083 8 mm thick at 5 mm/s speed and by hybrid plasma-MIG welding at 6.7 mm/s speed

mation, lowering electrode metal spatter, increasing welding speed, and reducing the width of the weld (Figure 13) and base metal softening zone (Figure 14).

More concentrated heating and increase of welding speed at application of hybrid plasma-MIG welding technology, compared to consumable-electrode welding, lead to an increase of both strength coefficient of the welded joint (from 0.90 to 0.95) and of weld metal (from 0.80 to 0.85) (Figure 15).

Conclusions

The most promising direction of development of plasma-arc welding of aluminium alloys is combined and hybrid application of two and more heat sources at welded joint formation. This allows increasing the welding speed, reducing electrode metal spatter, and lowering the level of welded structure distortion. One of the promising directions is hybrid plasma-MIG welding with ring cathode and axial feed of electrode wire.

There exist two main directions of development of equipment for hybrid plasma-MIG welding: development of specialized systems or of complex of equipment based on serial power sources for nonconsumable and consumable-electrode welding. For research laboratories, development of equipment complexes and not development of specialized systems is promising in the first place. Such an approach will allow a wider application of power sources capabilities, incorporated into their design, and flexible combination of different heat sources.

For plant conditions, it is possible to develop an equipment complex, proceeding from the anticipated product range, i.e. at maximum fast change of manufactured product range, provide power sources and software for the control system with broader technological capabilities.

Application of hybrid plasma-MIG welding, compared to regular consumable-electrode welding, allows increasing process efficiency, lowering electrode wire consumption, reducing the width of base metal softening zone, lowering spatter and improving the weld strength values.
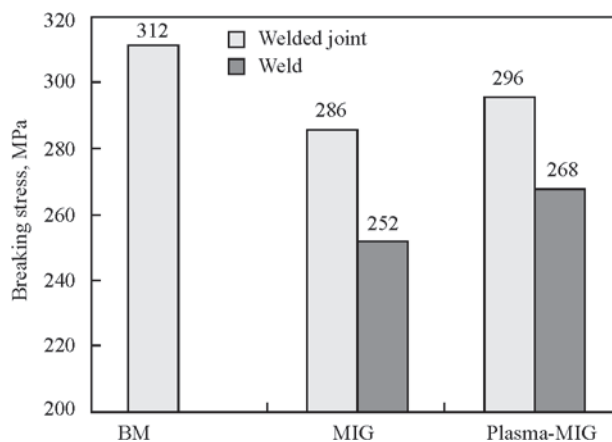
Figure 15. Strength of flat samples of base metal and welded joints of aluminium alloy 5083 8 mm thick produced by MIG welding at 5 mm/s speed and by hybrid plasma-MIG at 6.7 mm/s speed

1. Lieikens, A.C.H.J., Essers, W.G. *Method of and device for plasma arc welding*. Pat. 3,612,807 US. Int. Cl. B23k9/00. Publ. 1971.
2. Essers, W.G., Jelmorini, G. *Method of plasma-MIG welding*. Pat. 3,891,824 US. Int. Cl. B23k9/00. Publ. 1975.
3. Essers, W.G. *Method of and device for arc welding*. Pat. 4,039,800 US. Int. Cl. B23k9/00. Publ. 1977.
4. Essers, W.G. *Method of and device for plasma-MIG-welding*. Pat. 4,233,489 US. Int. Cl. B23k9/00. Publ. 1980.
5. Essers, W.G., Jelmorini, G., Tichelaar, G.W. *Method of and device for arc welding*. Pat. 4,174,477 US. Int. Cl. B23k9/00. Publ. 1979.
6. Essers, W.G. *Method of and device for arc welding*. Pat. 4,039,800 US. Int. Cl. B23k9/00. Publ. 1977.
7. Jelmorini, G. *Method and device for plasma-MIG welding*. Pat. 4,147,919 US. Int. Cl. B23k9/00. Publ. 1979.
8. Manz, A.F. *Method and torch for sustaining multiple coaxial arcs*. Pat. 4,048,465 US. Int. Cl. B23k9/00. Publ. 1977.
9. Brabader, W.A.J. *Welding torch*. Pat. 2004/0188406A1 US. Int. Cl. B23k9/173. Publ. 2004.
10. Lin Zhang, Timm Matus. *Plasma-MIG welding with plasma torch and with MIG torch*. Pat. 6,693,252 US. Int. Cl. B23k10/00. Publ. 2004.
11. Ignatchenko, G., Dykhno, I. *MIG-plasma welding*. Pat. 2005/0199593A1 US. Int. Cl. B23k9/12. Publ. 2005.
12. (2007) Hybrid welding: An alternative to SAW. *Welding J.*, **10**, 42–45.
13. Blechert, P. *Schweissbrenner zum Plasma-MIG-Schweissen*. Pat. 0168810A1 EP. Int. Cl. B23k28/00. Publ. 1985.
14. Kaika, V.I., Kutyr, A.S., Merkhin, V.M. et al. *Plasmotron for consumable-electrode welding*. USSR author's cert. 1557833A1. Int. Cl. B23k9/16. Publ. 1992.
15. Kaika, V.I., Ronsky, V.L., Kuzmenkov, L.G. et al. *Method of consumable-electrode plasma welding and plasmotron*. USSR author's cert. 1816250A3. Int. Cl. B23k10/00. Publ. 1993.
16. Merkle, W. *Plasma-MIG/MAG-Schweissbrenner*. Pat. 10327911A1 DE. Int. Cl. B23k10/02. Publ. 20.01.2005.
17. Matthes, K.-J., Kusch, M. (2000) Plasma-MIG-Schweissen. *Praktiker*, **5**, 182–188.
18. Shchitsyn, Yu.D., Tytkin, Yu.M. (1986) Plasma consumable-electrode welding of aluminium alloys. *Svarochn. Proizvodstvo*, **5**, 1–2.
19. Shchitsyn, Yu.D., Shchitsyn, V.Yu., Herold, H. (2003) Plasma welding of aluminium alloys. *Ibid.*, **5**, 36–42.
20. Makarenko, N.A., Nevidomsky, V.A. (2003) Thermal cycles in plasma-MIG surfacing. *The Paton Welding J.*, **1**, 43–45.
21. Bai Yan, Gao Hong-Ming, Qiu Ling (2010) Droplet transition for plasma-MIG welding on aluminium alloys. *Transact. of Nonferrous Met. Soc. China*, Vol. 20, 2234–2239.
22. da Cunha, T.V., Dutra, J.C. (2007) Processo plasma-MIG — contribuicao do arco plasma na capacidade de fusao do arame. *Soldagem Insp. Sao Paulo*, 12(**2**), 89–96.
23. Grinyuk, A.A., Korzhik, V.N., Shevchenko, V.E. et al. (2015) Main tendencies in development of plasma-arc welding of aluminium alloys. *The Paton Welding J.*, **11**, 31–41.

STRUCTURE AND SERVICE PROPERTIES OF HYBRID LASER-ARC WELDED JOINTS OF 14KhGN2MDAFB STEEL

L.I. MARKASHOVA, V.D. POZNYAKOV, E.N. BERDNIKOVA, S.L. ZHDANOV, V.D. SHELYAGIN and **T.A. ALEKSEENKO**
E.O. Paton Electric Welding Institute, NASU
11 Kazimir Malevich Str., 03680, Kiev, Ukraine. E-mail: office@paton.kiev.ua

The paper represents the results of experimental investigations of peculiarities in formation of structure and phase composition of welded joints from high-strength 14KhGN2MDABF steel at different speeds (v_w = 72, 90 and 110 m/h) of hybrid laser-arc welding. Information received at different structural levels (from grain to dislocation) is used for analytical evaluation of effect of the structural parameters on mechanical properties and fracture toughness of the welded joints depending on modes of laser-arc welding. The investigations of effect of the structural factors on mode of crack formation under conditions of different dynamic strength tests at external bend loading as well as cyclic loading were carried out for evaluation of a complex of welded joint service characteristics. A role of the structural factors in change of level of local internal stresses, i.e. sources of nucleation and propagation of cracks in the welded joint metal, is shown. The optimum technological modes of hybrid laser-arc welding are determined. They provide for the high indices of mechanical properties and crack resistance of metal under service conditions of external loading from point of view of structure and phase composition. 17 Ref., 2 Tables, 10 Figures.

As a rule, high-strength steels with yield limit more than 700 MPa are currently applied for critical machines and mechanisms having difficult for operation conditions. They in combination with the most optimum technological parameters of welding of such materials should provide for a necessary complex of service characteristics of the welded joints, first of all, their strength, ductility and crack resistance [1, 2]. The range of welding speeds in use of the classical technologies of mechanized metal arc welding for such steels makes v_w = 18–50 m/h at $w_{6/5} \approx$ 10–38 °C/s rate of cooling.

However, today advanced laser technologies find more and more application. Among them is a hybrid laser-arc (HLA) welding [3–5] which allows producing quality welded joints using higher welding speeds up to 110 m/h and $w_{6/5} \approx$ 30–100 °C/s. It significantly increases efficiency of the process (several times in comparison with arc welding) as well as provides for 8–15 % rise of strength indices and 1.5–2 times ductility of the welded joints. At that, a significant change of welding zone geometry shall be noted, i.e. 3–5 times reduction of width of weld and HAZ. Taking into account a significant change of process modes and, respectively, the welding zone geometry, noticeable changes are to be expected in the structures formed in the new type welded joints, which, as is well known, in many respects determine their properties [6–9].

In order to optimize the welding parameters, the most of process experiments in hybrid welding are dedicated to investigation of interaction between arc and laser, arc stabilizing and its spatial attachment by laser radiation, effect of shielding gas, arc voltage, welding speed and current on penetration depth [9–13]. Currently, the main task of technologists and researchers [14–17] is investigation of the peculiarities of laser and hybrid processes, their effect on weld formation, possible advantages and elimination of disadvantages of laser and arc constituents as well as effect of process parameters on structure formation in the welding zone.

The aim of present work is a detailed investigation of the peculiarities of phase and structural changes at all structural levels (from grain to dislocation) in the metal of joints produced using HL Awelding depending on parameters of technological process. Besides, a relevant task is the evaluation of role of specific structure-phase constituents, forming at different welding modes in optimizing the mechanical characteristics of welded joints, which are valuable for service conditions, namely indices of strength ductility and crack resistance.

Materials and investigation procedures. The work was carried out on samples of high-strength steel 14KhGN2MDAFB (%: 0.183C; 1.19Cr; 0.98Mn; 2.07Ni; 0.22Mo; 0.08V; 0.33Si; not more than 0.018P and 0.005S) of up to 10 mm thickness using welding wire Sv-10KhN2GSMFTYu (%: ≤0.1C; 0.7Cr; 0.4Mn; 0.22Mo; 0.15V; 0.24Si; not more than 0.007S) at the three following modes of HLA welding:

- 1st — v_w = 72 m/h, $I \sim$ 125 A, $U_a \sim$ 23 V;
- 2nd — v_w = 90 m/h, $I \sim$ 150 A, $U_a \sim$ 25 V;
- 3rd — v_w = 110 m/h, $I \sim$ 200 A, $U_a \sim$ 26 V.

Indicated modes provide for HAZ metal cooling in the temperature interval 600–500 °C at $w_{6/5}$ = = 58–62 °C/s rate. Nd:YAG laser DY 044 (Rofin Synar, Germany) to 4.4 kW power was used as laser radiation source and mixture Ar + CO_2 with 15–20 l/min consumption — as a shielding gas.

The structure-phase characteristics, i.e. size of grain and subgrain structure, distribution of phase precipitates, peculiarities of zones of brittle and ductile fracture, distribution of dislocation density in the weld metal and different areas of welded joint HAZ, were examined at all structural levels using complex of experimental methods of current physical materials science, including optical metallography (microscopes «Versamet-2» and «Neophot-32»), PHILIPS analytical scanning SEM-515 and JEOL transmission electron microscope JEM-200CX. Hardness of the examined metal was measured at LECO hardness gage M-400 at 0.1 kg loading.

The complex investigations provided for the evaluation of differential contribution of the separate structure-phase constituents and structural parameters in change of the integral values of strength $\sum \sigma_y$ and ductile fracture K_{1c} as well as local internal stresses $\tau_{l.in}$ (zones of nucleation and propagation of cracks) in different areas of the welded joints at applied modes of hybrid welding.

The results of mechanical tests (Table 1) determine that the highest indices of yield limit $\sigma_{0.2}$ and tensile strength σ_t are typical for welds made at v_w = 90 m/h.

However, in this case, the ductility index ψ is significantly reduced (1.6 times) in comparison with that at v_w = 72 and 110 m/h. The impact bending tests at temperature from +20 to –40 °C showed some increase of impact toughness in the weld metal of up to KCV_{+20} = 75.7 (at v_w = 72 m/h) and KCV_{-40} = 52.1 J/cm^2 (at v_w= 90 m/h). However, in the last case, KCV_{-40} is significantly reduced (1.4 times) (in comparison with v_w = 72 and 110 m/h) for HAZ metal.

Experiment results. The investigations were carried out for studying the changes of different phase constituents (upper and lower bainite B_U and B_L, martensite M, their volume fraction v, microhardness HV, as well as different structural parameters (dimension of grain, sub-grain structure — D_g, d_s), nature of dislocation density and distribution, and peculiarities of the fracture zone of welded joints (ductile, brittle etc.) depending on v_w = 72, 90 and 110 m/h. The experiments were performed for all the most significant zones of the welded joints, i.e. weld metal and HAZ.

Thus, the following is typical for the different zones of welded joint with a structure of base metal, consisting of bainite ferrite (B–F) grains with D_g = 15–25 μm and microhardness HV 2700–2850 MPa at v_w = 72 m/h. The structure of weld metal (Sv-10KhN2GSMFTYu) and HAZ (Figure 1, *a*) is B–M with prevailing ($V \sim$ 60–80 %) formation of structures of B_L with D_g = (30–120)×(170–350) μm in the weld metal at HV = 3660–4010 MPa (Figures 2, *a* and 3, *a*). Microhardness in an overheating area (HAZ I) at transfer from HAZ makes $HV \sim$ 3830–3900 MPa, and grain size for this zone reduces to $D_g \sim$ 30–60 μm (Figure 2, *d* and 3, *a*). In area of HAZ recrystallization the structure becomes more refined (2–4 times) at decrease of microhardness to HV = 3510–3660 MPa.

Table 1. Mechanical properties of HLA-welded joints of 14KhGN2MDAFB steel investigated

v_w, m/h	$\sigma_{0.2}$	σ_t	δ_5	ψ	KCV, J/cm^2, at T, ºC		
					Weld		HAZ
	MPa		%		+20	–40	–40
72	851.8	1068.3	12.7	59.6	61.4	35.7	93.5
	_963.6_	_1189.8_	_9.3_	_63.7_	_90.0_	_40.9_	79.9
	907.7	1129.0	11.0	61.6	75.7	38.3	_80.9_
							84.7
90	1138.1	1326.6	10.0	40.8	64.5	59.1	50.4
	_1156.3_	_1319.7_		_35.6_	_58.6_	_45.2_	61.7
	1147.2	1323.1		38.2	61.5	52.1	_65.7_
							59.2
110	991.5	1078.1	9.7	59.6	58.7	41.9	90.1
	_982.1_	_1088.9_	_14.0_		_81.2_	_29.7_	66.5
	986.8	1083.5	11.8		70.0	35.8	_96.7_
							84.4
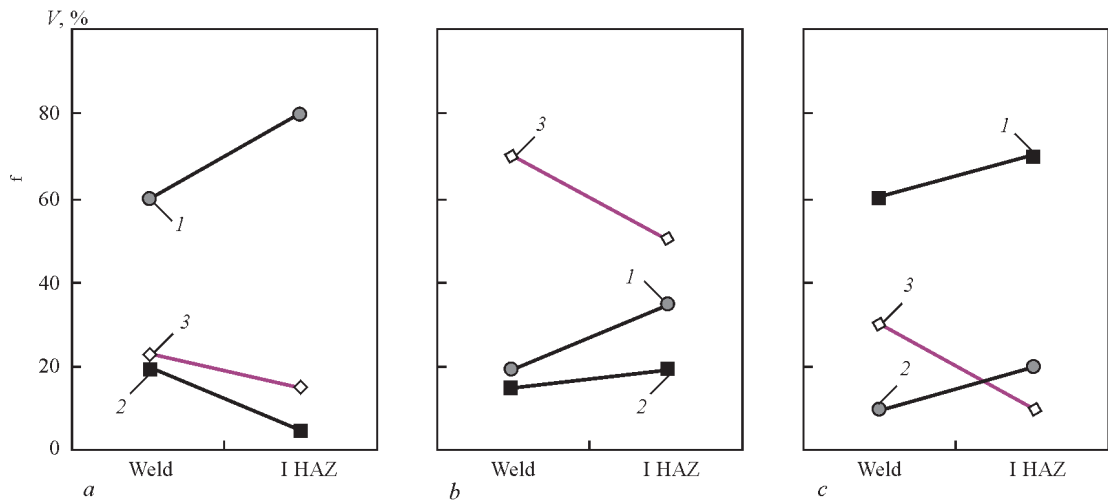
Figure 1. Change of volume fraction of structural constituents in weld metal and zone I of HAZ of HLA-welded joints at $v_w = 72$ (*a*), 90 (*b*), 110 (*c*) m/h: *1* — B_L; *2* — B_U; *3* — M

Formation of ferrite-bainite structure at $HV = 3360$–3510 MPa and $D_g = 5$–15 μm is typical at transfer to the base metal in area of incomplete recrystallization.

Thus, mainly B_L structure is formed at $v_w = 72$ m/h in the weld metal and HAZ, and at transfer from weld to HAZ the grain structure is 2–4 times refined at 12 % uniform reduction of microhardness.

Formation of mainly ($V \sim 50$–70 %) (Figure 1, *b*) martensite structure (tempered martensite) with $D_g \sim$ $\sim (30$–80)×(150–300) μm at $HV = 4050$–4422 MPa (Figures 2, *b* and 3, *b*) is typical for the weld metal at $v_w = 90$ m/h. The size of grain is somewhat reduced (to $D_g \sim 25$–50 μm) at transfer to the overheating area in HAZ with insignificant reduction of microhardness to $HV = 3830$–4050 MPa (Figures 2, *e* and 3, *b*). The HAZ structure is much more refined (2 times to $D_g = 10$–20 μm) with reduction of microhardness to

$HV \sim 3660$–3830 MPa as transfer to the base metal in area of recrystallization. Formation of F–B structure ($D_g = 10$–20 μm) at $HV = 3220$–3700 MPa is typical for the following area of incomplete recrystallization.

Increase of welding speed from 72 to 90 m/h results in a change of the phase composition of weld metal and HAZ from B–M to M type as well as relationship of the structural constituents in HAZ metal, i.e. 2–3 times reduction of B_L volume faction at increase (3 times) of M_{temp} fraction, that as a consequence provides for the maximum indices of strength, however, give rise to significant 1.6 times reduction (see Table 1) of ductility in the weld.

At the maximum $v_w = 110$ m/h the phase composition of weld metal and HAZ is represented by B–M structure with prevailing ($V \sim 60$–70 %) (Figure 1, *c*) formation of the B_U structures with $D_g = (20$–
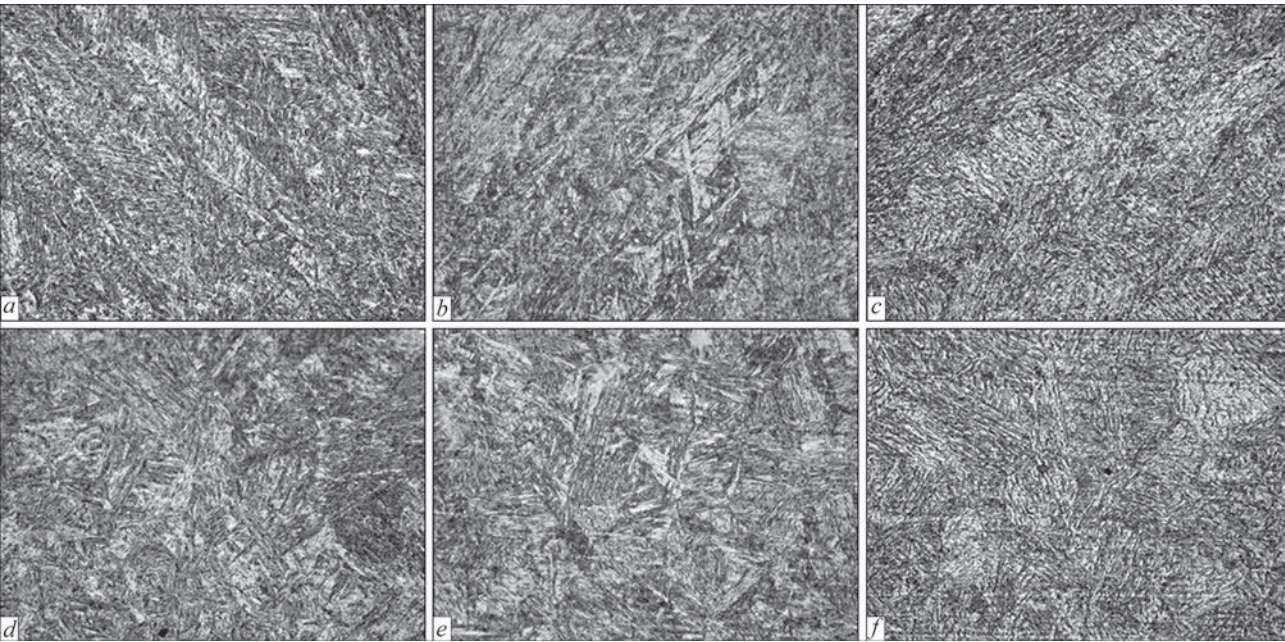
Figure 2. Microstructure (×500) of weld metal (*a–c*) and HAZ overheating area (*d–f*) at $v_w = 72$ (*a, d*), 90 (*b, e*) and 110 (*c, f*) m/h
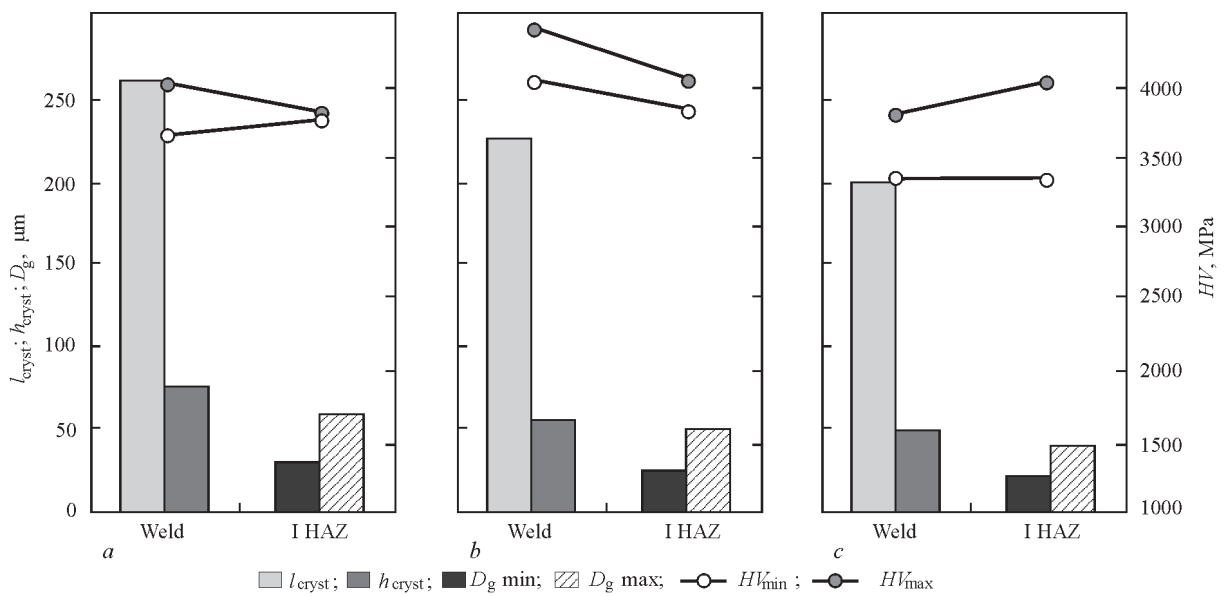
Figure 3. Change of average size of crystallites h_{cryst} and l_{cryst}, grain size D_g, microhardness HV in weld metal and HAZ at $v_w = 72$ (*a*), 90 (*b*) and 110 (*c*) m/h

80)×(150–250) μm and microhardness $HV \sim 3360$–4010 MPa (Figures 2, *c* and 3, *c*). However, the grain size is 2 times reduced to $D_g = 20$–40 μm (Figures 2, *f* and 3, *c*) at transfer to HAZ in the area of overheating, and the metal of incomplete recrystallization area is characterized by formation of F–B structure with $HV = 3360$–3510 MPa and $D_g = 5$–20 μm.

Thus, increase of welding speed to 110 m/h (regardless the fact that the phase composition of weld metal and HAZ overheating area are similar as at $v_w = 72$ m/h, i.e. B–M) promotes for significant reduction of volume fraction of B_L to 10–20 % and prevailing formation of B_U structure ($v = 60$–70 %). Such structural changes can result in non-uniform level of

Table 2. Change of volume fraction of fracture mode, size of facets of brittle intragranular chip, pits of ductile fracture for fracture zones in welded joint metal at different speeds of HLA welding

Fracture mode	T_{test}, °C	+20		−40		−40	
	Zone	I Weld	II Weld	I Weld	II Weld	I HAZ	II HAZ
		$v_w \sim 72$ m/h					
Brittle intragranular	V, %	–	–	50–60	80–90	–	5
	d_{fac}, μm	–	–	10–50	7–50	–	7–10
Ductile	V, %	100	100	40–50	10–20	100	95
	d_{pit}, μm	1–3	1–5	1–3	1–3	1–5	1–10
		$v_w \sim 90$ m/h					
Brittle intragranular	V, %	1–2	–	40–50	70–80	–	20
	d_{fac}, μm	5–7	–	20–50	10–50	–	7–14
Ductile	V, %	98	100	50–60	20–30	100	80
	d_{pit}, μm	1–3	1–3	1–3	1–3	1–6	1–50
		$v_w \sim 110$ m/h					
Brittle intragranular	V, %	20–30	10	70–80	95	–	35
	d_{fac}, μm	15–50	30–50	20–60	20–60	–	10–20
Ductile	V, %	70–80	90	30–40	0–5	100	65
	d_{pit}, μm	1–4	1–4	1–3	1–3	1–10	1–7
Note. Zone I — zone of fracture nucleus near the notch; II — zone of main crack propagation.							
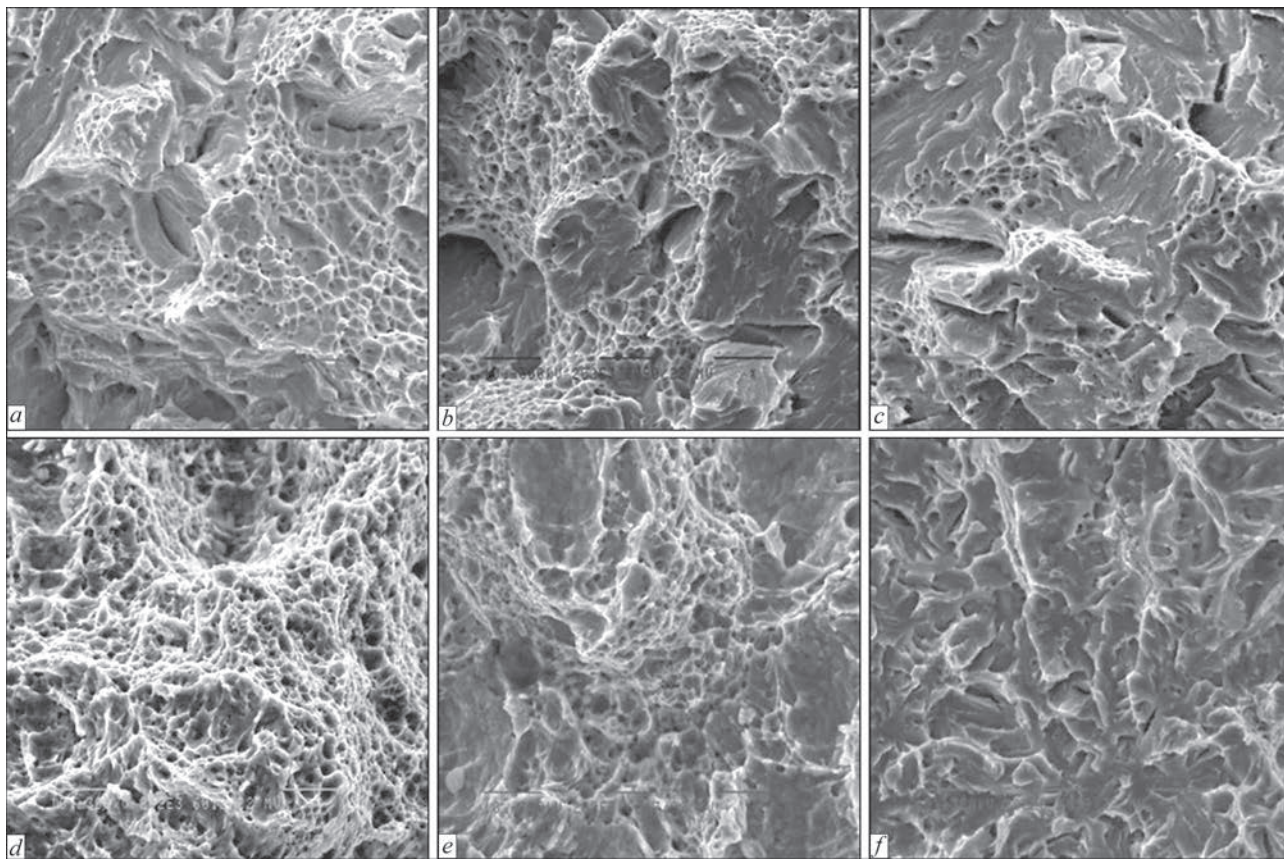
Figure 4. Microstructure (×2020) of fracture surface of weld metal (*a*–*c*) and HAZ (*d*–*f*) of HLA-welded joints in zone of main crack at T_{test} = –40 °C: *a, d* — v_w = 72; *b, e* — 90; *c, f* — 110 m/h

the mechanical properties along the welding zone and reduction of welded joint crack resistance.

Dynamic loading. The investigations of structural changes and their effect on dynamic strength of the welded joint metal depending on welding speed showed the following (Table 2; Figure 4). The results of fractographic SEM examinations of the fractures allowed making a comparison of facture mode of welded joint depending on test temperature in different fracture zones. Thus, ductile fracture type is mainly typical for weld metal at all speeds of welding and T_{test} = +20 °C. However, amount (up to ~ 2 %) of areas of brittle intracrystalline chip in zone I is somewhat increases at v_w = 90 m/h. In the case of v_w = 110 m/h the portion of brittle fracture increases to ~ 30 %.

The joint metal at v_w = 72 and 90 m/h and T_{test} = –40 °C is characterized by a mixed type of fracture, i.e. brittle in combination with ductile pit relief in zone I to ~ 40–55 %; in zone II to 70–80 % of brittle chip (Figure 4, *a*, *b*). Increase (1.3 times) of volume fraction of brittle fracture to ~75–95 % (Figure 4, *c*), coarsening of chip facets and increase of forming cracks extension are observed at v_w = 110 m/h.

Ductile mode fracture with pit size of 1–10 μm (see Table 2) is observed in the nucleus zone I of HAZ at T_{test} = –40 °C for all speeds of welding. In the zone of main crack propagation II at v_w = 72 m/h the frac-

ture has mainly ductile mode (Figure 4, *d*) with single areas (V ~ 5 %) of quasi-brittle constituent. v_w = 90 m/h promotes for the increase of volume fraction of quasi-brittle chip to V ~ 20 % (Figure 4, *e*) and that at v_w = 110 m/h makes V ~ 35 % (Figure 4, *f*). At that, the facets' size is also enlarged in 1.3 times.

Thus, the structure forming at v_w = 72 m/h is the optimum metal structure of welds and HAZ in the dynamic strength tests from point of view of fracture mode at different test temperatures.

Cyclic loading. The HLA-welded joints, made at v_w = 72 m/h, were used for investigation of effect of external loading. They were subjected to cyclic bend loading at cycle stress σ_{-1} = 60 MPa up to development in it of 2 mm length fatigue crack from notch apex at N = 800,000 cycles of loading.

Figure 5, *a* shows the general view of the fracture surface of sample being examined. The following zones can be outlined on fracture macrostructure, i.e. I — zone of slow propagation of crack in the direction from external (side) surface of the fracture; and II — zone of accelerated (main) crack propagation.

Zone I has smoothed surface that indicate the first stage, i.e. fracture nucleation (slow crack propagation). The dimensions of zone I were around 180–230 μm. This stage is characterized by crack nucleation and their propagation over slip planes. Pres-
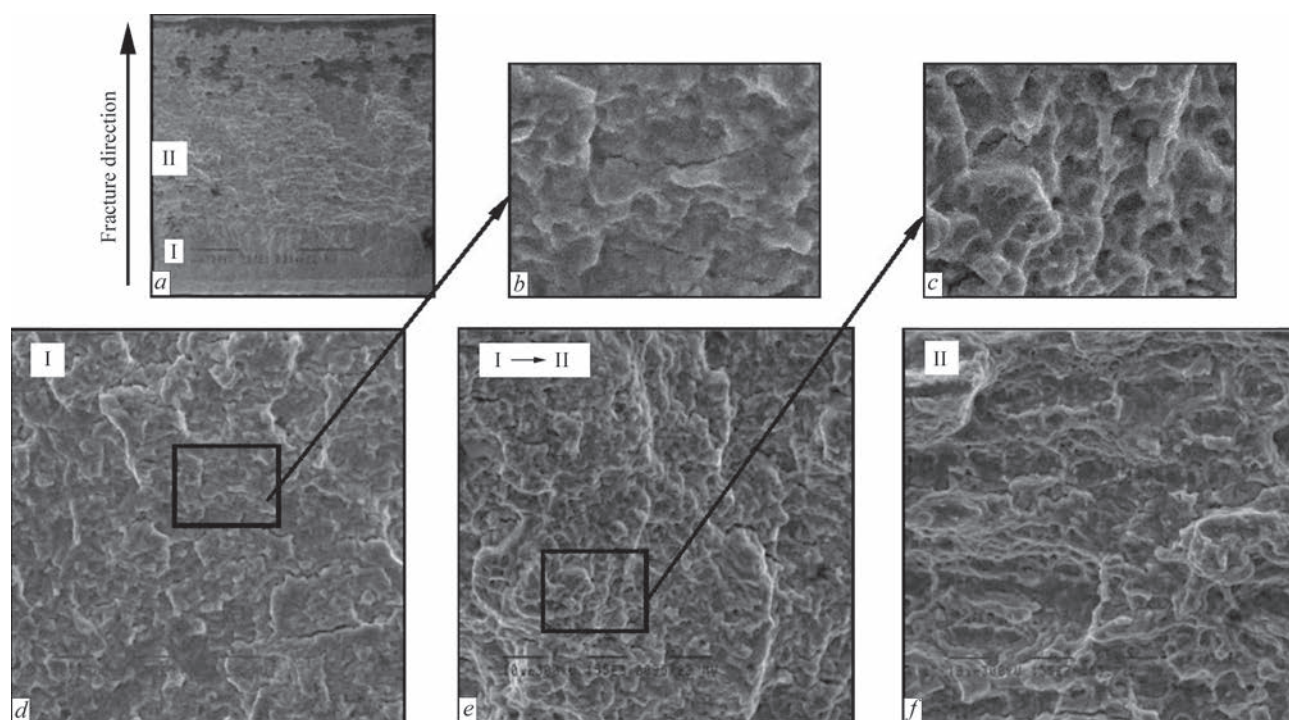
Figure 5. Fracture surface of HLA-welded joint (v_w = 72 m/h) after cyclic bend loading (σ_{-1} = 60 MPa, N = 800,000 cycles): *a* — zone of fracture nucleus; *b* — area of transfer of fracture nucleus to main crack; *c* — main fracture (×1550); *d*, *e* — corresponding fragments of fracture surface (×4 magnification)

ence of zone I indicates some duration of the stage of fracture nucleation and, respectively, duration of the process of fatigue crack propagation at nucleation stage, i.e. the welded joint under given conditions of external loading has a crack propagation resistance. The mode of fracture in zone I is quasi-brittle with the local areas of ductile fracture (Figure 5, *b*, *d*). A transfer to the main fracture zone from zone I to zone II is characterized by a shift of fracture mode, namely to ductile pit type (Figure 5, *c*, *e*, *f*).

Thus, the structural changes from point of view of mode of HLA-welded joint fracture under conditions of external cyclic bend loading (σ_{-1} = 60 MPa), apparently, should provide for the best properties of strength and crack resistance of metal under service conditions in the case of v_w = 72 m/h.

Examination of fine structure. The detailed TEM examinations were also carried out. They provide for the possibility to study the peculiarities of fine structure of welded metal and its parameters, i.e. change of density and mode of dislocation distribution in different structural constituents (in internal volumes and along the structural boundaries), nature of forming substructure, effective distance between carbide phases and their size. In this connection the following is determined for the welded joints produced at v_w = 72 m/h (optimum structure) and v_w = 110 m/h (gradient structure).

Formation of the internal substructure with uniform distribution of volume density of dislocations to $\rho \sim (4-6) \cdot 10^{10}$ cm^{-2} (Figure 6, *a*) is observed in the weld metal at v_w = 72 m/h in B_L grains, and dislocation density makes $\rho \sim 8 \cdot (10^{10}-10^{11})$ cm^{-2} in M_{temp} structures. B_L grain fragmentation is typical for HAZ metal, i.e. 10–20 % refinement of lath B_L structure is observed that is accompanied by certain increase of dislocation density (Figure 6, *b*).

The following is typical for the fine structure of welded joint in the case of v_w = 110 m/h, i.e. integral value of dislocation density in weld metal and HAZ rises, mainly B_U structure is formed at the maximum increase of dislocation density to $\rho \sim 1.5 \cdot 10^{11}$ cm^{-2} (Figure 6, *c*, *d*).

Thus, it is shown that the most uniform distribution of dislocation density at formation of B_L structure is provided in HLA welding with v_w = 72 m/h.

Analytical estimations of mechanical and strength properties. The experimental data allowed carrying out an analytical estimation of differential contribution of all structures and their parameters, namely size of grain D_g, subgrains d_s, dislocation density ρ, inter-carbide distances, volume fraction of structures forming along the welding zone in weld metal and in overheating areas, in change of the integral value of yield limit $\sum \sigma_y$ of the welded joints depending on welding mode [3–5]. At that, the integral $\sum \sigma_y$ value (according to equation including known dependencies of Hall–Petch, Orowan et al. [6–8]) is the sum value consisting of series of constituents:
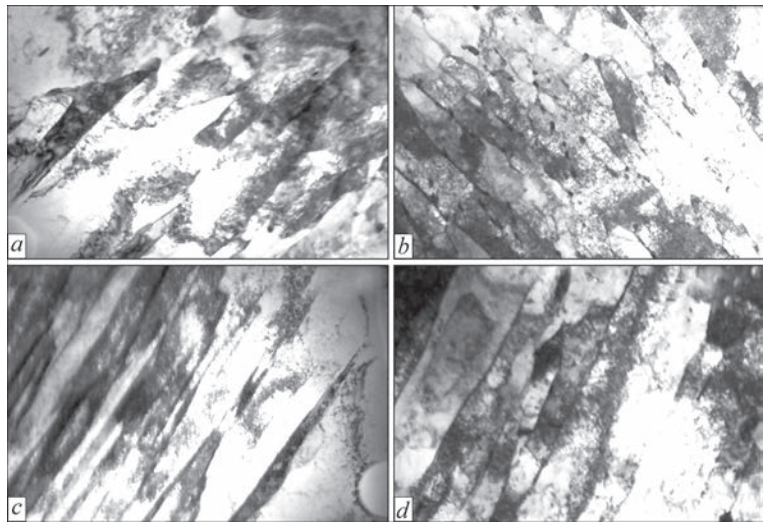
Figure 6. Fine structure of weld metal (*a, c*) and HAZ (*b, d*): *a, b* — B_L at $v_w = 72$ m/h (*a* — ×30000; *b* — ×20000); *c, d* — B_U at $v_w = 110$ m/h (*c, d* — ×30000)

$$\Sigma\sigma_y = \Delta\sigma_0 + \Delta\sigma_{s.s.} + \Delta\sigma_g + \Delta\sigma_s + \Delta\sigma_d + \Delta\sigma_{d.h},$$

where $\Delta\sigma_0$ is the resistance of type of metal lattice to free dislocation movement (lattice friction stress or Peierls–Nabarro stress); $\Delta\sigma_{s.s}$ are the hardening of solid solution by alloying elements (according to the Mott–Nabarro theory); $\Delta\sigma_g$ and $\Delta\sigma_s$ is the hardening due to change of size of grains and subgrains (in accordance with Hall–Petch dependence); $\Delta\sigma_d$ is the dislocation hardening caused by inter-dislocation interaction (based on the Taylor–Seger–Mott–Hirsch theory); $\Delta\sigma_{d.h}$ is the dislocation hardening (due to disperse phases by Orowan) [10–14].

The following is determined as a result of estimations of the changes in welded joint zones of such a strength characteristic as σ_y. The calculation value of yield limit in the weld metal and HAZ at $v_w = 72$ m/h makes $\Sigma\sigma_y \sim 917$ and 1077 MPa, respectively, and the maximum contribution in the yield limit is introduced by substructure ($\Delta\sigma_s \sim 318$–356 MPa), dispersion ($\Delta\sigma_d \sim 253$–295 MPa) and dislocation hardening ($\Delta\sigma_{d.h} \sim 157$–180 MPa) (Figure 7, *a*). At that, the

contribution of such a type of structural constituent as B_L is the maximum one (Figure 7, *b*).

In the case of $v_w = 110$ m/h the total value of yield limit rises (in comparison with $v_w = 72$ m/h) per 10–15 % (Figure 8), that is caused by certain grain structure refining (see Figure 3, *c*) and 1.3 times increase of the integral value of dislocation density.

Fracture toughness. The calculation values of fracture toughness index, estimated on dependence $K_{1c} = (2E\sigma_{0.2}\delta_{cr})^{1/2}$ [15] (where E is the Young's modulus; $\sigma_{0.2}$ is the calculation value of strengthening; δ_{cr} is the value of crack critical opening) according to the data of substructure parameters as well as substitution of K_{1c} and σ_y showed the following (Figures 8 and 9).

In as-welded state at $v_w = 72$ m/h $K_{1c} \sim 14$–37 MPa·m$^{-1/2}$ (Figure 9, *a, c*). It is kept on the level of $K_{1c} \sim 20$–33 MPa·m$^{1/2}$ (Figure 9, *b, c*) as a result of application of external cyclic bend loading ($\sigma_{-1} = 60$ MPa, $N = 800000$). This indicates the same crack resistance even under cyclic loading of this welded joint due to formation of B–M structure (mainly B_L).
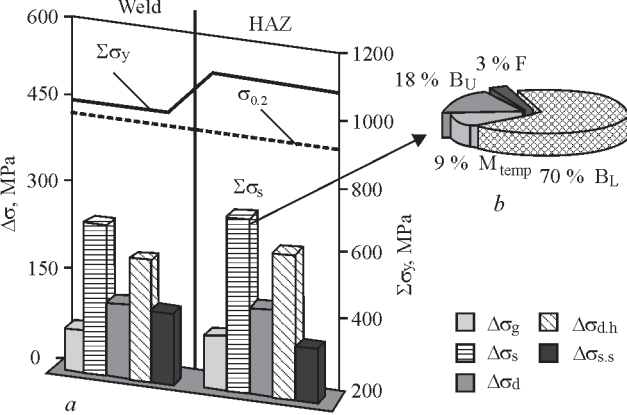
Figure 7. Contribution of different constituents of structural hardening $\Delta\sigma$ in calculation value of yield limit $\Sigma\sigma_y$ of weld metal (*a*), and contribution of structural constituents in change of substructural hardening $\Delta\sigma_s$ at $v_w = 72$ m/h (*b*)
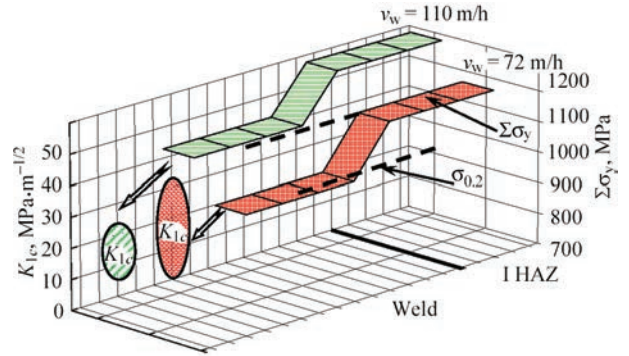
Figure 8. Change of average calculation value of yield limit $\Sigma\sigma_y$ and fracture toughness K_{1c} for zones of weld and I HAZ HLA welding at $v_w = 72$ and 110 m/h
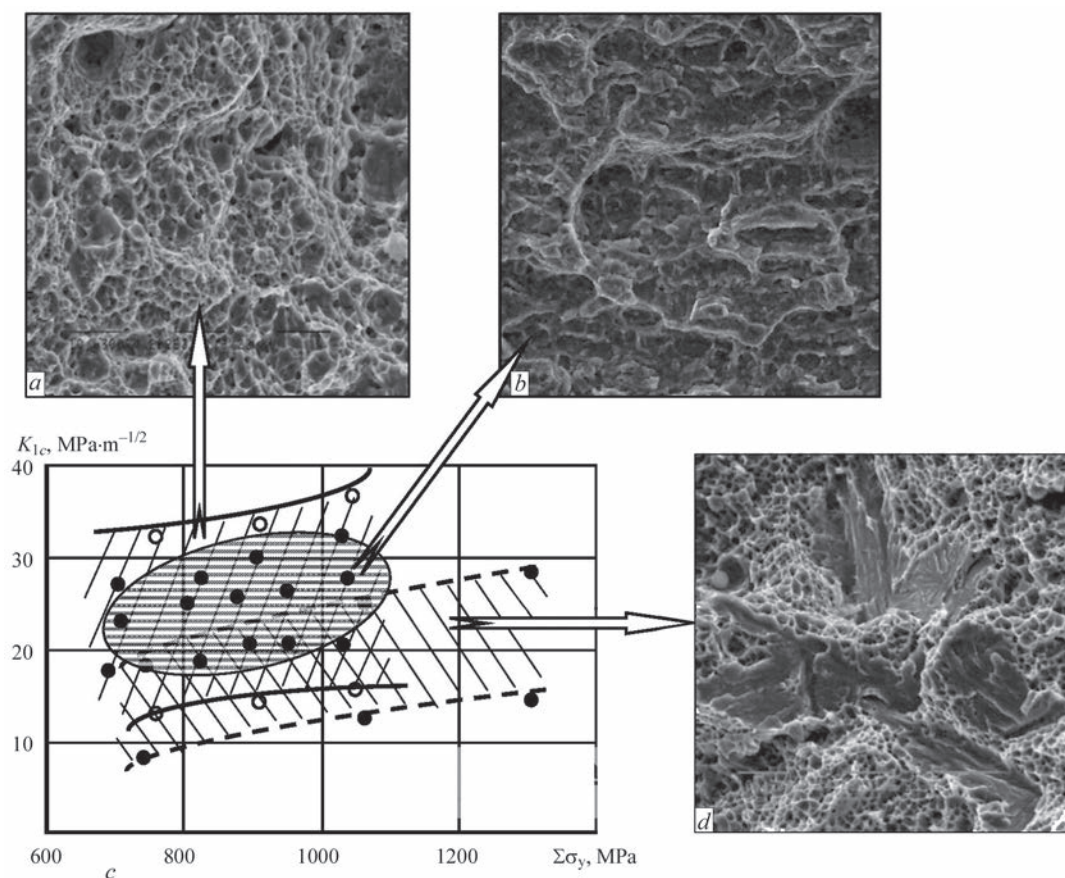
Figure 9. Change of calculation values of strength $\sum\sigma_y$ and fracture toughness K_{1c} of weld metal (*c*), patterns of 100 % ductile fracture after welding at v_w = 72 m/h (*a*) and cyclic loading (*b*) and 20–30 % brittle intragranular chip at v_w = 110 m/h (*d*) (×2020)

At that, the substructure, and mainly B_L, make the largest contribution in metal hardening and increase of fracture toughness (Figure 9). K_{1c} index (Figure 9, *c*) in the case of v_w = 110 m/h is significantly (30 %) reduced that results in a brittle intragranular fracture (Figure 9, *d*). The latter is mainly caused by a formation of other type structure, namely B_U, with corresponding non-uniform distribution of dislocation density.

Crack resistance (local internal stresses). Carried examinations of fine structure also allowed performing the estimation of change of local internal stresses $\tau_{l.in}$, i.e. zones of crack nucleation and propagation. The estimations were carried out using known dependence $\tau_{in} = Gbh\rho/[\pi(1 - \nu)]$ (where G is the shear modulus; b is the Burgers vector; h is the foil thickness; ν is the Poisson's ratio; ρ is the dislocation density) [10, 16, 17].

It was determined that the maximum values of $\tau_{l.in} \sim 1900$–2800 MPa (that makes $(0.2$–$0.35)\tau_{theor}$), are formed at v_w = 110 m/h in the places of elongated dislocation accumulations ($\rho = 1.5\cdot10^{11}$ cm^{-2}) along the B_U boundaries. This results in nucleation of microcracks in these zones and reduction of crack resistance of the welded joints (Figure 10, *a*,

b). The lowest values $\tau_{l.in} \sim 1500$–1900 MPa are typical for the welded joints produced at v_w = 72 m/h, which is promoted by formation of fine-grain and fragmented B_L structures in the welding zone in combination with uniform distribution of the dislocations (Figure 10, *c*, *d*).

As a consequence it is determined that the optimum strength, ductility and crack resistance of the HLA-welded joints of high-strength steel are provided at v_w = 72 m/h, that is caused by formation of the most disperse structures — B_L, fine-grain M_{temp} in the absence of elongated dislocation accumulations (concentrators of $\tau_{l.in}$).

Conclusions

1. The complex investigations at all structural levels were used for studying the structure-phase state of the main zones of welded joints of high-strength steel 14KhGN2MDAFB produced at different modes of hybrid laser-arc welding. It is shown that increase of welding speed from 72 to 110 m/h provokes for changing in relationship of phase constituents (lower bainite, upper bainite and martensite) forming in the welding zones, i.e. B_L volume fraction is reduced to 10–20 %, at prevailing B_U volume fraction (60–70 %)
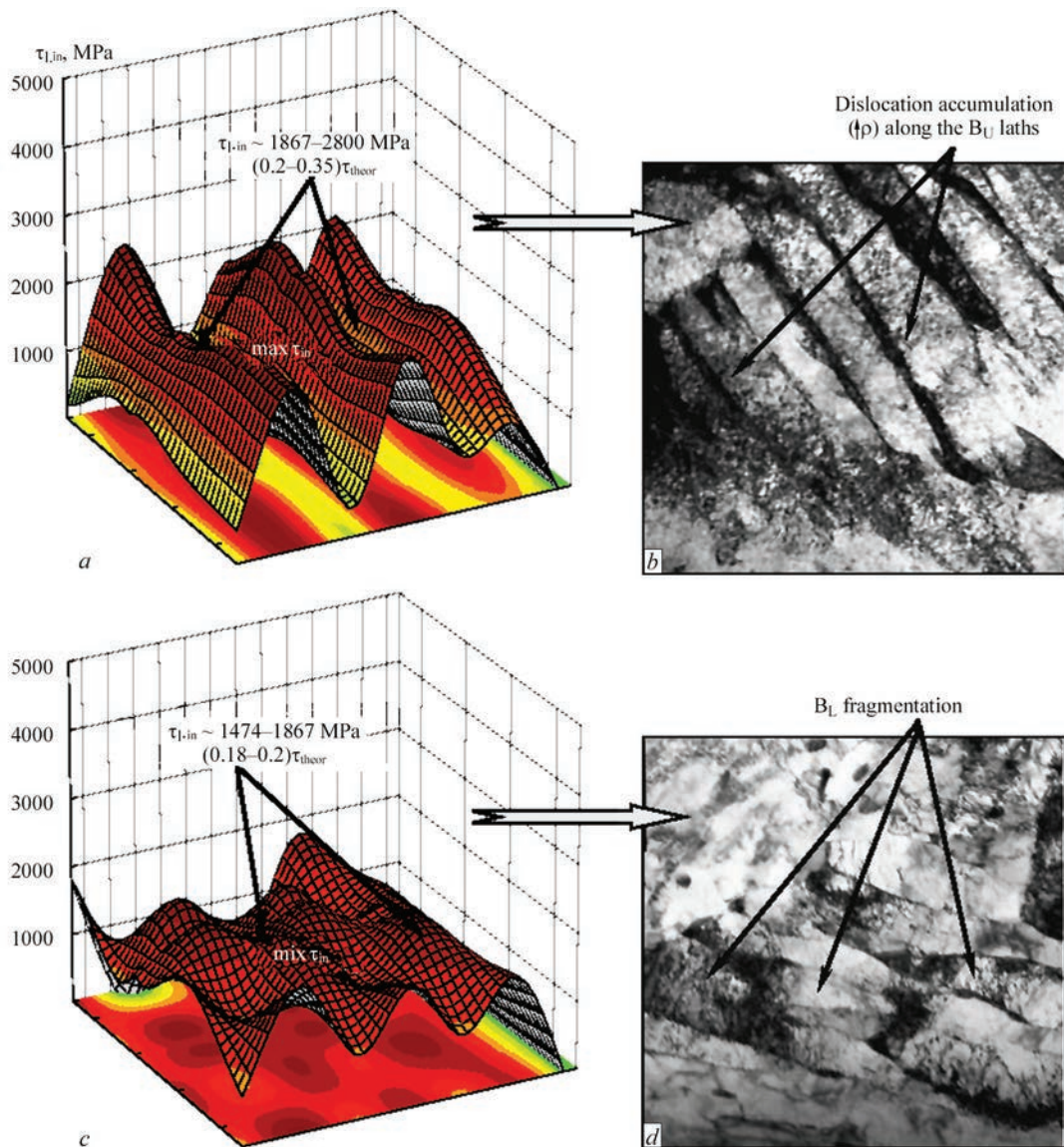
Figure 10. Distribution of local internal stresses $\tau_{l.in}$ in weld metal of structural zones of B_U at $\nu_w = 110$ m/h (a, b — ×20000) and B_L at $\nu_w = 72$ m/h (c, d — ×30000)

and M (10–30 %). Presence of the gradients of structural constituents dimensions, microhardness as well as dislocation density is typical at $\nu_w = 110$ m/h.

2. Combination of examination at different structural levels with analytical estimations of the mechanical properties of welded joints along the welding zone allowed showing that the constituents of lower bainite and formation of substructure at $\nu_w = 72$ m/h make the largest contribution in metal hardening $\sum\sigma_y$ and increase of fracture toughness K_{1c}. At that, increase of the crack resistance of welded joint under conditions of external dynamic (T_{test} from +20 to –40 °C) and cyclic loading ($\sigma_{-1} = 60$ MPa, $N = 800,000$ cycles) is provided. Rise of welding speed to $\nu_w = 110$ m/h causes 30 % reduction of K_{1c} index at some increase of metal hardness (10–15 %) due to preferable formation of upper bainite structures.

3. The estimations of level of local internal stresses taking into account distribution of dislocation densities in the elongated structural zones of their concentration showed that the maximum $\tau_{l.in} \sim$ ~ 1900–2800 MPa, corresponding to $(0.2$–$0.35)\tau_{theor}$, are formed at $\nu_w = 110$ m/h along the boundaries of upper bainite lath that results in brittle fracture and reduction of crack resistance of the welded joints.

4. The maximum strength, ductility and crack resistance are provided by formation of the structures of B_L and M_{temp} (fine-grain), and uniform distribution of dislocations in absence of the extended dislocation accumulations, i.e. concentrators of local internal stresses.

1. (1965) *High-strength steel*: Coll. Ed.by L.K. Gordienko. Moscow: Metallurgiya.
2. Houdremont, E. (1959) *Special steels*. Moscow: Metallurgizdat.

3. Paul, K., Ridel, F. (2009) Hybrid laser welding — joining the efforts. *Fotonika*, **1**, 2–5.

4. Kah, P., Salminen, A., Martikainen, J. (2010) Laser-arc hybrid welding processes (Review). *The Paton Welding J.*, **6**, 32–40.

5. Shelyagin, V.D., Khaskin, V.Yu. (2002) Tendencies in development of laser-arc welding (Review). *Ibid.*, **6**, 25–28.

6. Shorshorov, M.Kh., Belov, V.V. (1972) *Phase transformations and properties of steels in welding*. Moscow: Nauka.

7. Markashova, L.I., Poznyakov, V.D., Berdnikova, E.N. et al. (2013) Specifics of structure of high-strength steel welded joints formed in laser welding conditions. In: *Proc. of 6th Int. Conf. on Laser Technologies in Welding and of Materials Processing* (21–31 May 2013, Katsiveli, Crimea, Ukraine), 51–55.

8. Poznyakov, V.D., Shelyagin, V.D., Zhdanov, S.L. et al. (2015) Laser-arc welding of high-strength steels with yield strength of more than 700 MPa. *The Paton Welding J.*, **10**, 19–24.

9. Markashova, L.I., Grigorenko, G.M., Poznyakov, V.D. et al. (2009) Influence of thermal cycles of welding and external loading on structural-phase variations and properties of joints of 17Kh2M steel. *Ibid.*, **7**, 18–25.

10. Markashova, L.I., Poznyakov, V.D., Berdnikova, E.N. et al. (2014) Effect of structural factors on mechanical properties and crack resistance of welded joints of metals, alloys and composite materials. *Ibid.*, **6/7**, 22–28.

11. Markashova, L.I., Shelyagin, V.D., Kushnaryova, O.S. et al. (2014) Structural-phase state and mechanical properties of 38KhN3MFA steel surface layers formed under conditions of laser and laser-plasma alloying. In: *Proc. of 7th Int. Conf. on Mathematical Modelling and Information Technologies in Welding and Related Processes* (15–19 Sept. 2014, Odessa, Ukraine), 43–47.

12. Conrad, H. (1973) Model of strain hardening for explanation of grain size effect on metal flow stress. In: *Super-fine grain in metals*, 206–217. Moscow: Metallurgiya.

13. Petch, N.J. (1953) The cleavage strength of polycrystals. *J. Iron and Steel Inst.*, 174(**1**), 25–28.

14. Kelly, A., Nickolson, R.B. (1966) *Precipitation hardening*. Moscow: Metallurgiya.

15. Romaniv, O.N. (1979) *Fracture toughness of structural steels*. Moscow: Metallurgiya.

16. Stroh, A.N. (1954) The formation of cracks as a result of plastic flow. *Proc. of Roy. Soc. A*, 223(**1154**), 404–415.

17. Cottrell, A.H. (1958) *Dislocations and plastic flow in crystals*. Moscow: Metallurgiya.

COMPARATIVE EVALUATION OF PROPERTIES OF HIGH-STRENGTH N-A-XTRA-70 STEEL WELDED JOINTS PRODUCED USING ARC, LASER AND HYBRID LASER-ARC METHOD

V.D. POZNYAKOV, V.D. SHELYAGIN, S.L. ZHDANOV, A.V. BERNATSKY and **A.V. SIORA**

E.O. Paton Electric Welding Institute, NASU
11 Kazimir Malevich Str., 03680, Kiev, Ukraine. E-mail: office@paton.kiev.ua

In the work the comparative evaluation of mechanical properties of butt welded joints of N-A-XTRA-70 high-strength steel of 8 mm thickness, produced using arc, laser and hybrid laser-arc welding, was carried out. Mechanical tests on static tension and impact bending with V-notch showed that the values of static strength are increased with decrease in heat input of arc welding, and the values of ductility remain almost unchanged. At the same time, the values of impact toughness of weld and HAZ metal are approximately 1.5–1.8 times reduced. This is connected with the fact that at increase in welding speed from 18 to 50 m/h the phase composition of weld metal changes from ferrite-bainite to bainite-martensite. In laser welding, the values of static strength of weld metal are by 18–20 % reduced and the ductility 1.8 times increases with increase in welding speed and cooling rate of HAZ metal. With increase in speed of laser welding from 40 to 50 m/h the phase composition of weld metal changes from martensite to martensite-bainite (with martensite fraction exceeding 60 %). In hybrid welding, the increase in welding speed leads to 10–15 % increase in the values of static strength and ductility. These changes occur because of the fact that the fraction of phase components changes. In the molten metal of specimens produced using laser method, and in the deposited metal produced using arc and hybrid methods the ultra-low concentrations of diffusion hydrogen content are observed, namely 0.07, 0.2–0.3 and 0.4 ml/100 g, respectively. 10 Ref., 1 Table, 1 Figure.

The high-strength low-alloyed steels with yield strength of 600–900 MPa are used for manufacture of heavy-loaded welded structures in construction and mechanical engineering [1–4]. Their application provides reduction in mass of structures, increases service reliability and longevity of machines, mechanisms and constructions. Especially the use of high-strength steels in manufacture of handling machinery is effective.

The metallurgical processes of HSLA steel welding should meet two basic requirements: provide minimum saturation of weld metal with hydrogen, and producing the weld metal with optimal chemical composition of limited content of carbon and harmful impurities (sulfur and phosphorus) and nonmetallic inclusions [1]. Both requirements are connected, firstly, with the need in preventing the cold crack formation in the metal of different welded joint zones and, secondly, with the need in producing weld and HAZ metal with sufficiently high level of mechanical properties.

In the recent years in the world in order to reduce deformations and improve the quality of welded thin-wall metal structures for manufacture of products of steels of ferritic-pearlite class the technological processes are ever widely offered based on the use of laser and hybrid laser-arc welding methods [5–10]. In our opinion, this approach may be acceptable also for welding of high-strength bainite-martensite steels. However, considering the fact that these steels are prone to formation of hardening structures and have an increased tendency to delayed fracture, which is intensified under the influence of diffusion hydrogen, it becomes necessary to investigate the features of weld metal saturation with hydrogen, running of thermodeformational cycles in laser and HLA welding process as compared to the arc process and to establish their effect on the structure and properties of welded joints of high-strength bainite-martensite steels.

The aim of this work is the comparative evaluation of properties of butt joints of N-A-XTRA-70 high-strength steel (wt.%: 0.15 C; 0.63 Si; 0.85 Mn; 0.65 Cr; 0.12 Ni; 0.13 Mo; 0.04 Al; 0.01 S; 0.015 P; 0.015 N_2) 8 mm thick welded using arc, laser and hybrid method. In arc welding, solid wire Union NiMoCr (wt.%: 0.17 C; 0.53 Si; 1.68 Mn; 0.12 Cr; 1.54 Ni; 0.62 Mo; 0.011 S; 0,017 P) of 1 mm diameter was used. The welding was performed at I_w =

= 230–250 A, U_a = 28–32 V in the gas mixture of Ar + 18 % CO_2, at v_w = 18, 30, 40 and 50 m/h.

Laser welding without filler metal was carried out in the mixture of Ar + 18 % CO_2, at v_w = 40 and 50 m/h, power of laser radiation P = 4.4 kW and defocusing ΔF = –2 mm.

In HLA welding solid wire Union NiMoCr of 1 mm diameter was used. The welding was performed in the mixture of Ar + 18 % CO_2, at v_w = 72 and 90 m/h, P = = 4.4 kW, ΔF = –1.5 mm, I_w = 120–130 A, and U_a = = 22–24 V.

For welded joints, produced with equal value of heat input $Q_w \sim$ 3 kJ/cm, in case of application of laser welding (Figure 1, *a*) the volume of remelted metal is lower than that in hybrid welding (Figure 1, *b*). This is explained by occurring of the so-called hybrid effect consisting in non-additivity of the combined effect of laser and arc power sources on the material being welded [8].

To investigate the influence of thermal cycles on the structure and properties of HAZ metal of welded joints of steel N-A-XTRA-70 the works were carried out on fixation of heating and cooling processes in laser and hybrid welding. The results of the carried out experiments evidence that the cooling rate in the temperature range of 600–500 °C in HLA welding is about 61–63 °C/s, and in laser welding $w_{6/5}$ = 65–103 °C/s.

To carry out mechanical tests the specimens on static tension were manufactured from welded joints (type I according to GOST 6996–66) and impact bending (type XI according to GOST 6996–66) with V-notch. The specimens were tested on tension at room temperature, and on impact strength at 20, –20 and –40 °C.

The carried out mechanical tests showed (the Table) that with decrease in heat input of arc welding
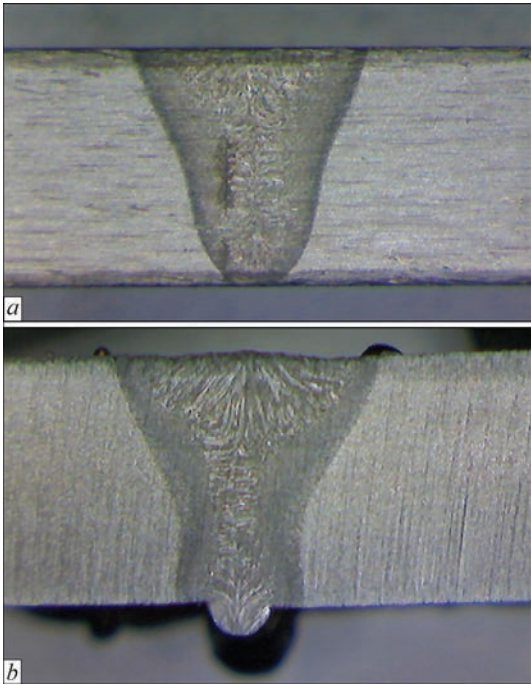
Macrostructure of cross sections of butt welded joints of N-A-XTRA-70 steel (δ = 8 mm) produced using laser (*a*) and hybrid laser-arc (*b*) methods at equal Q_w = 3 kJ/cm

the values of static strength $\sigma_{0.2}$ increase from ~731 to ~822 MPa and $\sigma_t \sim$ 817–910 MPa, and the values of ductility are almost unchanged and amount on average to $\delta_5 \sim$ 19 %, and $\psi \sim$ 63 %. At the same time, the values of impact toughness of weld and HAZ metal are approximately 1.5–1.8 times decreased. As the results of metallographic analysis show, it is connected with the fact that with increase in welding speed from 18 to 50 m/h, the phase composition of weld metal is changed from ferrite-bainite to bainite-martensite and the microhardness increases by 30 %.

The results of carried out investigations of influence of laser and HLA welding conditions on mechanical properties of weld metal and welded joints of

Mechanical properties of base N-A-XTRA-70 steel metal and welded joints produced using arc, laser and hybrid laser-arc welding with wire Union NiMoCr of 1 mm diameter in the Ar + CO_2 mixture

Object of investigation (method; v_w, m/h)	$\sigma_{0.2}$	σ_t	δ_5	ψ	KCV, J/cm², at T, °C					
					+20	–20	–40	+20	–20	–40
	MPa		%		Weld			HAZ		
BM	790.0	850.0	18.3	66.0	N/D	N/D	50.0	N/D	N/D	N/D
WJ (AW; 18)	731.1	817.1	19.5	65.0	181.6	–	109.2	217.9	–	218.0
WJ (AW; 30)	777.7	871.0	19.7	63.2	145.7	–	81.6	232.7	–	223.1
WJ (AW; 40)	826.7	915.0	18.4	60.9	140.3	–	91.3	246.3	–	212.3
WJ (AW; 50)	822.0	905.0	18.8	64.5	138.9	–	93.7	242.6	–	213.5
WJ (LW; 40)	1043.9	1227.7	6.0	24.9	N/D	15.5	8.7	90.6	84.0	59.2
WJ (LW; 50)	854.5	1050.8	10.0	42.4	52.5	13.8	7.3	N/D	N/D	N/D
WJ (HLAW; 72)	961.0	1196.0	6.2	28.0	113.0	83.4	59.1	102.5	102.3	76.8
WJ (HLAW; 90)	1082.0	1259.0	9.3	33.3	113.1	N/D	72.5	94.3	N/D	72.6

N-A-XTRA-70 high-strength steel of 8 mm thickness prove (see the Table) that in laser welding the values of static strength of weld metal are reduced by 18–20 % and the values of ductility are 1.8 times increased with increase in welding speed and cooling rate of HAZ metal. The results of metallographic examinations show that with increase in speed of laser welding from 40 to 50 m/h the phase composition of weld metal changes from martensite to martensite-bainite (with martensite fraction exceeding 60 %).

In HLA welding, the increase in welding speed leads to 10–15 % increase in the values of static strength. As the results of metallographic examinations show, these changes occur because of the fact that the share of phase components changes: at $v_w = 72$ m/h, $B_L > B_U + M$; at $v_w = 90$ m/h, $B_L < B_U + M$.

The investigations on determination of diffusion hydrogen in the deposited metal during arc, laser and hybrid welding were carried out using chromatographic method. The specimens of $25 \times 15 \times 15$ mm with deposited and molten metal were cooled in liquid nitrogen and then placed to the chromatograph chamber for the analysis of the evolved hydrogen content. Due to the fact that laser welding was carried out without the filler wire, it is not possible to attribute the volume of released hydrogen to the weight of deposited metal. Taking into account the latter, the content of diffusion hydrogen in the metal was determined according to its volume in the molten metal and was compared to the volume of hydrogen in the deposited metal of arc- and HLA-welded specimens.

The obtained results of investigations show that under the mentioned conditions and methods of welding the ultra-low concentrations of diffusion hydrogen content are observed, namely: 0.2–0.3 and 0.4 ml/100 g, respectively, in the deposited metal of specimens, produced using arc and hybrid methods. In laser welding the diffusion hydrogen content in the molten metal is even lower and amounts to 0.07 ml/100 g.

In conclusion, it should be noted that comparative evaluation of properties of butt welded joints of steel N-A-XTRA-70 produced using arc, laser and hybrid method with wire Union NiMoCr of 1 mm diameter in the mixture of $Ar + CO_2$ showed that hybrid welding allows providing a sufficiently high level of mechanical properties of welded joints, low content of diffusion hydrogen in weld metal from the point of view of ensuring the high resistance to cold crack formation.

1. Musiyachenko, V.F. (1976) Bases of welding metallurgy and technology of high-strength low-alloy steels: Course of lectures for specialists-welders. In: *Int. seminar-practical training of UN on welding*. Kiev: Naukova Dumka.
2. Musiyachenko, V.F., Mikhoduj, L.I. (1987) *Arc welding of high-strength alloy steels*. Moscow: Mashinostroenie.
3. Pokhodnya, I.K., Shvachko, V.I. (1997) Physical nature of hydrogen induced cold cracks in welded joints of high-strength structural steels. *Avtomatich. Svarka*, **5**, 3–10.
4. Markashova. L.I., Poznyakov, V.D., Berdnikova, E.N. et al. (2014) Structure and properties of high-strength steel joints under external static loading. In: *Transact. on building, materials science, machine-building*, Issue 73, 213–219. Dnepropetrovsk: PGASA.
5. Moore, P.L., Howse, D.S., Wallach, E.R. (2004) Microstructures and properties of laser/arc hybrid welds and autogenous laser welds in pipeline steels. *Sci. and Techn. of Welding and Joining*, Vol. 9, Issue 4, 314–322.
6. Kah, O., Salminen, A., Martikainen, J. (2010) Laser-arc hybrid welding processes (Review). *The Paton Welding J.*, **6**, 32–40.
7. Atabaki, M., Ma, J., Yang, G. et al. (2014) Hybrid laser/arc welding of advanced high strength steel in different butt joint configurations. *Materials and Design*, **64**, 573–587.
8. Shelyagin, V.D., Khaskin, V.Yu., Bernatsky, A.V. et al. (2010) Prospects of application of laser and hybrid technologies of welding steels to increase service life of pipelines. *The Paton Welding J.*, **10**, 29–32.
9. Gu, X.Y., Duan, Z.Z., Gu, X.P. et al. (2015) Microstructure and mechanical properties of laser-MAG hybrid welded thick-section weathered steel joint. *Int. J. Advanced Manufact. Techn.*, Vol. 81, Issue 5, 825–831.
10. Grigoryants, A.G. (2015) Special features of laser welding using fibre and CO_2 lasers. *Welding Int.*, Vol. 29, Issue 12, 968–973.

3D-PRINTING OF METALLIC VOLUMETRIC PARTS OF COMPLEX SHAPE BASED ON WELDING PLASMA-ARC TECHNOLOGIES (Review)

V.N. KORZHIK[1], **V.Yu. KHASKIN**[1], **A.A. GRINYUK**[1, 2], **V.I. TKACHUK**[1],
S.I. PELESHENKO[3], **V.V. KOROTENKO**[1, 2] and **A.A. BABICH**[1]

[1]E.O. Paton Electric Welding Institute, NASU
11 Kazimir Malevich Str., 03680, Kiev, Ukraine. E-mail: office@paton.kiev.ua
[2]NTUU «Kiev Polytechnic Institute»
37 Pobeda Ave., 03056, Kiev, Ukraine. E-mail: mail@KPI.ua
[3]South China University of Technology
510641, Guangzhou, PRC. E-mail: sviatoslav@qq.com

Manufacturing complex-shaped metal products by 3D-printing is becoming ever more urgent in modern industry. Laser technologies (SLS- and SLM-processes) are most often applied for this purpose, while electron beam technologies (EBF$_3$) are used less often. Both of them are characterized by quite high cost and low efficiency. This paper deals with new tendencies in application of welding technology for 3D-printing of complex metallic products, including those complemented by concurrent or subsequent machining. It is shown that application of welding technologies to produce volumetric metallic products significantly lowers their manufacturing cost at simultaneous increase in productivity, compared to SLS- and SLM-processes. The most promising welding technology of 3D-printing is plasma-arc process with application of wires or powders. It allows at comparatively low heat input creating quality volumetric products with 3–50 mm thickness from Fe, Ni, Co, Cu, Ti, Al alloys, as well as composite materials containing refractory components. Application of welding technologies allows producing both comparatively small and long products, not requiring any finish machining (for instance, growing stiffeners on large-sized panels, manufacturing honeycomb panels, building structures, etc.). Combination of welding technologies of 3D-printing with concurrent or finish machining (mostly, by CNC milling) allows manufacturing ready for use metal products of complex profile. 19 Ref., 2 Tables, 8 Figures.

K e y w o r d s : 3D-printing, metal products, welding technologies, machining, materials, equipment

At present 3D-printing or rapid prototyping of complex-shaped volumetric products is considered to be the technology of XXI century, which will fundamentally change the structure of industrial production and economy, will enable computer-aided design of parts, flexible and fast manufacturing of different products, redistribution of production from large enterprises to small ones or manufacturing parts directly at user facility [1]. 3D-printing is the technology of additive manufacturing. The process starts with obtaining virtual design data through computer modeling with application of CAD software. The machine for 3D-printing reads the data from CAD model file; CAM program modules are used to divide (cut) the part into layers, for each of which the tool movement trajectory is automatically generated, which can take into account a multitude of technological and geometrical factors. In total, all the programs for each layer form a control program, in keeping with which the CNC manipulator tool moves. The tool deposits successive layers of liquid, powder or sheet material, creating a physical model from a set of cross-sections.

These layers, corresponding to virtual cross-sections created in CAD model, are automatically connected to create the final shape.

There are different processes of 3D-printing, but they are united by that the prototype is made by layer-by-layer deposition of material. The main advantage of rapid prototyping consists in that the prototype is created in one step, and the geometrical model of the part proper is used as input data for it. Therefore, there is not need for planning the sequence of technological processes, special equipment for material processing at each manufacturing stage, transportation from one machine tool to another one, etc.

Among the known and rather widely applied now processes of 3D-printing we can note such techniques as stereolithography [2], fused deposition modeling (FDM) [3], and selective laser sintering (SLS) [4]. Such processes, with all their effectiveness, have one essential limitation: plastic is used in them as the main structural or binder material that considerably limits the range of manufactured items as to operating temperature, loads, mechanical strength and other values.

Enhancing the capabilities of 3D-printing requires availability of technologies of producing high-strength volumetric products from metals and alloys, including those of a high hardness. A number of US research centers (for instance, NASA's Langley Research Center, Houston and Johnson Space Centers, Hampton) perform development of electron beam process of manufacturing freeform metal items (EBF$_3$) [5]. Here, the electron beam is used as the energy source for melting the fed wire in vacuum. This procedure was demonstrated on aluminium and titanium alloys, which are of interest for aerospace applications [6]. In our opinion, it can be also extended to Ni- and Fe-based alloys. However, application of this process is limited by the need to apply expensive and complex vacuum equipment.

One of the promising technologies of producing high-strength metallic volumetric products is selective laser melting (SLM), ensuring item formation by fusing powders of different metals and alloys by the laser beam [7]. This technology enables producing complex metallic volumetric products with a high degree of detailing of their elements and high density (up to 99 %), as well as high dimensional accuracy (±50 μm).

On the other hand, with all its effectiveness and flexibility SLM process also has a number of limitations, narrowing its application (Table 1):

● need to apply expensive and energy-consuming equipment with a high service cost that results in high cost of 3D-printing process and leads to a high cost of manufactured products;

● relatively low productivity of 3D-printing (usually not more than 10 cm^3/h of incremental metal for the most widely applied machines);

● material limitations, namely for SLM expensive powders with strict requirements on granulometric and chemical composition and other characteristics are used;

● insufficiently high strength characteristics of manufactured items.

In view of the above-said, consideration of welding technologies for 3D-printing of complex-shaped metal products is urgent, as welding, at higher productivity, also allows realization of the principle of additive manufacturing, namely layer-by-layer formation of 3D structures. Moreover, welding technologies were developed long before appearance of 3D-printing, and are much more mature and less costly. Therefore, it is highly relevant to use welding processes in development of cost-effective method of manufacturing maximum dense metallic volumetric parts and tools [8].
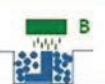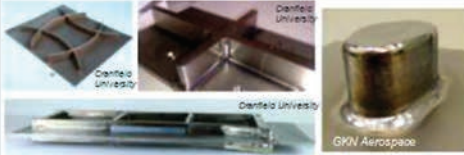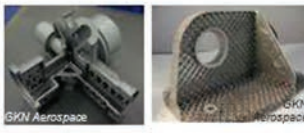
Work [9] gives the following chronology of the attempts to apply welding technologies for fabrication of 3D structures of a complex-shape:

● in 1926 Baker patented «application of electric arc as the heat source to produce bulk objects by spraying molten metal into the deposited layers»;

● in 1971 Yujie patented manufacture of a high-pressure vessel, using submerged-arc welding, electroslag technology and TIG welding to produce items with functionally-gradient walls;

● in 1983 Kussmaul used shape welding to manufacture large-sized products from high-strength steel (20MnMoNi5) of 79 t weight;

● in 1993 Prinz and Weiss patented a combined technology of incrementing material, using welding with milling in CNC machine tools (shape deposition manufacturing — SDM);

● in 1994–1999 the Cranfield University developed shaped metal deposition (SMD) technology for

Table 1. Comparison of the most widely accepted SLM technologies of 3D-printing of metallic products with new plasma-arc melting technology based on plasma-arc welding

Characteristic	Technology of 3D-printing of metallic products			
	SLM			PAM
	LENS company	POM company	AeroMet company	
Used equipment characteristic	Nd:YAG-laser, 1 kW power	CO$_2$-laser, 2 kW power	CO$_2$-laser, 14 kW power	Based on welding, 2–20 kW power
Productivity by incremental metal, cm^3/h	8	8	160	>1000–15000
Capability of processing along axes (degrees of freedom)	3 axes	3 axes	3 axes	4–5 axes
Type of material used for 3D-printing	Metal powder			Powders of metals, alloys, composite materials, powder mixtures. Solid and flux-cored wire
Material utilization factor, %	About 40	About 40	About 70	More than 90
Application fields	Manufacture and repair of small-sized expensive complex-shaped parts			Manufacture and repair of medium- and large-sized expensive complex-shaped parts for various applications
Tentative cost of main equipment units (per 1 kW of power)	Laser cost: 80,000–120,000 USD			Welding equipment cost: 1000–5000 USD

Table 2. Main technologies of additive manufacturing with application of local melting processes [17]

	Spraying				Powder/Mould		
	Plasma (wire)	EB (wire)	Laser (wire)	Laser (powder)	Laser (powder)	EB (powder)	Binder (powder)
Process schematic							
Illustration							
Description	Free spraying of wire using arc plasma	Spraying of wire molten by laser or electron beam in a chamber		Deposition of powder molten by laser in a chamber	Laser or electron beam selective melting in mould located in a chamber		Powder/binder system, requiring melting in the downhand position
Application	High-rate melting of material and its spraying technology allow growing almost precise items			Precise and almost finished sprayed parts	New generation prismatic components with highly complex geometry		Complex-shaped parts with inner cavities for cars

manufacturing engine shells for Rolls Royce Corporation (Great Britain).

There are also data on attempts made in the 1960s in Germany to create 3D metal structures, using shape welding. Based on this process, such companies as Krupp and Thyssen organized manufacturing of large-sized parts of a simple geometry, for instance, high-pressure vessels of up to 500 t weight [10]. Successful attempts of arc welding application for manufacturing large-sized metal structures and products from austenitic steels were made by the Babcock & Wilcox Company (USA) in the form of development of technology named Shape Melting [11]. As was already noted, Rolls Royce Corporation is pursuing arc welding application as the technology providing high forming productivity and lowering the level of wastes that may be generated at traditional processing during fabrication of items from expensive alloys [12]. At present this Corporation is successfully introducing this technology for manufacturing different aircraft parts from expensive Ni- and Ti-base alloys.

In addition to the above examples, research work on 3D arc welding is conducted in University of Nottingham (Great Britain), Wollongong University (Australia) and Southern Methodist University in Dallas (Texas, USA) [13]. Research teams from Indian Institute of Technology (Mumbai) and Fraunhofer Institute of Production Technology and Automation presented their conceptual ideas of combining a welding operation with milling. Characteristic defects in volumetric product forming by welding methods were

also studied and ways to eliminate them were developed [14]. Need to monitor the temperature of incremental layers was also studied. Special attention was given to creation of products from titanium [15] and nickel [16] alloys for aerospace industry applications. On the whole, main welding and related technologies for additive manufacturing can be presented in the form of Table 2 [17].

PWI work also confirmed the fundamental possibility of forming large-sized volumetric structures by arc welding. One of the striking examples can be creation of 3D welded sculptures and pictures from titanium alloy by G. Dochkin using his own unique method developed in mid-1970s [18]. Individual production problems were also solved, related to manufacture of unique products for defense industry.

The above studies were mostly focused on applicability for 3D-printing of such welding processes as gas metal arc welding (GMAW) and gas tungsten arc welding (GTAW). These processes ensure good metallurgical adhesion, as well as protection of weld pool and incremental layers of products from oxide formation. However, these processes with their availability, also have such disadvantages as considerable size of HAZ and quite large dimensions of incremental layer that leads to generation of undesirable temperature gradients and residual stress accumulation. More over, mostly standard welding wire is used as consumable material to form volumetric products that limits the chemical composition and properties of these items.
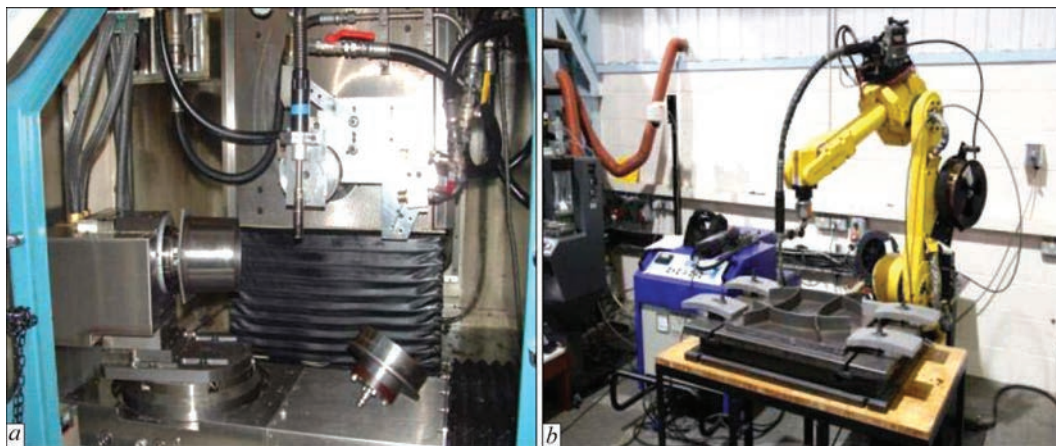
Figure 1. Complexes for realization of additive welding technologies [9]: *a* — five-axes system with CNC milling and WAAM technology; *b* — WAAM process without machining realized using an anthropomorphous robot

The above drawbacks can be eliminated by application of microplasma or plasma-arc melting, as well as microplasma or plasma-arc welding. These welding technologies are capable of providing a new level of 3D-printing, both compared to arc welding processes (GMAW, GTAW), and compared SLM, in view of the following advantages:

● temperature in plasma arc flame can reach 30000 ºC, that is essentially higher than in standard electric arc. Therefore, plasma can melt practically any refractory material for layer-by-layer incremental manufacturing of volumetric products;

● minimum heating of earlier deposited layers at product formation, less than 5 % heat penetration into base metal;

● absence of metal spatter when building-up the layers, their extremely low mixing;

● possibility of adjusting in a broad range the thickness (0.5–5.0 mm) and width (1.5–50.0 mm) of deposited metal layer in additive building-up of volumetric products;

● ability to adjust the composition of gas atmosphere (reducing, inert, oxidizing) during additive building-up of layers in product forming;

● high cost-effectiveness and productivity of the process (by 2–3 times and more);

● applicability of a wide range of consumable materials (powders of metals, alloys, composite materials, powder mixtures, solid and flux-cored wires), including those from Fe, Ni, Co, Cu, Ti, Al alloys, as well as composite materials, containing refractory components (carbides, borides, and other for instance, WC, Cr_3C_2, TiC, TiB_2), refractory materials, composite materials with refractory components;

● possibility of changing metal composition during item formation, producing items with graded structure.

At present, advanced research institutes and industrial corporations of economically developed countries pursue applied research on development of plasma-arc melting and welding technologies, as well as other welding technologies of 3D-printing of metal products. Let us consider some characteristic examples of such studies.

Cranfield University developed different complexes for realization of additive welding technologies — both with machining during layer building-up and without it (Figure 1) [9]. Manufacturing volumetric products in these complexes is based on wire-arc

Figure 2. Examples of volumetric products from carbon steel S355 manufactured by WAAM technology [9]: *a* — panels with crossing stiffeners without machining; *b* — cylinder machined after manufacturing

Figure 3. Shell casing of 160 mm diameter and 800 mm length with 8 to 18 mm wall thickness of 32 kg weight from high-strength steel made by WAAM technology (pulsed MIG welding) with productivity of 4 kg/h before (*a*) and after (*b*) machining [9]

additive manufacturing (WAAM) technology (Figure 2). Products are made from various materials, for instance, carbon steel, titanium and aluminium alloys, etc. Here, both standard (continuous or pulsed) and constricted electric arc, i.e. plasma, can be used (Figure 3). One of the promising directions of WAAM technology application is fabrication of large-sized honeycomb structures (Figure 4).

Southern Methodist University in Dallas studied the variants of laser, arc and plasma-arc technologies of manufacturing 3D objects with simultaneous or finish machining (CNC milling) [13]. Respective technological complexes were developed, and a number of engineering solutions were proposed, allowing manufacture of both relatively simple and quite complicated products (Figure 5). In particular, investigations were conducted in the field of microplasma powder building-up of volumetric products (Figure 6). Fundamental possibility of producing gradient composite structures by such a method was demonstrated. Analysis of the features and prospects for the above welding technologies showed that for the most high-efficient and cost-effective manufacturing of quality volumetric products with wall thickness of 3 to 50 mm, application of plasma-arc powder deposition of layers of 0.5–5.0 mm height in one pass is the optimum variant.

In addition to machines and mechanisms, welding technologies of 3D-printing also allow creation of building structures. Development of new MX3D technology can be an example [19]. MX3D project was created by JORIS LAARMAN LAB in cooperation with ACOTECH and HAL (Holland). New technology has enormous potential, as it allows quickly creating complex metal constructions without erection of any accompanying supporting structures, for instance, scaffolding or intermediate supports. During
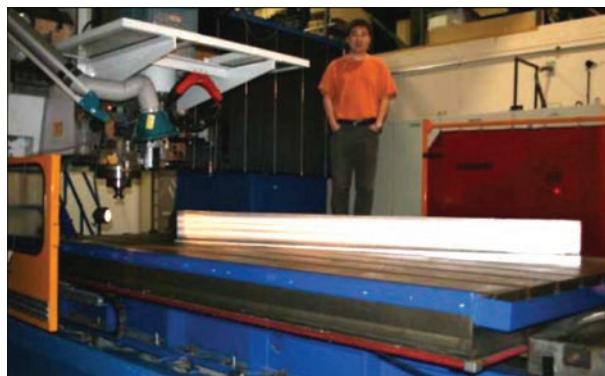
Figure 4. Aluminium honeycomb beam structure of 3 m length with higher rigidity [9]

3D welding, the man or welding robot creates his own support and moves ahead on the constructed structure. It speeds up and simplifies construction. More over, MX3D can be fully robotized, and can operate round the clock.
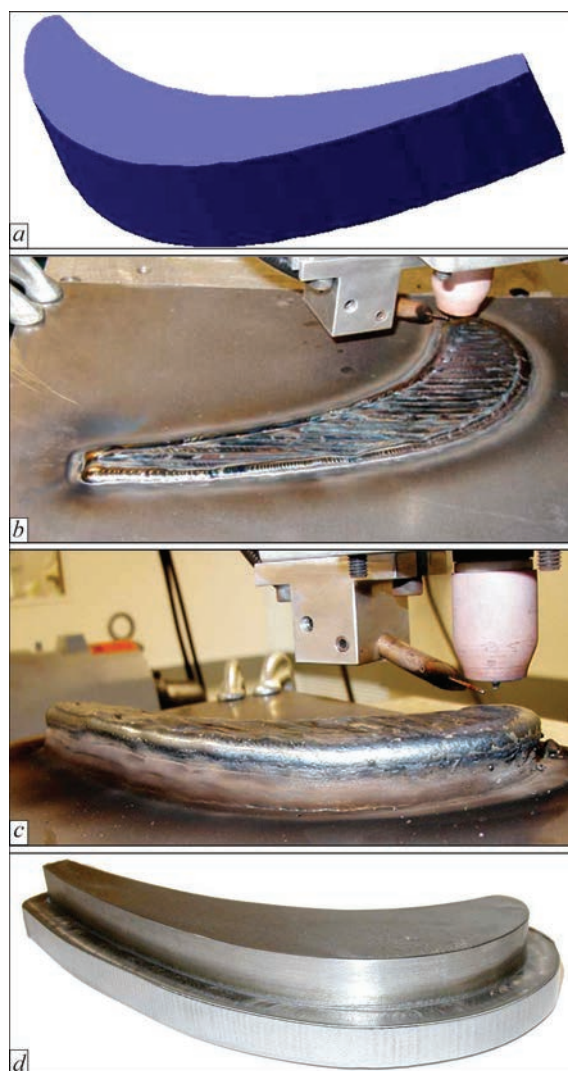

Figure 5. Process of manufacturing blade turbine by combination of arc surfacing and CNC milling: *a* — CAD model; *b* — start of GTA surfacing; *c* — end of GTA surfacing; *d* — blank after CNC milling [13]
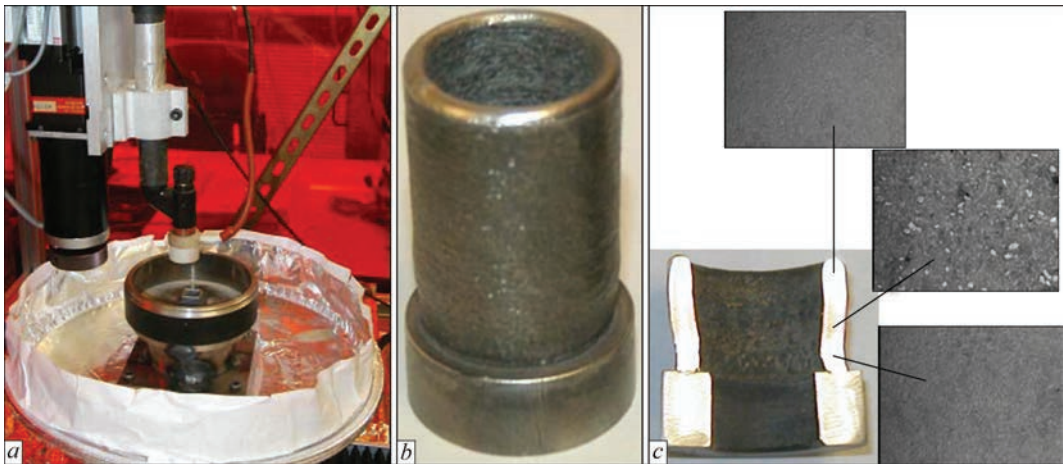
Figure 6. Microplasma powder growing of volumetric products [13]: *a* — laboratory unit; *b* — hollow cylinder of uniform structure (tool steel H-13); *c* — creation of gradient composite H-13 + tungsten carbide structure
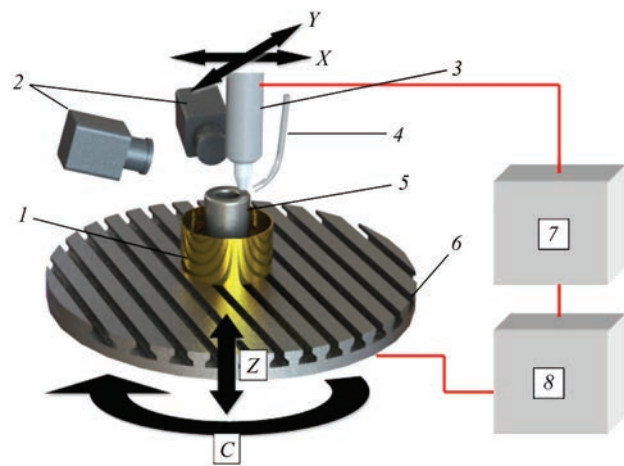

Figure 7. Schematic of unit for plasma-arc 3D-printing of volumetric products (for designations see the text)

Generalization of data, given and analyzed in publications, allows suggesting the following approach to fabrication of volumetric products, using welding technologies: computer modeling of the item, its manufacture by plasma-arc technology with application of wire or powder under the conditions of monitoring temperature and forming, machining of minimum required number of item sections. To realize such an approach, it is rational to separately apply the system for plasma-arc 3D-printing (Figure 7), and to perform machining in CNC milting and/or lathe machine tool. We believe it is not rational to combine the processes of 3D-printing and finish machining within one multi-axis all-purpose unit.

After development of a computer model of the grown part (using CAD system, for instance Solidworks), it is automatically (using CAM system, for instance Lazy CAM, Art CAM) separated into layers with generation of control programs for each of the layers, which are loaded into the system of CNC complex (see Figure 7). Growing of part *5* is performed in shielded (for capturing welding spatter and unused powder) zone *1*, located on rotating table *6*, with the capability of performing rotation *C* and step-by-step vertical displacement *Z*. Transferred arc plasmatron *3* is mounted on the carriage of *xy*-manipulator, providing precise movement along coordinates *X* and *Y*. Filler wire or powder is fed into the torch *3* coverage area using system *4*. Process monitoring is performed by system *2*, including two CCD-cameras, located at 90° angle to each other, and thermal imager. Here, not only forming of part *5*, but also its temperature
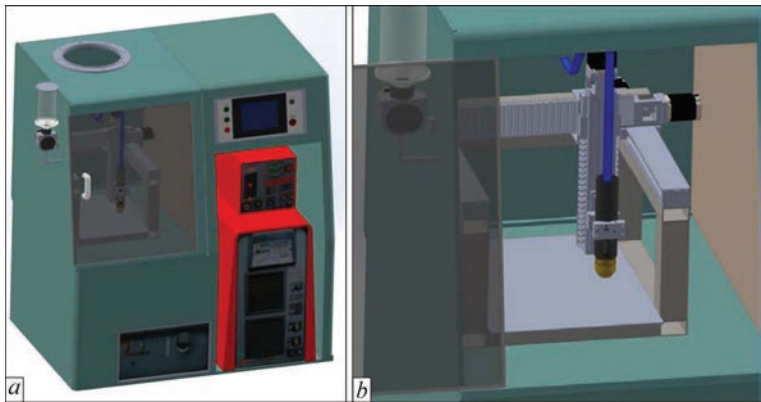
Figure 8. PWI-designed complex for manufacturing 3D objects based on technologies of plasma-arc welding and surfacing: *a* — general view; *b* — three-coordinate manipulator with plasmatron

state, is monitored. Systems *4* and *2* are also located on the carriage. Plasmatron *3* is powered by source *7*, and 3D-printing process is controlled by CNC system *8*. After growing part *5*, it can be transferred to machining station, can be treated directly in the system, in which it was created, or left untreated, if required quality of its surfaces has been achieved.

At present, PWI performs manufacturing of equipment for creation of 3D objects based on plasma-arc welding and surfacing. For this purpose, a complex was designed on the basis of three-coordinate manipulator, fitted with plasmatron with power source, filler wire feeder and CNC system (Figure 8). The complex is controlled using a common controller with the capability of exchange of data on 3D-printing modes and of control commands with the computer. Performed work allowed development of a number of unified systems of different typesizes for 3D-printing of metallic volumetric parts of a complex shape, based on plasma-arc technologies.

Conclusions

1. Application of welding technologies to produce metallic volumetric parts allows considerable lowering of their manufacturing cost at simultaneous increase in productivity, compared to SLS- and SLM-processes.

2. The most promising welding technology of 3D-printing is plasma-arc technology with application of wires or powders. It allows creating at comparatively low heat input quality volumetric products with wall thickness from 3 to 50 mm from alloys based on Fe, Ni, Co, Cu, Ti, Al, as well as composite materials, containing refractory components.

3. Application of welding technologies allows producing both comparatively small and long items, not needing finish machining (for instance, growing stiffeners on large-sized panels, creating honeycomb panels, building structures, etc.).

4. Combination of welding technologies of 3D-printing with concurrent or finish machining (most often CNC milling) allows manufacturing finished metal items of complex profile.

1. Kruth, J.P., Leu, M.C., Nakagawa, T. (1998) Progress in additive manufacturing and rapid prototyping. *CIRP Annals-Manufact. Techn.*, 47(**2**), 525–540.

2. (2009*) Laser technologies for treatment of materials: Current problems of fundamental studies and applied developments:* Monograph, Chapter: Laser technologies of rapid prototyping and direct fabrication of 3D objects. Moscow: Fizmatlit.

3. Slyusar, V.I. (2003) Fabber-technologies. New tool for 3D modeling. *Elektronika: Nauka, Tekhnologiya, Biznes*, **5**, 54–60.

4. Deckard, C.R., Beaman, J.J. (1987) Recent advances in selective laser sintering. In: *Proc. of 14th Conf. on Production Research and Technology* (Michigan, 1987), 447–451.

5. Kablov, E.N. (2015) Additive technologies as the dominant of national technology initiative. *Intellekt & Tekhnologii*, 2(**11**), 52–55.

6. Bruce, M.R., Riley, S.F., Cola, M.J. et al. (2012) Measurement and simulation of titanium alloy deposit temperature in electron beam additive manufacturing. In: *Trends in Welding Research:* Proc. of 9th Int. Conf. (Chicago, USA, 4–8 June 2012), 963–969.

7. Kruth, J.P. (2004) Selective laser melting of iron-based powder. *J. Mater. Process. Technol.*, Vol. 149, 616–622.

8. Karunakaran, K.P., Suryakumar, S., Vishal Pushpa et al. (2010) Low cost integration of additive and subtractive processes for hybrid layered manufacturing. *Robotics and Computer-Int. Manufact.,* 26(**5**), 490–499.

9. Colegrove, P., Williams, S. (2013) High deposition rate high quality metal additive manufacture using wire + arc technology. http://xyzist.com/wp-content/uploads/2013/12/Paul-Colegrove-Cranfield-Additivemanufacturing.pdf

10. Venuvinod, P.K., Weiyin Ma (2004) Rapid prototyping: Laser-based and other technologies. In: *Springer Science + Buisness Media*. New York.

11. Doyle, T.E., Ryan, P.M. *Cooling workpieces being manufactured by shape melting*. Pat. EP0340939A1 (US4857694). Int. Cl. B23K9/04, B23K37/003, B23K37/00F. Publ. 8.11.89.

12. Martina, F. (2014) Investigation of methods to manipulate geometry, microstructure and mechanical properties in titanium large scale wire + arc additive manufacturing. In: *School of Aerospace, Transport and Manufacturing*. Cranfield University.

13. Kovacevic, R. (2003) Development of machine for rapid manufacturing/repair. In: *The 2003 CTMA Symp.* (Salt Lake City, USA, March 31–April 3,2003), *www*.engr.smu.edu/rcam

14. Alhuzaim, A.F. (2014) *Investigation in the use of plasma arc welding and alternative feedstock delivery method in additive manufacture*: Thesis submitted in partial fulfillment of the requirements for the degree of Master of Sci. General Engineering. University of Motana.

15. Baufeld, B., Van der Biest, O., Gault, R.S. (2010) Additive manufacturing of Ti–6Al–4V components by shaped metal deposition: Microstructure and mechanical properties. *Materials & Design*., Vol. 31, 106–111.

16. Clark, D., Bache, M.R., Whittaker, M.T. (2008) Shaped metal deposition of a nickel alloy for aero engine applications. *J. Materials Proc. Techn.*, Vol. 203, 439–448.

17. Chad, H. (2014) Metallic additive manufacturing: Comprehensive overview and findings on 3D-printing for construction. http://www2.iceaustralia.com/ei/images/cmic14/cmicpresentations/plenary/henry.pdf

18. (2015) Art of Grigory Dochkin. In: *CWELD — equipment and materials for welding and cutting,* 01.08.2015; http://adiosgroup.ru/?p=242

19. (2015) 3D-welding from MX3D will print-out the bridge above the water, 17.06.2015; http://weldworld.ru/news/razraborki/5583-3d-svarka-ot-mx3d-raspechataet-most-nad-vodoy.html

USING THE THEORY OF GROWING BODIES IN CALCULATION OF STRESS-STRAIN STATE OF THE PARTS MANUFACTURED APPLYING ADDITIVE CLADDING TECHNOLOGIES

I.K. SENCHENKOV[1], **I.A. RYABTSEV**[2], **E. TURYK**[3] and **O.P. CHERVINKO**[1]

[1]S.P. Timoshenko Institute of Mechanics, NASU
3 Nesterov Str., 03057, Kiev, Ukraine. E-mail: ang@imech.freenet.kiev.ua
[2]E.O. Paton Electric Welding Institute, NASU
11 Kazimir Malevich Str., 03680, Kiev, Ukraine. E-mail: office@paton.kiev.ua
[3]Institute of Welding
16-18 Bl. Czeslaw Str., 44-100, Gliwice, Poland. E-mail: eugeniusz.turyk@gliwice.pl

Proceeding from the theory of growing bodies and unified model of flow, a model was developed for assessment of thermomechanical state of the part in multilayer cladding, as well as finite-element procedure of numerical realization of the model. In the case of cladding (building-up) a cylinder along its side surface it was established that the schematic of one-time building-up allows rather quickly obtaining qualitative evaluations of the level of stresses and strains at analysis of different variants of technological solutions for multilayer cladding of parts. However, it does not allow for the significant inhomogeneity and cellular structure of distributions, but just describes the smooth averaged change of characteristics of stresses and strains along the cylinder. It does not even allow studying such fine technological points as influence of different schematics of deposited bead overlapping on stress-strain state of the part. In this case, it is recommended to use the procedure of calculation by the schematic of bead-by-bead building-up (deposition). Generally satisfactory agreement of calculated and experimental data is indicative of the validity and reliability of the developed approach to modeling the thermomechanical processes in multilayer cladding of parts. 14 Ref., 9 Figures.

Keywords: cladding, additive technologies, theory of growing bodies, stress-strain state, residual stresses, deposited beads, deposited layers

By the generally accepted definition, additive technologies are technologies of manufacturing complex-shaped parts by 3D computer model by successive layer-by-layer deposition of material [1–4]. According to this definition, cladding can also be regarded as an additive technology. So far, however, at development of additive technologies with application of welding heat sources, attention was focused on laser and electron beam [5, 6]. Less attention was paid to other methods, in particular cladding, as additive technologies. Not enough attention at analysis was also given to the fact that layer-by-layer deposition of molten metal in additive technologies leads to formation of a certain stress-strain state (SSS) in finished parts, which may result in residual deformations or crack initiation in them.

Experimental methods of SSS investigation are expensive and labour-consuming processes, providing quite limited information. Therefore, development of models and procedures of mathematical modeling of stress-strain and microstructural state of the parts during incrementing, residual state, as well as stresses during operation, is a highly urgent task.

The objective of this work is development of a model and procedure of calculation of SSS of parts, manufactured with application of additive cladding technologies. The procedure is based on the theory of growing bodies [7], which simulates multilayer cladding process to the greatest extent [8].

Mechanical behaviour of material is described by Bodner–Partom model [9], which includes the following relationships in rectangular Cartesian system of coordinates *Oxyz:*

● law of flow and equation of plastic incompressibility

$$\dot{\varepsilon}_{ij} = \dot{\varepsilon}_{ij}^{p} + \dot{\varepsilon}_{ij}^{e}, \dot{\varepsilon}_{kk}^{p} = 0, \quad i, j = x, y, z; \quad (1)$$

● Prandtl–Reuss law of flow

$$\dot{\varepsilon}_{ij} = \frac{D_0}{J_2^{1/2}} \exp\left[-\frac{1}{2}\left(\frac{K_0 + K}{\sqrt{3J_2}} \right)^{2n} \right] s_{ij}, \quad (2)$$

where

$$J_2 = \frac{1}{2} s_{ij} s_{ij}; \quad s_{ij} = \sigma_{ij} - \frac{1}{3}\delta_{ij}\sigma_{kk};$$

$$\sigma_{kk} = \sigma_{xx} + \sigma_{yy} + \sigma_{zz};$$

● evolution equation for isotropic strengthening parameter

$$\dot{K} = m_1(K_1 - K)\dot{W}_p, \quad K(0) = 0, \qquad (3)$$

where $\dot{W}_p = \sigma_{ij}\dot{\varepsilon}_{ij}^p$; D_0, K_0, K_1, m_1, n are the model parameters;

● Hooke's law

$$\sigma_{kk} = 3K_V(\varepsilon_{kk} - 3\alpha(\theta - \theta_0)),$$
$$s_{ij} = 2G(e_{ij} - \varepsilon_{ij}^p), \quad e_{ij} = \varepsilon_{ij} - \frac{1}{3}\varepsilon_{kk}\delta_{ij}, \qquad (4)$$

where G, K_V, α are the moduli of shear, volume compression and coefficient of linear thermal expansion.

Relationships are complemented by universal equations of quasi-static equilibrium and heat conductivity, as well as respective boundary and initial conditions.

Two models of the process of multilayer cladding of parts are considered. The first is bead-by-bead layer-by-layer cladding (Figure 1, *a*), the second is one-time layer-by-layer cladding (Figure 1, *b*).

The first incremental model allows for deposition of each individual bead in each of the layers. In the second model, called one-time cladding, theory of growing bodies is used for modeling successive one-time deposition of each individual layer. The time interval between joining these beads or layers, their dimensions, material temperature, cooling time, etc. are selected from the condition of their equivalence to geometrical, energy and other parameters of technological process of cladding.

Two approaches are used in modeling of bodies growing during cladding. The first envisages plotting FE-mesh, which covers both the clad part, and all the layers to be deposited in the future. Thus, the number of nodes of FE-mesh does not change during numerical modeling. The essence of the second, more cost-effective approach consists in successive joining of incremental material elements. Here, the number of finite elements changes. The regions of cladding in the first approach or the clad element in the second approach are initially ascribed the properties of «void» material, which is regarded as thermoelastic material with the following characteristics:

$$E = 0; \quad \nu = 0,5; \quad \alpha = 0, \qquad (5)$$

where E is the modulus of elasticity, and ν is the Poisson's coefficient.

Value of Poisson's coefficient $\nu = 0.5$ was selected from the condition of correspondence to the properties of molten (incompressible) material, with which the element will be filled. Here, only forming deformation can occur. Thermophysical properties of the «void» are taken to be the same as those of deposited metal. Therefore, the element is «empty»
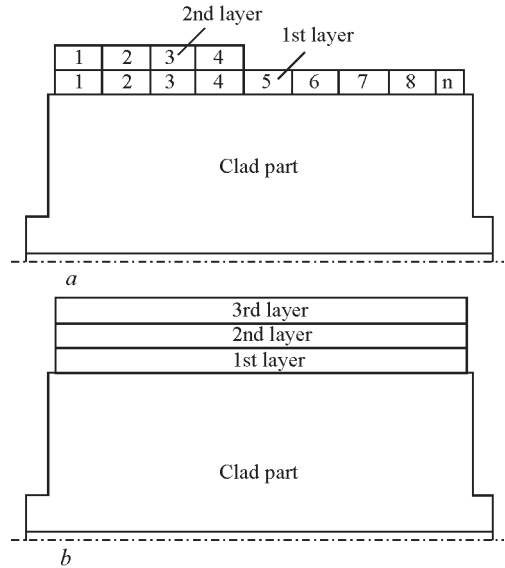
Figure 1. Schematics of models of multilayer cladding: *a* — bead-by-bead layer-by-layer (figures show bead numbers in the sequence of their deposition in each layer); *b* — one-time layer-by-layer

only in terms of mechanics. During filling, which is regarded as the process developing in time, «empty» elements of FE-mesh will be filled by material melt being deposited. The calculations allow for the fact that during element filling (cladding) the entire FE-mesh is deformed, both the one covering the part, and the «empty» elements.

Let at the moment of filling t^*, a certain empty element of mesh $\Delta V(t^*)$ adjacent to built-up surface have deformation ε_{ij}^*, and let it be filled with material melt of temperature θ^*, being non-stressed at the moment of filling. Then, in the clad element

$$\sigma_{ij} = 0, \quad i, j = x, y, z \text{ at } t = t^*. \qquad (6)$$

Condition (6) in terms of determining equation $\sigma_{ij} = \sigma_{ij}(\varepsilon_{kl}, \theta)$ can be written as $\sigma_{ij}(\varepsilon_{kl}^*, \theta^*) = 0$ in mesh element

$$\Delta V(t^*)i, j, k, l \leftrightarrow x, y, z. \qquad (7)$$

Equality (7) points to absence of stresses (condition (6)) in clad element ΔV, which has initial deformation ε_{ij}^* at filling temperature θ^*.

It is assumed that non-elastic deformation of deposited metal is absent at moment of time t^* of mesh element filling:
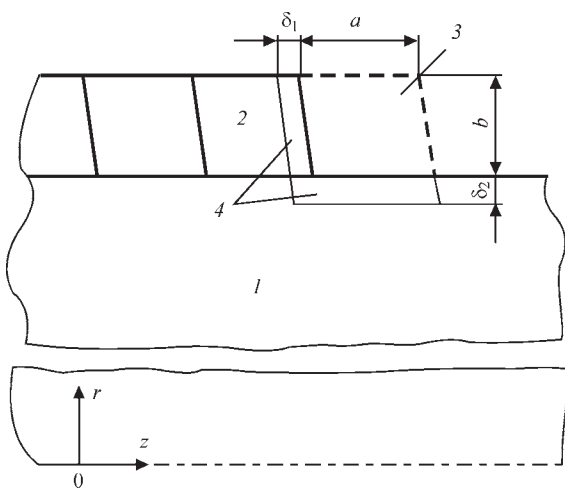
$$\varepsilon_{ij}^p(t^*) = 0 \text{ in mesh element } \Delta V(t^*). \qquad (8)$$

To satisfy conditions (2) and (3), it is necessary at $t > t^*$ to modify the equation of Hooke's law for isotropic material (4) as follows:

$$s_{ij} = 2G_f(e_{ij} - \varepsilon_{ij}^p - e_{ij}^*),$$
$$\sigma_{kk} = 2K_f(\varepsilon_{kk} - \varepsilon_{kk}^* - 3\alpha_f(\theta - \theta^*)), \qquad (9)$$

and to assume in equations (2) and (3):

Figure 2. Schematic of filling (cladding) of N-th bead: *1* — part; *2* — earlier deposited $(N–1)$-th bead; *3* — region responsible for next N-th bead, which is to be filled (before filling — «empty» region); *4* — regions of subsurface volume heated by welding arc in the part and in earlier deposited bead; δ_1 — width of heated region in material of $(N–1)$-th bead during deposition of N-th bead; δ_2 — width of heated region in base metal during deposition of N-th bead (dash-dot line — part axis)

$$\varepsilon_{ij}^{p}(t^*) = 0, \quad K(t^*) = 0, \quad K_0(t^*) = K_{0f}(\theta^*). \quad (10)$$

Here, lower index f indicates that the parameters pertain to deposited layer material.

Thus, in order to satisfy condition (6) in subsurface built-up layer, for all elements of clad material determining equations (1)–(4) are individualized by those specific values of strain ε_{ij}^{*} and temperature θ^*, at which their filling occurred at moment of time $t = t^*$.

As an example, let us consider spiral cladding of side surface of a cylinder. The schematic of deposited layer filling by individual beads in meridian section (see Figure 1, *a*) is given in Figure 2.

Let the start of deposition of N-th bead correspond to moment of time $t = t_N$. The process is realized in the following sequence:

1. In time interval $(t_N, t_N + t_Q)$, where t_Q is the effective time of source operation, simultaneous heating of the following regions takes places: (*a*) — «empty» region *3* by uniformly distributed heat source of power Q_K (index K means cladding); (*b*) — adjacent region *4* by welding arc, which is a bulk heat source of power Q_L (index L means arc).

2. At moment $t_N = t_N + t_Q$ both the sources switch off and «filling» of region *3* occurs, which is understood to be replacement in this region of «empty» material with (1) properties by material described by system of equations (1)–(4), allowing for modifications (9) and (10), where ε_{ij}^{*} and θ^* are the strains and temperatures in nodal points of region *3* at the moment of filling.

3. In time interval (t_{N+Q}, t_{N+1}) cooling takes place due to heat conductivity in-depth of the part and heat exchange with the environment.

4. At moment of time $t = t_{N+1}$ a new mechanically «empty» element is joined and the process is repeated.

Heat coming to the body at cladding is determined by the following relationship:

$$\overline{Q} = \eta_T(\eta_{\dot{E}} + \eta_{\dot{Y}})IU\Delta t_1 = \overline{Q}_{\dot{E}} + \overline{Q}_{\dot{Y}}, \quad (11)$$

where η_T is the effective power coefficient; $\eta_{\dot{E}}$ is the effective efficiency of part heating by the arc; $\eta_{\dot{Y}}$ is the effective efficiency of heating by electrode metal drops; $\overline{Q}_{\dot{E}}$ and $\overline{Q}_{\dot{Y}}$ are the heats transferred to the part body by the arc and coming to the electrode:

$$\overline{Q}_{\dot{E}} = \eta_T\eta_{\dot{E}}IU\Delta t_1, \quad \overline{Q}_{\dot{Y}} = \eta_T\eta_{\dot{Y}}IU\Delta t_1, \quad (12)$$

where Δt_1 is the time of deposition of a number of beads, which is determined, proceeding from geometrical dimensions of clad surface and deposition rate.

Respective bulk powers of heat sources are calculated by the following formulas:

$$Q_{\dot{E}} = \frac{\overline{Q}_{\dot{E}}}{V_{\dot{E}}t_Q}, \quad Q_{\dot{Y}} = \frac{\overline{Q}_{\dot{Y}}}{V_{\dot{Y}}t_Q}, \quad (13)$$

where $V_{\dot{E}}$ is the volume of the region, in which the heat source operates, derived by rotation of plane figure *4* or *3* of meridian section about the part axis; $V_{\dot{Y}}$ is the volume of the region derived by rotation of figure *3* (see Figure 2); t_Q is the effective time of heat source operation.

The following values of the set of geometrical parameters are assumed for filling schematic (see Figure 2): $\delta_1 = 10^{-3}$ m; $\delta_2 = 0.5\cdot10^{-3}$ m; a and b parameters were determined by bead width and height. Values of δ_1, δ_2, and t_Q were selected using numerical experiment from the condition of approximate equality of temperatures in volumes $V_{\dot{E}}$ and $V_{\dot{Y}}$ at the moment of filling of the region of bead *3* by molten material.

The following values of the given parameters were assumed at determination of heat input [8]: $\eta_T = 0.6$; $\eta_{\dot{E}} = 0.8$; $\eta_{\dot{Y}} = 0.2$. Calculations were performed using physico-mechanical characteristics of respective materials. Boundary problem of thermomechanics was solved by FEM. Detailed description of numerical procedure is given in [10–12].

We will give comparison of the results of calculation of residual SSS, derived in terms of schematics of gradual and one-time building-up (see Figure 1).

A cylinder from steel 35KhM built-up by two layers of Cr–Ni steel 10Kh18N10 with austenitic-ferritic structure is considered as an example. Cylinder diameter $D = 0.126$ m, and length is $L = 0.25$ m. Thickness of the first and second layers is the same and equal
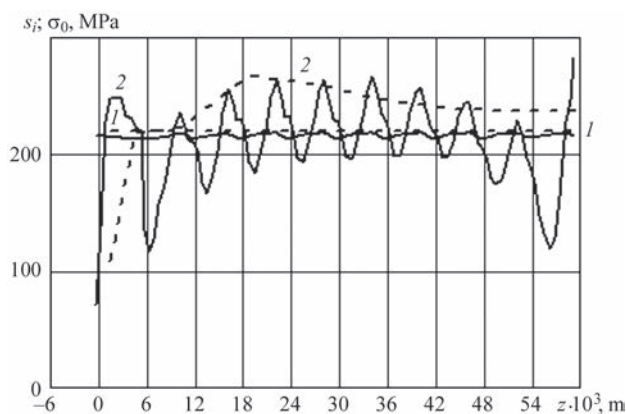
Figure 3. Intensity of stresses s_i (*1*) and mean stress σ_0 (*2*) in the first deposited layer after deposition of the second layer

to 2.3 mm. Cladding is performed with preheating to $\theta = 300$ °C.

In the schematic of gradual building-up 10 beads are deposited in each layer to reduce the volume of computations. Calculations showed that the end effects are localized in the zones of the first and the last three beads. Therefore, in the region between the third and seventh beads residual SSS is in place, which can be associated with the region of regular state of the main part of fully built-up cylinder.

Intensity of stress tensor deviator

$$s_i = J_2^{1/2},$$

non-elastic deformation intensity

$$\varepsilon_i^p = \left(\frac{1}{2} e_{ij}^p e_{ij}^p \right),$$

and mean normal stress

$$\sigma_0 = (\sigma_{rr} + \sigma_{zz} + \sigma_{\varphi\varphi}) / 3$$

are used as SSS characteristics.

Intensity s_i is responsible for non-elastic processes and fracture by ductile mode. Mean stress generally identifies tension ($\sigma_0 > 0$) or compression state.

Figures 3 and 4 show the distributions of SSS characteristics along Oz line at $r = 0.064$ m (half of first layer thickness) (here and below solid lines cor-
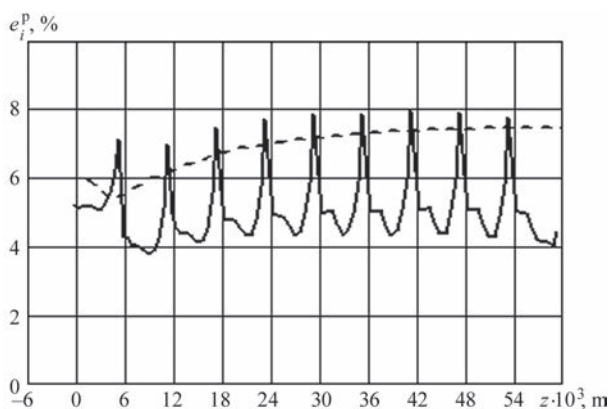
Figure 4. Intensity of residual non-elastic strains in the first deposited layer after second layer deposition
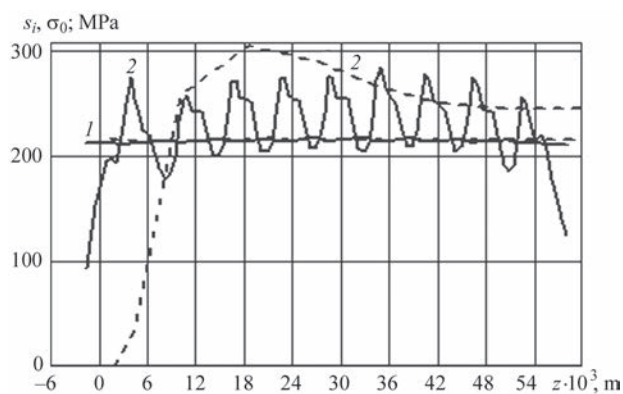
Figure 5. Intensity of stresses s_i (*1*) and mean stress σ_0 (*2*) in the second deposited layer

respond to the schematic of bead-by-bead deposition, and dash lines indicate one-time layer-by-layer deposition).

Distributions along the median line $r = 0.064$ m of residual stresses and strains, which formed in the second built-up layer after its cooling to 20 °C, are represented in Figures 5 and 6.

Analysis of presented results leads to the following conclusions:

1. Schematic of one-time layer-by-layer building-up does not allow for the non-uniform cellular structure of distributions, but describes a smooth averaged change of stress and strain characteristics along the built-up cylinder.

2. Schematic of one-time layer-by-layer building-up corresponds to more extended zones of end disturbances of SSS.

3. In the region of regular distribution of SSS characteristics, calculation results for one-time layer-by-layer schematic are in satisfactory agreement with the results derived on the basis of bead-by-bead deposition schematic. For this reason, the instant layer-by-layer schematic can be used in simplified calculations.
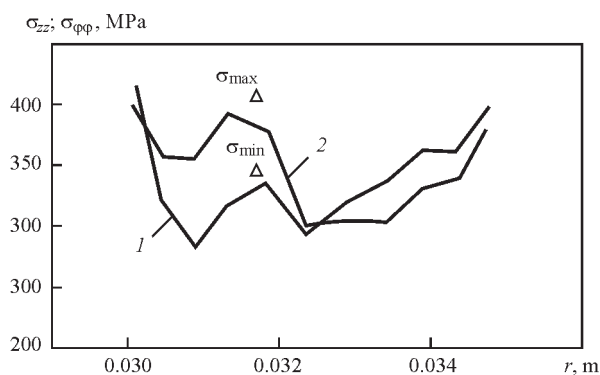
Results of numerical modeling are compared with experimental data. Measurements were performed by hole-drilling method [13, 14].
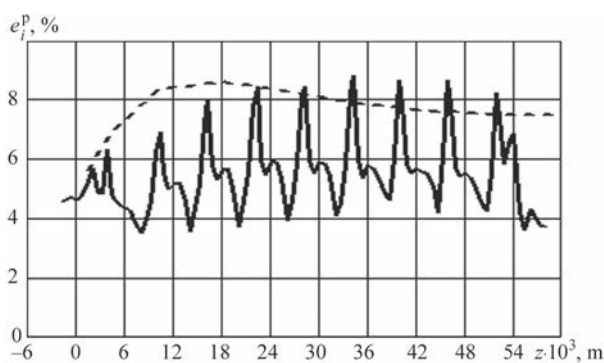
Figure 6. Intensity of residual non-elastic strains in the second deposited layer
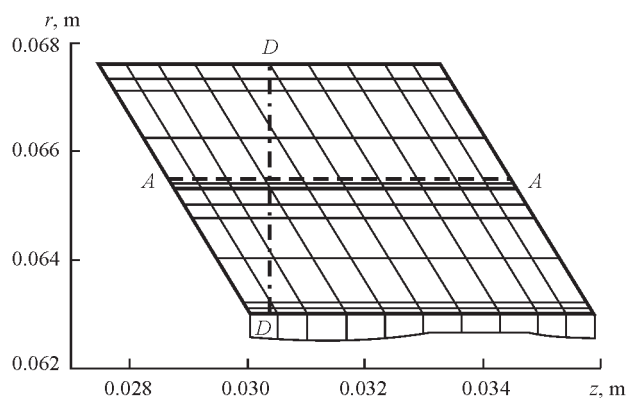
Figure 7. Schematic fragment of deposited layers: *dash-dot line D–D* — hole axis; *dashed line A–A* — hole depth; *thin lines* — FE-mesh

Figure 8. Axial (*1*) and circumferential (*2*) stress along line *A–A* in deposited layer fragment given in Figure 7

Investigations were conducted on sixth bead at two-layer bead-by-bead deposition of layers. Respective fragment of built-up layer is shown in Figure 7. Holes of 1.6 mm diameter were drilled to depth $\Delta r = 2.2$ mm in the center of the bead located in section $z = 0.0304$ m, to measure the residual stresses.

Figure 8 shows calculated axial distributions of components σ_{zz} and $\sigma_{\varphi\varphi}$ in section *A–A*. Triangles indicate experimental values of maximum and minimum principal stresses σ_{min} and φ_{max}. It is seen that stress components change quite significantly within the bead. However, good agreement of data is in place in the considered section.

It is more convenient to perform comparison with application of radial stress distributions in built-up layer. According to experimental procedure, measured stresses correspond to and should be compared with the following calculated values in this section:

$$\sigma_{min} = \Big\langle \min \big(\sigma_{zz}(r), \sigma_{\varphi\varphi}(r)\big)\Big\rangle_{\Delta r},$$

$$\sigma_{max} = \Big\langle \max \big(\sigma_{zz}(r), \sigma_{\varphi\varphi}(r)\big)\Big\rangle_{\Delta r}.$$

Here, $\langle f(r)\rangle_{\Delta r}$ designates the following value averaged by hole depth:
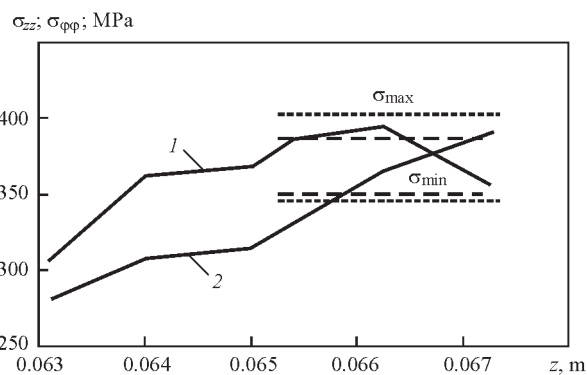
Figure 9. Distribution of residual axial σ_{zz} (*1*) and circumferential $\sigma_{\varphi\varphi}$ (*2*) stresses across deposited layer thickness in section $z = 0.0304$ m: *dotted lines* — experimental values of principal stresses averaged over thickness in deposited layer; *dashed lines* — calculated values of these parameters

$$\langle f(r)\rangle = \frac{2}{r_0^2 - (r_0 - \Delta r)^2} \int_{r_0 - \Delta r}^{r_0} f(r)r\,dr,$$

where r_0 is the outer radius of built-up bead.

Figure 9 shows the calculated distributions along the radius of components of stresses σ_{zz} and $\sigma_{\varphi\varphi}$ in the studied section.

One can see that maximum and minimum principal stresses are not related to any one component. So, component $\sigma_{\varphi\varphi}$ prevails on the surface, and in deeper-lying layers the maximum value is determined by component σ_{zz}.
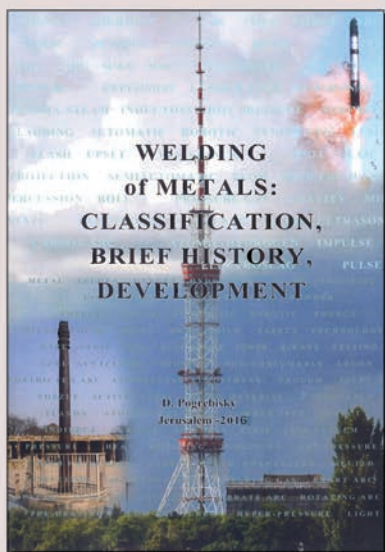
Conclusions

1. Theory of growing bodies and unified model of flow were used as the basis for development of the model of evaluation of thermomechanical state of the part during multilayer cladding, as well as FE procedure of numerical realization of the model. Generally satisfactory agreement of calculated and experimental data is indicative of validity and reliability of the developed approach to modeling the thermomechanical processes in multilayer cladding.

2. In the case of cladding (building-up) a cylinder along its side surface it is found that the schematic of one-time building-up allows quickly enough deriving qualitative evaluation of the level of stresses and strains at analysis of different variants of technological solutions for multilayer cladding of parts. It, however, does not allow for the considerable non-uniform and cellular structure of distributions, but just describes the smooth averaged change of stress and strain characteristics along the cylinder. It does not allow studying such fine technological points as the influence of different schematics of deposited bead overlapping on the part SSS. In this case, it is recommended to apply the procedure of calculation by the schematic of bead-by-bead building-up (deposition).

1. Balyakin, A.V., Smelov, V.G., Chempinsky, L.A. (2012) Application of additive technologies for development of combustion chamber parts. *Vestnik SamaraGAKU*, 34(**3**), 47–51.
2. Marya, S., Hascoet, J.Y., Panigrah, S.K. et al. Additive manufacturing, derivative of welding and joining technology: A literature review. *IIW Doc. XII-2185–14; IV-1195–14*.
3. Smurov, I.Yu., Konov, S.G., Kotoban, D.V. (2015) About implementation of additive technologies and production in national industry. *Novosti Materialovedeniya. Nauka i Tekhnika*, 14(**2**), 11–20.
4. Kovalev, O.B. (2015) Fundamental problems of modeling and diagnostics of processes in laser technologies of additive production of 3D metal pieces. In: *Proc. of 11th All-Union Congress on Fundamental Problems of Theoretical and Applied Mechanics* (Kazan, Russia, 20–24 Aug. 2015), 1836–1838.
5. Makhnenko, V.I., Kravtsov, T.G. (1976) *Thermal processes in mechanized surfacing of parts of circular cylinder type*. Kiev: Naukova Dumka.
6. Makhnenko, V.I., Velikoivanenko, E.A., Kravtsov, T.G. et al. (2001) Numerical studies of thermomechanical processes in surfacing of shafts of ship mechanisms. *The Paton Welding J.*, **1**, 2–10.
7. Arutyunyan, N.Kh., Drozdov, A.D., Naumov, V.E. (1987) *Mechanics of growing of viscous-elastic-plastic bodies*. Moscow: Nauka.
8. (2006) *Technology of welding, brazing and cutting*: Encyclopedia, Vol. III-4. Ed. by B.E. Paton. Moscow: Mashinostroenie.
9. Bodner, S.R. (2000) *Unified plasticity — an engineering approach:* Final report. Haifa: Israel IT.
10. Ryabtsev, I.A., Senchenkov, I.K. (2013) *Theory and practice of surfacing operations*. Kiev: Ekotekhnologiya.
11. Ryabtsev, I.A., Senchenkov, I.K., Turyk, E. (2015) *Surfacing, materials, technologies, mathematical modeling*. Gliwice: Silesia PI.
12. Senchenkov, I.K., Ryabtsev, I.A., Turyk, E. et al. (2005) Calculation of residual stresses in multilayer helical cladding of cylindrical parts on the base of theory of growing of viscous-plastic bodies. *Svarochn. Proizvodstvo*, **9**, 18–25.
13. *ASTM Standard E 837*: Standard test method for determining residual stresses by the hole drilling strain-gage method.
14. (1993) *Measurement of residual stresses by the hole drilling strain gage method*. Measur. Group Inc. Tech. Note.

ELECTRON BEAM 3D-DEPOSITION OF TITANIUM PARTS

S.V. AKHONIN, E.L. VRZHIZHEVSKY, V.Yu. BELOUS and **I.K. PETRICHENKO**

E.O. Paton Electric Welding Institute, NASU

11 Kazimir Malevich Str., 03680, Kiev, Ukraine. E-mail: office@paton.kiev.ua

At present 3D-printing and additive technologies are given a lot of attention in research centers all over the world. In connection with the fact that titanium is a reactive metal, electron beam technologies appear to be the most promising for development of the technology of metal 3D-deposition of parts from titanium-based alloys. The work is a study of the possibility of development of electron beam deposition of complex shapes from commercial titanium. Deposition was performed with application of 2-coordinate manipulator and moving work table, the part was formed on a titanium substrate, titanium welding wire of VT1-00 grade was used as filler material. Parts of rectilinear shape of 35 mm height and of cylindrical shape of 45 mm height with 10 mm wall thickness were produced. Deposited layer structures were studied, and absence of metal porosity in cylindrical and rectilinear deposits was noted. Structure of deposited metal layers is similar to that of cast metal of commercial titanium VT1-0. Microhardness of metal of the part produced by electron beam 3D-deposition with application of VT1-00 welding wire corresponds to the level of micorhardness of cast metal of commercial titanium VT1-0. It is shown that electron beam deposition technology allows producing parts of a complex shape from titanium of a homogeneous structure. 4 Ref., 9 Figures.

At present 3D-printing and additive technologies are given a lot of attention in research centers all over the world [1]. In case of fabrication of metal parts, technologies are developed, which use laser (so-called SLS-technologies [2]) or electron beam as the heat source. Sciaky Company specializing on development of welding technologies and equipment is developing a technology, according to which the part is created by the method of layer-by-layer deposition of material in the melt, formed by the electron beam (so-called Electron Beam Direct Manufacturing) [3].

In connection with the fact that titanium is a reactive material, EB technologies in the vacuum chamber,

Figure 1. Schematic of EB 3D-deposition of body of revolution with application of continuously maintained pool: *1* — manufactured item; *2* — manipulator; *3* — EB gun; *4* — rod of feed mechanism holder; *5* — feed mechanism; *6* — rotary table with vertical displacement mechanism

providing the most reliable protection of molten and cooling metal, are seen by us as the most promising for development of the technology of direct manufacturing of metal parts from titanium by 3D-deposition of metallic materials [4]. In this case, it is possible to use standard welding consumables, widely applied for performance of welding and surfacing operations.
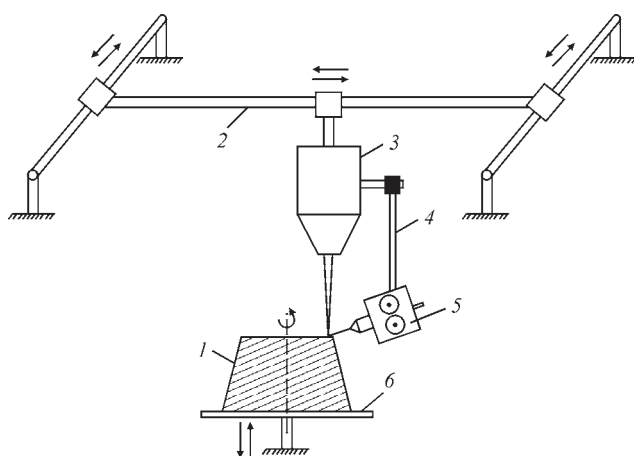
The objective of the work was studying the possibility of producing parts from a titanium alloy by the method of EB 3D-deposition with application of titanium-based filler wires.

EB 3D-deposition was performed in upgraded UL-144 unit, fitted with ELA 60/60 power unit, special welding gun and specialized feed mechanism for feeding the filler wire in electron beam chamber.

During performance of the work, the possibility of manufacturing two types of parts was studied, namely of the shape of body of revolution, and of rectilinear shape.

Application of the body of revolution to manufacture 3D-parts is a simpler task. Performed studies allowed optimizing the technology of 3D-deposition with application of continuously maintained molten metal pool. Schematic of the process of EB 3D-deposition of the body of revolution is shown in Figure 1.

Continuously maintained pool of molten metal was used at 3D-deposition of the part — sleeve, which is the body of revolution. During 3D-deposition of the body of revolution, the EB gun moves in the horizontal plane together with the mechanism for feeding filler metal in the form of wire. The part is
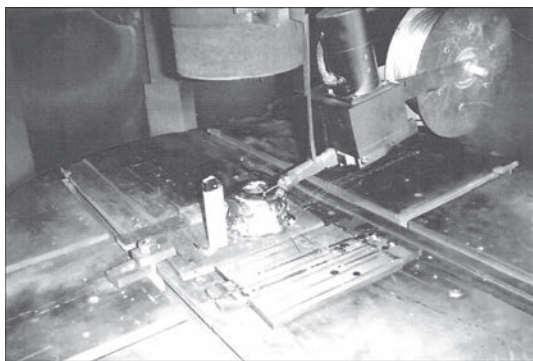
Figure 2. Position of the part of the shape of body of revolution and filler wire feed mechanism in the chamber of EB unit

formed on a water-cooled forming substrate, making rotational motion. As the layer is deposited, the table with the fixed part and water-cooled forming substrate moves downwards. Here, the distance between the filler wire and EB gun cathode is fixed, and does not change during the process of making of the entire part. An example of the part, having the shape of the body of revolution, is shown in Figures 2 and 3.

However, technological capabilities of the method of 3D-deposition with application of continuously maintained pool are limited. Technology of layer-by-layer 3D-deposition with application of periodically formed molten metal pool opens up many more possibilities.

A technique was experimentally worked out to make a part of a rectilinear shape, which is a vertical wall, formed on a metal substrate. In 3D-deposition of a rectilinear part, EB gun and feed mechanism move in the horizontal plane, here the distance between the filler wire and EB gun cathode is also fixed, and does not change during the process of manufacturing of the entire part. As the layer is deposited, the table with the fixed part and substrate moves downwards. Beam scanning and focusing were performed by a special program, to ensure the required dimensions of molten metal pool.

In the case of 3D-deposition of a part of a rectilinear shape, after deposition of the next layer, molten metal pool was formed in the starting point anew.
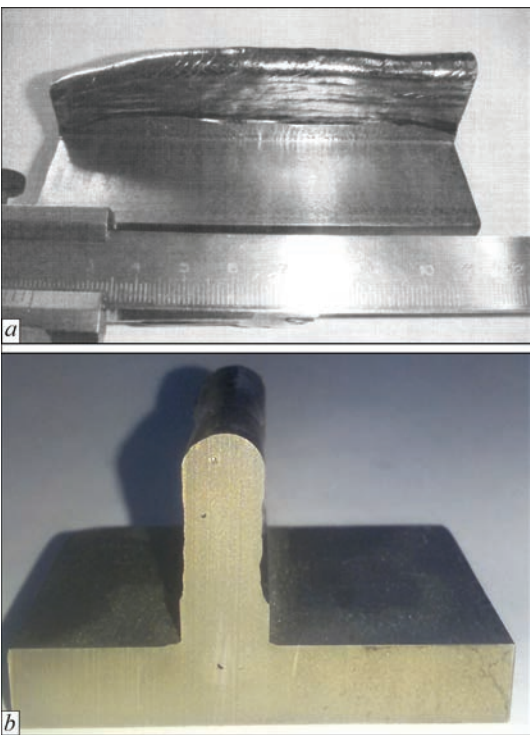
Figure 4. Sample of rectilinear-shaped part manufactured by EB 3D-deposition with application of periodically formed molten metal pool: *a* — appearance; *b* — rectilinear part cross-section

3D-deposition of a rectilinear-shaped part was performed on a substrate of titanium of VT1-00 grade 10 mm thick. During deposition, the substrate moved in the vertical direction, and the EB gun and feed mechanism moved in the horizontal plane. Number of layers required for the wall of a part of 35 mm height and 8 mm width was 18 passes. Filler wire feeding, creation of molten metal pool and pool movement over the formed part surface were performed by an automatic complex program. The program allows changing the height and width of the formed part wall in a broad range. An example of a rectilinear-shaped part is given in Figure 4.

Conducted studies of manufactured parts showed that in the case of application of VT1-00 welding wire as building material for EB 3D-deposition, and of commercial titanium VT1-00 10 mm thick as the substrate material, the deposited layer structure is similar
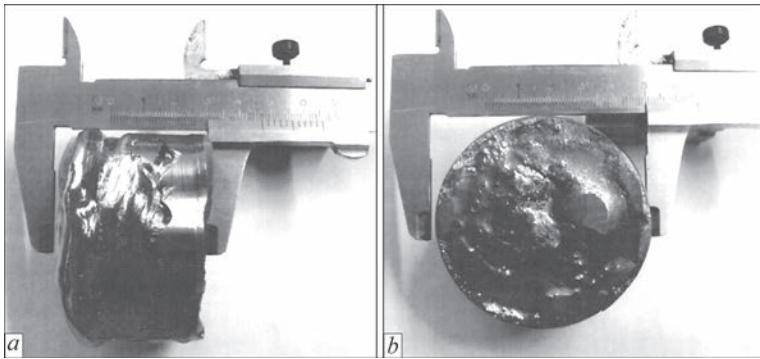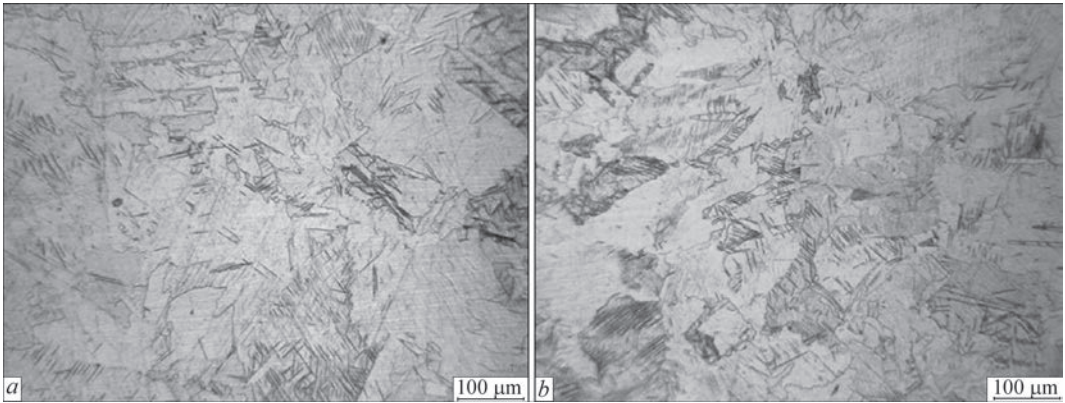

Figure 3. Appearance of the part of the shape of body of revolution: *a* — side view; *b* — top view
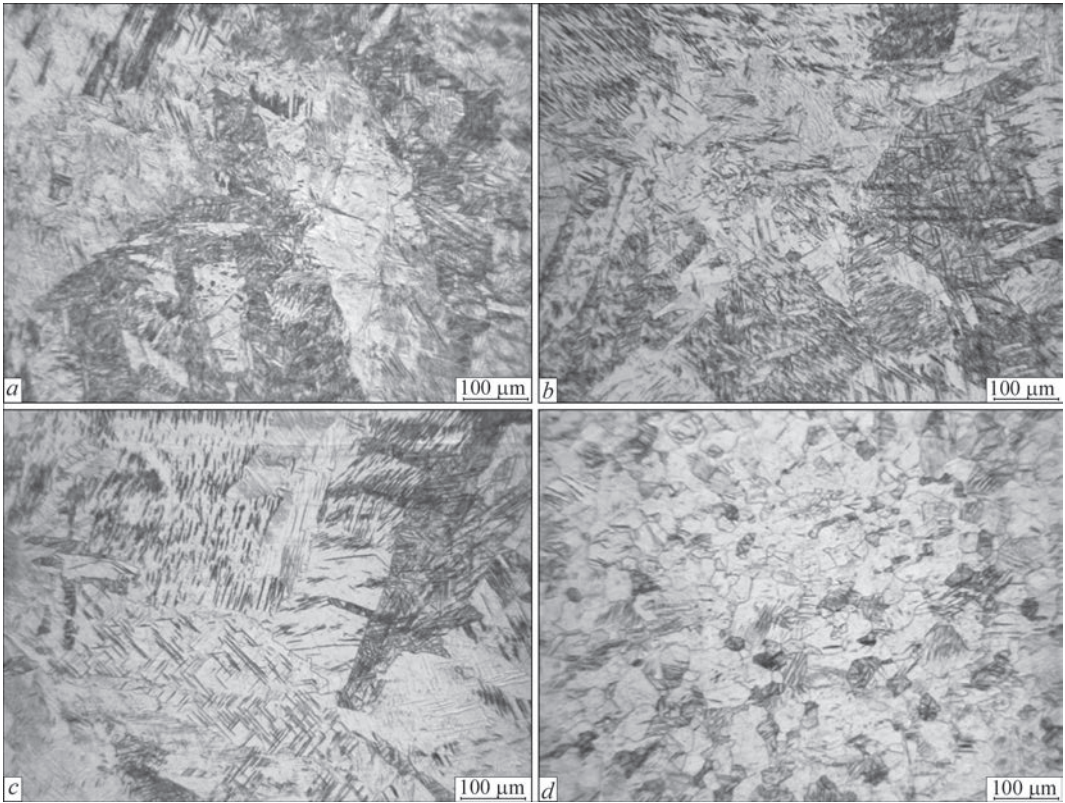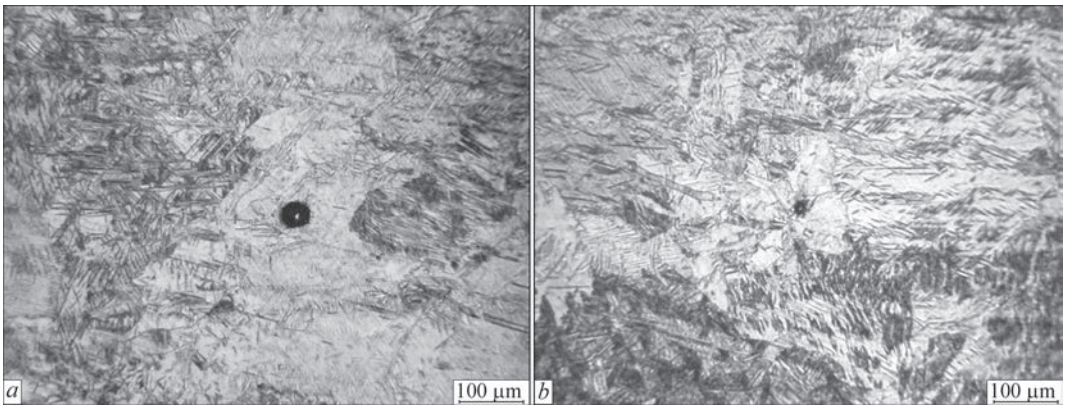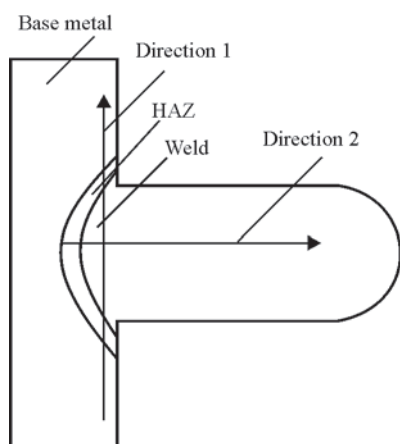
Figure 5. Structure of metal of a rectilinear part manufactured by EB 3D-deposition: *a–c* — deposited metal*; d* — substrate metal

Figure 6. Structure of HAZ metal of a rectilinear part made by EB 3D-deposition: *a* — near deposited metal; *b* — near substrate metal

Figure 7. Structure of deposited metal of a rectilinear part made by EB 3D-deposition

Figure 8. Schematic of measurement of microhardness of deposited metal of a rectilinear part made by EB 3D deposition

to that of cast metal of the base alloy. Deposited metal of filler wire of VT1-00 grade consists of coarse irregular-shaped grains with serrated boundaries (Figure 5, *a–c*), grain size being 0.5–3.0 mm, and most of the grains have twins. Substrate metal has more fine-grained structure and consists of equiaxed grains of α-phase of 10–50 μm size (Figure 5, *d*) with twins present in some grains.

Despite the fact that deposition was performed in several layers, no fusion zones between the layers are revealed structurally in the cross-section. Figure 6 presents microstructures of the metal of HAZ from the deposit. HAZ region, where the metal went through phase recrystallization during deposition, consists of grains of irregular shape with serrated boundaries, similar to deposited metal. Size of HAZ grains decreases with greater distance from the deposited metal (Figure 6). Twins are also present in HAZ metal grains. No defect, characteristic for EBW, such as microporosity, was found during deposited metal examination.

However, one pore of about 35 μm diameter (Figure 7, *a*) and several fine pores of less than 10 μm diameter (Figure 7, *b*) were detected, when studying deposited metal of rectilinear part of 10×25 mm cross-section. No other defects were found. Small number of pores is, probably, attributable to greater duration of molten metal pool existence, compared to welding modes.

Measurement of microhardness of deposited metal of a rectilinear part (Figure 8), made by EB 3D-depo-
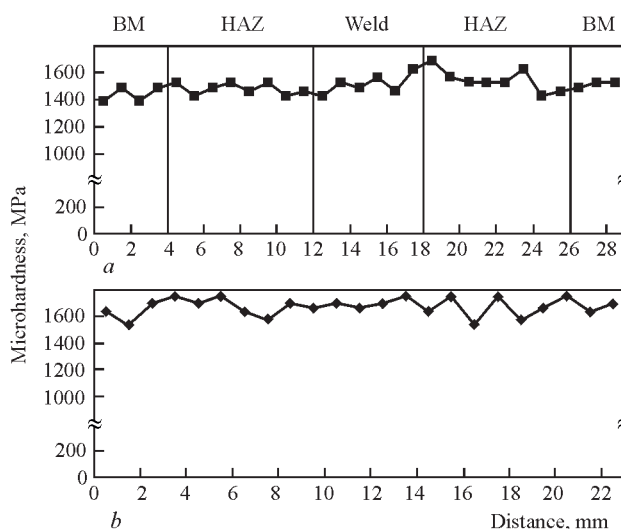
Figure 9. Microhardness of deposited metal of a rectilinear part manufactured by EB 3D-deposition in direction 1 (*a*) and 2 (*b*) (acc. to Figure 8)

sition, showed that its microhardness is on the level of substrate metal, that leads to the assumption that mechanical properties of deposited part metal will correspond to the level of cast metal of base titanium alloy (Figure 9).

Conclusions

1. A technique of 3D-deposition was developed which allows manufacturing two types of parts of the shape of bodies of revolution and of rectilinear shape.

2. In the case of application of titanium α-alloy VT1-00 as base metal, deposited layer structure is similar to that of cast metal of base titanium alloy.

3. Microhardness of metal of the part made by EB 3D-deposition corresponds to the level of microhardness of cast metal of base titanium alloy.

1. Hideki Kyogoku (2015) The current status and outlook for metal additive manufacturing in Japan. *Metal Additive Manufact.,* 1(**3**), 31–39.
2. Dutta, B., Froes, F.H. (2015) The additive manufacturing (AM) of titanium alloys. In: *Titanium powder metallurgy*, 447–468.
3. Xiaoqing Wang, Xibing Gong, Kevin Chou (2015) Scanning speed effect on mechanical properties of Ti–6Al–4V alloy processed by electron beam additive manufacturing. In: *Proc. of 43rd North American Manuf. Res. Institution of SME*, Vol. 1, 287–295.
4. Whittaker, D. (2015) Development in the additive manufacturing of titanium at PM titanium. *Metal Additive Manufact.*, 1(**3**), 53–60.

APPLICATION OF ADDITIVE TECHNOLOGIES FOR GROWING LARGE PROFILED SINGLE CRYSTALS OF TUNGSTEN AND MOLYBDENUM

V.A. SHAPOVALOV, V.V. YAKUSHA, A.N. GNIZDYLO and **Yu.A. NIKITENKO**

E.O. Paton Electric Welding Institute, NASU
11 Kazimir Malevich Str., 03680, Kiev, Ukraine. E-mail: office@paton.kiev.ua

The paper considers application of additive welding technologies with regard to growing the super large single crystals of refractory metals. Main methods of tungsten and molybdenum single crystals production from liquid phase were analyzed. The perspectives of plasma-induction technology for growing the large plane single crystals of tungsten and molybdenum are shown. A process scheme of additive growth of the plane single crystals of refractory metals using plasma-induction method is described. It is determined that the developed method provides for the possibility of flexible regulation of thermal field of single crystal being grown. Application of local molten zone, formed by low power plasma arc with the parameters typical for welding processes, allows growing the tungsten large single crystals of 210×180×20 mm size. The crystals are formed under conditions of heating with inductor high-frequency field to the temperature typical for hot deformation range. Given are the results of investigation of structural perfection of the growing crystals which verify the fact that the conditions of single crystals formation in plasma-induction zone melting provide for higher quality of single-crystalline structure than the methods, in which additional heating (electron beam and plasma-arc) is not used. It is determined that the plasma-induction process is characterized by formation of the regular dislocation structures, for which dislocation coalescence in low-angel boundaries are typical. 9 Ref., 7 Figures.

K e y w o r d s : additive welding technologies, plasma-arc zone melting, tungsten and molybdenum single crystals, dislocation substructure

Growing the tungsten and molybdenum single crystals has own peculiarities related with physical properties of these metals, in particular, high melting temperature. Specifically high melting temperature determined two melting methods based on application of highly-concentrated heat sources, i.e. electron beam and plasma arc. The electron beam heating [1] gained the largest application in commercial production of single crystals.

A traditional scheme of tungsten single crystal growing is a non-crucible zone melting or methods of growing with floating zone (Figure 1). The crystals grown using indicated method have perfect structure
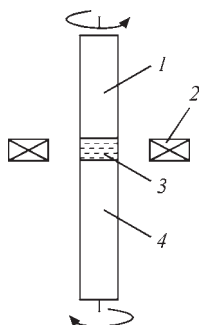
Figure 1. Scheme of vertical non-crucible zone melting: *1* — polycrystalline rod; *2* — heater; *3* — «floating» zone; *4* — single crystal

and smooth surface, irregularies and roughness of which depend on stability of process modes, namely stability of keeping the power, generated by ring-cathode EB gun, and stability of zone movement. However, at all relative simplicity of the growing method a serious drawback, namely crystal diameter limitation, was found. Increase of diameter rises EB gun power, molten zone volume, overheating temperature and possibility of melt run over. The process became unstable. The crystals produced with such a method had maximum diameter 25 mm for tungsten and 30 mm for molybdenum [2].

Found difficulties were partially solved by using a periphery zone melting. But, this method did not allow significant increase of diameter of grown crystals. Besides, diameter increase provoked rise of crystal stresses that resulted in deterioration of single-crystal structure [3, 4].

Application of low-temperature plasma and usage of modified Verneuil method (Figure 2) reviled the possibilities of technology development in scope of crystal diameter increase and capability of growing the profiled single crystals.

The crystals grown with the help of plasma arc heating had more rough surface, some geometry deviation was observed (Figure 3), and number of struc-
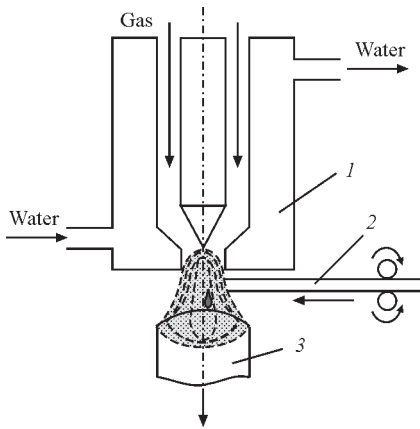
Figure 2. Scheme of growing the single crystals of refractory metals using plasma-arc heating: *1* — plasmatron; *2* — rod; *3* — crystal

Figure 4. Scheme of unit for additive growing the refractory metal single crystals using plasma-induction method: *1* — plasmatron; *2* — consumable rod; *3* — inductor; *4* — single crystal; *5* — hearth; *6* — rod feeder; *7* — plasma arc

tural disturbances was an order higher the same index for the crystals grown using EB heating [5].
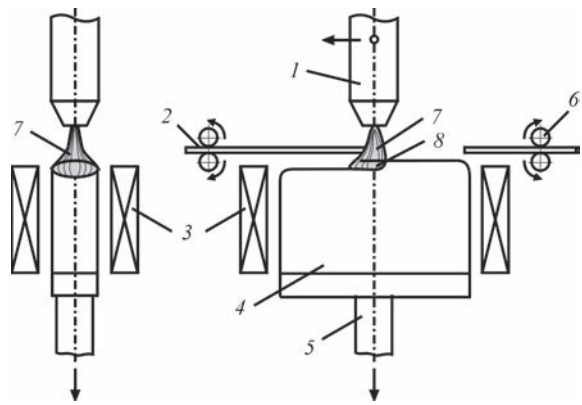
Further improvement of the technology of tungsten and molybdenum single crystal growing took place due to development at the PWI of a new method for growing the large single crystals by plasma-induction zone melting. The main differences of the method are heating of growing single crystal by high-frequency field energy, preventing the metal pool run over using electro-magnetic forces appearing at interaction of inductor current and current induced in the crystal, and the most important, layer-by-layer (additive) growth of single crystal due to movement of local metal pool, replenished by means of remelting of consumable polycrystalline rod (Figure 4).

Namely application of a local metal pool, formed by a low power plasma arc, with parameters typical for welding processes, allowed developing indicated method for growing super large profiled single crystals of tungsten and molybdenum of 210×180×20 mm size (Figure 5) [6].

Essence of the method lies in the fact that plasmatron by reciprocating motion moves a metal pool, which is replenished from remelted rods and forms a layer-by-layer crystal, reminding arc surfacing. After each plasmatron pass the single crystal moves downward per deposited layer height, thus, providing stable conditions, in which growing process takes place. The crystal is formed under conditions of heating by

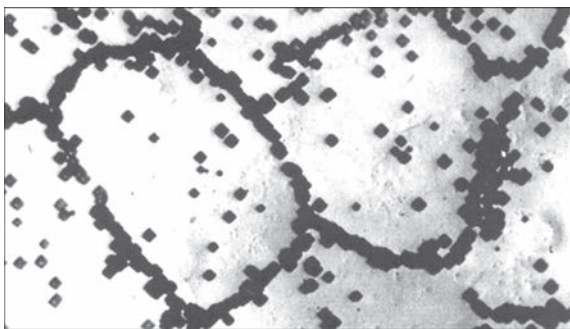high-frequency inductor field to temperatures typical for hot deformation range.

It is a well-known fact that dislocation displacement takes place at these temperatures under simultaneous effect of external stresses and temperature. The dislocations are not rigidly tightened to «their» slip plane and can migrate from one plane to another, selecting the easiest way. It is considered as additional degree of freedom of dislocation. Such an irregular dislocation movement rises the possibility of their hitting. Therefore, on the one hand, amount of cases of their annihilation (dislocation density decrease) rises, and, on the other hand, there is a tendency to formation of regular dislocation structures, for which coalescence of dislocations in low-angle boundaries is typical (Figure 6). The conditions of single crystal formation provides for higher quality of single-crystal structure than the methods, which do not use additional heating (electron beam and plasma arc) [7].

The crystals grown using indicted method have less smooth side surface, but it does not prevent their application without additional treatment as the billets for large-format rolling.

There are interesting results of crystal structure investigation using optical and X-ray methods. Fig-

Figure 3. View of tungsten single crystal grown using plasma-arc heating

Figure 5. Tungsten single crystals made by plasma-induction method

Figure 6. Microstructure (×400) of tungsten (flatness (001))

Figure 7. X-ray topogram of angle scanning of reflection: *a* — longitudinal; *b* — cross section of crystal

ure 7 shows the results of X-ray examination of single crystals.

The comparative investigations show that the structure of such crystals is more perfect than plasma-arc one, large macromosaic structure is virtually absent. Further accumulation of experimental facts allows optimizing regulation of structure formation in crystal growing.
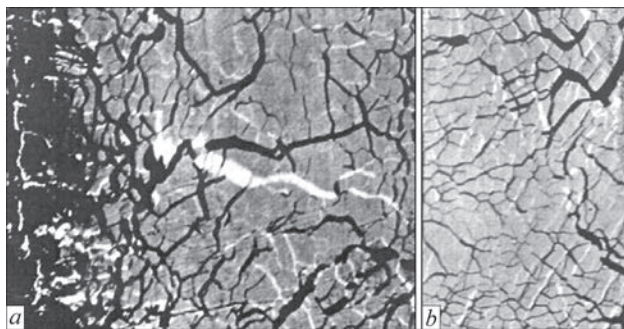
Development of additive welding technologies applicable to growth of super large single crystals allows creating new material and expanding it application in the following areas [8, 9]:

● X-ray devices (shields, anticathodes);

● electronics (targets for spraying, crucibles for growing oxides and nitrides single crystals);

● electrical engineering (connectors and wires);

● laser equipment (mirrors for optical and X-ray lasers);

● nuclear power engineering (thermionic converters of space power plants, ITER diverters, elements of active part);

● aerospace engineering (nozzle).

Conclusions

1. Analysis of existing opproaches for producing single crystals allows making a conclusion that the plasma-induction method does not have disadvantages typical for earlier developed methods, and provides for the widest possibilities for process of growing super large profiled tungsten single crystals.

2. Conditions of single crystal formation in plasma-induction zone melting provide for higher quality of single-crystal structure than the methods, in which additional heating is not used. Plasma-induction method is characterized by formation of regular dislo-

cation structures, for which coalescence in low-angel boundaries is mainly typical.

3. The most perspective directions in application of large oriented single crystals are heat and X-ray shields, ITER diverters, shells of emitters of thermionic converters of nuclear power units, mirrors of power lasers etc.

1. Manokhin, A.I., Burkhanov, G.S. (1987) State-of-the-art of problem of metal single crystals. In: *High-frequency and single crystal metallic materials*, 5–13. Moscow: Nauka.
2. Kervalishvili, I.D., Shchelkin, Yu.F. (1982) Heat conditions — factor determining the manufacturing of perfect crystals. *Fizika i Khimiya Obrab. Materialov*, **5**, 70–78.
3. Predtechensky, B.S., Starostina, L.S. (1972) Dislocations in molybdenum single crystals produced by zone melting. In: *Growth and defecfs of metal crystals*, 213–217. Kiev: Naukova Dumka.
4. Glebovsky, V.G., Semenov, V.N., Lomejko, V.V. (1987) Influence of crystallization conditions on structural perfection of tungsten single crystals. In: *High-pure and single-crystal metallic materials*, 38–42. Moscow: Nauka.
5. Savitsky, E.M., Burkhanov, G.S., Raskatov, N.N. (1978) Application of plasma heating for growing the single crystals of refractory metals. In: *Metal single crystals*, 5–10. Moscow: Nauka.
6. Shapovalov, V., Yakusha, V., Manulyk, A. (2015) Large refractory metals single crystals grown by plasma-induction zone melting. In: *Proc. of 24th Int. Materials Research Congress* (Cancun, Mexico, 16–20 Aug., 2015).
7. Shapovalov, V.A., Yakusha, V.V., Nikitenko, Yu.A. (2014) Investigation of temperature field of profiled tungsten single crystals made by plasma-induction method. *Sovr. Elektrometallurgiya*, **3**, 31–35.
8. Smirnov, V.P. (2008) Thermonuclear power as the major international innovative project. *Ros. Khimich. Zhurnal*, **6**, 79–94.
9. Filatov, O.G., Mazul, I.V. (2003) NII EFA experimental complex for simulation of operational factor of first wall of ITER reactor. *Voprosy Atomn. Nauki i Tekhniki*, **3**, 3–31.

3D ADDITIVE TECHNOLOGIES

doi.org/10.15407/tpwj2016.06.24

ADDITIVE MANUFACTURING OF METAL PRODUCTS (REVIEW)

V.V. ZHUKOV, G.M. GRIGORENKO and **V.A. SHAPOVALOV**
E.O. Paton Electric Welding Institute, NASU
11 Kazimir Malevich Str., 03680, Kiev, Ukraine. E-mail: office@paton.kiev.ua

Different characteristics of methods of additive manufacturing of metal products were considered. The prospects of technologies using metal wire as a consumable material were noted. The current state of research works in the field of additive manufacturing of layer-by-layer electric arc volumetric surfacing was shown. 20 Ref., 3 Tables, 10 Figures.

K e y w o r d s : additive manufacturing, prototyping, shape formation and structure control, laser surfacing using consumable wire, freeform fabrication using electron beam, electric arc volumetric layer-by-layer surfacing

The term «additive manufacturing» (AM) is used to define a group of technological methods of rapid prototyping, which allow creating solid, 3D products of different materials according to 3D computer model [1]. ASTM F2792-12A Standard provides definition to the term AM as the «method of joining materials, at which layer-by-layer creation of the object according to the preset digital three-dimensional model occurs». The first AM methods, which appeared in the early 1980s, were mainly specialized in manufacture of products of polymer plastics and rubbers. At present, these methods found a successful commercial application in such fields as aerospace production, mechanical engineering, medicine, architecture and design, consumer electronics, jewelry production and military industry [2–5]. Along with the development of AM methods using polymeric materials as consumables, the methods were also developed using metal alloys.

The possibility of manufacturing metal product of a final shape or a shape close to final one within a one technological operation is seen challenging in the field of direct manufacturing. The conventional field of application of manufacturing method at the other equal conditions can be represented as a dependence of form complexity on number of products. Figure 1 represents the area of AM application in the field of metallurgical manufacturing [6]. AM methods can be competitive if it is necessary to manufacture a small number of products or parts of complex shapes, or products with the specified structure.

As compared to classical methods of manufacturing (including machining on milling machine-tools with computer control (CNC), AM methods have certain advantages like:

● possibility of full automation of the process of product designing (including the stage of designing a digital 3D model), which reduces the number of man-hours required for fabrication of product, and reduces the total time of fabrication in general;

● competitiveness of AM methods application for manufacture of products of expensive titanium and nickel alloys because of the low coefficient of material consumption. This advantage is especially important in the aerospace industry and manufacture of parts, which are often characterized by high coefficients of material consumption (Figure 2).
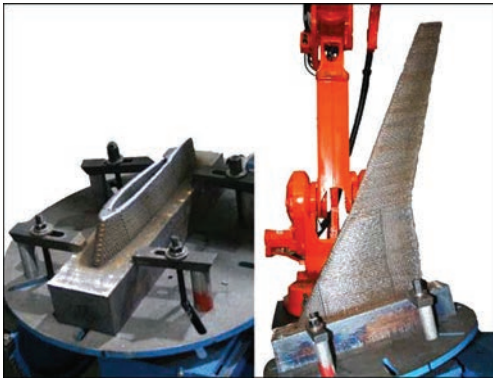
In Table 1 different AM methods are shown, grouped according to standard ASTM F2792. This standard assumes subdividing the AM methods in the field of manufacturing metal products according to the used principle based on melting (sintering) of powder bed; based on binder injection on the powder bed; based on surfacing using concentrated power source; based on laminating of sheet metal material.

It should be noted that the majority of methods were patented in the 1990s in connection with expi-
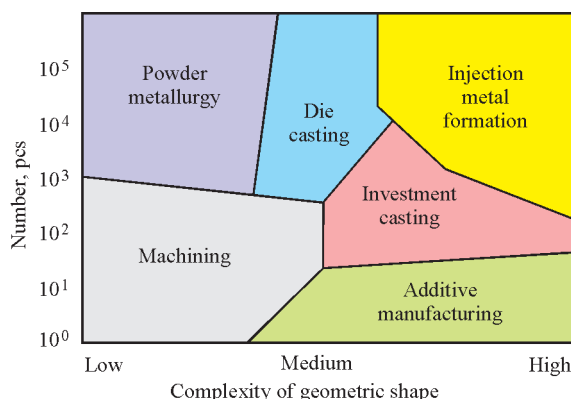
Figure 1. Quality position of AM application area relatively to the widespread methods of manufacturing [6]

© V.V. ZHUKOV, G.M. GRIGORENKO and V.A. SHAPOVALOV, 2016

ISSN 0957-798X THE PATON WELDING JOURNAL, No. 5-6, 2016 137

Figure 2. Model of wing designed according to WAAM technology [7]

ration of patents [3, 8], many variants of one and the same method appear. In Table 1 the names of methods most cited in the literature are given.

The methods of additive manufacturing of metal products have distinctive features. In Table 2 the comparison of some technological characteristics of different AM methods is presented.

The methods using powder as a consumable material are introduced wider at the moment as compared to the methods using wire as a consumable material due to the possibility of manufacturing products at a high geometric accuracy. In addition, the methods using metal powder allow producing products of powder metallic compositions, which is inherent to powder metallurgy. However, the efficiency of powder AM methods is very low, which is estimated by tens of grams per minute, which limits the possibility of their application for manufacture of large-sized products. In addition, the need in protection chamber and peculiarities of transportation and storage of metal powder
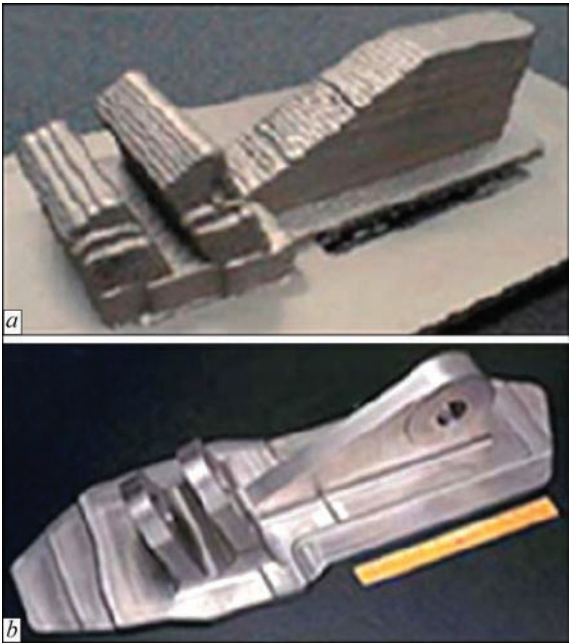
Figure 3. Semi-product (*a*) of part (*b*) manufactured by WFLB method

materials impose certain difficulties on application of powder AM methods. Laser engineered net shaping and the similar methods, using the principle of deposition by metal powder supplied in a jet of shielding gas to the area of laser beam action, although do not require the protective chamber for surfacing, nevertheless, because of spilling the powder, they require isolation of working area and individual protection for service personnel [6, 13].

AM methods using wire as a consumable material, as compared to powder AM methods possess 100 % efficiency of material use, as well as significantly

Table 1. Classification of AM methods according to the used principle

Principle	Name of method/original name	Consumable material
Fusion of powder bed	Selective laser sintering (SLS) [9]	Metallic powder
	Selective laser melting (SLM) [10]	
	Electron beam melting (EBM) [11]	
Injection of binder on powder bed	Powder bed and inkjet 3D printing (3DP) [12]	
Surfacing using concentrated power source	Laser engineered net shaping (LENS) [13]	
	Wire fed laser beam (WFLB) [14]	Wire
	Electron beam freeform fabrication (EBF$_3$) [15]	
	Wire and arc additive manufacturing (WAAM) [16]	
Lamination of metal sheets	Ultrasonic additive manufacturing (UAM) [17]	Sheet metal, foil

Table 2. Technological characteristics of some AM methods [6]

Used material	Name of method	Height of deposited layer, μm	Surfacing rate, g/min	Accuracy of performance, mm	Surface roughness, μm
Powder	LC*	–	1–30	(±0.025)–(±0.069)	1–2
	SLM	20–100		±0.04	9–10
	SLS	75	~0.1	±0.05	14–16
	DLF*	200	10	±0.13	~20
Wire	WAAM	~1500	12	±0.2	200
	EBF$_3$	–	Up to 330	Low	High
*Laser consolidation (LC) and Direct light fabrication (DLF) methods are the varieties of LENS method.					

Table 3. Results of mechanical tests of metal produced using electric arc additive surfacing

Orientation of specimen cutting out	Tensile strength, MPa	Elongation, %
Vertical	489	35.0
Horizontal (top)	484	22.5
Horizontal (bottom)	499	33.1

higher mass productivity, which justifies the application of methods for creating large-sized products. Despite the low accuracy and rough surface, the methods using wire as a consumable material, allow producing semi-products at considerable saving of material at the subsequent stages of treatment (Figure 3).

During investigation of metal of products manufactured according to the AM technologies using wire and powder [6] the similarity of microstructure of the specimens, manufactured using different methods, was noted. Nevertheless, the presence of some porosity in the metal of products manufactured according to AM technology using consumable powder was noted.

AM methods, using wire as a consumable material, depending on the concentrated power source can be divided into laser, electron beam and electric arc. It is noted [14] that laser AM methods are characterized by a high accuracy as compared to other methods using wire. Nevertheless, the laser methods of volumetric surfacing have low (2–5 %) power efficiency. The methods of electron beam additive surfacing possess the much higher power efficiency (15–20 %), but initially the method of electron beam surfacing of metallic freeforms was developed in NASA for challenging application in space [15] and requires using the equipment to create a vacuum environment. Accordingly, the size of parts produced by the electron beam surfacing using wire is limited by the size of the vacuum chamber (taking into account the equipment placed in it). Moreover, the need in operation with vacuum equipment imposes certain difficulties in the application of the method.

As compared to laser and electron beam surfacing, electric arc surfacing of freeforms involving the
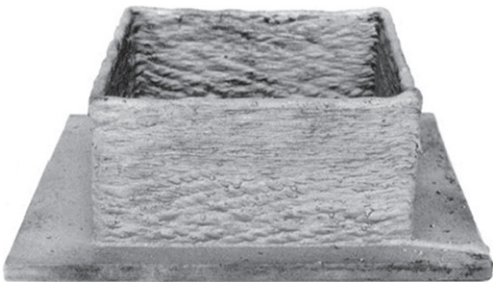

Figure 4. Experimental product manufactured using method of electric arc additive surfacing

methods of electric arc welding using consumable or non-consumable electrode in shielding gas has significant power efficiency. Some methods of TIG or MIG welding can reach the power efficiency of up to 90 % [6]. Nevertheless, all the AM methods using wire possess a number of common features, such as residual stresses and deformations of a product caused by intensive heating, relatively low accuracy of fabrication and characteristic «staged» surface.

However, AM methods using wire and, in particular, the methods of electric arc AM remain a challenging and developing area of metallurgical manufacturing [8]. At the moment, there are relatively few publications devoted to the AM problem based on arc welding technology. And though the first articles devoted to electric arc additive surfacing appeared in the 1990s [3, 18], the problem of weld metal structure formation, and the problems associated with weld shaping under the non-stationary conditions of heat dissipation remain unsolved and relevant [15, 19].

Using method of electric arc welding already in 1992 the researchers of the Nottingham University fabricated a volumetric product of the rectangular box type (Figure 4) of steel of the following composition: wt.%: 0.08 C, 0.9 Si, 1.5 Mn. The height of the product wall was 100 mm, and it was manufactured in 70 welding passes.

The analysis of mechanical characteristics of the produced metal showed a slight discrepancy during tensile testing of the specimens, cut along and across the welding direction (Table 3).
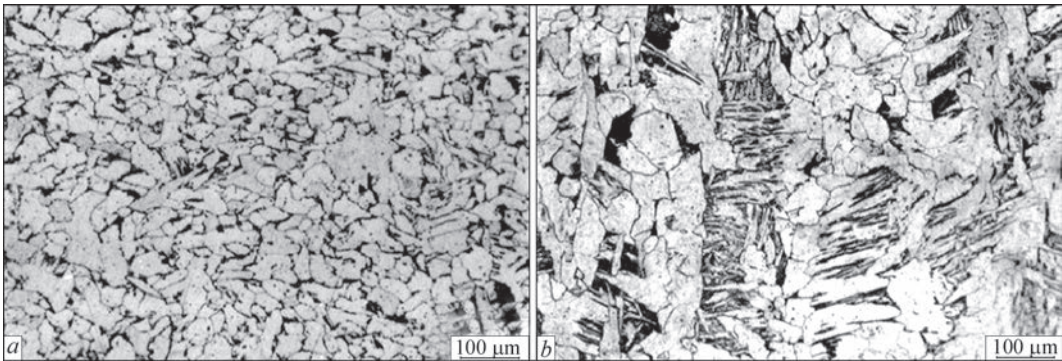

Figure 5. Macrostructure of product manufactured using method of electric arc additive surfacing in middle (*a*) and top (*b*) of the product wall
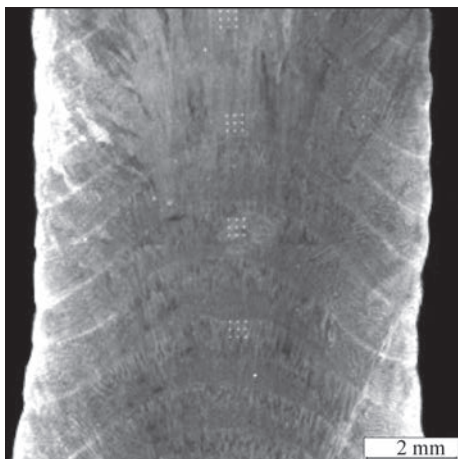
Figure 6. Macrostructure of cross-section of vertically deposited wall of steel 308S93 using electric arc AM method

The results of measuring Vickers hardness (under 10 kg load) showed increase in values from the bottom to the top of the wall of the product from *HV* 146.3 to 172.6 respectively. This increase in hardness can be connected with tempering processes taking place when applying surfacing beads. Nevertheless, the study of microstructure showed that in 99.5 % of the cases, the metal of specimens has a uniform, equiaxial ferrite-pearlite structure with grain size of about 60 μm (Figure 5, *a*). However, for the local area limited by the last surfacing layer, the presence of dendritic grains size of approximately 600×100 μm is characteristic (Figure 5, *b*).
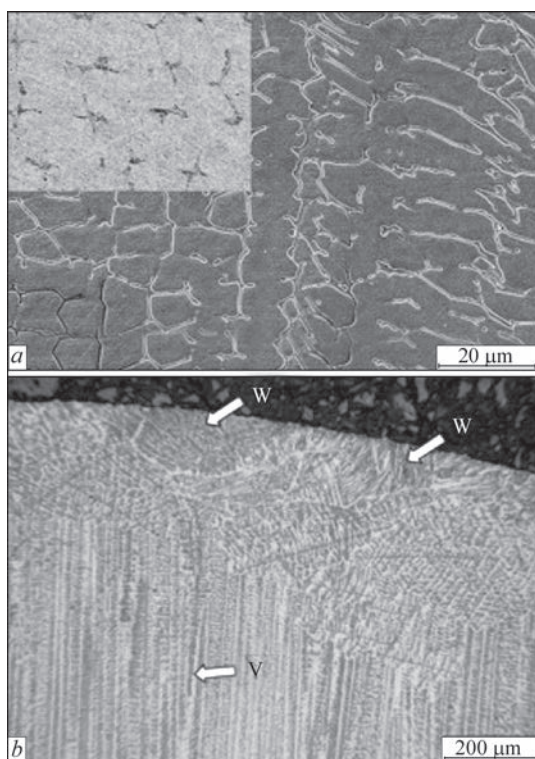
Figure 7. Microstructure of cross-section of weld of vertically electric arc AM-deposited wall of steel 308S93 in the middle (*a*) and top (*b*) of wall: V — lengthy acicular ferrite formations; W — Widmanstaetten ferrite

The area of the last deposited layer does not undergo a repeated (and the subsequent cycles) heating as the previous layers do. With this fact the deterioration in relative elongation of specimens, cut from a wall top of the fabricated product, can be associated.

The researchers also note changes in geometry of the deposited layers with increase in height of the deposited metal.

The authors of work [19] carried out the similar investigations on austenitic stainless steel 308S93. Alongside a «box» with wall length of 130×130 mm, wall height of 31 mm grown in 30 welding passes and wall thickness of 8 mm was fabricated. The surfacing parameters were as follows: 2 m/min wire consumption; 160 A welding current; 0.25 m/min travel speed of welding head.

The results of investigations of macrostructure of the wall cross-section (Figure 6) showed the L-shaped deposited layers, repeating the weld reinforcement shape.

The microstructure of metal consists mainly of ferrite and austenite (Figure 7, *a*) in the form of disoriented equiaxial crystallites, whereas the structure in the area of the latter (upper) layer (Figure 7, *b*) consists of extended ferritic needles oriented in accordance with heat dissipation, and the areas of Widmanstaetten ferrite.

Average hardness value was *HV* 186±15 at 100 g load. The mechanical tests showed the average value of tensile strength of 537 MPa at average relative elongation of 59 %. Also the researchers noted a tendency to deterioration of metal properties from the bottom to the top of the deposited wall.

In work [18] the results of investigations in the area of possibility of formation of different geometric elements of the created product are given. In particular, the selection of modes was carried out to create a horizontal ceiling wall (Figure 8, *a*). As a result the product with multidirectional planes without changes in inclination of priming plate during fabrication process was created (Figure 8, *b*).

It should be noted that many researchers [7, 15, 18, 19], dealing with the problems of electric arc volumetric surfacing, focus their attention mainly on the questions of shaping. At the same time, some of them [6] carry out investigations in the field of accuracy of embodiment of the product shape and achievement of preset properties, such as influence of scanning parameters and geometric weld parameters on quality of the surface after deposition (Figure 9), or influence of residual stresses and deformations on the degree of accuracy of product fabrication by changing the program of scanning (Figure 10).
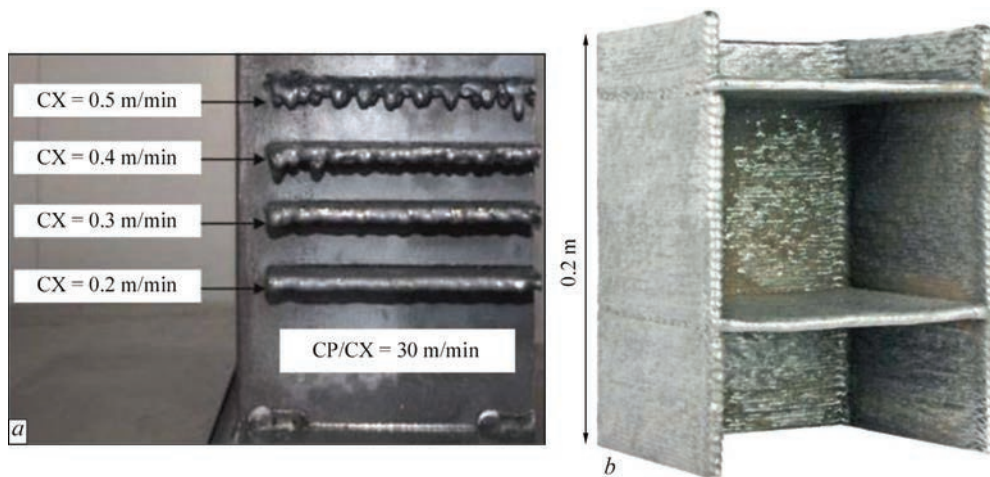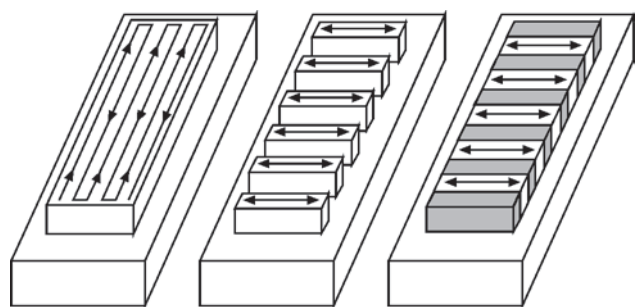
Figure 8. Selection of surfacing modes (*a*) for creation of hinged horizontal surfaces (*b*)
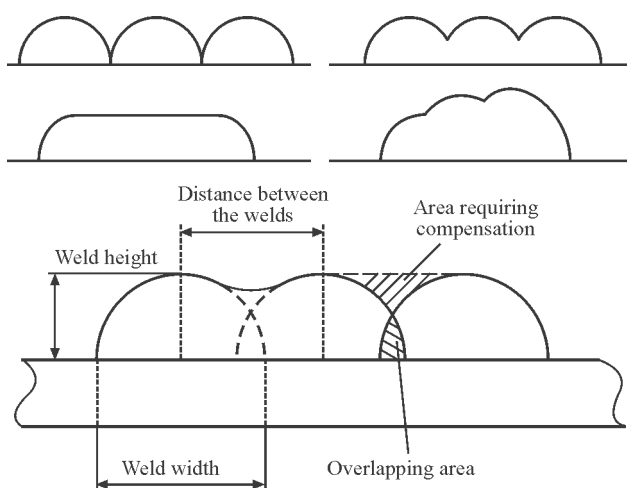
Figure 9. Peculiarities of weld geometry and influence of surfacing tool positioning on quality of the deposited surface

Figure 10. Variants of scanning movement of surfacing tool in process of creating the «wall» type element

complex product with the elements of different massiveness.

At the moment, at the PWI all the preconditions exist to create the technology of volumetric layer-by-layer electric arc automatic surfacing of volumetric metal products.

However, from the point of view of quality and reliability of metal product the primary feature is structure of metal rather than shape of the product. Although, in the case of metal products fabrication using spatial layer-by-layer surfacing the shape of the deposited weld is rigidly connected with the conditions of heat dissipation and, respectively, with the conditions of formation of inner structure of the metal, the primary task of metal product formation should remain a structural factor.

The approaches of structure control in the layer-by-layer ingot formation, developed at the E.O. Paton Electric Welding Institute [20], can be applied for creating metal products of complex geometric shape. The features of geometrical weld parameters formation depending on cooling conditions should be not a primary cause of the investigation, but a consequence and a technological feature, which should be taken into account, not trying to produce a uniform formation of layers, that is impossible under the condition of producing a uniform structure during fabrication of

1. Wong, K.V., Hernandez, A. (2012) A review of additive manufacturing. *Int. Scholarly Res. Network Mechanical Eng.*; *http*://downloads.hindawi.com/journals/isrn/2012/208760.pdf
2. Rizwan, Ali P.M., Hara Theja, C.R., Syed Mahammad Syed Sheb et al. (2015) Review on diverse materials applied for additive manufacturing. *Int. J. Res. in Applied Sci. & Eng. Techn.*, Vol. 3, Issue VII, 16–20; *http*://www.ijraset.com/fileserve.php?FID=2945
3. Wohlers, T., Gornet, T. (2014) *History of additive manufacturing*: Wohlers Report. *http*://wohlersassociates.com/history2014.pdf
4. Guessasma, S., Zhang, W., Zhu, J. et al. (2016) Challenges of additive manufacturing technologies from an optimisation perspective. *Int. J. Simulation and Multidisciplinary Design Optimization*, **6**; *http*://www.ijsmdo.org/articles/smdo/pdf/2015/01/smdo150009.pdf
5. (2015) Quadrennial Technology Review. *http*://energy.gov/sites/prod/files/2015/09/f26/Quadrennial-Technology-Review-2015_0.pdf
6. Ding, D., Pan, Z., Cuiuri, D. et al. (2015) Wire-feed additive manufacturing of metal components: Technologies, developments and future interests. *Int. J. Advanced Manufac. Techn.*, 81(**1–4**), 465–481; *http*://www.researchgate.net/publication/275973182_Wire-feed_additive_manufacturing_of_met-

al_components_technologies_developments_and_future_interests

7. Williams, S.W., Martina, F., Addison, A.C. et. al. (2015) Wire + arc additive manufacturing. *Mater. Sci. and Techn.*; *http*://www.researchgate.net/publication/277921887_WireArc_Additive_Manufacturing.

8. Frazier, W.E. (2014) Metal additive manufacturing: A review. *J. Mater. Eng. and Perform.*, 23(**6**), 1917–1928; *http*://link.springer.com/article/10.1007/s11665-014-0958-z/fulltext.html

9. Simchi, A., Petzoldt, F., Pohl, H. (2003) On the development of direct metal laser sintering for rapid tooling. *J. Materials Proc. Techn.*, **141**, 319–328; *http*://www.ibrarian.net/navon/paper/On_the_development_of_direct_metal_laser_sinterin.pdf?paperid=21177098

10. Kruth, J.P., Mercelis, P., van Vaerenbergh, J. et.al. (2004) Binding mechanisms in selective laser sintering and selective laser melting. In: *Proc. of Solid Freeform Fabrication Symp.* (Austin, USA), 44–59; *http*://sffsymposium.engr.utexas.edu/Manuscripts/2004/2004-06-Kruth.pdf

11. Pal, D., Patil, N., Stucker, B.E. (2012) Prediction of mechanical properties of electron beam melted Ti6Al4V parts using dislocation density based crystal plasticity framework. In: *Proc. of Solid Freeform Fabrication Symp.* (Austin, USA), 37–43; *http*://sffsymposium.engr.utexas.edu/Manuscripts/2012/2012-40-Pal.pdf

12. Michaels, S., Sachs, E.M., Cima, M.J. (1992) Metal parts generation by three dimensional printing. In: *Proc. of Solid Freeform Fabrication Symp.* (Austin, USA), 244–250; *http*://sffsymposium.engr.utexas.edu/Manuscripts/1992/1992-28-Michaels.pdf

13. Atwood, C., Griffith, M., Harwell, L. et. al. (1998) Laser engineered net shaping (LENS™): A tool for direct fabrication of metal parts. In: *Proc. of 17th Int. ALEO Congress* (Orlando, USA), 16–19; *http*://digital.library.unt.edu/ark:/67531/metadc621198/

14. Brandla, E., Baufeldb, B., Leyensc, C. et al. (2010) Additive manufactured Ti–6Al–4V using welding wire: Comparison of laser and arc beam deposition and evaluation with respect to aerospace material specifications. *Laser Assisted Net Shape Eng.*, Vol. 5, Pt B, 595–606; *http*://www.sciencedirect.com/science/article/pii/S1875389210005134

15. Dave, V.R., Matz, J.E., Eagar, T.W. (1995) Electron beam solid freeform fabrication of metal parts. In: *Proc. of Solid Freeform Fabrication Symp.* (Austin, USA), 64–70; *http*://sffsymposium.engr.utexas.edu/Manuscripts/1995/1995-09-Dave.pdf

16. Jandric, Z., Labudovic, M., Kovacevic, R. (2004) Effect of heat sink on microstructure of three dimensional parts built by welding-based deposition. *Int. J. Machine Tools and Manufac.*, 44(**7/8**), 785–796; *https*://www.smu.edu/~/media/Site/Lyle/RCAM/Publications/Effect %20of %20heat %20sink %20 on %20microstructure %20of %20three-dimensional.ashx

17. Friel, R.J., Harris, R.A. (2013) Ultrasonic additive manufacturing — A hybrid production process for novel functional products. In: *Proc. of 7th CIRP Conf. on Electro Physical and Chemical Machining*, Vol. 6, 35–40; *http*://www.sciencedirect.com/science/article/pii/S2212827113000784

18. Dickens, P.M., Pridham, M.S., Cobb, R.C. et al. (1992) Rapid prototyping using 3-D welding. In: *Proc. of Solid Freeform Fabrication Symp.* (Austin, USA), 280–290; *http*://sffsymposium.engr.utexas.edu/Manuscripts/1992/1992-32-Dickens.pdf

19. Skiba, T., Baufeld, B., van der Biest, O. (2009) Microstructure and mechanical properties of stainless steel component manufactured by shaped metal deposition. *ISIJ Int.*, 49(**10**), 1588–1591; *http*://www.jstage.jst.go.jp/article/isijinternational/49/10/49_10_1588/_pdf

20. Shapovalov, V.A. (2015) Control of metal structure in process of solidification. *Sovr. Elektrometallurgiya*, **2**, 51–54.

DEPENDENCIES OF DISCRETE-ADDITIVE FORMATION OF MICROVOLUMES OF METAL BEING SOLIDIFIED IN MULTI-LAYER MICROPLASMA POWDER SURFACING OF NICKEL ALLOYS

K.A. YUSHCHENKO, A.V. YAROVITSYN and **N.O. CHERVYAKOV**
E.O. Paton Electric Welding Institute, NASU
11 Kazimir Malevich Str., 03680, Kiev, Ukraine. E-mail: office@paton.kiev.ua

Peculiarities of heat input, bead cross-section area and efficiency were investigated at single-layer microplasma powder surfacing of nickel heat-resistant alloy JS32 on narrow substrate of 1–2 mm thickness. It is determined that series of its modes using 5–15 A welding current differs by the minimum heat input. Calculated evaluation of stress-strain state of a welded joint was carried out for its minimum and maximum level during building-up of edge of a plate using single- and three-layer surfacing. It is shown that the value of heat input in microplasma surfacing determines a width of plastic deformation zone and value of sum plastic deformations as a result of reheating in multi-layer surfacing. New technological principles were proposed for selecting the modes of multi-layer and 3D-microplasma powder surfacing of the parts from nickel heat-resistant alloys, providing the minimum heat input in a part and regulating requirements to welding current value, time of existence of metal of weld micropool in molten state and its volume. 20 Ref., 2 Tables, 10 Figures.

K e y w o r d s : microplasma powder surfacing, narrow substrate, nickel heat-resistant alloy JS32, effective power of part heating, heat input, bead cross-section area, volume of weld micropool, surfacing efficiency, stress-strain state of welded joint

It is a well known fact that the value of heat input is a very important process parameters which characterizes weld pool dimensions, duration of its existence and area of HAZ part heated to more than 600 °C temperature in fusion welding of structural steels [1].

The value of heat input under conditions of shielded-gas, submerged-arc and coated-electrode welding using more than 50 A current can lie in 0.87–3.78 kJ/mm range (bridge structures) [2], and is 0.6–0.9 kJ/mm for orbital TIG welding of technological pipelines [3]. The value of heat input in welding of low-alloy steels susceptible to quenching is reasonable to regulate based on conditions of cooling of HAZ metal in 600–500 °C interval and diagrams of anisothermal austenite decay [1–3]. In microplasma welding, the value of heat input, as a rule, lies in 20–35 J/mm range at proportional value of current and welding speed in the range of 2–49 A and 5–87 m/h, respectively, for metal of 0.1–0.5 mm thickness [4].

Heat input value can make 0.25–3 kJ/mm [5] applicable to repair of edges in the parts of aircraft GTE from nickel heat-resistant alloys by single-layer microplasma powder surfacing (MPPS) on narrow substrate using current up to 35 A [6]. A quality of base–deposited metal welded joint in multi-layer MPPS of nickel heat-resistant alloys according to crack suscep-

tibility criteria depends on the value of total heat input and surfacing efficiency [7, 8].

Aim of the work is an investigation of relationship of heat input and size of bead section (volume of welding micropool) in single-layer MPPS on narrow substrate of 1–2 mm width and at 5–15 A current with partial feed of powder of nickel heat-resistant alloys containing strengthening γ′-phase of more than 45 vol.%.

Experiment procedure and experimental data processing. Surfacing was carried out under conditions of free formation over the edge of (30–40)×(90–100) mm size plate from austenite stainless steel of 1, 1.6 and 2 mm thickness. A distance from surface being deposited to outer cut of plasmatron made 5 mm. A filler powder of nickel heat-resistant alloy JS32 [9] from +63 to –160 μm fraction was used. The experiments were carried out on UPNS-304M2/M3 unit. Mass of a powder portion, which is fed in a column of microplasma arc, made on average 0.14 g. Microplasmatron PPS04 with nozzle channel diameters of 2.5 (plasma) and 4.5 mm (focusing) was used. Higher grade argon on GOST 10157–79 was taken as a plasma (Q_{pl} = 1 l/min) and transporting (Q_{tr} = 4–5 l/min) gas, and Ar + 5 % H_2 mixture was applied as a shielding gas (Q_{sh} = 7 l/min).

In process of bead formation in a discrete-additive mode the welding micropool after filling by a portion
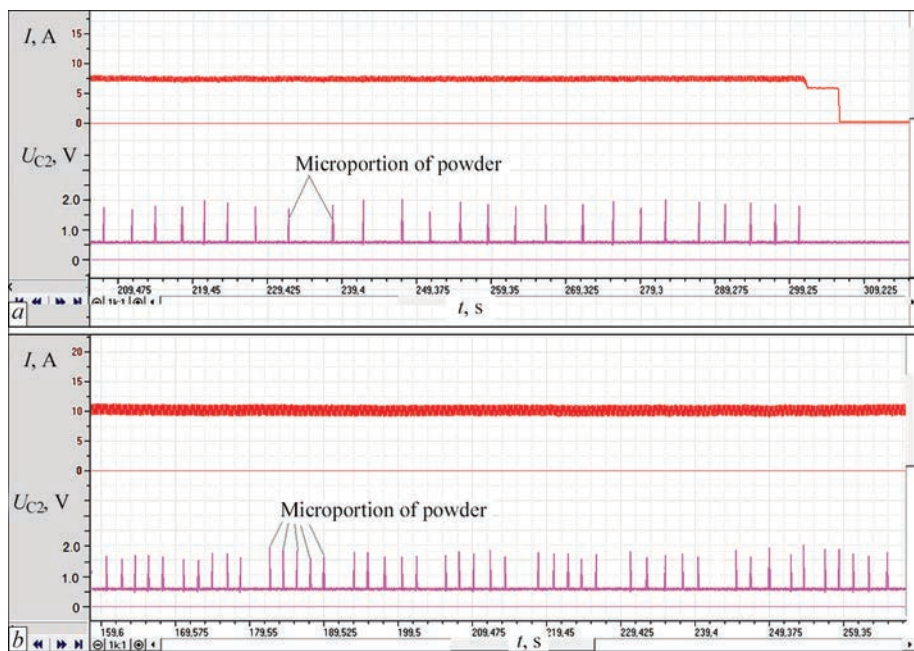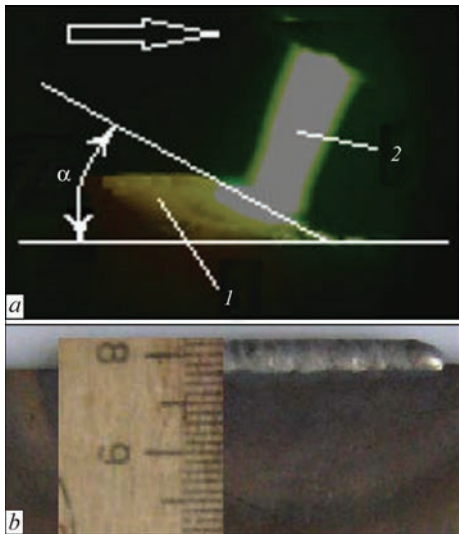
Figure 1. Fragments of oscillograms of MPPS on narrow substrate of 1.6 mm width with different amount of microportions of filler powder being fed in weld micropool: *a* — 1 portion; *b* — series from 5 portions; U_{C2} — control signal of feeder operating mechanism corresponding to feed of 1 microportion

of liquid filler is moved forward, and its new volume is again filled. In different series of experiments it was successively increased due to input in a weld pool mirror from 1 to 5 microportions of powder (Figure 1) simultaneously with step-by-step change of welding current in 5–15 A range. A period of the disperse filler portion feeding lied in the range of t_f = 1.5–5.0 s and was selected in such a way [5] as to provide a base metal wetting angle α = 30–60° (Figure 2, *a*) on a deposit leading edge proceeding from stable formation of set bead shape. If this condition was fulfilled at t_f = 1.5–1.8 s in smooth increase of welding current

Figure 2. Peculiarities of bead formation in deposition on narrow substrate of 1–2 mm wigth: *a* — wetting angel α of base and deposited metal on deposit leading edge; *b* — view of deposited bead; *1* — deposited bead; *2* — microplasma arc (arrow shows surfacing direction)

and feed of single microportions of JS32 powder, then further a disperse filler was introduced in a stationary welding micropool by series of 2–5 microportions. A base metal penetration depth in all the experiments did not exceed 1.5 mm, and fraction of base metal in deposited one made up to 20 %. An example of bead deposited on narrow substrate is shown in Figure 2, *b*.

Procedure [7] was used for processing the experimental data and calculation of power indices of surfacing modes. Heat input (taking into account effective efficiency of part heating [1]) was determined as a relationship of microplasma arc heat Q_Σ entered in anode to given length L of elliptic cylinder of deposited bead. Its cross-section area F_b was calculated on procedure [8].

Analysis of experimental data. The results of experiments (Figure 3) indicate that the weld micropool of cross-section to 35 mm^2 (approximate volume to 125 mm^2) is kept on a narrow substrate of 1–2 mm width under conditions of free formation of the deposited bead. This corresponds to effective height of deposited metal* h = 3–4 mm. A dependence $F_p = f(q_s)$ in 75–250 W and 1.5–35 mm^2 range is respectively described by a power function of $F_p = aq_s^n$ type, the coefficients of which change with narrow substrate width change. Its rise provokes for reduction of inclination of given dependence to abscissa axis, i.e. building up of the cross-section of deposited bead in rise of q_s >175 W value takes place more intensively,

_____

*Height of rectangle of width δ inscribed in contour of deposited bead cross-section and from below limited by primary level of nonfused surface of narrow substrate [8].

Table 1. Characteristics of modes of MPPS on narrow substrate of 1–2 mm width corresponding to heat input Q_Σ/L minimum

δ, mm	q_s, W	F_b, mm²	$\frac{Q_\Sigma/L,}{J/mm}$	v_d, m/h	G_d, g/min
1.0	145	6.5	490	1.15	0.9
1.6	170	5.5	700	0.90	0.75
2.0	195	7.5	600	1.15	0.9
Note. Based on experimental data.					

including due to increase of a coefficient of application of disperse filler at expansion of weld micropool [10].

It is determined that a series of modes of MPPS differs by the minimum heat input 490–700 J/mm (Figure 4; Table 1) under conditions of discrete-additive formation of the bead on narrow substrate. Such modes are characterized by:

● value of effective arc heat power, which is 25–40 W more than its corresponding value sufficient for the beginning of stable formation of the metal being deposited;

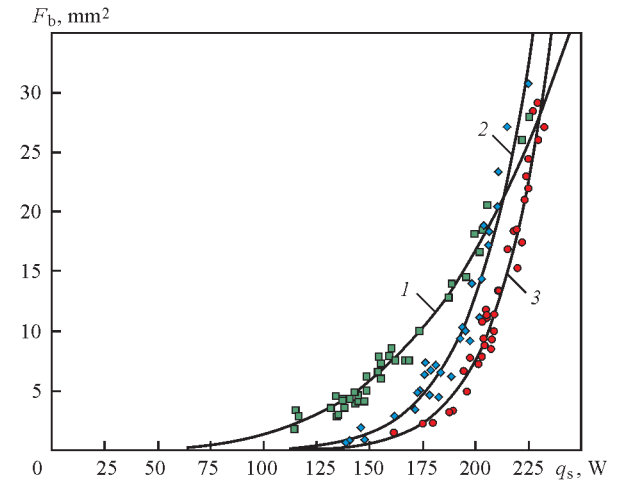● 5.5–7.5 mm² bead cross-section area and effective height of the deposited metal to 2.0–2.5 mm.

Thus, it is shown that position of the minimum of heat input corresponds to welding current and being 2.5–3.5 A more than its value, at which fusion of narrow substrate base metal takes place.

Increase of heat input in 2–2.5 times at 30–40 W reduction of the effective heat power of microplasma arc from a value of heat energy minimum is caused by a rise of arcing time between feeding the powder microportion for providing corresponding contact angle between base and deposited metal on the deposit leading edge and stable bead formation. 2.5–3 times increase of heat input on the right from the value of minimum heat input was promoted by the necessity of increase of arcing time at entering a series from 2–5 microportions of filler powder into a stable mirror of the micropool.

Sequential increase of effective heat power of the microplasma arc and surfacing efficiency promotes for changes of its rate in 0.4–1.2 m/h range (Figure 5). Its maximum values of 0.95–1.25 m/h are observed at F_b = 5.5–7.5 mm². Further, the deposition rate is delayed to 0.4–0.6 m/h, that is caused by increase of time of micropool filling with the metal being deposited. It is determined that the modes of narrow substrate surfacing, corresponding to the minimum heat input $Q\Sigma/L$ and the maximum deposition rate virtually match (see Figures 3–5 and Table 1), namely $q_s \le 10$ W ($I \le 0.63$ A); $\Delta v \le 0.05$ m/h; $\Delta Q_\Sigma/L \le 10$ J/mm.

Deposition efficiency changes in G_{d1} 0.1–2.3 g/min range in proportion to Q_Σ/L = 490–1800 J/mm (Figure 6). It makes 0.55–1.20 g/min at the minimum values of heat input.

The heat input is in direct proportion to frequency of feed of powder microportions, area of deposited

Figure 3. Dependence of cross-section area of deposited bead F_b on effective arc heat power q_s in deposition on narrow substrate (here and in Figures 4–6: *1* — substrate width of 1; *2* — 1.6; *3* — 2 mm)
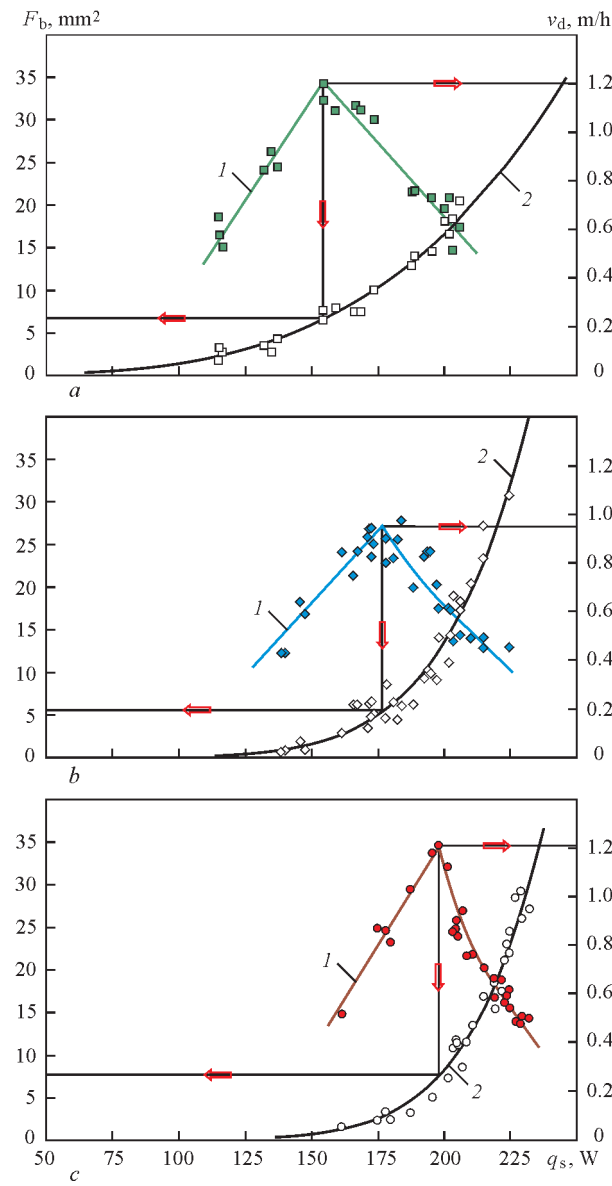
bead cross-section area and deposition efficiency in MPPS on narrow substrate of 1–2 mm width with the minimum penetration depth of base metal. Indicated factors can vary its value in 2.4–3.7 times.

Evaluation of stress-strain state of welded joint in single- and multi-layer surfacing on narrow substrate. Relationship of experimental data (see Figures 4–6) with earlier published results [7, 8] allows assuming that the SSS indices of base–deposited metal welded joint can significantly vary even under conditions of limited effective arc heat power (q_s = = 100–250 W) and base metal penetration depth (to 1.5 mm) in MPPS on narrow substrate of 1–2 mm width with different levels of Q_Σ/L = 490–2000 J/mm.

The corresponding estimation was based on determination of longitudinal compressive strain ε_{xx}^0 in a thin plate with $T(z)$ temperature gradient according to calculation scheme of Boley and Weiner [11] in ultimate heating condition and work [12] (approximated evaluation of stresses and deformations of a free band
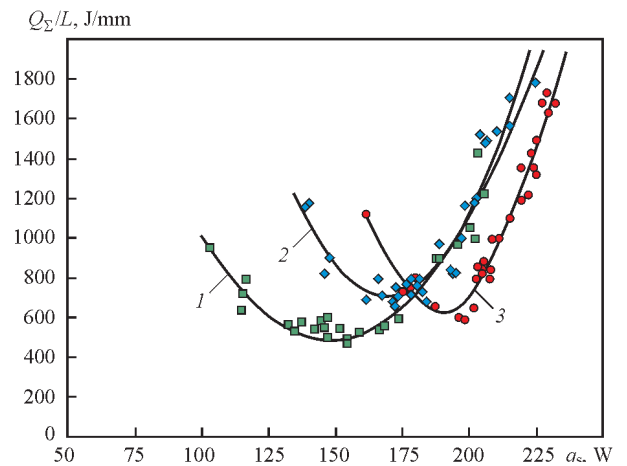
Figure 4. Dependence of heat input Q_Σ/L on effective arc heat power q_s in deposition on narrow substrate

Figure 5. Dependence of cross-section area of deposited bead and deposition rate on effective arc heat power in surfacing on narrow substrate
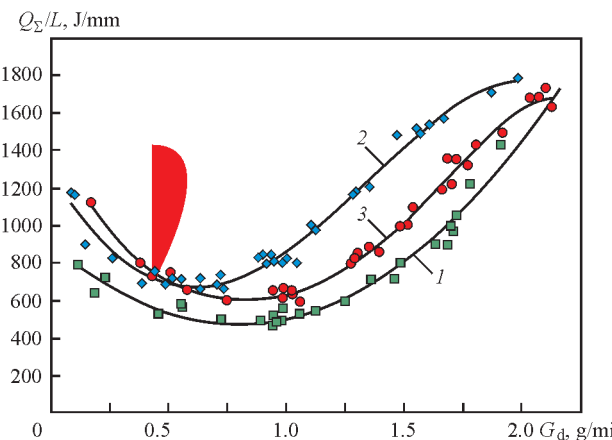
Figure 6. Dependence of heat input Q_Σ/L on efficiency of deposition G_d on narrow substrate

appearing in deposition of bead on one of its longitudinal edges [12–14]).

The following mathematical model was used for calculation of longitudinal deformations in single-axis stressed state appearing in a thin plate with temperature gradient T along axis z:

$$\varepsilon_{xx}^0 = \frac{\alpha(T)}{[1-v]} \times$$

$$\times \left[[T(z)dz + \frac{1}{b}\int_0^b T(z)dz + \frac{12z}{b^3}\int_0^b T(z)zdz \right]; \quad (2)$$

$$\varepsilon_{xx}^y = \frac{\sigma_y(T)}{E(T)}, \quad (3)$$

where ε_{xx}^0, ε_{xx}^y are the complete and elastic longitudinal deformation, respectively; $\alpha(T)$ is the coefficient of linear thermal expansion, l/°C; $E(T)$ is the Young's modulus, MPa; $v = 0.5$ is the Poisson's ratio; b is the size of narrow substrate in the direction of axis z, m.

The following assumptions and simplifications were taken in the mathematical model described above:

● bead is deposited simultaneously over the whole length of plate edge;

● thermal-deformation processes take place in elastic state, and plastic deformation is determined as a difference of total longitudinal deformations ε_{xx}^0 and elastic longitudinal deformations ε_{xx}^y at set temperature value;

● thermal physical dependencies $\alpha(T)$, $E(T)$ and $\sigma_y(T)$ for JS32 alloy with crystallographic orientation <001> were taken based on data of works [15, 16] considering their additional extrapolation from 1000–1100 °C to solidus temperature T_S during nickel heat-resistant alloy solidification;

● in boundary heating state the temperature distribution was set by exponential function of $T(z) = T_{max}e^{-kz^2}$ type, where $T_{max} = T_S$ condition is fulfilled in point $z = 0$.

Such an approach using temperature gradient function $T(z)$ allowed evaluating the longitudinal deformations $\varepsilon_{xx}^0(T)$ for real conditions of single- and three-layer surfacing on narrow substrate of 1–2 mm width, where the base and deposited metal is nickel heat-resistant alloy JS32 <001> with 62–65 vol.%. of strengthening γ'-phase. Different modes/conditions of surfacing were modeled by selecting the values of coefficient k based on provisions of isotherm 600 °C (Figure 7).

Evaluation of the compressive longitudinal deformations in the points of the maximum heating temperatures $T_{max1} > T_{max2} > T_{max3}$ (on current fusion line and its previous positioning levels in the depth of narrow substrate) where indices 2 and 3 are the increasing serial numbers of earlier deposited beads

relatively to current surfacing) was also carried out taking into account the effective (0.5 mm) height of the deposited layer for laser and microplasma process (1.5–5.0 mm) at three-layer surfacing. Figure 8 shows the results of numerical evaluation of gradient of longitudinal deformations $\varepsilon^0_{xx}(T)$ along axis z for single- and three-layer surfacing of nickel heat-resistant alloy JS32 under ultimate heating condition.

Evaluation of the SSS in single-layer surfacing of thin plate edge shows that the maximum $\varepsilon^0_{xx} \approx 7.5$ % and do not depend on value of temperature gradient in HAZ, and amplitude of change of $|\Delta\varepsilon^0_{xx}|$ in the base metal depth under different conditions varies insignificantly from 7.5 to 9.5 %. Reduction of the corresponding temperature gradient from 3350 to 70 °C/mm ($Z_{600\,°C}$ = 0.22–10.5 mm) promotes for expansion of HAZ area, subjected to plastic deformation, in more than 20 times.

The plastic defamation zone makes 3–10 mm for 490–2000 J/mm heat input, corresponding to the conditions of MPPS on 1–2 mm narrow substrate. Evaluation of the SSS in three-layer surfacing of the
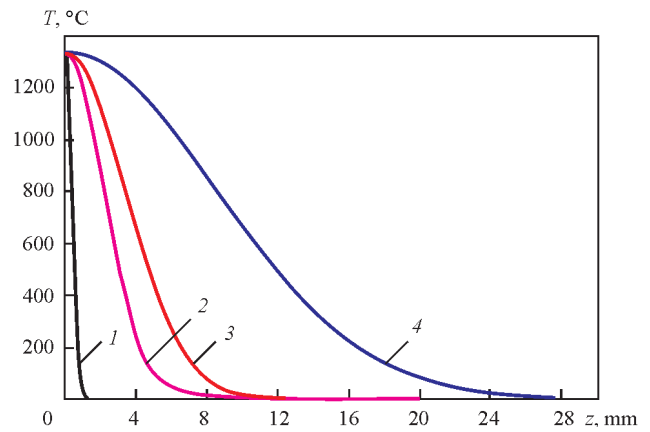
Figure 7. Assumed exponential distributions of $T(z)$ function typical for the following modes of surfacing on 2 mm narrow substrate: 1 — $Z_{600\,°C}$ = 0.22 mm, laser powder surfacing [17–19]; 2, 3 — $Z_{600\,°C}$ = 2.2 and 4.2 mm, MPPS at heat input modes less than 1000 J/mm; 4 — $Z_{600\,°C}$ = 10.5 mm, MPPS at modes with heat input approximately 2000 J/mm

thin plate edge shows that increased values of heat input (approximately 1800–2000 J/mm) provides for 40–65 % increase of the total plastic deformations in process of reheating in comparison with its values of less than 1000 J/mm (see Figure 8; Table 2). The total
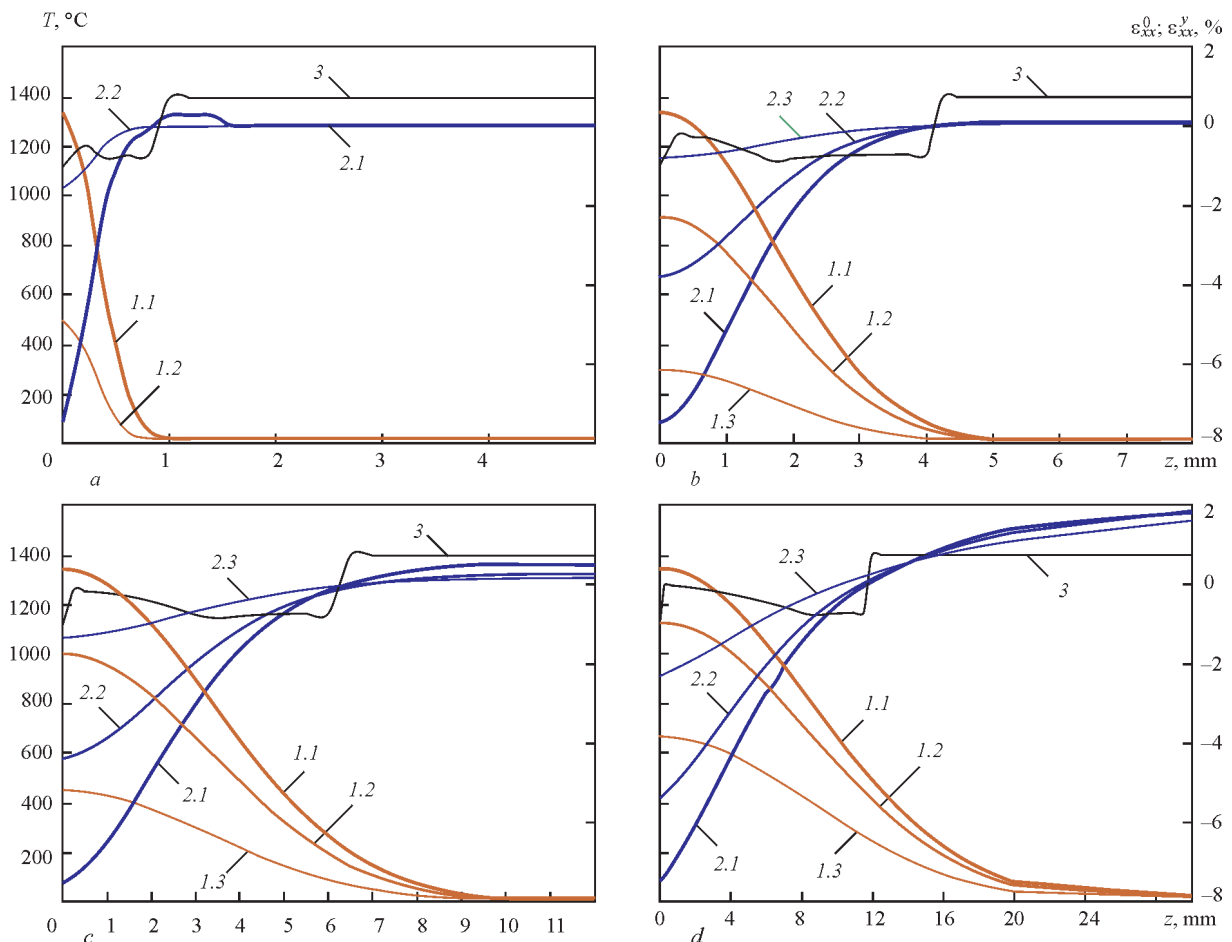
Figure 8. Change of total ε^0_{xx} distribution in HAZ under conditions of ultimate heating in three-layer surfacing on JS32 <001> narrow substrate: 1.1, 1.2, 1.3 — $T(z)$ distribution from fusion line for the last deposited bead and in reheating of two previous ones, respectively; 2.1, 2.2, 2.3 — $\varepsilon^0_{xx}(z)$ distribution from fusion line for the last deposited bead and in reheating of two previous ones, resprctively; 3 — $\varepsilon^y_{xx}(z)$ distribution from fusion line in the last deposited bead at $Z_{600\,°C}$ = 0.22 (a), 2.2 (b), 4.2 (c) and 10.5 (d) mm

Table 2. Distribution of $|\Delta\varepsilon^0_{xx}|$ at maximum heating and total $\sum |\Delta\varepsilon^0_{xx}|$ values of amplitudes of longitudinal deformation change depending on temperature gradient $Z_{600°C}$ in HAZ for 3-layer deposition on narrow 1–2 mm substrate (acc. to Figure 8)

Layers of surfacing	$\|\Delta\varepsilon^0_{xx}\|$, %, at $Z_{600°C}$, mm			
	0.22	2.2	4.2	10.5
First (current)	7.5	7.6	8.0	9.4
Secons	1.5	3.8	4.6	7.2
Third	–	0.8	1.5	3.9
$\sum\|\Delta\varepsilon^0_{xx}\|$	9.0	12.2	14.1	20.5

values of amplitudes $\sum|\Delta\varepsilon^0_{xx}|$ change under ultimate heating condition for three-layer surfacing on 1–2 mm narrow substrate at $Q_\Sigma/L < 1000$ J/mm does not exceed the maximum values of ductility of alloy JS32 <001> in testing for uniaxial tension (14.5 % at $T \leq 1000$ °C, [16]). Together with already obtained practical results [7, 8, 20] this allows validating the principal possibility for preserving a technological strength in multi-layer MPPS on narrow substrate without a relaxing heat treatment after deposition of each bead.

Evaluation of possible technological effect in full-scale modelling of three-layer MPPS with heat input less than 1 kJ/mm. A full-scale modelling of technologically probable shape of the bead cross-section, deposited on 2 mm narrow substrate, per 1 layer with heat input 2000 J/mm (Figure 9, *a*) and per 3 layers with 600 J/mm heat input of layer-by-layer surfacing (Figure 9, *b*), was carried out in the computer-aided process documentation engineering system Compas-3D V12.

The total heat inputs were taken according to procedure [7] as the criteria of comparative evaluation, and effective height of surfacing *h* and area of bead side reinforcements $2\Delta F_2$ (see Figure 9) — according to procedure [8]. It is determined that transfer to
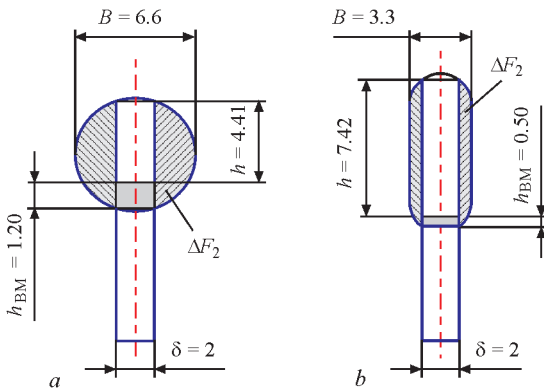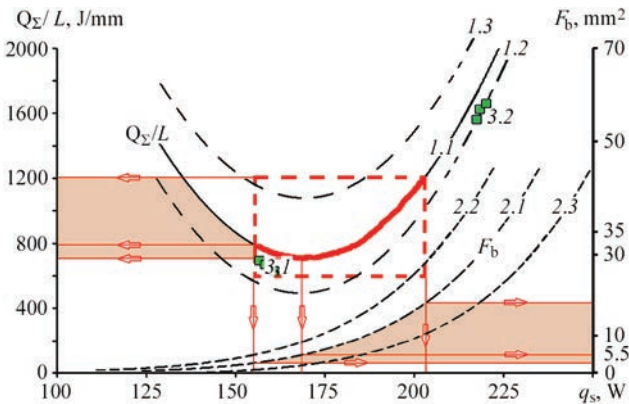
three-layer surfacing with $Q_\Sigma/L = 600$ J/mm, together with reduction of the total heat inputs in the part by approximately 10 %, allows increasing the effective surfacing height by about 70 % and reducing indirect losses of filler powder (values of machining allowance of deposited bead) roughly in 2 times.

Discussion of investigation results. MPPS with discrete-additive formation can be realized in a range of process parameters, lower boundary of which is limited by the effective power of microplasma arc sufficient for base metal fusion, and upper one — by the limiting volume of weld pool, which can be hold on vertically fixed narrow substrate. Such formation in single-layer surfacing on 1–2 mm narrow substrate using Ar + 5 % H$_2$ shielding gas is characterized by the following indices: effective heat power of microplasma arc $q_s = 100$–250 W; heat input $Q_\Sigma/L = 490$–2000 J/mm; average $v_d = 0.4$–1.25 m/h; bead cross-section of 1.5–35 mm^2 (weld pool volume approximately from 3 to 125 mm^3); deposition efficiency of 0.1–2.3 g/min.

Series of modes inside the set range is differ by the lowest heat input 490–700 J/mm, which respectively provides for the lowest total heat input in the part, and being determined by the following combination of indices, i.e. time of existence of metal of weld micropool in molten state of not more than 3–6 s; cross-section area of deposited bead 5–8 mm^2; volume of weld micropool approximately 15–25 mm^3; fraction of base metal in deposited metal 0.2; height of deposited bead 1.5–2.5 mm; deposition efficiency 0.55–1.0 g/min; average $v_d = 0.9$–1.25 m/h.

It was preliminary determined that the considered base–deposited metal welded joints of JS26–JS32 and JS32–JS32 systems at increase of the average total heat input to 5 kJ/mm demonstrate cracks, which are sufficiently easily determined by penetrant test-

Figure 9. Full-scale modelling of cross-section of beads deposited on 2 mm narrow substrate with heat input of 2000 (*a*) and 600 (*b*) J/mm: *B* — deposited bead width; h_{BM} — depth of base metal penetration; *h* — effective height of deposited bead; ΔF_2 — cross-section area of bead side reinforcement which is removed at further machining

Figure 10. Basic principles for selection of MPPS rational modes depending on Q_Σ/L, F_b and effective q_s: *1.1*, *2.1* — dependences of Q_Σ/L and F_b for basic variant of modes (Ar + 5 % H$_2$); *3.1*, *3.2* — rationally and irrational selected pulsed modes; *1.2*, *2.2* — proposed change due to optimizing the composition of shielding gas/ shielding conditions of weld micropool/quality of disperse filler; *1.3*, *2.3* — modes which differ by irrational selection of process parameters, filler powder quality indices or structure of microplasmatron nozzle assembly

ing. Limitation of heat input of layer-by-layer surfacing at certain maximum allowable values of the total heat input in the part, at which no tendency to crack formation can be observed in the considered welded joints, allows significantly increasing number of layers of the deposited metal and, respectively, height of repaired section on the edge of part of aircraft GTE.

From point of view weldability of nickel heat-resistant alloys, the modes of multilayer surfacing (in prospect 3D surfacing) with the lowest heat input are also the most preferable due to 2.0–3.3 times reduction of width of zone of plastic deformations in HAZ and decrease total plastic deformations in process of reheating by 40–65 %, in comparison with the mode at $Q_s/L = 1800$–2000 J/mm.

Figure 10 proposes the generalized algorithm for selection of rational modes of layer-by-layer MPPS based on keeping the principle of heat input minimum (by example for the 1.6 mm narrow substrate). A dashed lines show the range of surfacing modes, which performance of further optimization of its parameters is reasonable by means of application of pulsed surfacing modes, improvement of the conditions for shielding of weld micropool and increase of filler wire quality. The lower values of effective arc heat power, heat input and width of deposited bead, in comparison with corresponding values of indicated indices for direct welding current, are the additional criteria for reasonable choice of process parameters of corresponding surfacing modes with pulsed welding current.

Conclusions

1. Range of the MPPS process parameters on narrow substrate of 1–2 mm width was evaluated in discrete-additive formation of deposited metal at welding current 5–15 A. It is determined that the series of its modes in Ar + 5 % H_2 shielding gas differs by the lowest heat input 490–700 J/mm and is characterized by limitation of bead cross-section and time of existence of weld pool metal in molten state in the 5–8 mm^2 and 3–6 s range, respectively.

2. It is shown that such modes of multilayer surfacing of nickel heat-resistant alloys with high content of strengthening γ'-phase differ by 2–3.3 times reduction of the width of plastic deformation zone in HAZ and 40–65 % decrease of the total plastic deformations in the process of reheating. The expected technological effect at approximately similar total heat input is also 2 times reduction of machining allowance value and 70 % increase of effective height of the deposited metal.

3. The new technological principles were proposed for selection of the modes of multi-layer or 3D MPPS of the parts from nickel heat-resistant alloys. They lie in providing the lowest possible level of heat input of

such a process, first of all, due to regulation of deposited bead cross-section and time of existence of weld micropool metal in molten state.

1. Frolov, V.V., Vinokurov, V.A., Volchenko, V.N. et al. (1970) *Theoretical principles of welding*. Moscow: Vysshaya Shkola.
2. Karasev, M.V., Grebenchuk,V.G., Rabotinsky, D.N. et al. (2009) Investigation of influence of semiautomatic gas mixture shielded welding conditions using rectifiers of VD-506DK type with flux-cored wire Power Bridge 60M on mechanical and viscous-plastic properties of deposited metal in welding of bridge structures. *Svarka i Diagnostika*, **4**, 19–25.
3. Shipilov, A.V., Konovalov, A.V., Brovko, V.V. et al. (2011) Control of welded joint structure in orbital TIG welding of industrial pipelines of compressor stations. *Izvestiya VUZav,*. Series Mashinostroenie, **6**, 44–52.
4. Paton, B.E., Gvozdetsky, V.S., Dudko, D.A. et al. (1979) *Microplasma welding*. Kiev: Naukova Dumka.
5. Yarovytsyn, O.V. (2009) *Microplasma powder surfacing of refractory nickel alloys containing 45-65 % of γ'-phase*: Syn. of Thesis for Cand. of Techn. Sci. Degree. Kiev: PWI.
6. Gladky, P.V., Pereplyotchikov, E.F., Ryabtsev, I.A. (2007) *Plasma surfacing*. Kiev: Ekotekhnologiya.
7. Yarovitsyn, A.V. (2015) Energy approach in analysis of microplasma powder surfacing modes. *The Paton Welding J.*, **5/6**, 14–21.
8. Yushchenko, K.A., Yarovitsyn, A.V., Khrushchov, G.D. et al. (2015) Analysis of process of bead shaping in cladding on narrow substrate. *Ibid.*, **9**, 20–27.
9. Melekhov, R.K., Pokhmursky, V.I. (2003) *Structural materials of power equipment. Properties. Degradation*. Kiev: Naukova Dumka.
10. Yushchenko, K.A., Yarovitsyn, A.V., Yakovchuk, D.B. et al. (2013) Some techniques for reducing filler powder losses in microplasma cladding. *The Paton Welding J.*, **9**, 30–36.
11. Boley, B., Weiner, J. (1964) *Theory of thermal stresses*. Moscow: Mir.
12. Okerblom, N.O. (1948) *Welding strains and stresses*. Moscow; Leningrad: MAShGIZ.
13. Talypov, G.B. (1973) *Welding strains and stresses*. Leningrad: Mashinostroenie.
14. Nedoseka, A.Ya. (1998) *Principles of calculation and diagnostics of welded structures*. Kiev: Indprom.
15. Budinovsky, S.A., Kablov, E.N., Muboyadzhan, S.S. (2011) Application of analytical model for determination of elastic stresses of multilayer system in solving of problems on development of high-temperature heat-resistant coatings of aircraft turbine blades. *Vestnik MGTU im. N.E. Baumana,* Series Mashinostroenie, 26–37.
16. Golubovsky, E.R., Svetlov, I.L., Khvatsky, K.K. (2005) Principles of change of axial and azimuthal anisotropy of strength properties of heat-resistant nickel single crystals for GTE blades. *Aviats.-Kosmich. Tekhnika i Tekhnologiya*, 26(**10**), 50–54.
17. (2001) Melt pool size control in thin-walled and bulky parts via process maps. In: *Proc. of 12th Solid Freeform Fabrication Symp.* (Austin: Univ. of Texas), 432–440.
18. Vasinonta, A., Beuth, J.L., Griffith, M. (2007) Process maps for predicting residual stress and melt pool size in the laser-based fabrication of thin-walled structures. *J. Manufact. Sci. and Eng.*, 129(**1**), 101–109.
19. Aggaransi, P., Beuth, J.L. (2007) Localized preheating approaches for reducing residual stress in additive manufacturing. *Ibid.*, 709–720.
20. Zhemanyuk, P.D., Petrik, I.A., Chigilejchik, S.L. (2015) Experience of introduction of the technology of reconditioning microplasma powder surfacing at repair of high-pressure turbine blades in batch production. *The Paton Welding J.*, **8**, 39–42.

APPLICATION OF WELDING TECHNOLOGIES FOR SUPPRESSION OF LIQUATION IN LARGE INGOTS

V.A. SHAPOVALOV

E.O. Paton Electric Welding Institute, NASU

11 Kazimir Malevich Str., 03680, Kiev, Ukraine. E-mail: office@paton.kiev.ua

The problem of liquation continuously attracts an attention of metallurgists and it is especially acute in producing of large ingots. Dendritic liquation can deteriorate the ingot so that it can occurr to be unsuitable for manufacture of large critical-purpose parts. It is shown that the main cause of liquation is a low rate of solidification. Its increase is impossible in melting of large ingots by using the traditional technologies. Therefore, one of the ways of suppression of the dendritic liquation is a stage-by-stage surfacing (formation) of ingots by using the welding technologies. The article gives the experimental data confirming the feasibility of the ingot structure control independently of its sizes. The fields of application of the suggested approach for manufacture of critical products are predicted. 10 Ref., 5 Figures.

K e y w o r d s : dendritic liquation, coefficient of distribution, rate of solidification, ESR, VAR, EBR, PAR, macro- and microstructure

Liquation is the non-homogeneity of chemical composition, occurred at its crystallization. There is dendritic and zonal liquation. The dendritic liquation for alloys results in decrease of corrosion resistance, reduction in ductility, formation of lineage structure in pressure treatment, decrease in solidus temperature, hazard of fusion of grain boundaries during heat treatment, instability of structure and properties of metal with time. Zonal liquation can be positive, negative, carbide, off-center (cord-type) and gravity. The cause of liquation is the different solubility of the alloying component or impurity in solid and liquid phases (Figure 1).

The ratio of concentration of impurities in a solid phase γC_s to concentration of impurities in a liquid phase C_1 is the coefficient of distribution

$$K = \frac{C_s}{C_1}.$$

In metallurgical processes $K < 1$ and depends on temperature and rate of solidification (for most alloying elements and impurities). At rapid (instantaneous) hardening $K = 1$. At very slow solidification $K = K_0$, where K_0 is in equilibrium. With lower K the liquation is stronger.

Usually, its value is given in handbooks for the equilibrium state.

Under the real conditions it is necessary to mention about the effective coefficient of distribution (Figure 2) which is determined by formula [1]
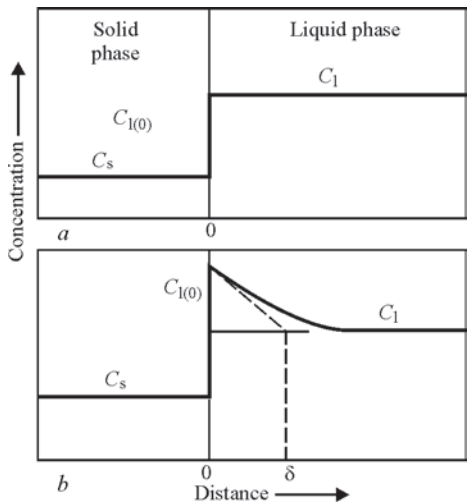
Figure 1. Scheme of distribution of impurities at the interface of solid and liquid phases in equilibrium (*a*) and non-equilibrium (*b*) conditions (δ — thickness of diffusion layer)
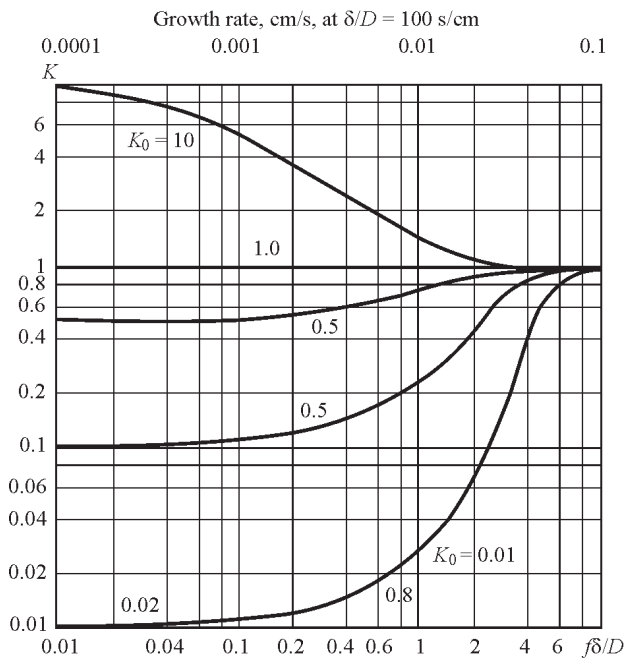
Figure 2. Effective coefficient of distribution versus value of given rate of movement of the solidified metal boundary [1]
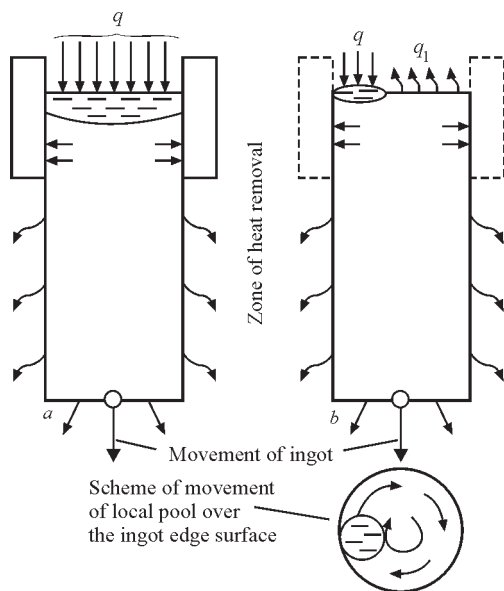
Figure 3. Scheme of supply and removal of heat from ingot: *a* — diameters of pool and ingot are equal; *b* — local metal pool

$$K = \frac{K_0}{K_0 + (1 - K_0)e^{-f\delta/D}},$$

where f is solidification rate, cm/s; δ is the thickness of diffusion layer adjacent to the front of crystallization and enriched with impurity, cm; D is the coefficient of impurity diffusion, cm²/s.

The traditional technical procedures for prevention of the liquation are the following: control of temperature of poured metal; control of thermal field at the pool surface; adding of coolers; electromagnetic stirring, vibro-treatment; reverse rotation of metal; ultrasonic treatment; electrohydraulic pulse treatment; treatment of melt with immersed oscillating rod.

Unfortunately, the efficiency of traditional technical procedures is decreased with increase in the ingot weight. Therefore, the development of new methods
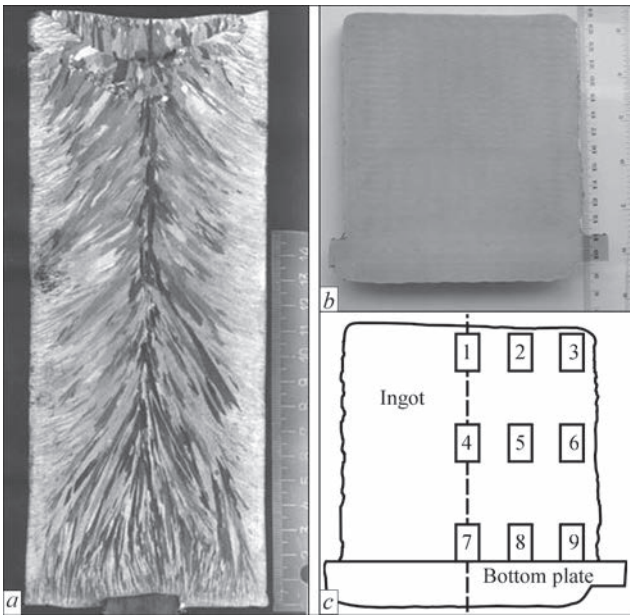

Figure 4. Microstructure of plasma-arc remelted ingot (*a*) and ingot produced using layer-by-layer surfacing by local welding power source (*b*), and map of specimens sampling (*c*)

of producing large ingots is urgent. The main cause of liquation is the low rate of solidification, and it is decreased non-linearly with increase in the ingot mass.

The way of the liquation prevention is the increase in the rate of solidification (crystallization) up to such a value which will provide the effective coefficient of distribution of impurities and alloying elements, which is $K \approx 1$.

The traditional methods of producing large ingots, including also the special metallurgy, cannot solve this problem. In case of exceeding the critical diameter of the ingot the crystallization, typical for VAR, ESR, EBR and PAR ingots of a small diameter, is violated and the processes lose their advantages [2–4]. The heat removal from the ingot middle downward and through a lateral surface is limited, and at the top
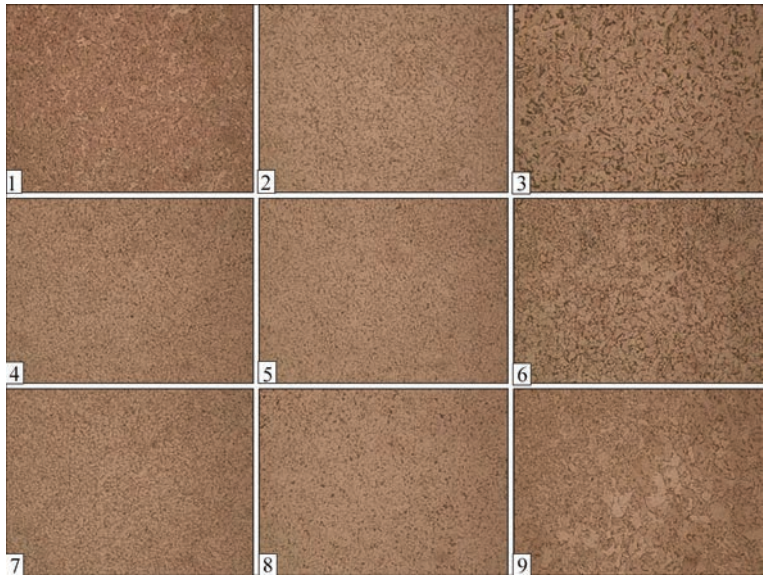
Figure 5. Microstructure (×200) of specimens of ingot metal produced by increment during movement of small metal pool

the overheated metal pool covers all the ingot cross section (Figure 3, *a*).

To solve the problem, i.e. the increase in solidification rate, it is necessary to organize the heat outflow. This possibility appears if the metal pool would have small sizes, and the rest top edge surface of the ingot would be solid with heat dissipation into the furnace atmosphere (Figure 3, *b*; flow q_1). Then, it would be possible to control the rate of crystallization and liquation processes by stirring the metal pool over the surface being surfaced at a high rate.

The problem of liquation can be solved by applying the welding technologies. Small weld pool by sizes and high speed of welding or surfacing, reaching several meters per minute, allows predicting the desired result with confidence. The welding processes are the most frequently applied in 3D-technologies for manufacture of products of the preset rather intricate shape. The processes of producing powerful turbine rotors are described in [5], the examples of prospects of manufacture of nuclear reactor bodies are given in [6]. The published works are devoted mainly to the shape formation, but there is negligible number of works, in which the attention is paid to the control of structure (liquation).

Our scientific interests belong to the area of structure control, first of all, and, secondly, to shape formation. Thus, by reducing the rate of movement of local metal pool to the area of small values (mm/min) and using a single-crystalline primer we produce the single crystals, the sizes of which are theoretically not limited [7, 8]. The crystals inherit structure and crystallographic orientation of the primer. With increase in the speed of welding source movement by 5–10 times as compared to rate of melting of ingots in known remelting processes, we can obtain random and rapid mass nucleation of crystals in a metal pool and, as a result, produce the fine-crystalline structure [9, 10]. Convinced results about the wide possibilities of structure control as compared with traditional PAR are given in Figure 4 (when sizes of ingots are commensurable).

In PAR the ingot structure has two zones: zone of hardened crystals, and zone of large directed crystals, i.e. dendrites. Moreover, the transcrystallization is observed in the axial zone. In the ingot, produced as a result of its increment during movement of a small metal pool, a fine-grain structure is observed. Results of metallographic investigations show that the grain value is within the ranges of 8–9 (Figure 5). But, it is most important that the grain size does not almost depend on place of sampling the specimens from ingot: middle, top, or bottom. In realization of such a technological approach the effect of a scale factor on the ingot structure formation is eliminated, that, in its turn, opens up the great opportunities of increasing the service properties of the product, produced of such ingots, and leads to the metal saving as the scale factor is accepted to be equal to 1, the value of which is usually decreased with increase in product dimensions. In addition, weight of the ingot can maximum approach the weight of the ready product, so, there is no need to cut out the bottom and head parts (this is one third of the large ingot weight).

The control of structure and liquation processes is rather important in manufacture of critical-purpose products, for example, discs of the aircraft engines. In practice, this can be replacement of a complicated and expensive powder technology.

Conclusions

1. Ineffective application of traditional technologies for control of liquation processes in crystallization of large ingots is shown.

2. Application of welding technologies for control of liquation processes is grounded.

3. Feasibility of producing homogeneous structure across the entire ingot section, including bottom and head parts, is confirmed.

4. Prospects of application of the developing method for melting of critical-purpose ingot and billets are shown.

1. (1961) *Technology of semiconductor materials*. Ed. by G. Bridgers et al. Moscow: Oborongiz.
2. Flemings, M. (1977) *Solidification processing*. Ed. by A.A. Zhukov. Moscow: Mir.
3. Nekhenzi, Yu.A. (1948) *Steel casting*. Moscow: GINTL ChTsM.
4. Mitchell, A., Belestain, A.S. (1985) Factors influencing temperature and solidification of ingots in ESR. *Elektroshlak. Pereplav*, Issue 6, 192–198.
5. Datta, R., Million, K., Zimmermann, H. (2003) Shape welding with MnMoNi alloys for heavy components. *Welding and Cutting*, 55(**4**), 216–224.
6. Diltey, U., Stein, I., Berger, C. et al. (2006) Future prospects of shape welding. *Ibid.*, 5(**3**), 164–172.
7. Shapovalov, V.A., Latash, Yu.V., Zholud, V.V. et al. (2001) Large flat tungsten and molybdenum single crystals and methods of its production. In: *Proc. of 7th Int. Symp. on Pure Metals* (Kharkov, 2001), 39–42.
8. Shapovalov, V.A., Latash, Yu.V., Borimskaya, S.T. et al. (2001) Oriented tungsten single crystals: Producing, examination and application. *Metally*, **1**, 6–64.
9. Shapovalov, V.A., Grigorenko, G.M. (2015) Suppression of liquation processes in large ingots. *Sovr. Elektrometallurgiya*, **1**, 26–30.
10. Shapovalov, V.A., Tsykulenko, K.A., Shapovalov, E.V. et al. (2015) Formation of large ingot by method of moving of local metal pool. *Elektrometallurgiya*, **2**, 36–43.

RESISTANCE WELDING OF COATED STEEL PLATES IN THE ASPECT OF ENVIRONMENTAL CONDITIONS

J. MATUSIAK and **J. WYCIŚLIK**
Institute of Welding
16-18 Bl. Czeslawa Str., 44-100, Gliwice, Poland. E-mail: joanna.wycislik@is.gliwice.pl

In the industry, resistance welding has always been regarded as the process without significant adverse effect on the work environment. The research literature of the last years dealing with investigations into fume and chemical factors of resistance welding was the only reason that has directed the attention of specialists on working safety to the amount and type of pollutants emitted during this process. The article presents research, conducted at Instytut Spawalnictwa in Gliwice, into the emission of pollutants generated during spot resistance welding of steel plates with various protective coatings. The article demonstrates the research station and methodology of determination of total fume, carbon monoxide, nitrogen oxides and organic matters. The examination of fume and gas emission was conducted during resistance welding of electrolytic and hot-dip coated plates, covered with zinc, zinc-iron alloy, aluminium with the admixture of silicon as well as zinc-epoxy double layer coatings. The comparative analysis of the research results was aimed at the determining the impact of coating type and welding current on emission of fumes and gases during resistance welding of plates with different thickness. 17 Ref., 3 Tables, 9 Figures.

K e y w o r d s : *spot resistance welding, coated steel sheets, pollutants emission*

In the literature on industrial medicine and research into factor having the adverse impact on the safety work conditions, welding of metal coated plates is associated with a disease called metal fume fever [1–7]. This disease is caused by zinc, aluminium and magnesium compounds. Its symptoms resemble the symptoms of influenza and appear usually approximately four hours after the exposition. In the assessment of occupational hazards the metal fume fever is recognised as the risk appearing very quickly after the exposure to the agents causing the disease. Moreover, the fever is accompanied by the characteristic symptom called «Monday morning fever», consisting in the fact that the patient's condition deteriorates after a longer rest. Repeated occupational expositions to the high concentration of zinc oxides (ZnO) lead to lesions in the respiratory system. The metal fume fever is recognised as a direct reason for asthma development initiated by the occupational agents [3]. During welding of aluminium coated plates, fumes containing aluminium oxide Al_2O_3 and silicon dioxide (silica) are the main compounds affecting work conditions and influencing workers health [2]. Aluminium belongs to the elements of toxic action on human body and tends to accumulate in the liver, kidneys, pancreas, bones and brain tissue. Current research data indicate that aluminium reduces the activity of central nervous system, blocking the action potential of neurons.

The process of resistance welding was regarded in the industry as the technology not affecting adversely the work environment. The research results into the issues of the factors harmful to the workers' health during resistance welding performance have drawn the attention of the specialists in industrial safety on the amount and type of pollutants generated by this process.

Resistance welding of paint coated plates or plates covered with combination of metal, paint and organic coatings is associated with the generation of chemical compounds belonging to the aromatic hydrocarbons group, e.g. benzene, toluene, ethyl benzene, xylene, phenol and cresol as well as polycyclic aromatic hydrocarbons (PAHs) to the work environment [4]. Those substances after penetrating into the human body cause poisoning and occupational diseases. During resistance welding of steel plates with protective coatings, fume containing zinc, iron, aluminium, manganese and silicon is always generated while carbon monoxide generation belongs the gas emission process [5, 6].

Pollutant emission rate research during resistance welding. This article presents the research conducted in the experimental station at Institute of Welding in Poland aimed at the determination of the correlation between the selected resistance welding parameters and amount of pollutants being generated [8–10]. The investigation into fume and gas generation was conducted for hot-dip coated plates with zinc, zinc-iron alloy coatings as well as with coating of aluminium with admixture of silicon.

Table 1. Materials used in research into fume and gas generation during spot resistance welding [8–10]

Steel grade (material thickness, mm)	Coating type	Surface type/Surface protection
Hot-dip coated plates with Zn coating (Z type)		
HX 260 LAD (1.2) HX 300 LAD (1.2) HX 300 LAD (1.5)	Z100 MBO	MBO: MB — high quality of zinc coating/ O — oiling
HX 420 LAD (1.2)	Z140 MBO	
DX 53D (1.5)	Z140 MBO	
Hot-dip coated plates with Zn–Fe alloy coating (ZF type)		
DX 53D (1.2) DX 53D (1.4)	ZF100 RBO	RBO: RB — high quality of Zn–Fe alloy surface/ O — oiling
HCT 600 (1.2) HCT 600 (1.8)	ZF100 RBO	
DX 52D (1.5)	ZF140 RBO	
Hot-dip coated plate with Al–Si alloy coating (AS type)		
DX 53D (0.6)	AS120	
Double-sided electrolytic-coated plates		
DC04 (1.2)	ZE75/75 A	A: Normal coated surface/ No additional protection
DC04 (2.0) ZSTE 280BH (0.6)	ZE75/75 APO	APO: A — normal coated surface/ P — additional phosphate coating O — oiling
Double-layer zinc–epoxy electrolytic-coated plate		
LAC 320Y400T (1.5)	ZE/EG + OC2 GardoProtect 9498	OC: O — oiling C — chemical passivation

The plates used in research had coating thicknesses from 5 to 20 μm with additional surface protection by oiling. The electrolytic-coated plates had 7.5 μm thick zinc coating on their both sides and were additionally protected by oiling and phosphating. The investigation of pollutants during spot resistance welding was performed also for electrolytic zinc-coated plates with coating thickness of 5 μm with additional coating of 5 μm thick epoxy layer. The double-layer coating was protected by oiling and chemical passivation. Materials used during the research into the generation of fume and gas during spot resistance welding are given in Table 1, while Table 2 presents the parameters of resistance welding process.

Research station for the examination of fume and gas generation during resistance welding is composed of the following main components (Figures 1 and 2): fume chamber, exhaust system and spot welding machine of ZPa-130i type with the inverter controller HWS 2102IQ, equipped with computer control system for monitoring current and voltage using the program LOGWELD.

The experimental station and research methodology were developed in accordance with the require-

Table 2. Technological conditions for spot resistance welding used in pollutants emission investigations [8–10]
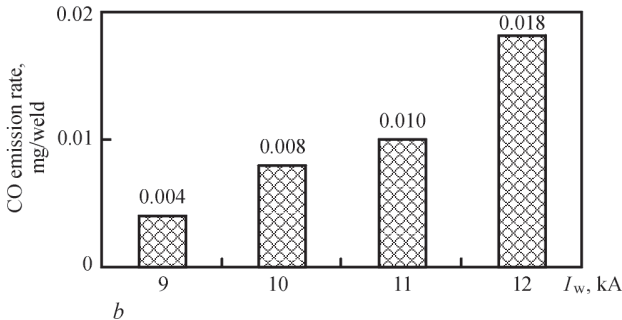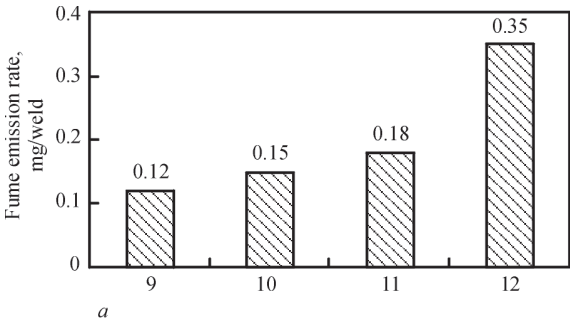
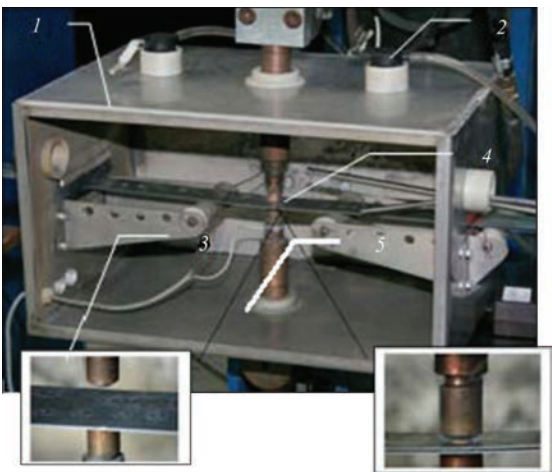| Material grade	Plate thickness, mm	Welding current, kA	Welding time, ms	Welding force, daN	Welding productivity, weld/min
HX 260 LAD/Z100 MBO	1.2	9–12	300	250	22–28
HX 300 LAD/Z100 MBO	1.2	9–11	300	250	22–24
HX 300 LAD/Z100 MBO	1.5	9–11	250	300	22–24
HX 420 LAD/Z140 MBO	1.2	9–11	300	250	22
DX 53D/Z140 MBO	1.5	9–12	250	300	22
DX 53D/ZF100 RBO	1.2	9–12	300	250	22–24
DX 53D/ZF100 RBO	1.4	9–11	250	300	22–24
HCT 600/ZF100 RBO	1.2	8–10	300	350	26–30
HCT 600/ZF100 RBO	1.8	9–11	250	350	22–24
DX 52D/ZF140 RBO	1.5	9–12	250	300	22
DX 53D/AS120	0.6	8.4–10.4	250	250	22
DC04/ZE75/75 A	1.2	9.5–12.5	300	300	22
DC04/ZE75/75 APO	2.0	9.5–12.2	250	300	22
ZSTE 280BH/ZE75/75 APO	0.6	7.4–10.5	250	250	22
LAC 320Y400T/ZE/EG + OC2	1.5	8.8–11.8	250	300	22

Figure 1. Research station for the examination of fume and gas generation during resistance welding: *1* — fume chamber of 0.03375 m³; *2* — welded workpiece; *3* — machine of ZPa-130i type; *4* — inverter controller HWS 2102IQ; *5* — aspirators; *6* — fume filter; *7* — gas analyser Testo-33/Testo-350; *8* — system for measuring and monitoring welding parameters

ments of PN-EN ISO 15011 standard [12–15]. Sampling of fume aimed at the specification of total fume generation is based on the gravimetric method. The principle of the examination is sampling the fume onto the measuring filters during resistance welding with productivity of 20–30 weld/min, in the hermetic chamber when exhaust system is switched on. It was assumed that the welding process duration in the chamber should be 60 s, since this time makes possible to obtain the increase of fume in the measuring filter enough to determine the mass of collected fume with the accuracy of up to 0.1 mg.

The examination of gas generation during resistance welding was conducted using direct method, therefore, analyzers Testo-33 and Testo-350 allowed for direct reading of gas concentration (NO, NO_2, CO) and temperatures. Research methodology, developed initially for the determining inorganic gases generation during resistance welding, suggests the measuring the concentration and emission rate of carbon monoxide and nitrogen oxides. Preliminary research revealed that the nitrogen oxides generation during welding processes is very limited. The conclusion reached during the preliminary research is in the conformity with the assumptions of EN ISO 15011-6:2010 standard [15], which in the case of inorganic gases generation during resistance welding recommends examination of carbon monoxide emission only.
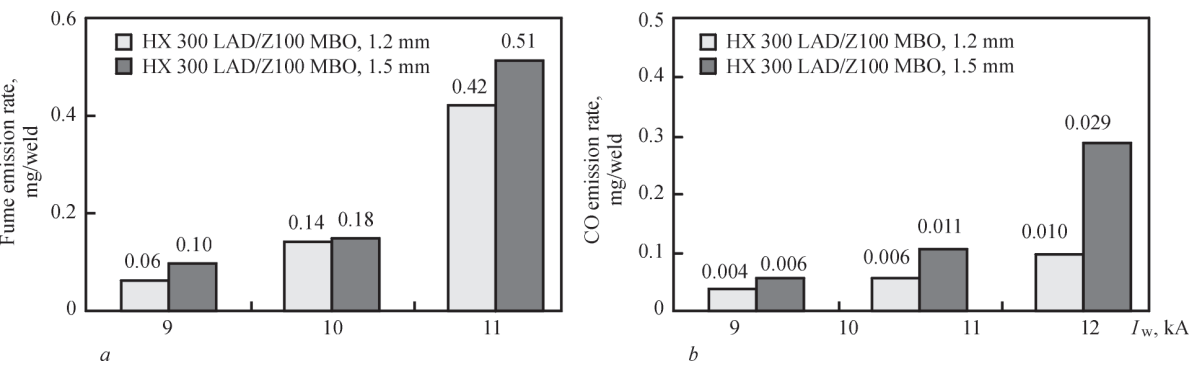

Figure 2. Fume chamber in experimental station for examination of fume and gas emission during spot resistance welding: *1* — fume chamber; *2* — fume filter; *3* — welded workpiece; *4* — electrodes; *5* — electrode around which welding fume is being formed [11]

Next step of research covered both the determination of chemical composition of fume and the examination of organic substances generation during resistance welding of selected coated plates.

Analysis of research results. The conducted tests of the pollutants generation rates during spot resistance welding of coated plates allowed for the conducting comparative analysis aimed at determination of the effect of welding current and plate thickness on fume and gas generation. The pollutants generation rates in similar welding conditions for different steel grades and various types of the coating were compared as well.

Impact of welding current on fume and gas emission rates. The investigation of fume and carbon monoxide generated during spot resistance welding revealed the impact of welding current on emission rate. Increase in welding current resulted in higher total fume generation and higher generation of carbon monoxide during welding of plates of the same thickness, same welding time and force. The relation between welding current and pollutants emission rate occurred in the case of all coated materials being tested. Taking into consideration welding of DX 53D/

Figure 3. Impact of current on fume (*a*) and CO (*b*) emission rates during spot resistance welding of hot-dip Zn-coated plate DX 53D/ Z140 MBO of 1.5 mm thickness

Figure 4. Emission of total fume (*a*) and CO (*b*) during spot resistance welding of HX 300 LAD/Z100 MBO 1.2 and 1.5 mm plates for various welding currents

Z140 MBO material (see Table 2), the increase of welding current from 9 to 12 kA resulted in three-fold fume generation and 4.5 times of CO emission rate growth (Figure 3).

Impact of thickness of material being welded on pollutants emission rate. The analysis of this issue was conducted for following coated plates: DX 53D/ZF100 RBO (1.2 and 1.4 mm thick), HX 300 LAD/Z100 MBO (1.2 and 1.5), HCT 600/ZF100 RBO (1.2 and 1.8) as well as DC04/ZE75/75 A (1.2) and DC04/ZE75/75 APO (2.0).

During welding HX 300 LAD/Z100 MBO plate, higher fume and CO emission rates were revealed for the 1.5 mm thick plate (Figure 4).

In the case of DX 53D/ZF100 RBO material 1.2 and 1.4 mm thick, for the same welding current, the higher emission of fume occurred for thinner plate. Similar relation took place for HCT 600/ZF100 RBO plates 1.2 and 1.8 mm thick. For resistance welding of electrolytic zinc-coated plates the comparative analysis was conducted for DC04/ZE75/75, 1.2 and 2.0 mm thick plates. These plates differed in the additional surface protection: the 1.2 mm plate did not have any protection while the 2.0 mm plate was additionally phosphated and oiled (PO type). Higher fume and CO emission rate for all current values occurred during welding 1.2 mm thick plate with zinc coating not protected additionally (Figure 5).

To sum up the research results of the pollutants generation during spot resistance welding, the unequivocal relation between fume and carbon monoxide emission rates and thickness of welded material cannot be established.

Impact of protection coating type on pollutants emission rates. The examination of pollutants emission rate during welding was conducted for five types of coatings differing in the method of applying, chemical composition, thickness and additional protection (Figure 6). The analysis of the research results have revealed that the type of protective coating affects the generation of total fume and carbon monoxide. During resistance welding LAC 320Y400T grade plate with double-layer coating, i.e. electrolytic zinc-coated plate with 5 μm thick zinc coating + epoxy protective coating of GardoProtect type, resulted in the highest fume and CO emission rates in comparison with Zn and zinc-iron coated plates. Fume generation during zinc- and epoxy-coated plates resistance welding can be even 3–5 times higher than that for hot-dip zinc-coated plates. The analysis of fume and CO emission rates during welding of hot-dip Zn- and Zn–Fe-coated plates and electrolytic Zn-coated plates (ZE type coating) revealed that for similar welding conditions, the highest pollutants emission rates occurred for the plates with ZF coating. The plates with Z and ZE coating types have similar pollutants emission rates. Research has revealed that fume and
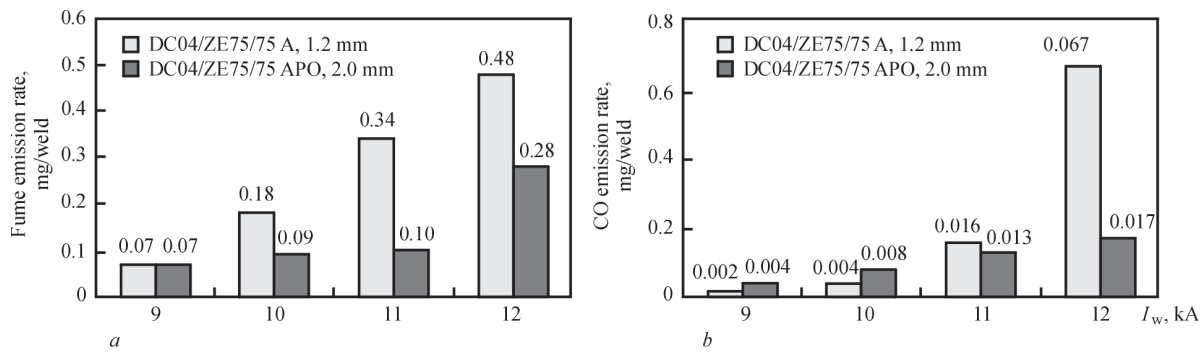
Figure 5. Emission of total fume (*a*) and CO (*b*) during spot resistance welding of 1.2 mm thick DC04/ZE75/75 A and 2.0 mm thick DC04/ZE75/75 APO plates for various welding currents
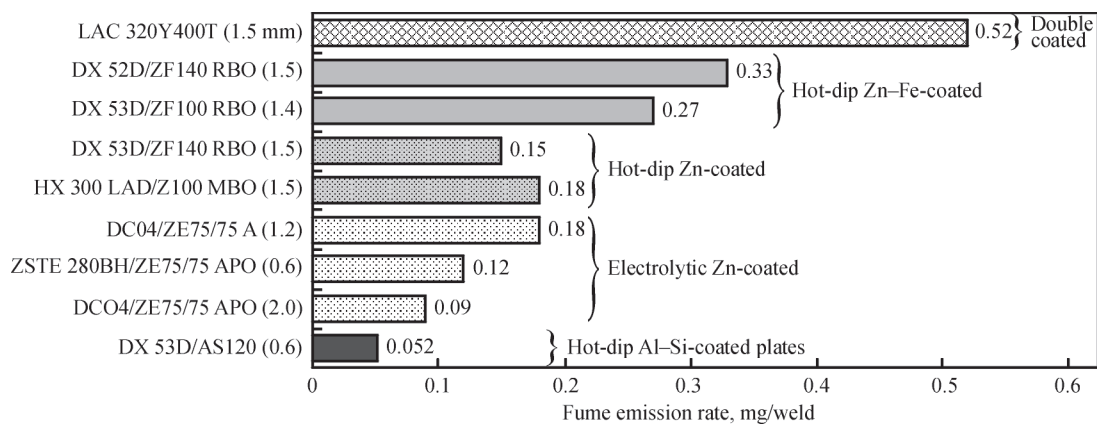
Figure 6. Total fume generation during spot resistance welding plates with various coatings at $I_w = 10$ kA

carbon monoxide emission rates are affected by the type of additional protection of the surface. During resistance welding of electrolytic zinc-coated plates of DC04/ZE75/75 A (no additional protection) and DC04/ZE75/75 APO grade (PO protection), fume generation is 2–3 times lower for the phosphated and oiled material.

Impact of coating thickness on pollutants emission rates. The analysis of coating thickness influence was carried out for similar material grades and thicknesses. They differed with the coating mass — 100 and 140 g/m^2–100 g/m^2 referred to coating thickness of 7 μm, and 140 g/m^2 — to 10 μm.

In case of hot-dip coated plates with Z type coating, the research of coating thickness influence was conducted for HX 300 LAD/Z100 MBO and HX 420 LAD/Z140 MBO materials 1.2 mm thick. The test results have shown that fume emission rate was 3–4 times higher for material with thicker coat-

ings (Figure 7, *a*). In case of CO, higher values of emission rate were also connected with Z140 MBO coating type, the difference was even seven-fold for $I_w = 10$ and 11 kA (Figure 7, *b*).

For hot-dip coated plates with ZF type coating the analysis was carried out for two similar material — DX 53D/ZF100 RBO (1.4 mm) and DX 52D/ZF140 RBO (1.5 mm). The test results have shown that at $I_w = 10$ and 11 kA the fume emission rates were 20 % higher for material with thicker coating (Figure 7, *c*). Also CO emission rates for the same welding current values were 10 % higher for ZF140 RBO coating type (Figure 7, *d*).

To summarize, it is possible to observe directly proportional relation between the coating thickness and the fume and CO emission rate, namely, the higher the coating thickness, the higher is the pollutant emission rate value.
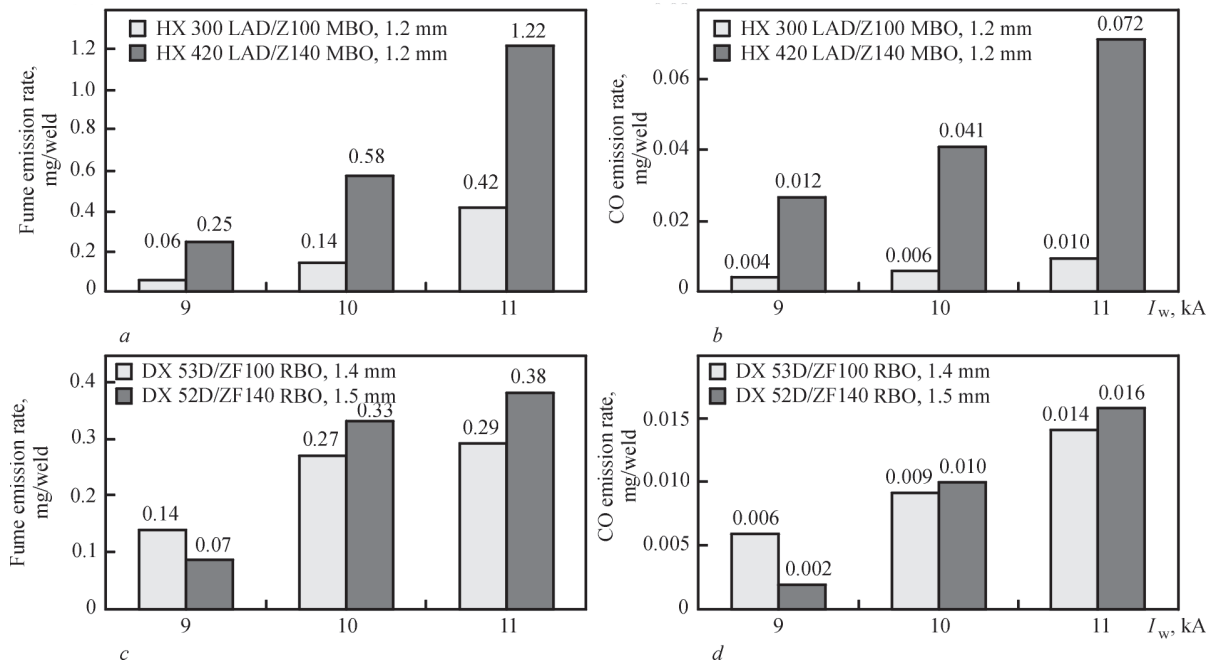

Figure 7. Impact of coating thickness of resistance-welded material on fume and CO emission rates

Table 3. Chemical composition of fume generated during spot resistance welding of coated plates

Type of coated plates	Fume chemical composition, %				
	Fe	Mn	Si	Zn	Al
DX 53D/ZF100 RBO	67.5	0.53	0.30	12.18	–
HCT 600/ZF100 RBO	69.6	1.16	0.27	8.11	–
HX 300 LAD/Z100 MBO	64.0	0.51	0.24	18.80	–
HX 260 LAD/Z100 MBO	62.3	0.62	0.28	16.30	–
DC04/ZE75/75 A	68.9	0.21	0.26	28.70	–
DC04/ZE75/75 APO	55.3	0.26	0.30	28.20	–
DX 53D/AS120	48.8	1.13	1.09	–	6.21

Chemical composition of fume generated during resistance welding of coated plates. Chemical analysis was conducted for several steel grades with different type of protective coatings. The testing was performed on fume arising for the chosen highest values of welding current (see Table 2). Chemical composition of fume is shown in Table 3.

Zinc content in the fume depended on the type of protective coating. The highest amount occurred during resistance welding of electrolytic zinc-coated plates (ZE75/75 coating thickness of 7.5 μm), the zinc content in fume was 28.2–28.7 %. Then during resistance welding of hot-dip zinc-coated plates (Z100 coating thickness of 7 μm) the zinc content in the fume amounted 16.3–18.8 %. Meanwhile in the case of plates with Zn–Fe alloy coating (ZF100 coating thickness of 7 μm) the zinc content in fume was from 8.11 to 12.18 %.

Organic substances emitted during resistance welding of coated plates. The quantitative analysis of organic substances was conducted for selected material grades: HCT 600/ZF100 RBO (1.8), LAC 320Y400T/ZE/EG + OC2 (1.5), DX 53D/Z140 MBO (1.5) and HX 420 LAD/Z140 MBO (1.2 mm thick) for $I_w = 11$ kA, and covered three groups of organic compounds:

● for BTEX compounds – benzene, toluene, ethyl benzene and o, m, p-xylene;

● for phenol, o-cresol and m + p cresol;

● for polycyclic aromatic hydrocarbons — naphthalene, acenaphthylene, fluorene, phenanthrene, benzo(a)anthracene, pyrene, chrysene, benzo(a)pyrene, benzo(k)fluoranthene.

The impact of the protection coating type on organic compounds emission rate during spot resistance welding is shown in Figures 8 and 9. Research has revealed that the type of anticorrosive coating and the additional protection technique of the outside layer influence the emission rate and the type of generated organic compounds. The highest generation of benzene — the substance of the proven carcinogenic action — occurred during resistance welding of HCT 600/ZF100 RBO grade plate. This plate was covered with coating of the increased quality from zinc–iron alloy and was additionally protected by oiling (see Figure 8).

The highest generation of three cresol isomers: ortho, meta and para — the substance of the probable carcinogenic action — occurred for plate LAC 320Y400T/ZE/EG + OC2 + GardoProtect 9498 with double-layer coating 1.5 mm thick at $I_w = 11$ kA.

The analysis of PAHs emission started with benzo(a)pyrene generation, since this hydrocarbon is the most thoroughly examined substance being defined as confirmed carcinogen and benzo(k)fluoranthene — the next substance of the high relative carcinogenic coefficient (0.1). Benzo(a)pyrene is the standard compound for the calculation of the carcinogenic action of other PAHs compounds. The highest emission of these substances occurred during welding of oiled zinc–epoxy double-layer coated and chemically passivated plate. In the case of resistance welding of Zn-
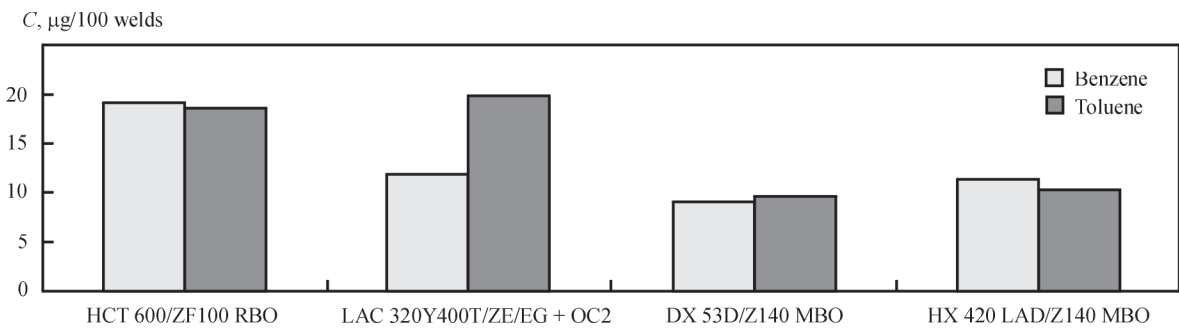
Figure 8. Emission of benzene and toluene during resistance welding of coated plates
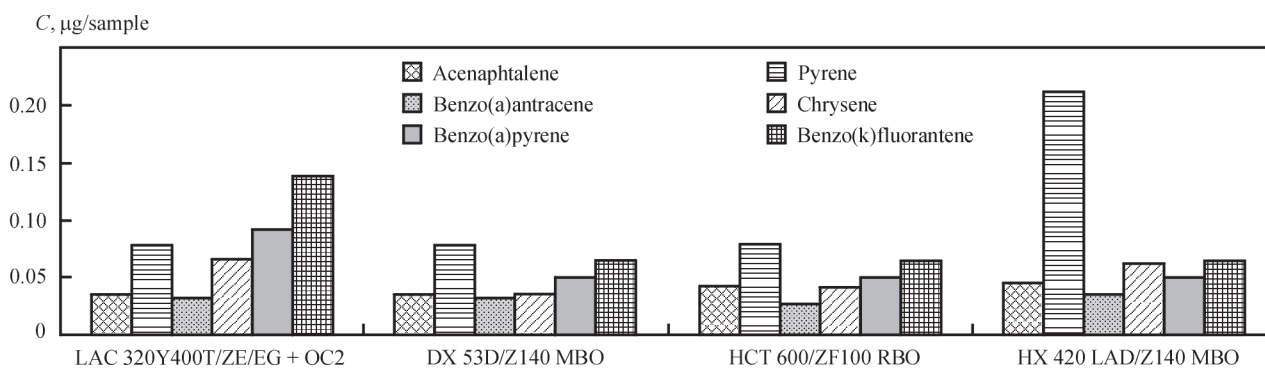
Figure 9. Impact of anticorrosion coating on emission rate of polycyclic aromatic hydrocarbons during resistance welding of plates with various coatings

and Zn–Fe-coated plates, the emission rates of benzo(a)pyrene and benzo(k)fluoranthene were below their determinability levels.

Also the emission rates of other polycyclic aromatic hydrocarbons identified in welding fumes: pyrene, chrysene and acenaphthalene; these substances are characterised by lower carcinogenic properties (see Figure 9).

All materials with protective coatings being resistance-welded were additionally protected by the oiling and chemical passivation processes. The decomposition of the oil and epoxy resin layers caused emission of organic compounds to the work environment. Especially high emission rate of these substances was associated with resistance welding of double-layer zinc- and epoxy-coated and additionally oiled plates.

Conclusions

The investigations of pollutants arising during spot resistance welding of plates with various protective coatings conducted at Instytut Spawalnictwa allowed for formulating following conclusions [8–10, 16, 17].

The fume and gas emission rates in welding depends on current: the increase of current results in higher generation of total fume, carbon monoxide and organic substances in welding of plates of the same thickness and applying the same welding time and welding force. The relation between welding current and pollutants emission rates occurs for all covered materials being tested.

The unequivocal relation between fume and gas emission rates and thickness of the welded material cannot be determined on the basis of the research results of pollutants generation during spot resistance welding of plates with various protective coatings.

The research revealed the impact of the protection coating type on emission rates of the total fume and carbon monoxide, namely, during resistance welding the highest results of fume and CO were identified for double-coated plates (with zinc–epoxy coating), then for plates with zinc-iron coatings. Plates with zinc and

zinc-iron coatings have the similar pollutants emission rates.

The results analysis confirmed the directly proportional relation between the coating thickness and the values of fume and CO emission rate.

The chemical analysis of fume covered the quantitative determination of Fe, Zn, Si, Mn and Al elements. The results of the chemical analysis of the fume being generated during resistance welding of plates with various coatings have revealed that the highest content of zinc in fume occurs in the case of electrolytic zinc-coated plates.

The process of resistance welding steel plates covered with protective coatings is associated with the emission of various organic substances. The compounds of the confirmed carcinogenic character emitted in this process are benzene and benzo(a)pyrene. The substances of suspected carcinogenic action being determined in resistance welding are cresols and polycyclic aromatic hydrocarbons.

1. (1999) *Austral. Occup. Health and Safety Comm.*: Welding fumes and gases.
2. Matczak, W., Gromiec, J.P. (2003) *Zasady oceny narażenia zawodowego spawaczy*. Łódź: Instytut Med. Pracy.
3. El-Zein, M., Infrnte-Rivard, C. (2005) Is metal fume fever a determinant of welding related respiratory symptoms and /or increased bronchial responsiveness? *Occup. Environmental Med.*, **62**, 688–694.
4. Legros, P., Lodi, P. (2008) Spot welding fumes: Characterization of organic coated steels. In: *Arcelor Innovation R&D.* Belgium.
5. Carter, G., Pengelly, I. (2008) Fume emissions from resistance welding through organic coatings: Establishing a method for generating safety data. In: *TWI Report 897/2008.*

6. Legros, P., Winne, V. (2007) *Eesistance welding fumes analysis of coated steels*. Res. Report. Arcelor Res. Industry, Gent.

7. (2002) *Fume emissions from resistance welding:* TWI Res. Report.

8. Matusiak, J., Wyciślik, J. et al. (2010) Badania emisji zanieczyszczeń przy zgrzewaniu rezystancyjnym blach z powłokami. In: *Res. Report of Institute of Welding*, Vol. 105.

9. Matusiak, J., Wyciślik, J. et al. (2011) Analiza wpływu warunków technologicznych innowacyjnych technik spajania różnych materiałów konstrukcyjnych z nowoczesnymi powłokami ochronnymi na stan środowiska pracy. In: *Res. Report of Institute of Welding*, Ma-34.

10. Matusiak, J., Wyciślik, J. Ocena zagrożeń w środowisku pracy przy zgrzewaniu rezystancyjnym punktowym, zgrzewaniu tarciowym z mieszaniem materiału zgrzeiny oraz zgrzewaniu ultradźwiękowym i wibracyjnym różnych materiałów konstrukcyjnych. Opracowanie zaleceń do profilaktyki zagrożeń z uwzględnieniem modyfikacji warunków technologicznych. In: *Zadanie realizowany w 2012. Program wieloletni pn. «Poprawa bezpieczeństwa i warunków pracy» etap II realizowane w latach 2011–2013*. Warszawa: Koord. CIOP PIB.

11. *PN-EN ISO 5182:2009*: Zgrzewanie rezystancyjne — Materiały na elektrody i sprzęt pomocniczy (oryg.).

12. *PN-EN ISO 15011-1:2010*: Zdrowie i bezpieczeństwo przy spawaniu i procesach pokrewnych — Metoda laboratoryjna pobierania próbek dymu i gazów. Część 1: Określanie wielkości emisji dymu podczas spawania łukowego i pobieranie dymu do analizy.

13. *PN-EN ISO 15011-4:2008/A1:2009*: Zdrowie i bezpieczeństwo przy spawaniu i procesach pokrewnych — Metoda laboratoryjna pobierania próbek pyłu i gazów. Część 4: Karty charakterystyki pyłu (oryg.)

14. *ISO 15011-5:2009*: Health and safety in welding and allied processes — Laboratory method for sampling fume and gases. Pt 5: Identification of fume and gases generated during welding and cutting through products composed wholly or partly of organic materials.

15. *ISO 15011-6:2010*: Health and safety in welding and allied processes — Laboratory method for sampling fume and gases. Pt 6: Procedure for quantitative determination of fume and gases from resistance spot welding.

16. Matusiak, J., Wyciślik, J. (2012) Zgrzewanie rezystancyjne blach stalowych z powłokami a emisja zanieczyszczeń do środowiska pracy. *Biul. Instytutu Spawalnictwa*, **3**, 20–28.

17. Matusiak, J., Wyciślik, J. (2012) Research into fume and gases emission during resistance welding of coated steels plates. *Hutnik — Wiadomości hutnicze*, **11**, 805–816.

MEASUREMENT-AND-ANALYTICAL SYSTEM FOR WELDING PARAMETERS AND NOISE LEVEL DURING MANUFACTURING PROCESS OF WELDED STRUCTURES

L. SZUBERT, P. SKOCZEWSKI, J. MATUSIAK and **J. WYCIŚLIK**

Institute of Welding

16-18 Bl. Czeslawa Str., 44-100, Gliwice, Poland. E-mail: leszek.szubert@is.gliwice.pl

This paper presents the design, technical possibilities and intended use of the multi-station measurement-analytical system for assessing welding process parameters and noise levels. The system is an innovative solution as regards the measurement technique related to welding parameters and acoustic pressure in production floors. Once implemented industrially, the system enables the monitoring and recording of noise levels in individual work centres as well as the monitoring and recording of technological conditions accompanying welding of various structures and products. 8 Ref., 1 Table, 9 Figures.

The use of welding technologies in industrial practice entails the necessity of testing and determining conditions related to health and safety at work. Welding belong to manufacturing processes significantly and unfavourably affecting the work environment. Presently, welding along with allied techniques constitute the most developed and established joining technology used when making structures and products of diverse materials and sizes in many industrial sectors. Various welding methods generate excessive noise being a physical factor having a definitely destructive effect on the worker's physical health and significantly deteriorating work conditions.

The exposure of individual welding shop workers to noise depends on numerous factors, particularly including concurrent work performed in individual production centres, welding current and arc voltage parameters and intensity of post-weld machining. The acoustic environment of a production floor where welded structures are made is hazardous to the worker's health and affects the efficiency of production. According to Instytut Spawalnictwa's research and experience, in many companies the excessive noise accompanying the making of welded structures constitutes a very urgent and important issue.

Having in view the foregoing, Instytut Spawalnictwa has developed an innovative measurement-analytical system for measuring and analysing welding process parameters and noise levels in technological floors [1]. The combination of measuring and recording functions of the system with analytical modules related to the making of welded structures and concerning acoustic conditions is an innovative solution enabling the control of manufacturing (welding) processes and that of the acoustic environment of work.

Outline of the system. In strict terms, the system is by definition a computer-based control-measurement, measurement-analytical and analytical-advisory system. The measurement system is an appropriately organised set of elements constituting a certain whole dedicated to obtaining measurement information from an object being tested and providing the user with this information in a usable form. The control system is tasked with verifying whether a measurement result is restricted within a certain range of boundary values. In turn, the role of the analytical system is to analyse collected information and enable the user to draw logical and practical conclusions. The advisory (expert) system, on the basis of collected information and using an appropriate algorithm, provides the user with a solution to a given problem. The term «computer-based» means that all of the functions enumerated above are performed using a computer system.

The system is composed of two layers, i.e. hardware and software. The hardware layer includes sensors, data acquisition cards, communication interface cards, computer system elements as well as the remaining elements, systems and electronic devices. The software layer includes software modules controlling the operation of the measurement system as well as software modules implementing the adopted functionality of the control-measurement system and

the adopted functionality of the analytical-advisory system.

According to a previously adopted assumption, the system is not dedicated to a specific type of welding station. It has been assumed that the system should be usable with many different types of welding stations. For this reason, the system architecture is sufficiently open and versatile so that the system could be used in various conditions. The multi-station character of the system means that system functions are implemented on many welding stations at the same time.

The system is experimental in nature and constitutes an innovative approach to the assessment of sounds emitted when welded structures are made in a production shop. The system incorporates the control-measurement functions of the system with analytical functions related to the making of welded structures and to acoustic conditions, as well as analytical-advisory functions aimed to reduce the level of sound by changing welding process parameters.

Functional description of the system. The system is relatively complex and its functionalities can be viewed in various ways [1]. The most general level involves the following functions:

● measuring/recording — acquisition of parameters connected with welding processes and parameters related to noise generated and emitted during production;

● storing (archiving) — transfer of recorded data from welding stations and data collected during acoustic measurements to the central storage unit (database server), where these data are stored and secured;

● analytical — analysis of collected data, calculating derivative quantities, the evaluation of welding processes and the assessment of noise levels;

● advisory — changes of technological parameters aimed to reduce noise levels;

● visualising — presentation of collected data.

The detailed description and characteristics of system functions are presented in the Table.

System architecture. The system can be characterised as a distributed multi-station analytical-measurement system connected (via a computer network) with a central computer (server) storing recorded parameters and data created on the basis of these parameters (Figure 1). The data can be accessed by users

Description of functions of the system for measuring and analysing welding parameters and noise when making welded structures [1]

Function	Description	Advantages
Recording of welding parameters	Measurement of quantities related to arc welding processes (MIG/MAG), i.e. welding current, arc voltage and wire feed rate	Possibility of obtaining detailed technological information on welding processes
Recording of noise parameters	Recording of acoustic pressure levels using correction (A, C)	Possibility of obtaining detailed information on noise present at selected production stations
Archiving of recorded parameters	Saving of recorded parameters in the database	Possibility of using data for further analysis and documentation of production processes
Automated information collection process	Recording, saving and processing of selected parameters are performed automatically by the measurement system	Unattended gathering of information on production processes
Visualisation and reporting of collected data	Presentation of collected information, recorded waveforms, calculated derivative quantities in various timeframes (shift, daily, monthly etc.) enables the system user to assess the process production in a bigger picture. Generation of daily, weekly etc. reports	Assessment and detection of trends and untypical changes of parameters
Analytical-advisory function for correlation of welding parameters and sound levels	On the basis of defined technological welding parameters it is possible to select/adjust an alternative set of parameters leading to the reduction of noise generated and emitted during production processes	Reduction of noise improving work conditions
System scalability	Universal module design of the system makes it possible to add more stations to the system and to add new functions connected with the analysis of collected data without reorganising the system	Module architecture of the system enabling its easy extension
Access via a computer network	Use of Ethernet for data transmissions. The possibility of incorporating the system into the network infrastructure of the production facility. As a result, collected data are available to all authorised workers using the computer network	Availability of the system
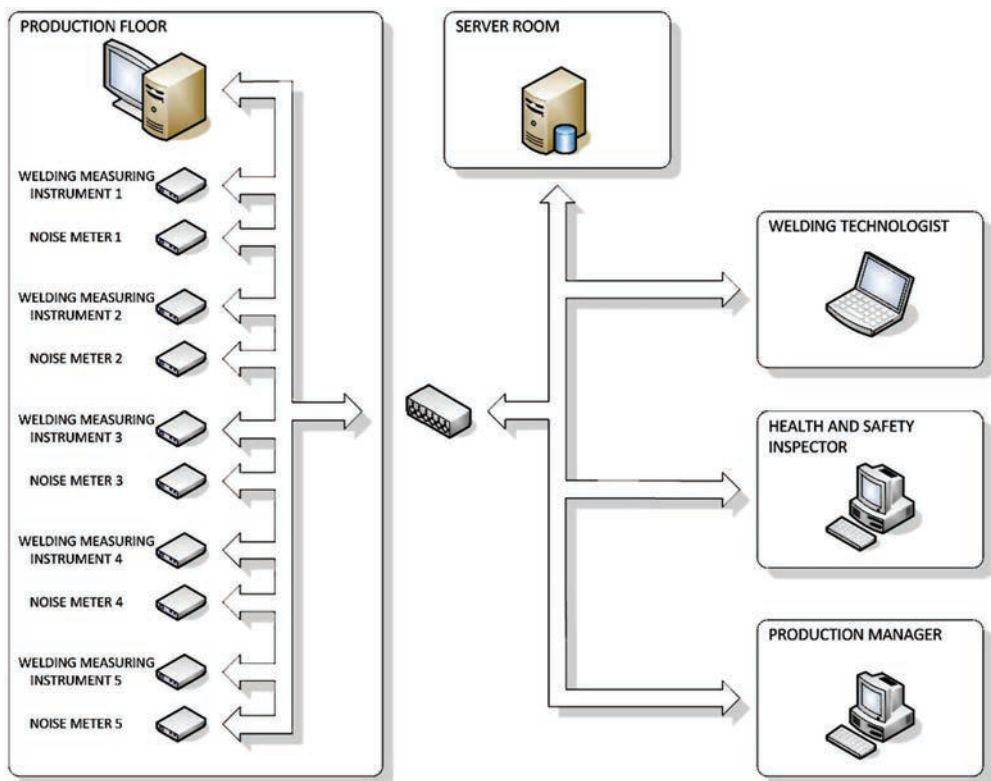
Figure 1. Measurement system architecture [1]

connected to the computer network and provided with appropriate software applications enabling the users to visualise and analyse collected information [2].

The system represents a typical example of client/server network architecture, where the central computer with the database (server) are the receiver of data generated by measurement modules installed at production stations and analytical software (clients) used by the main system users, i.e. welding technologists, health and safety inspectors and other personnel managing production processes.

The measurement system is composed of modules for measuring welding parameters (Figure 2), provided with three measurement channels, i.e. for measuring welding current, arc voltage and wire feed rate. The modules have been provided with appropriate measuring transducers, measurement cards and an industrial controller controlling the operation of the measurement module provided with an output for communication via Ethernet.

The operation of the measurement module is entirely autonomous. Its software automatically detects

Figure 2. Module for measuring technological parameters of welding processes [1–3]: *a* — module connected to welding power source; *b* — measurement module; *c* — transducer for measurements of filler wire feed rate installed in the feeder

Figure 3. Noise meter in the production floor

the commencement of welding process and afterwards, on the basis of momentary values, calculates systematically the average and root-mean-square values of recorded waveforms and sends this information to the server via the computer network.

The module for measuring noise intensity is presented in Figure 3. The system includes DSA-50 noise meter manufactured by Sonopan, provided with special software adjusted to the welding measurement system. The meter is equipped with special RS-232 digital output for communication with the master system. For this reason, the module is equipped with RS-232/Ethernet converter to enable communication between the meter and the server via the computer network.

Measurement-analytical system software. Because of the complex functionality of the system and due to the fact that the system has been created by many developers using various IT and measurement technologies, the system software has been divided into the following independent modules (applications) [5, 6]:

● monitor of parameters in the production floor — software for the visualisation of welding parameters and noise levels currently recorded at monitored production stations available in the production shop;

● software for the visualisation of collected data — presentation of collected data and calculated derivative quantities saved in the database, activated remotely by any computer connected to the computer network (e.g. from the office of welding technologist/ health and safety inspector);

● analytical-advisory module for the correlation of welding conditions and noise levels (activated remotely, e.g. from the office of welding technologist/ health and safety inspector);

● reporting software — generation of periodical reports on the basis of collected data stored in the database;

● software of recorders — software of measurement modules for recording welding parameters and the software of noise meters for recording noise level parameters.

The module structure has made it possible to implement required functions of the system, independently in individual modules, using the computer network for the exchange of data and the database as the element integrating the system in one whole.

The graphic interface of the application monitoring noise parameters (used in the production shop) is presented in Figures 4 and 5. The software window contains numbered bookmarks related to each noise meter (Meter 1÷5), List and Diagnostics bookmarks for controlling the application operation and communication between the application and noise meters.

Panel *1* presenting the diagram of noise levels displays equivalent 1-minute levels of acoustic pres-
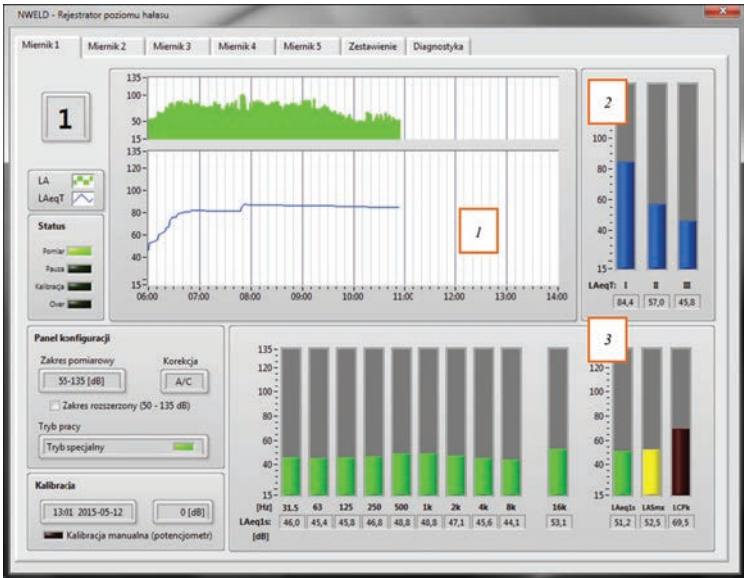

Figure 4. Monitor of acoustic pressure parameters: *1* — panel of acoustic pressure; *2* — panel presenting working changes; *3* — panel of analyser
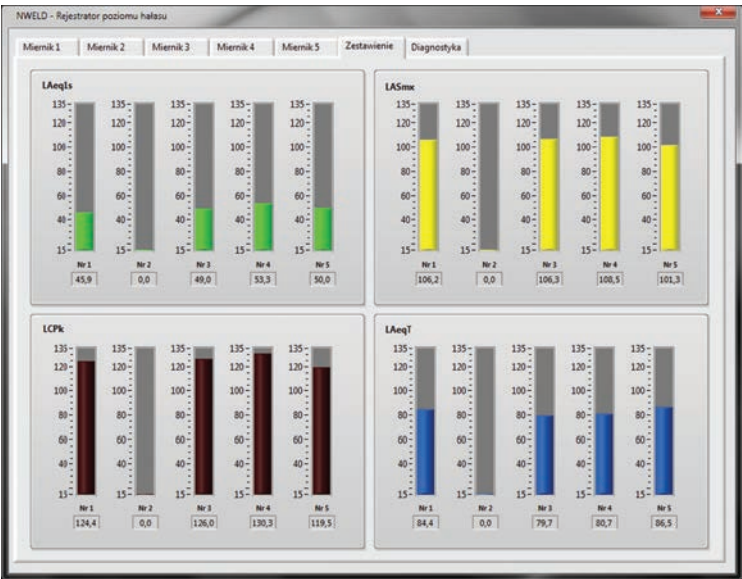
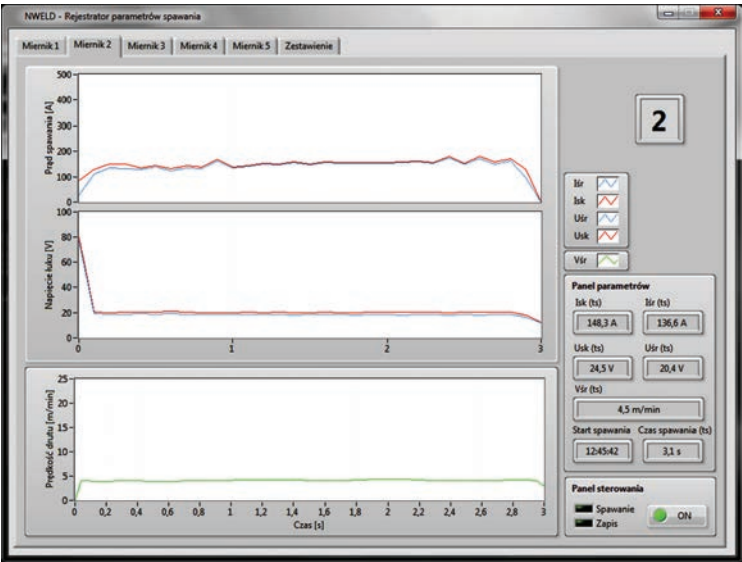**Figure 5.** Bookmark List of noise level monitor software

Figure 6. Main window of welding parameter monitor software
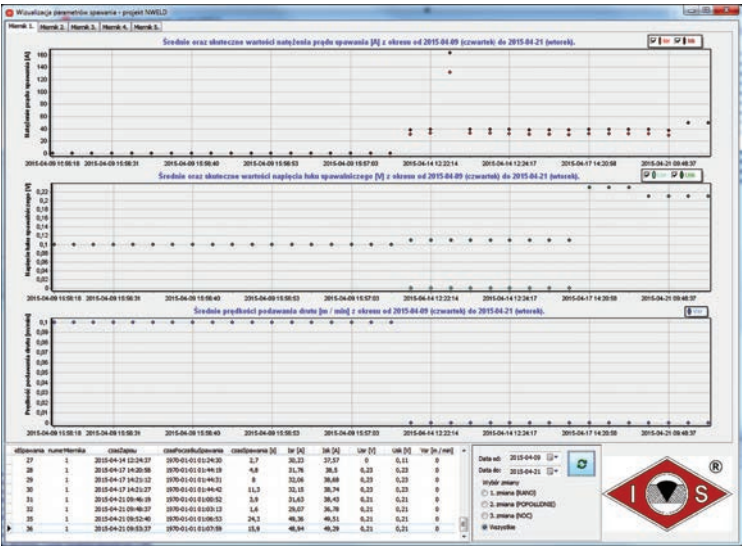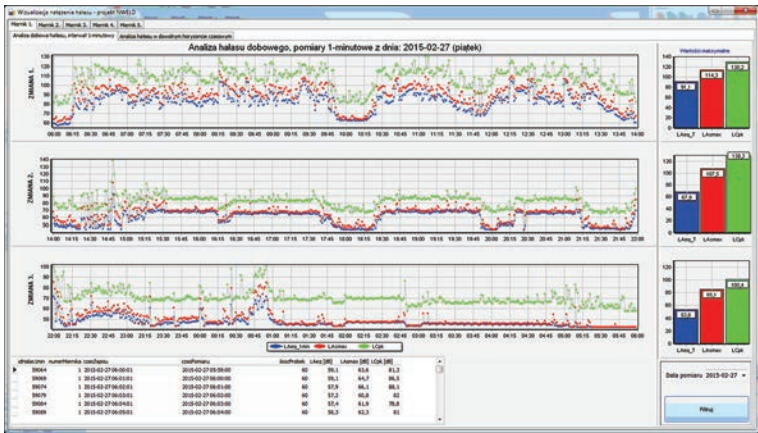

Figure 7. Main window of software for visualisation of welding process-related data

Figure 8. Main window of program for visualisation of data concerning noise intensity

sure (in the form of green bars) according to frequency characteristic *A* and changes of acoustic pressure equivalent to 8-hour working day (in the form of the blue line). Panel *2* showing working changes displays values for each working change of equivalent 8-hour acoustic pressure corrected according to characteristic *A*. Panel *3* of the analyser displays equivalent 1-second levels of acoustic pressure *A* for individual octaves. In addition to the panels enumerated above, the bookmark also contains the panel of configuration presenting the current configuration of noise meter and the panel of calibration presenting the information on the timing of the meter recent calibration.

The bookmark List is used for the simultaneous comparison of noise level values indicated by all 5 m:

● L_{Aeq1s} — equivalent *A*-weighted sound pressure level over 1-second duration;

● L_{ASmx} — maximum *A*-weighted sound pressure level;

● L_{Cpk} — peak *C*-weighted sound pressure level;

● L_{AeqT} — equivalent *A*-weighted sound pressure level over duration *T* (calculated since the start of the shift until the present moment).

The welding parameter monitor interface of a selected meter is presented in Figure 6. The program window contains the panel of graphs presenting waveforms of welding current and arc voltage (also root-mean-square current and root-means-square voltage) as well as wire feed rate recorded during welding. The control lights in the panel of parameters provide the following information (on an ongoing basis): root-mean-square values of welding current and voltage, average filler wire feed rate, welding start time, and welding process duration.

The bookmark List contains simple welding log in the form of table displaying the number of recently made welds. The log contains the following fields: meter number, welding start time, welding process duration, average welding current, root-mean-square welding current, average arc voltage, root-mean-square arc voltage, and average wire feed rate.

The primary function of the program is to preview present measurement results and archived data (Figure 7). The program window contains three graphs, namely, welding current, arc voltage and filler wire feed rate (average). The window also contains the panel allowing the selection of work shift and measurement date as well as the table containing information related to selected measurement such as date when the given weld was made, recording date, welding pro-
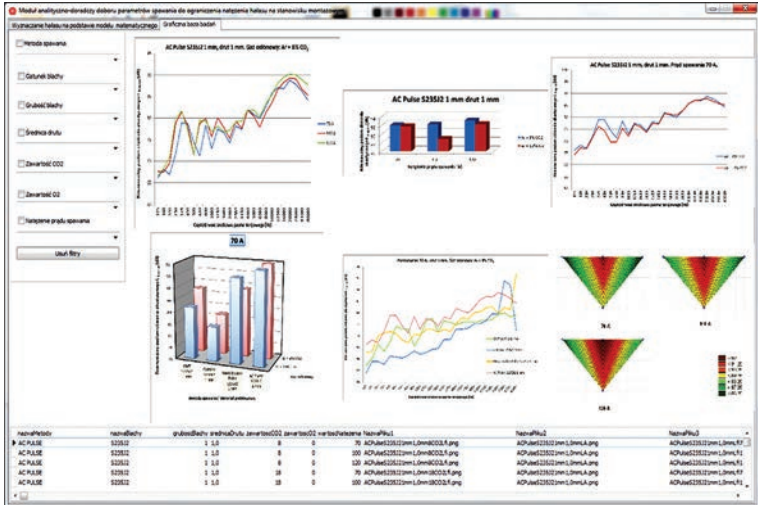
Figure 9. Analytical-advisory module for correlating welding parameters and noise levels [1, 7, 8]

cess duration and values of individual quantities being measured. In the graphs presented below, successive points correspond to average values of successively made welds. Clicking on any point opens the window containing time series plots of recorded parameters related to selected weld.

Figure 8 presents the program window for the visualisation of acoustic pressure measurement results. The window contains the graphs showing changes of acoustic pressure for each work shift, the table containing measurement results in the form of numeric values, and the panel for selecting measurement results. The window displays the following acoustic pressure values:

● $L_{Aeq,1m}$ — equivalent 1-minute level of acoustic pressure corrected according to frequency characteristic A;

● $L_{ASmx,1m}$ — maximum 1-minute root-mean-square value of acoustic pressure;

● $L_{Cpk,1m}$ — maximum momentary value of acoustic pressure, recorded in the 1-minute period, corrected according to frequency characteristic C.

An exemplary window of the analytical-advisory module for the correlation of noise levels and welding parameters is presented in Figure 9. The primary function of the module is to provide the possibility of predicting acoustic pressure values on the basis of developed statistical model. The model is based on multiple regression and describes the dependence of noise generated during the welding of sheets on factors having statistically significant effect on the level of noise. On the basis of research-related tests, the factors recognised as statistically significant are as follow [7, 8]:

● welding method;
● sheet grade and thickness;
● welding current;
● filler wire diameter;
● oxygen and carbon dioxide contents in shielding gas mixture.

An additional function of the module is the diagram-based presentation of comparative test results for various configurations of welding process parameters. It is possible to select the precise configuration of the above-named welding parameters.

Conclusion

The measurement-analytical system for assessing noise emitted during making welded structures enables the monitoring and recording of acoustic pressure levels in individual production centres (welding work stations) as well as the monitoring and recording of technological welding conditions. The system is provided with the analytical-advisory module for correlating welding conditions and noise levels. The

combination of its measuring and recording functions with the analytical-advisory module concerning the making of welded structures and acoustic conditions enables the control of manufacturing processes (welding and mechanical processes) as well as the acoustic control of the work environment aimed to comply with hygienic standards of occupational noise. The system has been provided with the universal (in terms of welding process applications in various sectors) and entirely innovative database of acoustic pressure levels for various welding methods. The base has been developed for selected welding methods and current-voltage parameters commonly used industrial practice. The database used in the analytical-advisory module is based on test results focused on acoustic pressure levels for numerous combinations of welding method–base material–filler metal–shielding gas–current-voltage parameters–filler wire feed rate.

The measurement-analytical system is a solution enabling the technological and acoustic monitoring of individual production steps as well as making it possible to implement modifications of technological conditions aimed to reduce the exposure of workers to noise. The use of the system when making welded structures is an important move aimed at the prevention of hazards affecting workers' health. In future, such an initiative is bound to improve work conditions and increase work efficiency.

1. Matusiak, J., Wyciślik, J., Szubert L. et al. Badania i opracowanie systemu pomiarowo-analitycznego dla oceny poziomu dźwięku emitowanego przy wytwarzaniu konstrukcji spawanych. In: *Report of project INNOTECH*, 2013–2015.

2. Noergaard, T. (2005) Embedded systems architecture: A comprehensive guide for engineers and programmers. Amsterdam: Elsevier.

3. Szubert, L., Skoczewski, P., Welcel, M. (2010) System rejestracji parametrów elektrycznych procesu spawania dla wielu stanowisk produkcyjnych. In: *Res. Report of Institute of Welding ST-284 (Fc-89)*.

4. Szubert, L. Skoczewski, P., Welcel, M. (2013) Rozbudowa możliwości systemu monitorowania procesu spawania. Opracowanie prototypu głowicy pomiarowej do rejestracji kluczowych parametrów spawania dla urządzeń spawalniczych typu MIG/MAG. In: *Res. Report of Institute of Welding ST-323 (Fd-125)*.

5. Stroustrup, B. (2010) *Programowanie. Teoria i praktyka z wykorzystaniem C++*. Gliwice: Helion.

6. Schwartz, B., Zaitsev, P. et al. (2009) *Wysoko wydajne MySql. Optymalizacja, archiwizacja, replikacja*. Gliwice: Helion.

7. Matusiak, J., Szłapa, P., Wyciślik, J. et al. (2014) Experimental tests on the effect of gas-shielded arc welding technological conditions on sound level. *Biul. Instytutu Spawalnictwa*, **5** 159–172, *http*://bulletin.is.gliwice.pl/index.php?go=current&ebis=2014_05_22

8. Matusiak, J., Wyciślik, J., Szłapa, P. et al. (2015) Hałas przy spawaniu łukowym w osłonie gazów. *Hutnik — Wiadomości hutnicze*, **3**, 202–211.

PATON PUBLISHING HOUSE

www.patonpublishinghouse.com

SUBSCRIPTION

The Paton WELDING JOURNAL

«The Paton Welding Journal» is Published Monthly Since 2000 in English, ISSN 0957-798X.

Автоматическая Сварка

«Avtomaticheskaya Svarka» Journal (Automatic Welding) is Published Monthly Since 1948 in Russian, ISSN 005-111X.

«The Paton Welding Journal» is Cover-to-Cover Translation of Avtomaticheskaya Svarka» Journal into English.

If You are interested in making subscription directly via Editorial Board, fill, please, the coupon and send application by Fax or E-mail.

The cost of annual subscription via Editorial Board is $348 for «The Paton Welding Journal» and $180 for «Avtomaticheskaya Svarka» Journal.

«The Paton Welding Journal» can be also subscribed worldwide from catalogues subscription agency EBSO.

SUBSCRIPTION COUPON
Address for journal delivery _____

Term of subscription since _____ 20 _____ till _____ 20 _____
Name, initials _____
Affiliation _____
Position _____
Tel., Fax, E-mail _____

We offer the subscription all issues of the Journal in pdf format, starting from 2009.

The archives for 2009−2014 are free of charge on *www.patonpublishinghouse.com* site.

ADVERTISEMENT
in «Avtomaticheskaya Svarka» and «The Paton Welding Journal»

External cover, fully-colored:
First page of cover
(190×190 mm) — $700
Second page of cover
(200×290 mm) — $550
Third page of cover
(200×290 mm) — $500
Fourth page of cover
(200×290 mm) — $600

Internal cover, fully-colored:
First/second/third/fourth page of cover (200×290 mm) — $400

Internal insert:
Fully-colored (200×290 mm) — $340
Fully-colored (double page A3) (400×290 mm) — $500

• Article in the form of advertising is 50 % of the cost of advertising area
• When the sum of advertising contracts exceeds $1001, a flexible system of discounts is envisaged

Size of journal after cutting is 200×290 mm